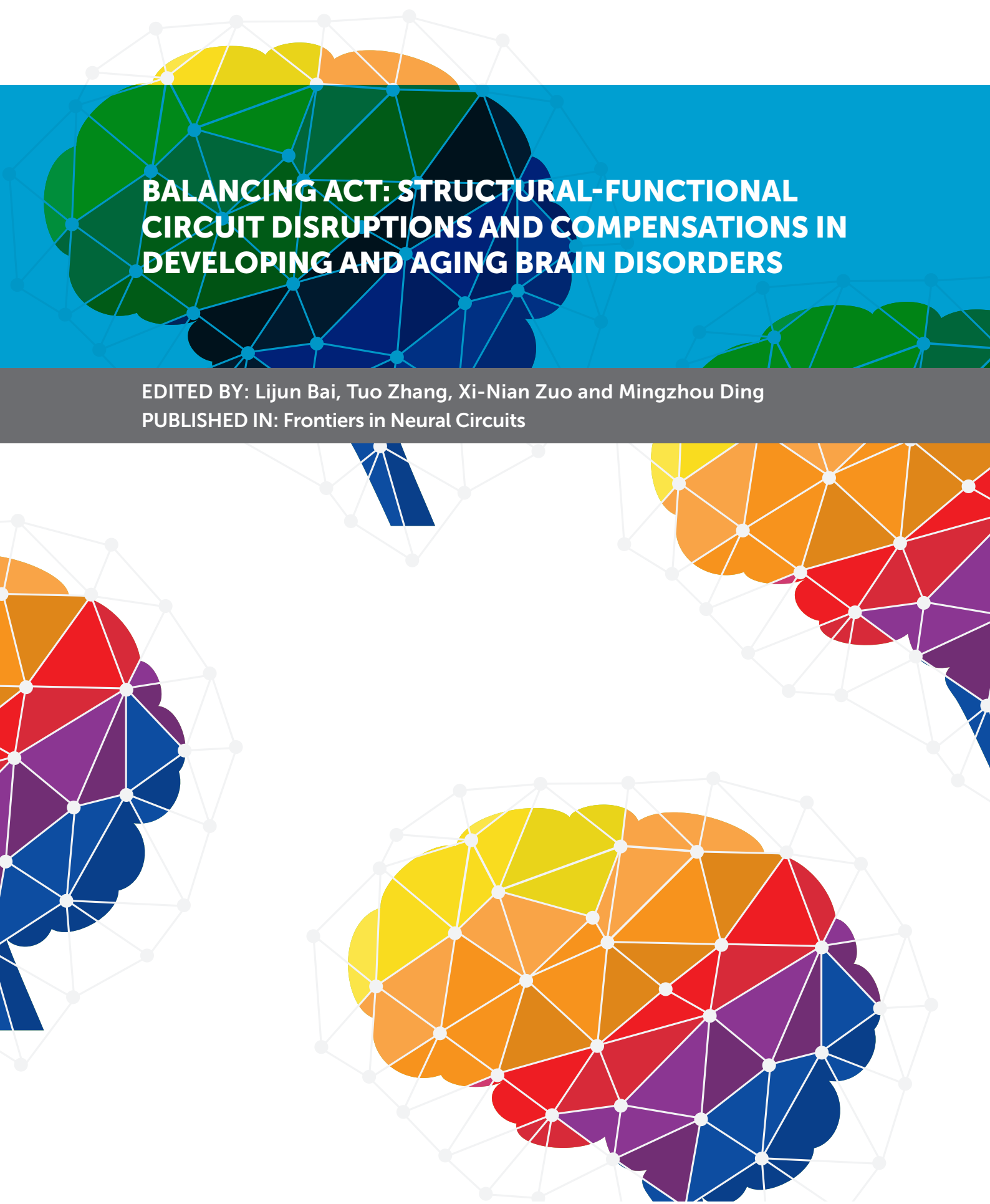

BALANCING ACT: STRUCTURAL-FUNCTIONAL CIRCUIT DISRUPTIONS AND COMPENSATIONS IN DEVELOPING AND AGING BRAIN DISORDERS

EDITED BY: Lijun Bai, Tuo Zhang, Xi-Nian Zuo and Mingzhou Ding

PUBLISHED IN: Frontiers in Neural Circuits

frontiers Research Topics

frontiers

ISSN 1664-8714
ISBN 978-2-88963-486-6
DOI 10.3389/978-2-88963-486-6

About Frontiers

Frontiers is more than just an open-access publisher of scholarly articles: it is a pioneering approach to the world of academia, radically improving the way scholarly research is managed. The grand vision of Frontiers is a world where all people have an equal opportunity to seek, share and generate knowledge. Frontiers provides immediate and permanent online open access to all its publications, but this alone is not enough to realize our grand goals.

Frontiers Journal Series

The Frontiers Journal Series is a multi-tier and interdisciplinary set of open-access, online journals, promising a paradigm shift from the current review, selection and dissemination processes in academic publishing. All Frontiers journals are driven by researchers for researchers; therefore, they constitute a service to the scholarly community. At the same time, the Frontiers Journal Series operates on a revolutionary invention, the tiered publishing system, initially addressing specific communities of scholars, and gradually climbing up to broader public understanding, thus serving the interests of the lay society, too.

Dedication to Quality

Each Frontiers article is a landmark of the highest quality, thanks to genuinely collaborative interactions between authors and review editors, who include some of the world's best academicians. Research must be certified by peers before entering a stream of knowledge that may eventually reach the public - and shape society; therefore, Frontiers only applies the most rigorous and unbiased reviews.
Frontiers revolutionizes research publishing by freely delivering the most outstanding research, evaluated with no bias from both the academic and social point of view. By applying the most advanced information technologies, Frontiers is catapulting scholarly publishing into a new generation.

What are Frontiers Research Topics?

Frontiers Research Topics are very popular trademarks of the Frontiers Journals Series: they are collections of at least ten articles, all centered on a particular subject. With their unique mix of varied contributions from Original Research to Review Articles, Frontiers Research Topics unify the most influential researchers, the latest key findings and historical advances in a hot research area! Find out more on how to host your own Frontiers Research Topic or contribute to one as an author by contacting the Frontiers Editorial Office: researchtopics@frontiersin.org

BALANCING ACT: STRUCTURAL-FUNCTIONAL CIRCUIT DISRUPTIONS AND COMPENSATIONS IN DEVELOPING AND AGING BRAIN DISORDERS

Topic Editors:
Lijun Bai, Xi'an Jiaotong University, China
Tuo Zhang, Northwestern Polytechnical University, China
Xi-Nian Zuo, Institute of Psychology, Chinese Academy of Sciences, China
Mingzhou Ding, University of Florida, United States

Citation: Bai, L., Zhang, T., Zuo, X.-N., Ding, M., eds. (2020). Balancing Act: Structural-Functional Circuit Disruptions and Compensations in Developing and Aging Brain Disorders. Lausanne: Frontiers Media SA.
doi: 10.3389/978-2-88963-486-6

Table of Contents

frontiers in Neural Circuits

EDITORIAL
published: 15 January 2020
doi: 10.3389/fncir.2019.00083

Editorial: Balancing Act: Structural-Functional Circuit Disruptions and Compensations in Developing and Aging Brain Disorders

Lijun Bai[1]*, *Tuo Zhang*[2], *Xi-Nian Zuo*[3,4] and *Mingzhou Ding*[5]

[1] The Key Laboratory of Biomedical Information Engineering, Ministry of Education, Department of Biomedical Engineering, School of Life Science and Technology, Xi'an Jiaotong University, Xi'an, China, [2] School of Automation, Northwestern Polytechnical University, Xi'an, China, [3] Key Laboratory of Brain and Education, Nanning Normal University, Nanning, China, [4] Department of Psychology, University of Chinese Academy of Sciences, Beijing, China, [5] J. Crayton Pruitt Family Department of Biomedical Engineering, University of Florida, Gainesville, FL, United States

Keywords: neural circuits, neurobiology, neuroscience, developing and aging brain disorders, structural and functional brain connectivity

Editorial on the Research Topic

Balancing Act: Structural-Functional Circuit Disruptions and Compensations in Developing and Aging Brain Disorders

The last decade has witnessed an increasing interest in exploring the network connectivity of brain areas and communities. The disruption of brain networks has been linked to variable levels of neuropsychological dysfunctions observed in individual patients with brain disorders (Collin and van den Heuvel, 2013; Crossley et al., 2014). Understanding the course of these changes may help understand how they contribute to risk and resilience for both developing and aging brain disorders, and may offer personalized treatment opportunities. The balancing act of disruptions and compensations in large-scale structural-functional brain network organization across individuals in various brain disorders is still unclear (Bullmore and Sporns, 2009).

The transformative brain changes occurring during the course of childhood and adolescence are critical for the shaping of individual developmental trajectories in cognitive and social functions, adaptability, personality, and mental health (Dosenbach et al., 2010). The tremendous potential for neuroplasticity and environmental sensitivity also characterized this period of development and individualized the brain functional connectome during the course of adolescence and related patterns of maturation (Zielinski et al., 2010; Fair et al., 2012). The progress made on both neuroscience and computational sciences has motivated new approaches for studying brain structure and function from a complex systems perspective (Hagmann et al., 2008; Sharp et al., 2014). These current trends have suggested that connectivity-based methods may provide good tools in order to understand brain functioning in healthy subjects, as well as to study changes during lifespan, or during the time course of neurodegenerative diseases.

Brain connectivity refers to patterns of links connecting distinct units within the nervous system. It can be studied at different scales, and therefore, units or nodes can be defined as individual neurons, neural populations, or segregated brain regions, described by anatomical or

OPEN ACCESS

Edited and reviewed by:
Edward S. Ruthazer, McGill University, Canada

***Correspondence:**
Lijun Bai
bailijun@xjtu.edu.cn

Received: *12 November 2019*
Accepted: *19 December 2019*
Published: *15 January 2020*

Citation:
Bai L, Zhang T, Zuo X-N and Ding M (2020) Editorial: Balancing Act: Structural-Functional Circuit Disruptions and Compensations in Developing and Aging Brain Disorders. Front. Neural Circuits 13:83. doi: 10.3389/fncir.2019.00083

functional landmarks. Structural connectivity networks can be measured through white matter tracts quantified by diffusion tractography or correlations of morphological metrics; it can provide clue into structural architectural features. By contrast, functional connectivity networks mainly describe the connective properties of temporal coherences between blood oxygen level-dependent functional MRI signals from both local and distant brain regions; thus functional connectivity networks provide insight of a network perspective on brain dynamics. This Research Topic "Balancing act: structural-functional circuit disruptions and compensations in developing and aging brain disorders" brings together basic, clinical, and translational neuroscience research with brain circuit disruptions and compensations in developing and aging Brain Disorders. The discussions in this Research Topic report new integrated knowledge to understand developing and aging brain disorders.

Neurovascular imbalance is generally noted in the aging population and Alzheimer's disease (AD). It has been shown that regional cerebral blood flow (rCBF) is closely coupled with cerebral metabolism, and the relationship between network measures and rCBF provides insights into the mechanisms of connectivity disruptions in brain disorders. Hu et al. discussed the coupling of rCBF and functional connectivity strength (FCS) in Wilson's disease (WD) associated with mild cognitive impairments (MCI). They found that the CBF-FCS correlations of patients with WD were significantly decreased in the basal ganglia and the cerebellum and slightly increased in the prefrontal cortex and thalamus. Qi et al. evaluated the pattern of activity in the cerebral limbic network from the perspective of the cerebellum. Results indicated that the cerebellum was not compromised by Alzheimer pathology in the early stages of AD, and this pattern indicates that the sub-scale ventral attention network may play a pivotal role in functional compensation through the coupled cerebro-cerebellar limbic network in MCI, and the cerebellum may be a key node in the modulation of social cognition. Moreover, patients with cerebral vascular diseases exhibit widespread differences in functional connectivity across multiple cortical networks. Leukoaraiosis (LA) is associated with cognitive impairment in older people and associated with dysfunctional communications between the three basic brain networks, consisting of the default-mode network (DMN), salience networks (SNs), and the central executive network (CEN). Chen et al. presented the diminished negative correlations between the SN and DMN while positive correlation between the SN and CEN were enhanced as the cognitive impairment loads increased in patients with LA.

Traumatic brain injury (TBI) is a substantial public health problem, and can accelerate the aging process, leading to long-term structural and functional alterations to the brain. Wang et al. aimed to investigate the sex difference on whole-brain functional connectivity at the network level from a cohort of acute mild TBI patients since there were differential cognitive outcome by sex. Ye et al. investigated the changes of α-synuclein in blood serum and its relationship with default mode network (DMN) connectivity after acute mild TBI. The chronic consequences of TBI may contribute to the increased risk for early cognitive decline and dementia, primarily due to diffusion axonal injury. Yin et al. investigated longitudinal changes of white matter (WM) using diffusion tensor imaging (DTI) and their correlations with neuropsychological tests following mild TBI. They reported that increased fractional anisotropy values in some tracts at 1 month post-injury were positively associated with better performance on cognitive information processing speed at initial assessment.

Synaptic failure may critically impair information processing in the brain and may underlie many neurodegenerative diseases. Budak and Zochowski systematically analyzed how two types of synaptic failure (activity-independent and targeted, activity-dependent) affect two complementary (incoming and outgoing) scale-free network structures. Williams and Sun explored the layer and spectrotemporal architecture and laminar distribution of high-frequency oscillations (HFOs) in a neonatal freeze lesion model of focal cortical dysplasia (FCD). They provided the evidence that HFOs, particularly fast ripples, is a biomarker to help define the cortical seizure zone and understand cellular level changes underlying the HFOs. Infarction or aging in regions project to the pyramidal tract (PyT) would result in incomplete transmission of information to the PyT and concomitant decreases in motor planning and coordination abilities. Using the large population data of the HCP and high magnet gradient HARDI data, Wang et al. visualized the existence of the PyT in humans.

Cognitive aging research has identified several general patterns of compensatory neural activity. Most studies of neural compensation limited to a between-subject design, Samuel et al. examined the neural compensation from a fatigue paradigm and reflect neural activities typically associated with aging-related cognitive impairment. In the young cohort, they found that both behavioral performance and neural activity declined as the experiment progressed, reflecting the deleterious effects of cognitive fatigue. Both behavioral performance and neural activity did not decline as the experiment progressed in the older cohort, in contrast to the young. Pelzer et al. reviewed the literature regarding quantitative susceptibility mapping (QSM), MEG, and rs-fMRI detected changes in motor and non-motor symptoms in Parkinson's disease (PD).

Finally, the morphological features of gyri and sulci change during aging and development-related psychiatric disorders such as schizophrenia, reflecting a potential of gyral-sulcal indices as a biomarker for developmental and aging related disorders. Fluid intelligence, as a measure of higher-order relational reasoning, has been argued to be linked to specific functional outcomes and to variations in human neuronal structure and function. Yang et al. explored the temporal variability of cortical gyral-sulcal resting state functional activity and its association with fluid intelligence measures on the Human Connectome Project dataset, which provided novel insights to understand the functional relevance of gyri and sulci. Social anxiety and risk of mental disorders have increased in

the left-behind children (LBC). Fu et al. provided empirical evidence of altered brain structure in LBC compared to non-LBC, responsible for emotion regulation and processing, which may account for mental disorders and negative life outcome of LBC.

AUTHOR CONTRIBUTIONS

LB and TZ drafted the work and revised it critically for important intellectual content. All of the authors provide approval for publication of the content, agree to be accountable for all aspects of the work in ensuring that questions related to the accuracy or integrity of any part of the work are appropriately investigated and resolved, and made substantial contributions to the conception and design of the work.

FUNDING

This research was supported by the National Natural Science Foundation of China (Grant Numbers 81571752, 81771914), the Beijing Municipal Science and Tech Commission (Z161100002616023, Z171100000117012), the China - Netherlands CAS-NWO Programme (153111KYSB20160020), the National R&D Infrastructure and Facility Development Program of China, Fundamental Science Data Sharing Platform (DKA2017-12-02-21), and Guangxi BaGui Scholarship (201621).

REFERENCES

Bullmore, E., and Sporns, O. (2009). Complex brain networks: graph theoretical analysis of structural and functional systems. *Nat. Rev. Neurosci.* 10, 186–198. doi: 10.1038/nrn2575

Collin, G., and van den Heuvel, M. P. (2013). The ontogeny of the human connectome: development and dynamic changes of brain connectivity across the life span. *Neuroscientist* 19, 616–628. doi: 10.1177/1073858413503712

Crossley, N. A., Mechelli, A., Scott, J., Carletti, F., Fox, P. T., McGuire, P., et al. (2014). The hubs of the human connectome are generally implicated in the anatomy of brain disorders. *Brain* 137, 2382–2395. doi: 10.1093/brain/awu132

Dosenbach, N. U. F., Nardos, B., Cohen, A. L., Fair, D. A., Church, J. A., Nelson, S. M., et al. (2010). Prediction of individual brain maturity using fMRI. *Science* 329, 1358–1361. doi: 10.1126/science.1194144

Fair, D. A., Bathula, D., Nikolas, M. A., and Nigg, J. T. (2012). Distinct neuropsychological subgroups in typically developing youth inform heterogeneity in children with ADHD. *Proc. Natl. Acad. Sci. U.S.A.* 109, 6769–6774. doi: 10.1073/pnas.1115365109

Hagmann, P., Cammoun, L., Gigandet, X., Meuli, R., Honey, C. J., Wedeen, V. J., et al. (2008). Mapping the structural core of human cerebral cortex. *PLoS Biol.* 6,1479–1493. doi: 10.1371/journal.pbio.0060159

Sharp, D. J., Scott, G., and Leech, R. (2014). Network dysfunction after traumatic brain injury. *Nat. Rev. Neurol.* 10, 156–166. doi: 10.1038/nrneurol.2014.15

Zielinski, B. A., Gennatas, E. D., Zhou, J., and Seeley, W. W. (2010).Network-level structural covariance in the developing brain. *Proc. Natl. Acad. Sci. U.S.A.* 107, 18191–18196. doi: 10.1073/pnas.1003109107

Conflict of Interest: The authors declare that the research was conducted in the absence of any commercial or financial relationships that could be construed as a potential conflict of interest.

frontiers in Neural Circuits

ORIGINAL RESEARCH
published: 29 November 2018
doi: 10.3389/fncir.2018.00107

Sex Differences in Abnormal Intrinsic Functional Connectivity After Acute Mild Traumatic Brain Injury

Shan Wang[1†], Liuxun Hu[2†], Jieli Cao[1], Wenmin Huang[1], Chuanzhu Sun[1], Dongdong Zheng[2], Zhuonan Wang[3], Shuoqiu Gan[1,3], Xuan Niu[3], Chenghui Gu[2], Guanghui Bai[4], Limei Ye[4], Danbin Zhang[4], Nu Zhang[2], Bo Yin[2], Ming Zhang[3]* and Lijun Bai[1]**

[1]The Key Laboratory of Biomedical Information Engineering, Ministry of Education, Department of Biomedical Engineering, School of Life Science and Technology, Xi'an Jiaotong University, Xi'an, China, [2]Department of Neurosurgery, The Second Affiliated Hospital and Yuying Children's Hospital of Wenzhou Medical University, Wenzhou, China, [3]Department of Medical Imaging, The First Affiliated Hospital of Xi'an Jiaotong University, Xi'an, China, [4]Department of Radiology, The Second Affiliated Hospital and Yuying Children's Hospital of Wenzhou Medical University, Wenzhou, China

Mild traumatic brain injury (TBI) is considered to induce abnormal intrinsic functional connectivity within resting-state networks (RSNs). The objective of this study was to estimate the role of sex in intrinsic functional connectivity after acute mild TBI. We recruited a cohort of 54 patients (27 males and 27 females with mild TBI within 7 days post-injury) from the emergency department (ED) and 34 age-, education-matched healthy controls (HCs; 17 males and 17 females). On the clinical scales, there were no statistically significant differences between males and females in either control group or mild TBI group. To detect whether there was abnormal sex difference on functional connectivity in RSNs, we performed independent component analysis (ICA) and a dual regression approach to investigate the between-subject voxel-wise comparisons of functional connectivity within seven selected RSNs. Compared to female patients, male patients showed increased intrinsic functional connectivity in motor network, ventral stream network, executive function network, cerebellum network and decreased connectivity in visual network. Further analysis demonstrated a positive correlation between the functional connectivity in executive function network and insomnia severity index (ISI) scores in male patients ($r = 0.515$, $P = 0.006$). The abnormality of the functional connectivity of RSNs in acute mild TBI showed the possibility of brain recombination after trauma, mainly concerning male-specific.

Keywords: mild traumatic brain injury, sex difference, rs-fMRI, functional connectivity, independent component analysis

OPEN ACCESS

Edited by:
Tuo Zhang,
Northwestern Polytechnical University, China

Reviewed by:
Jie Lu,
Xuanwu Hospital, Capital Medical University, China
Zhenyu Liu,
Institute of Automation (CAS), China

****Correspondence:***
Bo Yin
76yinbo@163.com
Ming Zhang
zhangming01@mail.xjtu.edu.cn
Lijun Bai
bailijun@xjtu.edu.cn

[†]These authors have contributed equally to this work

Received: *26 September 2018*
Accepted: *13 November 2018*
Published: *29 November 2018*

Citation:
Wang S, Hu L, Cao J, Huang W, Sun C, Zheng D, Wang Z, Gan S, Niu X, Gu C, Bai G, Ye L, Zhang D, Zhang N, Yin B, Zhang M and Bai L (2018) Sex Differences in Abnormal Intrinsic Functional Connectivity After Acute Mild Traumatic Brain Injury. Front. Neural Circuits 12:107. doi: 10.3389/fncir.2018.00107

INTRODUCTION

Traumatic brain injury (TBI) is a substantial public health problem, and can accelerate the ageing process, leading to long-term structural and functional alterations to the brain (Benedictus et al., 2010; Cole et al., 2015). About 90% of TBI is classified as mild (Vos et al., 2002). It is worthy of attentions that one-quarter of mild TBI patients have post-concussive symptoms or other cognitive disorders (Bazarian et al., 2010). However, the heterogeneity of the injuries and the variability of cognitive symptoms make it problematic for management (Jenkins et al., 2016). Several factors are

associated with poor outcomes after mild TBI, of which, the most controversial is sex (Bazarian et al., 2010). In female group, sex steroids have been tested to demonstrate neuroprotective effects in severe TBI (Fakhran et al., 2014). Nevertheless, the effect of sex on outcome is still unclear after mild TBI. Understanding sex differences of brain injury mechanism after mild TBI may enhance the future diagnostic work-up in patients and lead to separate management strategies for patients with different sexes.

Previous studies about sex differences in cognitive outcome after mild TBI revealed controversial and interesting results. Controlled animal experiments have shown better cognitive outcomes among females after mild TBI (Bramlett and Dietrich, 2001; O'Connor et al., 2003; Bazarian et al., 2010). Evidence from a human study also finds that women have superior executive functioning when compared with men after acute TBI (Niemeier et al., 2014). Other studies show that women outperform men in the tasks of verbal memory and learning measures following TBI (Farace and Alves, 2000; Covassin et al., 2012). These results indicate that female sex is somehow neuroprotective. While, multiple observational studies in humans have demonstrated that females present worse outcomes following concussion compared with males (Broshek et al., 2005; Bay et al., 2009; Covassin et al., 2013; Hsu et al., 2015; Cancelliere et al., 2016). Specifically, females report more post-concussive symptoms with greater severity compared to males (Broshek et al., 2005; Bay et al., 2009; Covassin et al., 2012). Indeed, these observation studies may be confounded by many factors, especially by sociological pressures on male athletes, including the greater societal stigma with symptom reporting, resulting in underreporting by males (Fakhran et al., 2014). Therefore, more objective measurements, such as neuroimaging indices, are crucial in avoiding such bias.

The evaluation of resting-state functional connectivity is an appealing approach to assess activity differences among sexes (Filippi et al., 2013). A recent research has revealed that global connectivity was stronger in female network than in males with posttraumatic stress disorder (PTSD; Cao et al., 2018). However, resting-state fMRI studies in mild TBI focus on connectivity mainly in a limited number of predefined regions-of-interest (ROIs), not fully exploring large-scale brain functional connectivity (Mayer et al., 2011; Slobounov et al., 2011; Shumskaya et al., 2012). Though substantial evidence supports models of TBI as a condition characterized by altered brain connectivity, sex-related differences in functional connectivity are still less clear. Understanding the effects of sex difference after mild TBI on brain function and behavior is likely to require a widespread investigation on brain network connectivity. Indeed, several studies have characterized the resting-state networks (RSNs) using independent component analysis (ICA; Damoiseaux et al., 2006; De Luca et al., 2006). As declared by a study performed on a very large sample of healthy participants, these networks have a high reproducibility (Biswal et al., 2010). The assessment of RSNs allows us to evaluate the intrinsic functional connectome of the human brain among sexes (Filippi et al., 2013).

Most studies investigating functional connectivity have involved patients with moderate-to-severe TBI, or during the chronic stage of recovery (Caeyenberghs et al., 2012, 2013, 2014; Shumskaya et al., 2012). Importantly, reliable and valid indices of acute injury, which can elucidate underlying neuroanatomical injury mechanisms or be predictive for longer-term outcomes, are lacking in studies of mild TBI (Yuan et al., 2015). Thus, in the current study, we aimed to investigate the sex differences on whole-brain functional connectivity at the network level from a cohort of acute mild TBI patients, not biased by *a priori* region selection.

MATERIALS AND METHODS

Participants

A total of 61 patients with acute mild TBI within 7 days post-injury were recruited from the emergency department (ED) of a local hospital, between August 2016 and July 2017. All consecutively patients with non-contrast head CT due to acute head trauma enrolling from the local ED formed the initial population. Inclusion criteria for all mild TBI patient were based on the World Health Organization's Collaborating Centre for Neurotrauma Task Force (Holm et al., 2005): (i) Glasgow Coma Scale (GCS) score of 13–15 on presentation to the ED; (ii) one or more/any of the following: loss of consciousness (LOC) for less than 30 min, posttraumatic amnesia (PTA) for 24 or less hours, and/or other transient neurological abnormalities such as focal signs, seizure, and intracranial lesion not requiring surgery; and (iii) were aged 18 years or older. Mild TBI patients were excluded for: (i) a history of a previous brain injury, neurological disease, long-standing psychiatric condition, or concurrent substance or alcohol abuse; (ii) a structural abnormality on neuroimaging (CT and MRI); (iii) intubation and/or presence of a skull fracture and administration of sedatives; (iv) the manifestation of mild TBI due to medications by other injuries (e.g., systemic injuries, facial injuries, or spinal cord injury); (v) other problems (e.g., psychological trauma, language barrier, or coexisting medical conditions); and (vi) caused by penetrating craniocerebral injury. Among these patients, seven were excluded, five of whom had MRI contraindications, and two were left handedness. At last, 54 patients (27 males) were enrolled. In addition, 34 sex-, age- and education-matched healthy controls (HCs; 17 males) without neurologic impairment or psychiatric disorders participated in the study. All participants were right-handed according to the Edinburgh Handedness Inventory. All the subjects gave written, informed consent in person approved by a local institutional review board; the research procedures were approved by the Ethical Committee of The Second Affiliated Hospital of Wenzhou Medical University and conducted in accordance with the Declaration of Helsinki.

Clinical Assessment

Clinical assessments were performed within 48 h of MR imaging for all the participants. Neuropsychological tests included: (a) WAIS-III Digit Symbol Coding (DSC) to examine motor skill and memory; (b) Verbal Fluency Test to evaluate verbal

fluency including language ability, executive function and semantic memory (Troyer et al., 1997; Kreiner and Ryan, 2001). Self-assessment symptom questionnaires included: the Rivermead Post-Concussion Symptom Questionnaire (RPCS), Insomnia Severity Index (ISI; King et al., 1995; Bastien et al., 2001).

Image Acquisition

A non-contrast CT scan was performed on all consecutive patients following acute head injury with a 64-row CT scanner (GE, Lightspeed VCT). The MRI scans were acquired with the use of 3.0 T MRI scanner (GE 750). A custom-built head holder was used to prevent head movements. All participants were instructed to remain in a relaxed state without engaging in cognitive or motor activity and to keep their eyes closed. Alertness during the scan was confirmed immediately afterward. The MRI protocol involved the high-resolution T1-weighted 3D MPRAGE sequence (echo time (TE) = 3.17 ms, repetition time (TR) = 8.15 ms, flip angle = 9°, slice thickness = 1 mm, field of view (FOV) = 256 mm × 256 mm, matrix size = 256 × 256), single-shot, gradient-recalled echo planar imaging (EPI) sequence with 54 slices covering the whole brain (TR = 2,000 ms, TE = 30 ms, slice thickness = 3 mm, flip angle = 90°, FOV = 216 mm × 216 mm, matrix size = 64 × 64, voxel size = 3 mm × 3 mm × 3 mm), axial FLAIR (TR = 9,000 ms, TE = 95 ms, flip angle = 150°, thickness = 5 mm, slices = 20, FOV = 240 mm × 240 mm, matrix size = 173 × 256), axial susceptibility weighted imaging (SWI; TR = 37.8 ms, TE = 25 ms, flip angle = 15°, thickness = 2 mm, slices = 70, FOV = 230 mm × 230 mm, matrix size = 512 × 512), axial FLAIR (TR = 9,000 ms, TE = 95 ms, flip angle = 150°, thickness = 5 mm, slices = 20, FOV = 240 mm × 240 mm, matrix size = 173 × 256).

The presence of focal lesions and cerebral microbleeds was determined by an experienced clinical neuroradiologists (with 10 years' experience) who assessed multiple modalities of neuroimaging data acquired at baseline (T1-weighted, SWI, FLAIR) for all subjects in random sequence, blind to clinical information and group membership (patient or control).

Preprocessing of Resting State Data

Image preprocessing was accomplished using the FSL software package (Smith et al., 2004). First, the first 10 volumes of resting-state data were removed to allow for steady state equilibrium. Data preprocessing included the slice-timing, head-motion correction, normalization, spatially smoothing with a 6-mm full width at half maximum, linear trend removal, and band-pass filtering (0.01–0.08 Hz). Motion correction was performed by realigning fMRI time-series using a six-parameter rigid-body spatial transformation (Friston et al., 1995). In the normalization step, all BOLD data were aligned to their corresponding T1-weighted images, and normalized BOLD images were created by applying the transformation of T1-weigthed images to the ICBM152 template. Spurious variances (head motion, ventricular and white matter signal and the derivatives of each of these signals) were removed by multiple linear regression analysis.

Data analysis was performed using the FMRIB Software Library (FSL; FMRIB Software Library). Head motion in the resting state data was corrected using multi-resolution rigid body co-registration of volumes, as implemented in the MCFLIRT software (Jenkinson et al., 2002). Brain extraction was carried out in the BET software for motion-corrected BOLD volumes with optimization of the deforming smooth surface model, as implemented (Smith, 2002). Rigid body registration as implemented in the FLIRT software was used to co-register fMRI volumes to 3D MPRAGE (brain-extracted) volumes of the corresponding subjects and subsequently the 3D MPRAGE volumes to the MNI152 standard space (Jenkinson et al., 2002). The images were smoothed with a 6-mm full width at half-maximum (FWHM) Gaussian kernel.

Resting State Networks

Following the preprocessing, Multivariate Exploratory Linear Optimized Decomposition into Independent Components (MELODIC) tool within FSL was used to perform spatial group-ICA using multisession temporal concatenation. Datasets were temporally concatenated across all participants to create a single 4-dimensional dataset as input for MELODIC, to produce 25 independent component maps (IC maps) representing average resting state brain networks (RSNs).

The intrinsic functional connectivity was the connectivity among various regions within a RSN (Kumar et al., 2018). A dual regression approach was used to perform the between-subject analysis by voxel-wise comparisons of resting functional connectivity (Jenkinson et al., 2002; Nichols and Holmes, 2002; Beckmann and Smith, 2005; Cole et al., 2010; Kumar et al., 2018). We accomplished this procedure as follow. First, we used all group ICA spatial maps as spatial regressors against the preprocessed individual subject's fMRI data, which produced subject-specific time courses for each group ICA component. Then, these time courses were variance-normalized and linearly regressed for the subject's fMRI dataset. Individual spatial maps of each group ICA component were provided by the regression. Finally, we merged these individual spatial maps across subjects into single 4-dimensional files per ICA component. The voxel-wise group differences in intrinsic network functional connectivity between male and female patients were carried out using nonparametric permutation testing (5,000 permutations per contrast for each ICA component) in FSL (Kumar et al., 2018). Threshold-free cluster enhancement (TFCE) was used to control the multiple comparisons. The significance threshold was set to $P < 0.05$, Family-Wise Error (FWE) corrected. The results represented the group differences in functional connectivity for all RSNs.

Region of Interest Analysis

Region-of-Interest (ROI) analysis was then applied based on the regions showing significant differences on functional connectivity between male and female patients. Such analysis would provide us the ability to determine the size and location of the clusters, which showed significant differences between male and female patients. A single ROI mask was created according to the location and size of clusters in the specific RSN. Strengths of

functional connectivity of patients and HCs, were then extracted in an automated fashion by using the ROI mask along the individual spatial maps.

Additional Statistical Analysis

Statistical analyses were performed in SPSS 20.0. For each continuous variable, the normal distribution was measured by the Shapiro-Wilk test. The independent two-sample *t*-test and the Mann-Whitney test were used to compare group differences based on data normality, respectively. A Kruskal-Wallis test was conducted to assess the differences in age, education level and neuropsychologic test results in four groups (i.e., control male, control female, mild TBI male and mild TBI female). Chi-square analyses were applied to assess categorical variables. ROI-analysis among four groups were subjected to the univariate analysis of variance (ANOVA). Correlation analysis was also conducted between functional connectivity and clinical symptoms by using Pearson correlation coefficients.

RESULTS

Participant Characteristics

During the study, we employed 54 patients with mild TBI, all of which were recruited from the ED of the local Level-1 emergency center. None of patients were with visible contusion lesions using conventional neuroimaging techniques and exhibited cerebral microbleeds on SWI. Thirty-four (17 males) control subjects were included. No significant difference was seen between the HCs and patients with mild TBI in regard to age, sex and education level ($P > 0.1$).

For all the patients, no significant contusion or cerebral hemorrhage was found. The major mechanism of trauma was a motor vehicle collision injury [13 of 27 male patients (48.2%), 15 of 27 female patients (55.6%)], followed by assault [9 of 27 male patients (33.3%), 7 of 27 female patients (25.9%)], and fall was the last [5 of 27 male patients (18.5%), 5 of 27 female patients (18.5%)]. No significant differences in age and education level were found between male and female patients with mild TBI ($P > 0.05$).

Both female and male patients with mild TBI displayed deficits on all of the clinical assessments compared with their control counterparts. For both the male and female subjects, there were significant differences between patients and controls in the Rivermead Post-Concussion Symptom Questionnaire ($P < 0.001$), WAIS-III DSC score ($P < 0.05$), Verbal Fluency Test ($P < 0.05$), ISI ($P < 0.001$; **Table 1**). No significant sex differences were found for all assessments, neither in mild TBI nor HC groups (**Table 2**).

Resting-State Networks

Twenty-five components were computed in the entire subject group by the ICA. Based on visual inspection of the spatial map (biologic plausibility and comparability with previously reported RSNs), we sorted the components into functionally relevant RSNs and artifactual components related to physiologic/scanner noise and head motion. Seven components closely coincided

TABLE 1 | Demographic and behavioral statistics for male and female participants.

	Male participants			Female participants		
Characteristic	**Mild TBI group (*n* = 27)**	**Control group (*n* = 17)**	***P* value (Cohen's *d*)**	**Mild TBI group (*n* = 27)**	**Control group (*n* = 17)**	***P* value (Cohen's *d*)**
Demographic						
Age (years)	35.4 ± 9.7 (19–54)	32.8 ± 10.1 (22–53)	0.394 (0.272)	35.6 ± 9.4 (21–54)	33.1 ± 10.7 (20–54)	0.421 (0.254)
Education (years)	9.4 ± 3.5 (3–15)	10.7 ± 5.1 (1–17)	0.322 (−0.305)	9.5 ± 4.3 (0–16)	11.1 ± 4.8 (0–17)	0.270 (−0.351)
Clinical assessments						
RPCS	8.4 ± 5.8 (1–23)	1.3 ± 1.8 (0–7)	< 0.001 (1.669)	11.4 ± 6.4 (3–25)	2.4 ± 2.5 (0–9)	< 0.001 (1.915)
DSC	34.7 ± 13.7 (14–60)	50.7 ± 15.4 (14–60)	0.001 (−1.130)	36.7 ± 14.1 (9–60)	48.8 ± 15.7 (16–60)	0.011 (−0.833)
VF	17.1 ± 4.8 (9–27)	20.8 ± 6.7 (9–32)	0.042 (−0.641)	15.6 ± 4.8 (9–26)	19.1 ± 6.3 (8–31)	0.043 (−0.642)
ISI	5.9 ± 4.5 (0–17)	1.2 ± 2.6 (0–11)	< 0.001 (1.307)	8.8 ± 7.1 (1–24)	1.8 ± 2.2 (0–8)	< 0.001 (1.357)

Notes: DSC, WAIS-III Digit Symbol Coding score; VF, Verbal Fluency Test; RPCS, the Rivermead Post-Concussion Symptom Questionnaire; ISI, Insomnia Severity Index; In 2nd, 3rd, 5th, 6th column, numbers in parentheses are ranges. In 4th, 7th column, numbers in parentheses are for the Cohen's d effect size. P < 0.05 was considered statistically significant in all the tests.

TABLE 2 | Demographic and behavioral statistics for patients and control subjects.

	Patients with mild TBI			Control subjects		
Characteristic	**Male (*n* = 27)**	**Female (*n* = 27)**	***P* value (Cohen's *d*)**	**Male (*n* = 27)**	**Female (*n* = 27)**	***P* value (Cohen's *d*)**
Demographic						
Age (years)	35.4 ± 9.7 (19–54)	35.6 ± 9.4 (21–54)	0.996 (−0.012)	32.8 ± 10.1 (22–53)	33.1 ± 10.7 (20–54)	0.948 (−0.023)
Education (years)	9.4 ± 3.5 (3–15)	9.5 ± 4.3 (0–16)	0.945 (−0.019)	10.7 ± 5.1 (1–17)	11.1 ± 4.8 (0–17)	0.837 (−0.073)
Clinical assessments						
RPCS	8.4 ± 5.8 (1–23)	11.4 ± 6.4 (3–25)	0.073 (−0.507)	1.3 ± 1.8 (0–7)	2.4 ± 2.5 (0–9)	0.166 (− 0.502)
DSC	34.7 ± 13.7 (14–60)	36.7 ± 14.1 (9–60)	0.593 (−0.149)	50.7 ± 15.4 (14–60)	48.8 ± 15.7 (16–60)	0.726 (0.125)
VF	17.1 ± 4.8 (9–27)	15.6 ± 4.8 (9–26)	0.242 (0.328)	20.8 ± 6.7 (9–32)	19.1 ± 6.3 (8–31)	0.450 (0.270)
ISI	5.9 ± 4.5 (0–17)	8.8 ± 7.1 (1–24)	0.072 (−0.509)	1.2 ± 2.6 (0–11)	1.8 ± 2.2 (0–8)	0.441 (−0.276)

Notes: DSC, WAIS-III Digit Symbol Coding score; VF, Verbal Fluency Test; RPCS, the Rivermead Post-Concussion Symptom Questionnaire; ISI, Insomnia Severity Index; In 2nd, 3rd, 5th, 6th column, numbers in parentheses are ranges. In 4th, 7th column, numbers in parentheses are for the Cohen's d effect size. P < 0.05 was considered statistically significant in all the tests.

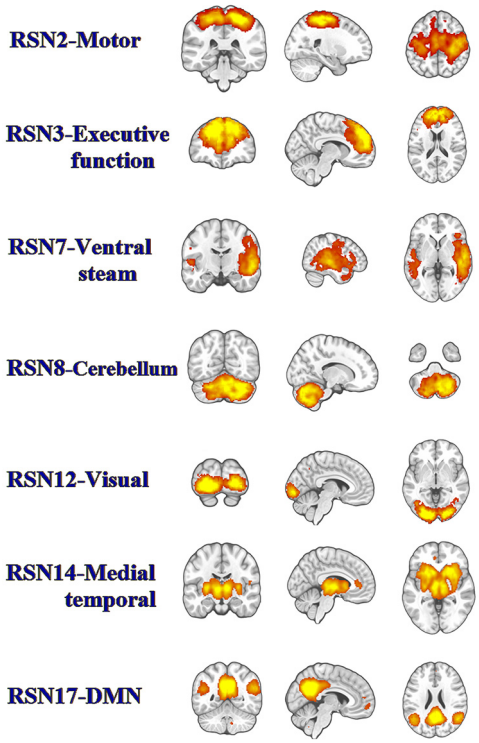

FIGURE 1 | The panel represents functionally relevant resting-state networks (RSNs) from the group independent component analysis (ICA) analysis of temporally concatenated datasets from both patients with mild traumatic brain injury (TBI) and control subjects. The left side of the brain corresponds to the left side in the image.

with prior reports (**Figure 1**; Shumskaya et al., 2012). RSN 2 corresponded to the motor network. The visual processing network was represented in the RSN 12. We also found two RSNs involved in high-order cognitive functions: the executive function network (RSN 3) and default mode network (RSN 17). RNS14 was medial temporal which located in the temporal lobe. RNS7 corresponded to the ventral stream. We identified another component that was rarely reported or examined thoroughly, namely the cerebellum (RSN 8).

Five RSNs showed significant voxel-wise differences in the spatial maps between male and female patients ($P < 0.05$, FWE corrected, **Figures 2**, **3**). Compared with females, male patients showed increased intrinsic functional connectivity within the motor network (RSN 2), executive function network (RSN 3), ventral stream network (RSN 7), and cerebellum (RSN 8). By contrast, male patients performed lower connectivity than female patients in the visual network (RSN 12).

ROI Data Analysis

Within these between-sex difference networks in patients, results of ANOVA demonstrated that intrinsic functional connectivity were significant different in clusters within the motor network ($P = 0.012$, $F_{(3,84)} = 3.91$), executive functional network ($P = 0.011$, $F_{(3,84)} = 3.96$), ventral stream network ($P = 0.004$, $F_{(3,84)} = 4.77$), cerebellum ($P = 0.003$, $F_{(3,84)} = 5.02$) and visual

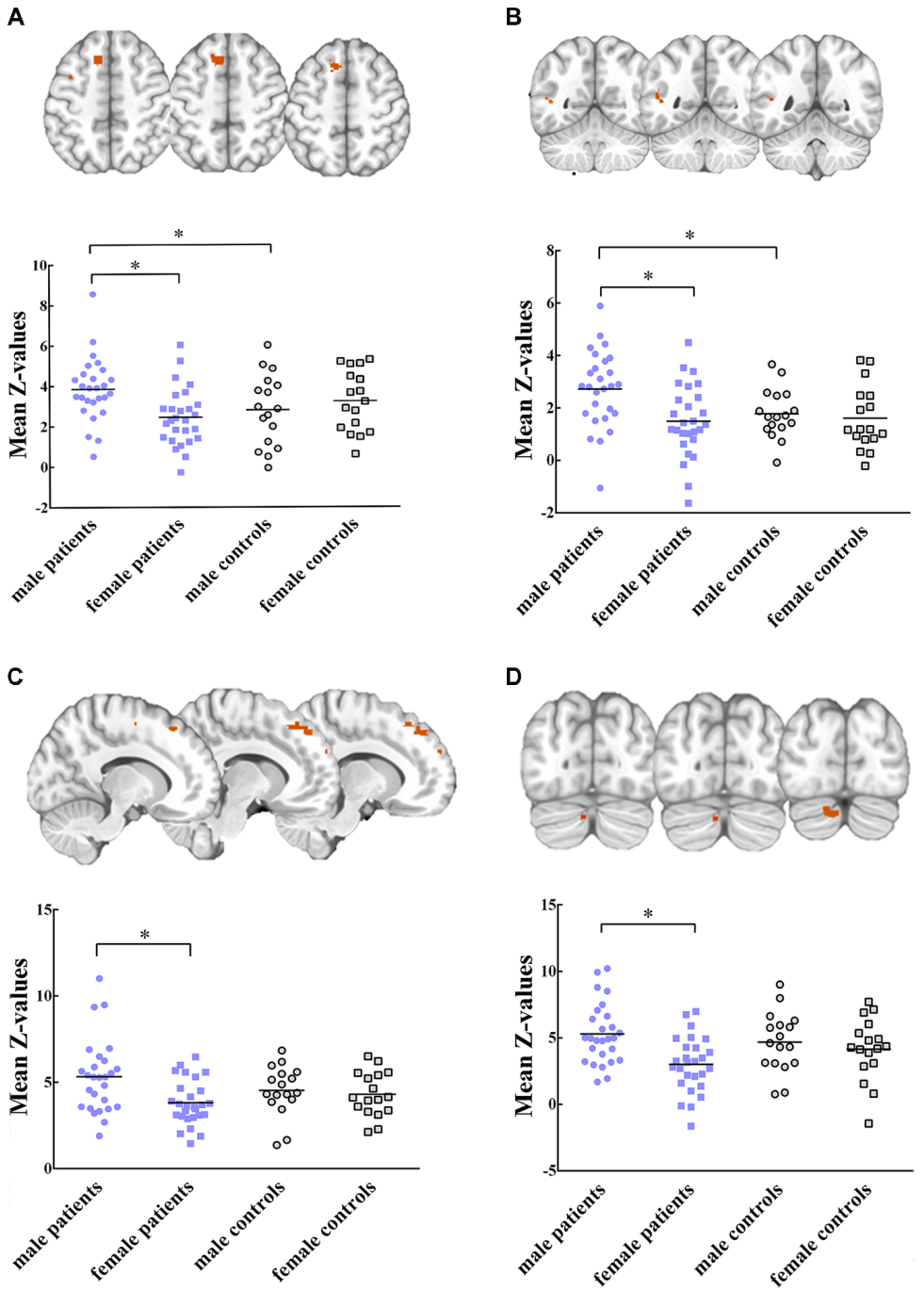

FIGURE 2 | Intrinsic functional connectivity differences between male and female patients within **(A)** motor network, **(B)** ventral stream network, **(C)** executive function network **(D)** cerebellum are showed increased connectivity in male patients. Maps were thresholded at $P < 0.05$ (family wise error (FWE) corrected). The left side of the brain corresponds to the left side in the image. Scatterplots are displayed for regions-of-interest (ROI)-analysis among groups. Significant effects are denoted with asterisks between two groups, under *post hoc* restricted least significant difference (LSD) tests.

network ($P = 0.004$, $F_{(3,84)} = 4.88$) among groups. *Post hoc* restricted least significant difference (LSD) tests of ANOVA further revealed that male patients had significant increased connectivity than male controls in the motor (RSN 2, $P = 0.033$) and ventral stream networks (RSN 7, $P = 0.021$). Male patients had lower connectivity strength in the visual network (RSN 12, $P = 0.028$) than male controls. No significant difference was found between female patients and female controls within these brain networks. In sum, the mild TBI effect on the sex difference was derived mainly from the male patients.

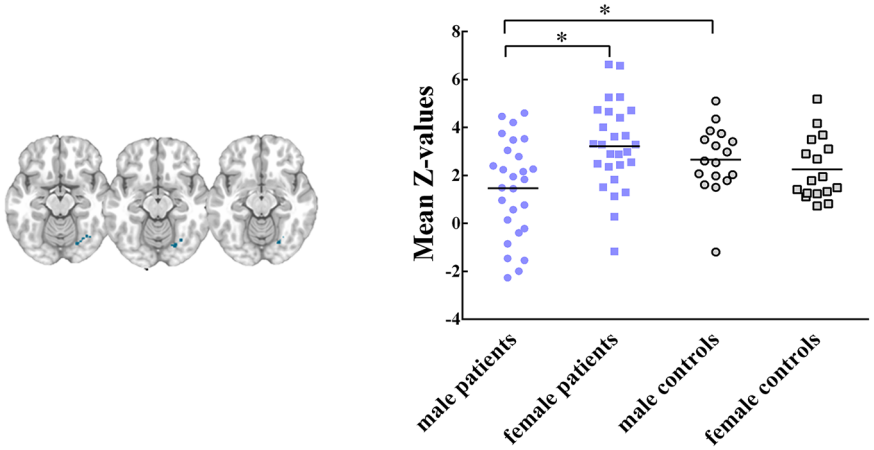

FIGURE 3 | Intrinsic functional connectivity differences between male and female patients within visual network, where showed decreased connectivity in male patients. Maps were thresholded at $P < 0.05$ (FWE corrected). The left side of the brain corresponds to the left side in the image. Scatterplots are displayed for ROI-analysis among groups. Significant effects are denoted with asterisks between two groups, under *post hoc* restricted LSD tests.

The Relationship Between Abnormal Functional Connectivity and Clinical Performance

Correlation analysis was then conducted and restricted into each brain network showing significant sex difference (RSNs 2, 3, 7, 8, 12) and clinical symptoms only in the male patients. Correlation analysis showed that functional connectivity within the executive function network (RSN 3) was positively correlated with ISI scores ($r = 0.515$, $P = 0.006$, **Figure 4**). A conservative corrected significance level of $P < 0.0125$ was considered following Bonferroni correction for the total number of clinical assessments involved (0.05/4).

DISCUSSION

Mild TBI is considered to induce abnormal resting state functional connectivity within intrinsic networks, however little is known about whether there is an effect of biological sex on response to TBI-related abnormalities (Shumskaya et al., 2012; Mayer et al., 2014). This study applied a whole-brain analysis to illustrate sex differences of resting-state functional connectivity from a network perspective after mild TBI. To the best of our knowledge, this is the first study to evaluate potential sex differences in the functional connectivity networks from a cohort of patients with acute mild TBI. The main findings of the present study are: (a) for the neuropsychological tests and self-report scales involved in the study, there were no significant differences between males and females either in mild TBI or control group; (b) however, male patients presented increased functional connectivity within motor, ventral steam, executive function and cerebellum networks, decreased connectivity within visual network compared with female patients; these identified RSNs have been previously associated with somatosensory and motor functions, executive control, self-related processing (Bressler and Menon, 2010); and (c) there was a positive correlation between functional connectivity within executive functional network and ISI scores in male patients.

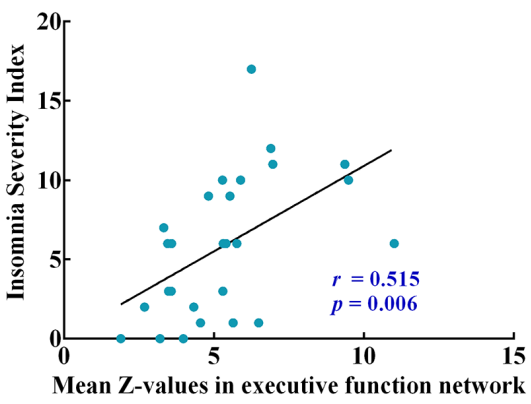

FIGURE 4 | The pearson correlation coefficient plots correlating mean Z-values of intrinsic functional connectivity in executive function network with insomnia severity index (ISI).

No sex difference was observed in clinical scales after mild TBI in our study. Previous studies have attempted to discover sex effect on mild TBI using clinical cognitive outcomes (Covassin et al., 2012, 2013; Hsu et al., 2015). However, results of these experiments are controversial. Some have suggested that females report worse outcomes and more post-concussive symptoms compared with males following concussion (Broshek et al., 2005; Covassin et al., 2012; Cancelliere et al., 2016). One has found that women have superior executive functioning when compared with men after TBI (Niemeier et al., 2014). In consistent with several studies, our results had shown no substantial difference in outcome with regard to sex (Cantu et al., 2010; Frommer et al., 2011). Observational studies may be confounded by sociological pressures on males, leading to underreporting by male subjects (Fakhran et al., 2014). Thus, it is essential to

develop a more objective measurement to evaluate the sex difference after injury.

In the present study, we selected seven functionally relevant RSNs. Between-group analysis reported the effects of sex difference on intrinsic functional connectivity within RSNs. Compared to female patients with mild TBI, male patients exhibited enhanced functional connectivity within the motor network (paracentral lobule, superior frontal gyrus, **Figure 2A**), ventral stream network (superior temporal gyrus, **Figure 2B**), executive function network (middle frontal gyrus, **Figure 2C**), and cerebellum (posterior lobe, **Figure 2D**). Male patients also presented higher connectivity than male controls in the motor and ventral steam network (**Figures 2A,B**). Motor network is involved in motor-learning, and it is suggested to have a potential role in disease-related functional connectivity alterations in motor tasks (Kumar et al., 2018). In a previous study, Shumskaya et al. (2012) find decreased functional connectivity within the motor-striatal network in the mild TBI group. Conversely, we observed increased connectivity in male patients when compared with either male HC or female patients. Nevertheless, there was no significant difference neither between female patients and female controls in the area, nor between male and female controls. We supposed that there might be physical male-specific stress response after acute injury. The ventral stream network is involved to the processing of visual information, as well as hearing (Tinelli et al., 2014; Dittinger et al., 2018). Our results showed significantly increased functional connectivity in the superior temporal gyrus in male patients. In executive function network, male patients showed greater connectivity than female patients on the middle frontal gyrus. A previous study suggest that increased connectivity found in the mild TBI group might lead to the increase of awareness from the external environment during the acute stage, and it might explain cognitive over-fatigue recounted by patients with mild TBI (Shumskaya et al., 2012). Similarly, damaged self-awareness has also been attested previously in patients with TBI with frontal lobe injury (Spikman and van der Naalt, 2010). Within cerebellum network, comparing to female patients, male patients showed increased connectivity on the anterior lobe and posterior lobe. However, few researches have investigated functional connectivity in cerebellum, since there is no region of interest in studies. A research about sex differences on cerebellum should be done in future. In brief, the hyper-connectivity in male patients indicated that men had a different strategy in information processing when suffering concussion.

Further, male patients showed significant decreased functional connectivity on occipital lobe, which considered to be one component of visual network (**Figure 3**), compared with female patients and male controls. The visual network is related to the processing of visual information, and visual dysfunctions in mild TBI include photosensitivity or photaesthesia, double vision and vision deficits (Goodrich et al., 2007; Cockerham et al., 2009). Visual dysfunction had been found to be associated with high level processing defects, such as the speed of understanding and reading (Capó-Aponte et al., 2012). Mild TBI may destroy the transmission of information, and then affect perception, cognition and behavior. In visual network, female patients showed no significant difference than female controls. We suspected that males had weaker visual adjustment ability with compensation than females following injury. For the acute mild TBI, females may have the ability to protect their visual network with production of some regulatory substance.

Moreover, a positive correlation between functional connectivity within executive function network and ISI scores was discovered in male patients, suggesting the hyperconnectivity in executive function network was detrimental to male's sleeping after mild TBI. One study has reported that the hyperconnectivity with dorsal medial prefrontal cortex (dlPFC) across the executive function network may explain impaired concentration, increased rumination and self-focus in major depressive disorder (Crowther et al., 2015). It has been demonstrated that a single night of sleep deprivation is harmful to cognitive abilities, ranging from phasic alertness to executive functions (Harrison et al., 2000; Doran et al., 2001; Muto et al., 2012). The fragmented sleep can also make impairments on hyper-arousal and executive dysfunction (Stoffers et al., 2014). The results in our study may indicate that males were more vulnerable than females when suffering mild TBI.

Several limitations of our present study should be noted. First, it cannot infer direct causal effects of sex differences from current results in the study. Sex differences on functional connectivity are the result of interaction between genetics and external environmental factors (Kaczkurkin et al., 2016). Nonetheless, in specific RSNs, the significant sex differences presented on functional connectivity suggest particular adjustment for males following mild TBI, and may represent an important mechanism. Second, current study about mild TBI is limited to the acute period. Long-term differences of functional connectivity or prognosis between male and female patients cannot be accomplished. Recent research had shown that the strength of these network connections would be increased or decreased in a rapid and reversible manner to achieve a dynamic network connection (DNC; Arnsten et al., 2010). We need a longitudinal follow-up instead of once time point study in future. Third, the hormone status, which has been shown to affect neuropsychologic data and image status, is not unified (Bhagia et al., 2010; Xu et al., 2010; McAllister et al., 2011; Tamargo et al., 2017; Yamakawa et al., 2017). The study variables cannot be completely controlled. Furthermore, a combination of imaging methods, such as SWI, diffusion tensor imaging for integrity of white matter cellulose, MR perfusion study and MR spectroscopy for metabolite study should be compared, which may help to understand the structural pathophysiology of mild TBI and the causes of sex differences, to draw a more statistically significant conclusion.

CONCLUSION

In summary, the current findings of our research confirmed that there were significant sex differences on functional connectivity within specific RSNs following mild TBI. Male patients showed hyper-connectivity than female patients in four of selected RSNs, including motor, ventral stream, executive function and cerebellum networks. Hypo-connectivity in male patients than

female patients was found in visual network, suggesting a king of female compensation mechanism. We found that the abnormality of the functional connectivity of RSNs in acute mild TBI showed the possibility of brain recombination after trauma, mainly concerning male-specific.

AUTHOR CONTRIBUTIONS

SW and LH performed the experiment, analyzed image data and drafted the manuscript. JC, WH, CS, ZW, SG and XN performed the experiment and statistical results. DDZ, CG, GB, LY, DBZ and NZ collected the data involved in the study. BY, MZ and LB designed the study and gave critical comments on the manuscript.

FUNDING

This research was supported by the National Natural Science Foundation of China under Grant Nos. 81571752, 81771914, National key research and development plan of China (2016YFC0100300), the Zhejiang Natural Science Foundation (Grant no. LY15H090016), Wenzhou Municipal Sci-Tech Bureau (Y20140577), and Fundamental Research Funds for the Central Universities (No. Xjj 2018229).

REFERENCES

Arnsten, A. F. T., Paspalas, C. D., Gamo, N. J., Yang, Y., and Wang, M. (2010). Dynamic network connectivity: a new form of neuroplasticity. *Trends Cogn. Sci.* 14, 365–375. doi: 10.1016/j.tics.2010.05.003

Bastien, C. H., Vallières, A., and Morin, C. M. (2001). Validation of the insomnia severity index as an outcome measure for insomnia research. *Sleep Med.* 2, 297–307. doi: 10.1016/s1389-9457(00)00065-4

Bay, E., Sikorskii, A., and Saint-Arnault, D. (2009). Sex differences in depressive symptoms and their correlates after mild-to-moderate traumatic brain injury. *J. Neurosci. Nurs.* 41, 298–309. doi: 10.1097/jnn.0b013e3181b6be81

Bazarian, J. J., Blyth, B., Mookerjee, S., He, H., and McDermott, M. P. (2010). Sex differences in outcome after mild traumatic brain injury. *J. Neurotrauma* 27, 527–539. doi: 10.1089/neu.2009.1068

Beckmann, C. F., and Smith, S. M. (2005). Tensorial extensions of independent component analysis for multisubject FMRI analysis. *Neuroimage* 25, 294–311. doi: 10.1016/j.neuroimage.2004.10.043

Benedictus, M. R., Spikman, J. M., and van der Naalt, J. (2010). Cognitive and behavioral impairment in traumatic brain injury related to outcome and return to work. *Arch. Phys. Med. Rehabil.* 91, 1436–1441. doi: 10.1016/j.apmr.2010.06.019

Bhagia, V., Gilkison, C., Fitts, R. H., Zgaljardic, D. J., High, W. M., Masel, B. E., et al. (2010). Effect of recombinant growth hormone replacement in a growth hormone deficient subject recovering from mild traumatic brain injury: a case report. *Brain Inj.* 24, 560–567. doi: 10.3109/02699051003601705

Biswal, B. B., Mennes, M., Zuo, X. N., Gohel, S., Kelly, C., Smith, S. M., et al. (2010). Toward discovery science of human brain function. *Proc. Natl. Acad. Sci. U S A* 107, 4734–4739. doi: 10.1073/pnas.0911855107

Bramlett, H. M., and Dietrich, W. D. (2001). Neuropathological protection after traumatic brain injury in intact female rats versus males or ovariectomized females. *J. Neurotrauma* 18, 891–900. doi: 10.1089/089771501750451811

Bressler, S. L., and Menon, V. (2010). Large-scale brain networks in cognition: emerging methods and principles. *Trends Cogn. Sci.* 14, 277–290. doi: 10.1016/j.tics.2010.04.004

Broshek, D. K., Kaushik, T., Freeman, J. R., Erlanger, D., Webbe, F., and Barth, J. T. (2005). Sex differences in outcome following sports-related concussion. *J. Neurosurg.* 102, 856–863. doi: 10.3171/jns.2005.102.5.0856

Caeyenberghs, K., Leemans, A., De Decker, C., Heitger, M., Drijkoningen, D., Linden, C. V., et al. (2012). Brain connectivity and postural control in young traumatic brain injury patients: a diffusion MRI based network analysis. *Neuroimage Clin.* 1, 106–115. doi: 10.1016/j.nicl.2012.09.011

Caeyenberghs, K., Leemans, A., Leunissen, I., Gooijers, J., Michiels, K., Sunaert, S., et al. (2014). Altered structural networks and executive deficits in traumatic brain injury patients. *Brain Struct. Funct.* 219, 193–209. doi: 10.1007/s00429-012-0494-2

Caeyenberghs, K., Leemans, A., Leunissen, I., Michiels, K., and Swinnen, S. P. (2013). Topological correlations of structural and functional networks in patients with traumatic brain injury. *Front. Hum. Neurosci.* 7:726. doi: 10.3389/fnhum.2013.00726

Cancelliere, C., Donovan, J., and Cassidy, J. D. (2016). Is sex an indicator of prognosis after mild traumatic brain injury: a systematic analysis of the findings of the world health organization collaborating centre task force on mild traumatic brain injury and the international collaboration on mild traumatic brain injury prognosis. *Arch. Phys. Med. Rehabil.* 97, S5–S18. doi: 10.1016/j.apmr.2014.11.028

Cantu, R. C., Guskiewicz, K., and Register-Mihalik, J. K. (2010). A retrospective clinical analysis of moderate to severe athletic concussions. *PM R* 2, 1088–1093. doi: 10.1016/j.pmrj.2010.07.483

Cao, X., Wang, L., Cao, C., Fang, R., Chen, C., Hall, B. J., et al. (2018). Sex differences in global and local connectivity of adolescent posttraumatic stress disorder symptoms. *J. Child Psychol. Psychiatry* doi: 10.1111/jcpp.12963 [Epub ahead of print].

Capó-Aponte, J. E., Urosevich, T. G., Temme, L. A., Tarbett, A. K., and Sanghera, N. K. (2012). Visual dysfunctions and symptoms during the subacute stage of blast-induced mild traumatic brain injury. *Mil. Med.* 177, 804–813. doi: 10.7205/milmed-d-12-00061

Cockerham, G. C., Goodrich, G. L., Weichel, L. T. C. E. D., Orcutt, J. C., Rizzo, J. F., Bower, C. O. L. K. S., et al. (2009). Eye and visual function in traumatic brain injury. *J. Rehabil. Res. Dev.* 46, 811–818. doi: 10.1682/JRRD.2008.08.0109

Cole, J. H., Leech, R., Sharp, D. J., and Alzheimer's Disease Neuroimaging Initiative. (2015). Prediction of brain age suggests accelerated atrophy after traumatic brain injury. *Ann. Neurol.* 77, 571–581. doi: 10.1002/ana.24367

Cole, D. M., Smith, S. M., and Beckmann, C. F. (2010). Advances and pitfalls in the analysis and interpretation of resting-state FMRI data. *Front. Syst. Neurosci.* 4:8. doi: 10.3389/fnsys.2010.00008

Covassin, T., Elbin, R. J., Bleecker, A., Lipchik, A., and Kontos, A. P. (2013). Are there differences in neurocognitive function and symptoms between male and female soccer players after concussions? *Am. J. Sports Med.* 41, 2890–2895. doi: 10.1177/0363546513509962

Covassin, T., Elbin, R. J., Harris, W., Parker, T., and Kontos, A. (2012). The role of age and sex in symptoms, neurocognitive performance and postural stability in athletes after concussion. *Am. J. Sports Med.* 40, 1303–1312. doi: 10.1177/0363546512444554

Crowther, A., Smoski, M. J., Minkel, J., Moore, T., Gibbs, D., Petty, C., et al. (2015). Resting-state connectivity predictors of response to psychotherapy in major depressive disorder. *Neuropsychopharmacology* 40, 1659–1673. doi: 10.1038/npp.2015.12

Damoiseaux, J. S., Rombouts, S. A. R. B., Barkhof, F., Scheltens, P., Stam, C. J., Smith, S. M., et al. (2006). Consistent resting-state networks across healthy subjects. *Proc. Natl. Acad. Sci. U S A* 103, 13848–13853. doi: 10.1073/pnas.0601417103

De Luca, M., Beckmann, C. F., De Stefano, N., Matthews, P. M., and Smith, S. M. (2006). fMRI resting state networks define distinct modes of long-distance interactions in the human brain. *Neuroimage* 29, 1359–1367. doi: 10.1016/j.neuroimage.2005.08.035

Dittinger, E., Valizadeh, S. A., Jäncke, L., Besson, M., and Elmer, S. (2018). Increased functional connectivity in the ventral and dorsal streams during retrieval of novel words in professional musicians. *Hum. Brain Mapp.* 39, 722–734. doi: 10.1002/hbm.23877

Doran, S. M., Van Dongen, H. P. A., and Dinges, D. F. (2001). Sustained attention performance during sleep deprivation: evidence of state instability. *Arch. Ital. Biol.* 139, 253–267. doi: 10.4449/aib.v139i3.503

Fakhran, S., Yaeger, K., Collins, M., and Alhilali, L. (2014). Sex differences in white matter abnormalities after mild traumatic brain injury: localization and correlation with outcome. *Radiology* 272, 815–823. doi: 10.1148/radiol.14132512

Farace, E., and Alves, W. M. (2000). Do women fare worse? A metaanalysis of gender differences in outcome after traumatic brain injury. *Neurosurg. Focus* 8:e6. doi: 10.3171/foc.2000.8.1.152

Filippi, M., Valsasina, P., Misci, P., Falini, A., Comi, G., and Rocca, M. A. (2013). The organization of intrinsic brain activity differs between genders: a resting-state fMRI study in a large cohort of young healthy subjects. *Hum. Brain Mapp.* 34, 1330–1343. doi: 10.1002/hbm.21514

Friston, K. J., Frith, C. D., Frackowiak, R. S. J., and Turner, R. (1995). Characterizing dynamic brain responses with fMRI: a multivariate approach. *Neuroimage* 2, 166–172. doi: 10.1006/nimg.1995.1019

Frommer, L. J., Gurka, K. K., Cross, K. M., Ingersoll, C. D., Comstock, R. D., and Saliba, S. A. (2011). Sex differences in concussion symptoms of high school athletes. *J. Athl. Train.* 46, 76–84. doi: 10.4085/1062-6050-46.1.76

Goodrich, G. L., Kirby, J., Cockerham, G., Ingalla, S. P., and Lew, H. L. (2007). Visual function in patients of a polytrauma rehabilitation center: a descriptive study. *J. Rehabil. Res. Dev.* 44, 929–936. doi: 10.1682/jrrd.2007.01.0003

Harrison, Y., Horne, J. A., and Rothwell, A. (2000). Prefrontal neuropsychological effects of sleep deprivation in young adults–a model for healthy aging? *Sleep* 23, 1–7. doi: 10.1093/sleep/23.8.1f

Holm, L., Cassidy, J. D., Carroll, L. J., Borg, J., and Neurotrauma Task Force on Mild Traumatic Brain Injury of the WHO Collaborating Centre. (2005). Summary of the WHO collaborating centre for neurotrauma task force on mild traumatic brain injury. *J. Rehabil. Med.* 37, 137–141. doi: 10.1080/16501970510027321

Hsu, H. L., Chen, D. Y., Tseng, Y. C., Kuo, Y. S., Huang, Y. L., Chiu, W. T., et al. (2015). Sex differences in working memory after mild traumatic brain injury: a functional MR imaging study. *Radiology* 276, 828–835. doi: 10.1148/radiol.2015142549

Jenkins, P. O., Mehta, M. A., and Sharp, D. J. (2016). Catecholamines and cognition after traumatic brain injury. *Brain* 139, 2345–2371. doi: 10.1093/brain/aww128

Jenkinson, M., Bannister, P., Brady, M., and Smith, S. (2002). Improved optimization for the robust and accurate linear registration and motion correction of brain images. *Neuroimage* 17, 825–841. doi: 10.1016/s1053-8119(02)91132-8

Kaczkurkin, A. N., Moore, T. M., Ruparel, K., Ciric, R., Calkins, M. E., Shinohara, R. T., et al. (2016). Elevated amygdala perfusion mediates developmental sex differences in trait anxiety. *Biol. Psychiatry* 80, 775–785. doi: 10.1016/j.biopsych.2016.04.021

King, N. S., Crawford, S., Wenden, F. J., Moss, N. E. G., and Wade, D. T. (1995). The rivermead post concussion symptoms questionnaire: a measure of symptoms commonly experienced after head-injury and its reliability. *J. Neurol.* 242, 587–592. doi: 10.1007/bf00868811

Kreiner, D. S., and Ryan, J. J. (2001). Memory and motor skill components of the WAIS-III digit symbol-coding subtest. *Clin. Neuropsychol.* 15, 109–113. doi: 10.1076/clin.15.1.109.1906

Kumar, M., Modi, S., Rana, P., Kumar, P., Kanwar, R., Sekhri, T., et al. (2018). Alteration in intrinsic and extrinsic functional connectivity of resting state networks associated with subclinical hypothyroid. *J. Neuroendocrinol.* doi: 10.1111/jne.12587 [Epub ahead of print].

Mayer, A., Ling, J., Allen, E., and Klimaj, S. (2014). Static and dynamic intrinsic connectivity following mild traumatic brain injury. *Brain Inj.* 28, 688–688. doi: 10.1089/neu.2014.3542

Mayer, A. R., Mannell, M. V., Ling, J., Gasparovic, C., and Yeo, R. A. (2011). Functional connectivity in mild traumatic brain injury. *Hum. Brain Mapp.* 32, 1825–1835. doi: 10.1002/hbm.21151

McAllister, T. W., Flashman, L. A., McDonald, B. C., Ferrell, R. B., Tosteson, T. D., Yanofsky, N. N., et al. (2011). Dopaminergic challenge with bromocriptine one month after mild traumatic brain injury: altered working memory and BOLD response. *J. Neuropsychiatry Clin Neurosci.* 23, 277–286. doi: 10.1176/appi.neuropsych.23.3.277

Muto, V., Shaffii-le Bourdiec, A., Matarazzo, L., Foret, A., Mascetti, L., Jaspar, M., et al. (2012). Influence of acute sleep loss on the neural correlates of alerting, orientating and executive attention components. *J. Sleep Res.* 21, 648–658. doi: 10.1111/j.1365-2869.2012.01020.x

Nichols, T. E., and Holmes, A. P. (2002). Nonparametric permutation tests for functional neuroimaging: a primer with examples. *Hum. Brain Mapp.* 15, 1–25. doi: 10.1002/hbm.1058

Niemeier, J. P., Perrin, P. B., Holcomb, M. G., Rolston, C. D., Artman, L. K., Lu, J., et al. (2014). Gender differences in awareness and outcomes during acute traumatic brain injury recovery. *J. Womens. Health* 23, 573–580. doi: 10.1089/jwh.2013.4535

O'Connor, C. A., Cernak, I., and Vink, R. (2003). Interaction between anesthesia, gender and functional outcome task following diffuse traumatic brain injury in rats. *J. Neurotrauma* 20, 533–541. doi: 10.1089/089771503767168465

Shumskaya, E., Andriessen, T. M. J. C., Norris, D. G., and Vos, P. E. (2012). Abnormal whole-brain functional networks in homogeneous acute mild traumatic brain injury. *Neurology* 79, 175–182. doi: 10.1212/WNL.0b013e31825f04fb

Slobounov, S. M., Gay, M., Zhang, K., Johnson, B., Pennell, D., Sebastianelli, W., et al. (2011). Alteration of brain functional network at rest and in response to YMCA physical stress test in concussed athletes: RsFMRI study. *Neuroimage* 55, 1716–1727. doi: 10.1016/j.neuroimage.2011.01.024

Smith, S. M. (2002). Fast robust automated brain extraction. *Hum. Brain Mapp.* 17, 143–155. doi: 10.1002/hbm.10062

Smith, S. M., Jenkinson, M., Woolrich, M. W., Beckmann, C. F., Behrens, T. E. J., Johansen-Berg, H., et al. (2004). Advances in functional and structural MR image analysis and implementation as FSL. *Neuroimage* 23, S208–S219. doi: 10.1016/j.neuroimage.2004.07.051

Spikman, J. M., and van der Naalt, J. (2010). Indices of impaired self-awareness in traumatic brain injury patients with focal frontal lesions and executive deficits: implications for outcome measurement. *J. Neurotrauma* 27, 1195–1202. doi: 10.1089/neu.2010.1277

Stoffers, D., Altena, E., van der Werf, Y. D., Sanz-Arigita, E. J., Voorn, T. A., Astill, R. G., et al. (2014). The caudate: a key node in the neuronal network imbalance of insomnia? *Brain* 137, 610–620. doi: 10.1093/brain/awt329

Tamargo, I. A., Bader, M., Li, Y. Z., Yu, S. J., Wang, Y., Talbot, K., et al. (2017). Novel GLP-1R/GIPR co-agonist "twincretin" is neuroprotective in cell and rodent models of mild traumatic brain injury. *Exp. Neurol.* 288, 176–186. doi: 10.1016/j.expneurol.2016.11.005

Tinelli, F., Bulgheroni, S., Mazzotti, S., Vago, C., Groppo, M., Scaramuzzo, R. T., et al. (2014). Ventral stream sensitivity in "healthy" preterm-born adolescents: Psychophysical And Neuropsychological evaluation. *Early Hum. Dev.* 90, 45–49. doi: 10.1016/j.earlhumdev.2013.10.006

Troyer, A. K., Moscovitch, M., and Winocur, G. (1997). Clustering and switching as two components of verbal fluency: evidence from younger and older healthy adults. *Neuropsychology* 11, 138–146. doi: 10.1037//0894-4105.11.1.138

Vos, P. E., Battistin, L., Birbamer, G., Gerstenbrand, F., Potapov, A., Prevec, T., et al. (2002). EFNS guideline on mild traumatic brain injury: report of an EFNS task force. *Eur. J. Neurol.* 9, 207–219. doi: 10.1046/j.1468-1331.2002.00407.x

Xu, Y. Q., McArthur, D. L., Alger, J. R., Etchepare, M., Hovda, D. A., Glenn, T. C., et al. (2010). Early nonischemic oxidative metabolic dysfunction leads to chronic brain atrophy in traumatic brain injury. *J. Cereb. Blood Flow Metab.* 30, 883–894. doi: 10.1038/jcbfm.2009.263

Yamakawa, G. R., Salberg, S., Barlow, K. M., Brooks, B. L., Esser, M. J., Yeates, K. O., et al. (2017). Manipulating cognitive reserve: pre-injury environmental conditions influence the severity of concussion symptomology, gene expression and response to melatonin treatment in rats. *Exp. Neurol.* 295, 55–65. doi: 10.1016/j.expneurol.2017.06.001

Yuan, W. H., Wade, S. L., and Babcock, L. (2015). Structural connectivity abnormality in children with acute mild traumatic brain injury using graph theoretical analysis. *Hum. Brain Mapp.* 36, 779–792. doi: 10.1002/hbm.22664

Conflict of Interest Statement: The authors declare that the research was conducted in the absence of any commercial or financial relationships that could be construed as a potential conflict of interest.

frontiers in Neural Circuits

ORIGINAL RESEARCH
published: 22 January 2019
doi: 10.3389/fncir.2019.00002

Cortical Layer and Spectrotemporal Architecture of Epileptiform Activity *in vivo* in a Mouse Model of Focal Cortical Malformation

*Anthony J. Williams and Qian-Quan Sun**

Department of Zoology & Physiology, University of Wyoming, Laramie, WY, United States

Our objective is to examine the layer and spectrotemporal architecture and laminar distribution of high-frequency oscillations (HFOs) in a neonatal freeze lesion model of focal cortical dysplasia (FCD) associated with a high prevalence of spontaneous spike-wave discharges (SWDs). Electrophysiological recording of local field potentials (LFPs) in control and freeze lesion animals were obtained with linear micro-electrode arrays to detect presence of HFOs as compared to changes in spectral power, signal coherence, and single-unit distributions during "hyper-excitable" epochs of anesthesia-induced burst-suppression (B-S). Result were compared to HFOs observed during spontaneous SWDs in animals during sleep. Micro-electrode array recordings from the malformed cortex indicated significant increases in the presence of HFOs above 100 Hz and associated increases in spectral power and altered LFP coherence of recorded signals across cortical lamina of freeze-lesioned animals with spontaneous bursts of high-frequency activity, confined predominately to granular and supragranular layers. Spike sorting of well-isolated single-units recorded from freeze-lesioned cortex indicated an increase in putative excitatory cell activity in the outer cortical layers that showed only a weak association with HFOs while deeper inhibitory units were strongly phase-locked to high-frequency ripple (HFR) oscillations (300–800 Hz). Both SWDs and B-S show increases in HFR activity that were phase-locked to the high-frequency spike pattern occurring at the trough of low frequency oscillations. The spontaneous cyclic spiking of cortical inhibitory cells appears to be the driving substrate behind the HFO patterns associated with SWDs and a hyperexcitable supragranular layer near the malformed cortex may play a key role in epileptogenesis in our model. These data, derived from a mouse model with a distinct focal cortical malformation, support recent clinical data that HFOs, particularly fast ripples, is a biomarker to help define the cortical seizure zone, and provide limited insights toward understanding cellular level changes underlying the HFOs.

Keywords: high frequency oscillations, epilepsy, spike wave discharge, single unit, neonatal freeze lesion

OPEN ACCESS

Edited by:
Lijun Bai,
Xi'an Jiaotong University, China

Reviewed by:
Matthew T. Colonnese,
George Washington University, United States
Aleksey V. Zaitsev,
Institute of Evolutionary Physiology and Biochemistry (RAS), Russia

****Correspondence:***
Qian-Quan Sun
neuron@uwyo.edu

Received: *08 September 2018*
Accepted: *07 January 2019*
Published: *22 January 2019*

Citation:
Williams AJ and Sun Q-Q (2019) Cortical Layer and Spectrotemporal Architecture of Epileptiform Activity in vivo in a Mouse Model of Focal Cortical Malformation. Front. Neural Circuits 13:2. doi: 10.3389/fncir.2019.00002

INTRODUCTION

Focal epilepsy is associated with the derangement of local neural network activity leading to hypersynchronous neuronal discharges (ictogenesis) in the affected brain tissues (van Diessen et al., 2013; Perucca et al., 2014; Ferrari-Marinho et al., 2015). High frequency oscillations (HFOs) have recently emerged as a sensitive biomarker of hyper-excitable tissues responsible for focal epilepsy (Brázdil et al., 2010; Ferrari-Marinho et al., 2015; van Klink et al., 2016; Cuello-Oderiz et al., 2018) and resection of brain regions with increased HFO rates has been associated with a high incidence of seizure-free outcome in clinical patients (Fujiwara et al., 2012; Fedele et al., 2016; Cuello-Oderiz et al., 2018). However, both physiological and pathological HFOs are common within cortical brain regions of epileptic patients (Matsumoto et al., 2013) though fast ripple activity (>250 Hz), Currently however, the spectral characteristics that distinguish physiological vs. pathological HFOs have not been clearly defined (Kerber et al., 2013; Frauscher et al., 2015).

Focal cortical dysplasia (FCD) is a common form of cortical malformation associated with a high incidence of epilepsy (Guerrini and Dobyns, 2014; Luhmann, 2016). Given the focal nature of FCD, many of these patients exhibiting refractory epilepsy are candidates for surgical resection of the affected brain tissue to relieve the epileptic condition (Sisodiya, 2000). The hyperexcitability that arises within the SOZ likely involves the accumulation of hypersynchronous unit activity that ultimately interferes with normal brain rhythms and can broadcast pathological activities to adjacent brain regions through low frequency propagation patterns (e.g., spike-and-wave seizure discharges). Recent evidence suggests that specific ictal patterns may indicate distinct network alterations driving epileptogenesis as demonstrated in drug-resistant epilepsy patients (Ogren et al., 2009; Ferrari-Marinho et al., 2016) and in animal models (Bragin et al., 2009; Lévesque et al., 2012). Distinct differences in network connectivity has also been demonstrated between different types of cortical malformations as demonstrated from cellular synaptic activity of epileptic tissues obtained from clinical patients (Cepeda et al., 2012). The spectrotemporal dissection of pathological waveforms obtained with high-density micro-electrode arrays including the analysis of cross-laminar and cross-frequency coupling may serve as useful high-resolution tools for studying the underlying pathologies and neural networks associated with different forms of epileptogenesis (Buzsáki and Silva, 2012; Ibrahim et al., 2014; Williams et al., 2016).

The epileptogenicity of FCD is likely related to an imbalance in the level of excitation to inhibition in the affected brain regions (Redecker et al., 1998; Avoli et al., 1999; Zhu and Roper, 2000; Eichler and Meier, 2008) The hyper-excitable zone of brain tissue can extend several millimeters from the core microgyric lesion (Jacobs et al., 1996, 1999b, 2009, 2012; Luhmann and Raabe, 1996; Roper et al., 1997; Redecker et al., 1998) and has been associated with alterations in expression of excitatory and inhibitory receptors in dysplastic and exfocal regions of freeze lesioned cortex (Zilles et al., 1998; Redecker et al., 2000). In particular, hyperexcitable regions are isolated to regions outside the microgyric core as experimental isolation of ectopic tissue or microgyria fail to remove the hyperexcitability (Jacobs et al., 1999a). In fact, accurate identification and complete resection of hyper-excitable tissues surrounding the microgyric lesion is a key factor that determines seizure-free outcome in FCD patients (Fujiwara et al., 2012; Guerrini and Dobyns, 2014; Moosa and Gupta, 2014). To date, the cellular and circuit features underlying paroxysmal discharges *in vivo* still have not been elucidated.

The aim of the current study was to assess the altered *in vivo* cortical neurophysiology of a recently characterized FCD model shown to be associated with the high prevalence of spike-wave discharges (SWDs; Sun et al., 2016). In this model, a distinct cortical microgyric cleft is consistently observed that results in close to a 90% incidence of SWDs in adult animals (Sun et al., 2016) similar to the neuropathology observed in FCD patients exhibiting cortical microgyria that also exhibit a high incidence of epilepsy (Luhmann, 2016). Here, we provide a comprehensive spectrotemporal analysis of the malformed cortex following hyper-excitable activation using anesthesia-induced burst-suppression (B-S; Williams et al., 2016). In our initial study (Williams et al., 2016) we found that this transitional state of anesthesia-induced hyper-excitability is significantly enhanced in animals exposed to a neonatal freeze lesion and often contains spike-wave components similar to that observed during SWDs in awake animals. In the current study, we extend our initial findings and focus on the incidence and laminar distribution of HFOs, one- and two-dimensional spectrotemporal mapping of altered local field potentials (LFPs), and characterization of hyperexcitable single-unit distributions across cortical lamina using commercially available linear micro-electrode arrays. Research into the underlying circuitries that control hypersynchronous activity as well as possible differential patterns between epileptic conditions that arise in disparate parts of the brain will be critical for understanding and ultimately treating these activities.

MATERIALS AND METHODS

All experiments were performed under protocols approved by the Institutional Animal Care and Use Committee (IACUC) of the University of Wyoming. Animals were housed in a vivarium maintained at 22–23°C on a 12:12 h light-dark cycle. Food and water were available *ad libitum*.

Freeze Lesion Model

Neonatal freeze lesions were induced in P0–1 pups (male and female CD-1) using a modification of the model described by Dvorak et al. (1978) to induce neocortical microgyria (right S1 somatosensory region) as previously described (Sun et al., 2016). Briefly, mice pups were immersed in wet ice until movement and response to tail pinch was absent. The skull was then exposed through a midline scalp incision and a freezing probe with a 1 mm diameter circular tip (cooled to −196°C in liquid nitrogen) was placed on the skull over the somatosensory cortex, 2 mm lateral to midline and 0.5 mm caudal to the Bregma

for 1–2 s. This procedure was routinely completed within 5 min and resulted in the development of a consistent microgyrus in the adult brain (e.g., **Figure 1A**). Control animals underwent a sham surgery (exposed to all surgical procedures minus the freeze lesion).

Extracellular Microelectrode Array Studies (Anesthetized Mice)

Extracellular signals were recorded using 16-electrode linear micro-electrode SmartProbe^{TM} arrays (NeuroNexus, Ann Arbor, MI, USA) from the right S1cortical region of anesthetized control (sham) and freeze lesion mice as previously described (Williams et al., 2016). The electrode array consisted of a single shank with 16 individual iridium electrodes (A1 × 16, 3 mm length, 15 μm thickness, each electrode separated by 100 μm space) with on-board electronics for digital conversion of the signals and linked to a SmartBox^{TM} control and data streaming system through a SmartLink headstage (NeuroNexus). These electrodes typically have a impedance of around 1.5 MΩ. The array was positioned perpendicular to the cortical surface to allow recording from both cortical and subcortical brain structures. Each signal was digitally filtered (1–10,000 Hz band-pass and 60 Hz notch filters), and recorded at a sample rate of 30 kHz using Smartbox 2.0 software (NeuroNexus). Additional off-line digital filtering was used to define LFPs (1–100 Hz) and multi-unit activity (MUA; 300–3,000 Hz). All recordings were obtained during B-S due to the hyperexcitable state of the brain during this level of anesthesia (Kroeger and Amzica, 2007; Amzica, 2009; Ferron et al., 2009), recently characterized in the freeze lesion model to be sensitive to changes in hyperexcitability of the epileptic brain (Williams et al., 2016). In brief, mice were anesthetized under isoflurane anesthesia (2%, delivered in oxygen) and secured in a stereotaxic frame (Stoelting, Wood Dale, IL, USA). A scalp incision was made to expose the skull over the right S1 area. The micro-electrode array was then advanced at an angle of 40° from vertical (∼1650-micron depth) into the S1 cortex (see **Figure 1A**) using a hydraulic micromanipulator (Narishige, Amityville, NY, USA). A reference electrode (silver wire) was placed in the skin flap of the scalp incision. The isoflurane anesthesia level was then reduced to 1.0% to induce B-S. Extracellular recordings began once stable baseline activity was observed. Signals were digitally filtered (1–7,500 Hz band-pass and 60 Hz notch filters), and recorded at a sample rate of 20 kHz using Smartbox 2.0 software (NeuroNexus).

Bipolar Field Potential Recordings (Unanesthetized Mice)

A screw free, glue-based electrode assembly system (Wu et al., 2008) was used to record LFPs from the brains of awake, behaving animals as previously described (Sun et al., 2016). In brief, mice were anesthetized (2% isoflurane, delivered in oxygen) and secured in a stereotaxic frame (Stoelting, Wood Dale, IL, USA) for electrode implantation. Bipolar electrodes were constructed of twisted pairs of polyimide-insulated stainless steel wires (125 μm diameter, California Fine Wire Co., Grover Beach, CA, USA) and connecting pins (Digikey, Thief River Falls, MN, USA). The electrodes were stereotaxically implanted through a small burr hole in the skull over the ipsilateral (right)

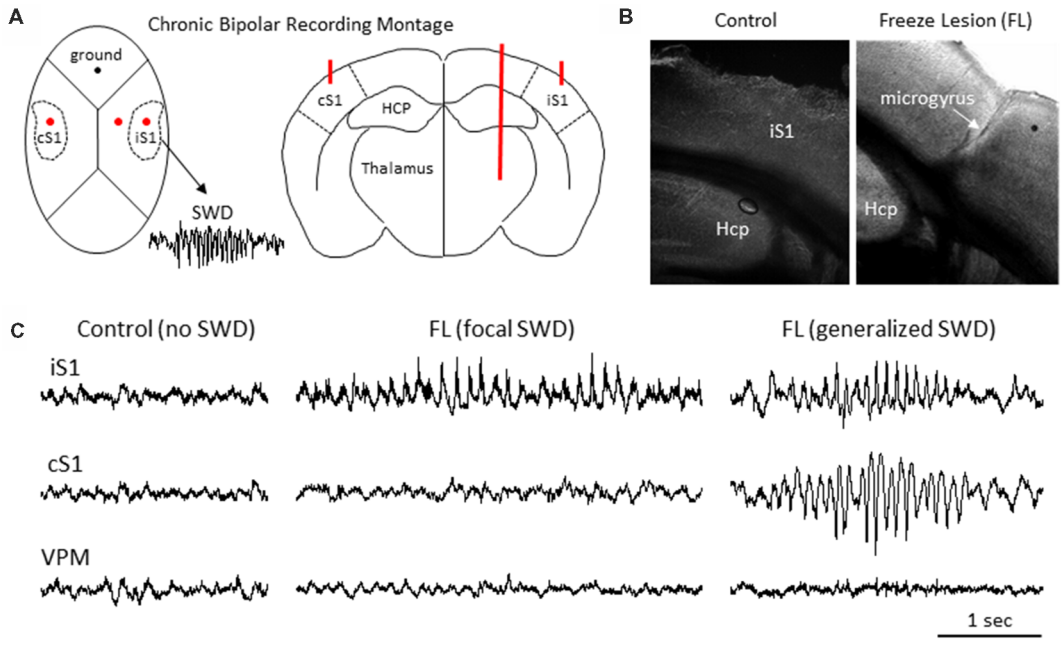

FIGURE 1 | Freeze lesion induced microgyrus and local field potential (LFP) recordings of spike-wave discharges (SWDs). **(A)** Diagram of mouse skull (left) and coronal brain section (right) indicating position of the chronic bipolar recording electrodes in the ipsilateral S1 (iS1), contralateral S1 (cS1) and thalamus. HCP, hippocampus. **(B)** Representative coronal section from the S1 cortical region of a control and FL mouse brain. **(C)** Examples of focal and generalized SWDs from FL animals that were generally confined to cortical regions and not observed in control animals.

S1 cortex (1.5 mm posterior and 3.5 mm lateral to Bregma) and glued in place with dental cement. A ground electrode was placed into the ipsilateral olfactory bulb area. Recording sessions were performed over 6–24 h with automated infrared activity tracking to detect animal movement in a circular recording arena that allowed for free movement of the animal. Electrographic signals were amplified (Model 1700 differential AC amplifier, A-M system, Carlsborg, WA, USA), digitized (Power 1401 A-D converter, Cambridge Electronic Design Limited, Cambridge, England), and continuously recorded (Spike2 software, Cambridge Electronic Design Limited, Cambridge, England) at a sample rate of 3.2 kHz.

Histopathology

Following completion of electrophysiology recordings, animals were anesthetized and transcardially perfused with 0.9% saline followed by 4% paraformaldehyde for histological analysis as previously described (Williams et al., 2016). In brief, brains were extracted, immersed in 4% paraformaldehyde for 24 h, and then transferred to 0.1 M phosphate buffer containing sequentially increasing levels of sucrose (10/20/30%, pH 7.4, 4°C) across three consecutive days. Brain issue was then cut into serial sections through the area of interest (50–300 μm thick). The back of the micro-electrode was swabbed with DiI (2 mg/ml in ethanol, Invitrogen Molecular Probes, Eugene, OR, USA) for visualization of the electrode track (e.g., **Figure 1A**). All sections were then mounted on glass slides with a DAPI mounting medium (Vectashield, Vector Laboratories, Burlingame, CA, USA), evaluated under a light/fluorescent microscope (Zeiss Axioskop 2, Ontario, CA, USA), and digitally imaged using Axiovision software (ver. 4.6, Zeiss).

Stereotaxic Viral Injection and Optogenetic Stimulation *in vivo*

Virus injection was performed in sham or FL mice aged P14-P16. Mice were anesthetized with 2% isoflurane (vol/vol) and maintained with oxygenated 1% isoflurane throughout surgery procedure. AAV2.1.CAG.hChR2(H134R)-mCherry (University of Pennsylvania Vector Core) was used. Viral vector (2 μl) was loaded into the tip (∼10 μm in diameter) of a beveled glass micropipette (Drummond Scientific Co., Broomall, PA, USA). A custom stereotactic apparatus was used to deliver viral vector to cortex through a small hole drilled into the skull. For local vS1 injection, virus was injected at two depths: 400 μm and 800 μm; for L4 injection, 400 μm and 600 μm. For each depth, a volume of ∼150 nl was injected within 1–2 min using a micromanipulator (MP-285-system, Sutter Instrument). Injection pipette was kept in place for 5 min for each depth after injection. Injected mice were put back to dam after 5–10 min recovery from anesthesia in a separate cage with a heating pad underneath. After weaning day, pups were separated and housed by gender until experiments. *Optogenetic*. We placed a multi-mode fiber optic patch cable *via* a 1.25 mm OD multimode ceramic zirconia ferrule (Precision Fiber Products, Inc., Milpitas, CA, USA) near the recording site. The multi-mode fiber optic patch cable was coupled to a blue laser which is triggered by a custom written program.

Data and Statistical Analysis

All recorded electrographic signal files were exported to NeuroExplorer (Nex Technologies, Madison, AL, USA) for off-line data analysis and visual inspection by an experimenter blinded to the test group. Each signal was digitally filtered using finite impulse response filters to define changes across a continuous array of frequency bands dependent on the sampling rate of the signals; low frequency (<25 Hz), gamma (25–100 Hz), low-frequency ripple (LFR; 100–300 Hz), high-frequency ripple (HFR; 300–800 Hz), and MUA (800–5,000 Hz). HFOs were identified as amplitude increases in the digitally filtered low and HFR bands (as demonstrated in **Figure 1B**) followed by a spectrograph analysis to evaluate increases in high-frequency spectral power (as demonstrated in **Figure 2**), a protocol similar to the techniques used for clinical detection of HFOs in epileptic patients (Zijlmans et al., 2012). Quantitative spectral analysis of discrete extracellular artifact-free recording samples (2–5 s duration) were analyzed during periods of B-S or SWDs to evaluate spectrotemporal changes in PSD and LFP coherence between channels using a previously described protocol (Williams et al., 2016).

Single-unit spike sorting of linear array recordings was conducted off-line with Spike2 using a combined template matching and principal component analysis protocol. Spike waveforms greater than 2 standard deviations above threshold were initially separated using automated template matching. Manual verification of separated spike waveforms was used to ensure consistent waveforms with refractory periods greater than 1 ms between spikes. Following initial separation of spikes, principal component analysis was used to classify neurons into well isolated groups with clearly separated cluster boundaries in 3-D space across each channel. Firing phase analysis was used to compare the firing rate of isolated single-units to distinct frequency oscillations: (1) spike field coherence (SFC) analysis was used to compare single-unit firing rate to specific frequencies across the LFP derived from the same signal; and (2) zero-phase oscillation timestamps were computed for each frequency band of interest and compared to individual single-unit spike rates to construct spike-phase histograms.

Following primary analysis, raw data was exported to Microsoft Excel for tabulation of statistical averages and standard error values or Sigmaplot (SYSTAT software Inc., San Jose, CA, USA) for graphical display (including spectral heat maps) and statistical analysis between groups. A multifactorial ANOVA was used to evaluate main effects and interactions when multiple independent variables were present followed by a Holm-Sidak *post hoc* analysis to evaluate significant differences between individual groups. A Fisher's Exact Test was used to assess significant differences in the relative proportion of responses between experimental groups. A P value of < 0.05 was considered significant.

RESULTS

Intracranial bipolar electrodes or linear micro-electrode arrays were used to evaluate electrophysiological disruption of the FL brain, with a particular focus on changes in the ultra-high

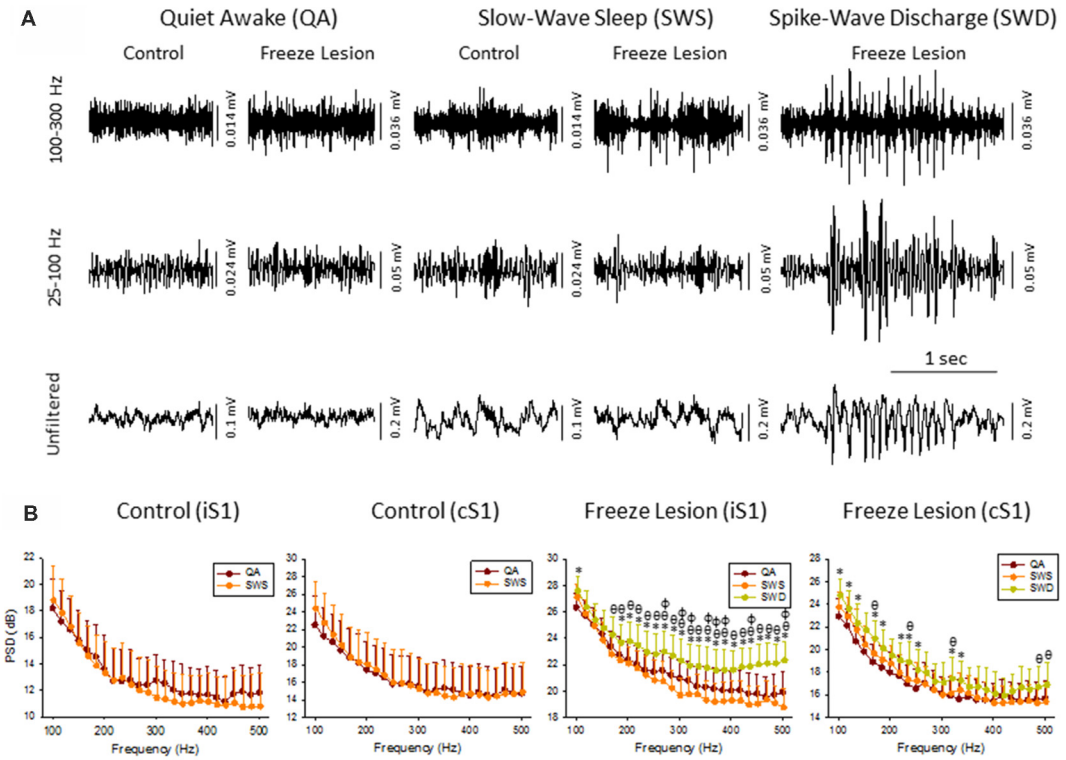

FIGURE 2 | High frequency oscillations (HFOs) across vigilance state and during SWD. **(A)** Sample LFP recordings of quiet awake (QA), slow-wave sleep (SWS), and SWDs in control and FL animals (iS1 recordings). Digital filtering of the field potential recordings revealed that SWDs were associated with an increased in HFOs (upper traces) as compared to the full spectrum recordings (lower traces). **(B)** Comparison of spectral power (i.e., PSD) levels across vigilance state and during SWDs in control (n = 5) and FL (n = 5–10) animals. $^{*}P < 0.05$ SWD vs. QA, $^{\theta}P < 0.05$ SWD vs. SWS, $^{\phi}P < 0.05$ QA vs. SWS (Holm-Sidak *post hoc* analysis).

frequency range (>100 Hz), in a total of 45 mice of either sex on a CD-1 background (12 controls: six male and six female, weight 33 ± 4 g; and 33 FL: 20 female and 13 male, weight 35 ± 4 g) ranging in age from 5 to 11 months old (8 ± 1 months). More detailed animal information for each experiment is provided in relevant "Results" section. Upon completion of the electrophysiological recordings, brain tissue was collected from a subset of animals to verify that animals exposed to a neonatal FL (n = 7) exhibited a distinct microgyrus within the right S1 region of the brain as compared to the normal cortical morphology of control animals (n = 6; **Figure 1B**).

Chronic Bipolar Field Potential Recordings (Unanesthetized, Fully Behaving Mice)

LFP recordings from three brain regions [ipsilateral S1 (iS1), contralateral S1 (cS1), and VPM, see **Figure 1A**] were evaluated for the presence of SWDs. Average age was 6.40 ± 0.98 months for control animals (N = 5 mice, weight = 35 ± 3 g, three male and two female) and 8.67 ± 0.54 months for FL animals (N = 17 mice, P > 0.05 between groups for age, 11 male and six female, weight = 33 ± 2 g). SWDs were defined as 10–12 Hz repetitive SWDs above baseline activity of at least 1 s in duration that occurred primarily during slow-wave sleep (SWS) as previously described in detail for this mouse model (Sun et al., 2016). Control animals exhibited no evidence of SWDs (0/5) while 83% (10/12) of FL animals exhibited either focal (5/10 recordings) or generalized (5/10 recordings) SWDs over the course of the recording session of about 12 h in each animal (**Figure 1C**). SWDs were confined to the cortical regions and were not evident in the subcortical (i.e., VPM) recordings in any of the 10 animals exhibiting SWDs.

Cortical LFP recordings were band-pass filtered to evaluate changes in HFOs across vigilance state and during SWDs (**Figure 2A**). Control animals exhibited relatively stable levels of background activity across periods of quiet awake (QA) and SWS (**Figure 2A**) with no significant differences in spectral power (100–500 Hz) in either brain hemisphere (**Figure 2B**). Freeze lesion animals exhibited similar levels of activity during QA and SWS, as compared to controls (**Figure 2A**) though there was a significant increase in spectral power between the two vigilance states above 250 Hz in the ipsilateral but not contralateral hemisphere (**Figure 2B**). In contrast to QA and SWS, a transient/oscillatory increase in HFO amplitude was observed during periods of SWD (**Figure 2A**). Significant increases in spectral power were also measured between SWDs and either vigilance state in both cortical hemispheres though stronger increases in PSD were observed in the iS1 as compared to cS1 (**Figure 2B**),

particularly for frequencies above 200 Hz that exhibited a 2–3 dB increase in spectral power as compared to either QA or SWS.

The increase in HF activity (>100 Hz) that occurred during SWDs presented as oscillatory wax-wane amplitude alterations locked to the spike-and-wave pattern of the SWD (**Figure 2A**).

Both SWDs and hyperexcitable B-S both show increases in HFR activity that were phase-locked to the high-frequency spike pattern of hyperexcitable brain waves occurring at the trough of low-frequency waves.

LFP recordings from the iS1 cortex of 11 *unanesthetized* animals (six males and seven females, age = 8 ± 2 months, weight = 31 ± 2 g) exposed to neonatal freeze lesion injury, and seven sham-treated controls (three male and four female mice, age = 7 ± 1 months, weight = 32 ± 2 g) were evaluated for the presence of SWDs and associated HFOs for comparison to the results obtained in the B-S model (i.e., anesthetized animals). SWDs were defined as 10–12 Hz repetitive SWD patterns above baseline activity of at least 1 s in duration that occurred primarily during SWS as previously described in detail for this mouse model (Sun et al., 2016). The cortical field potential recordings were band-pass filtered to evaluate changes in HFOs across frequency bandwidths up to 800 Hz (**Figure 3A**). In comparison to periods of non-ictal activity, a distinct pattern of HFO activity was observed in all freeze lesion animals during periods of SWD that presented as stereotypical transient/oscillatory increases in signal amplitude, particularly within the HFR band, locked to the SWD pattern (**Figure 3A**).

Direct comparison of the two forms of hyperexcitable activity observed from the same mouse FCD model indicated that amplitude-modulated increases in HFR activity occurred during either SWDs in unanesthetized, behaving animals or hyperexcitable spike-and-wave patterns observed during B-S in anesthetized animals. In both forms of epileptiform activities, the high frequency oscillatory amplitude modulations observed in the HFR band were phase locked to large amplitude spike deflections of the low frequency band (LFR) as demonstrated in **Figure 3B**. Average perievent histograms of changes in PSD (300–800 Hz) verified that the increases in HFR spectral power were centered on the spike deflections during either SWDs or B-S (**Figure 3C**). These data shows that the frequency distribution pattern of hyperexcitable B-S activities in anesthetized animals are similar to that of SWD in unanesthetized, behaving animals, and thus indicate a similar underlying neural mechanisms that were revealed in earlier results.

Neonatal Freeze Lesions Induced Laminar-Specific Increases in HFOs in the Malformed Cortex

Acute cortical field potential recordings were obtained using linear microelectrode arrays during hyperexcitable epochs of B-S in anesthetized mice (Williams et al., 2016) from one or

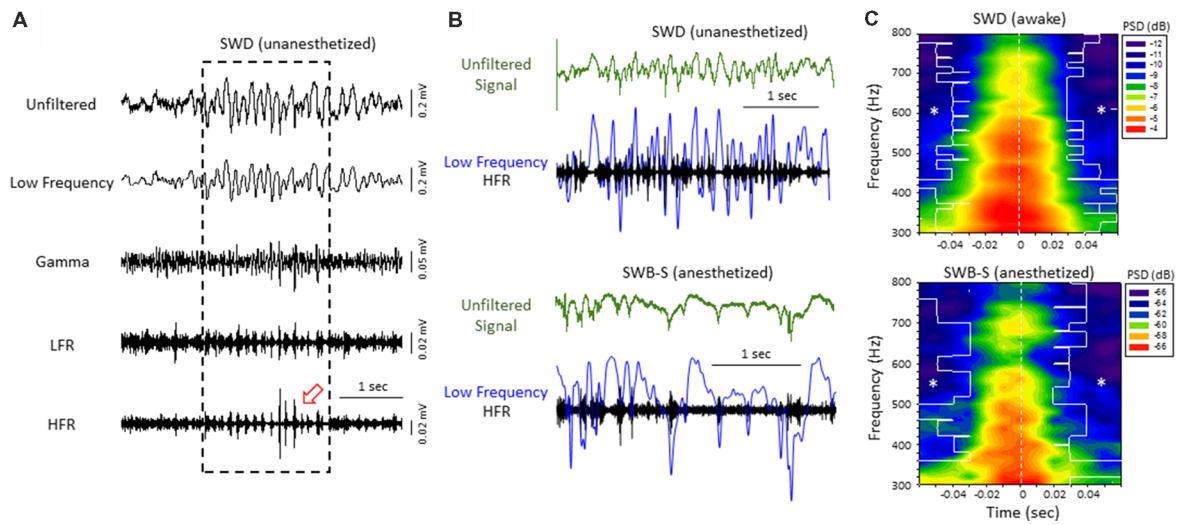

FIGURE 3 | High-frequency ripple (HFR) activity recorded from the iS1 cortex was locked to high-amplitude spike deflections observed in the low frequency band of both awake and anesthetized animals. **(A)** Example of a spontaneous SWD (awake) from the iS1 cortex and corresponding HFOs. Each signal was digitally filtered into spectral bandwidths for comparison as defined in **Figure 1**. Strong wax-and-wane amplitude oscillations (red arrow head) were commonly observed across the HFR spectrum locked to the large amplitude spike deflections of the SWD. **(B)** Representative traces from freeze lesion animals indicating that the oscillatory amplitude changes observed in the HFR band were locked to the spike-and-wave pattern of the low frequency band during both spontaneous SWDs (upper panel) and spike-wave burst-suppression (SWB-S) events (lower panel). In each example an overlay of the low frequency (blue trace) and HFR (black trace) bands are presented below each unfiltered trace (green) for comparison. **(C)** Average perievent spectrograms indicating that the increases in PSD within the HFR frequency band were centered on the "spike" of the spike-and-wave pattern that occurred during either SWDs (upper panel, $n = 5$) or B-S events (lower panel, $n = 6$). SWDs were recorded from the iS1 region of awake animals while the B-S events shown were recorded from the supragranular layer of the iS1 region of anesthetized animals. $^*P < 0.05$ compared to PSD values at time 0 for each frequency bin (Holm-Sidak *post hoc* analysis).

more distinct electrode penetrations within the iS1 cortex of seven control and 11 freeze lesion animals. Average age was 7.93 ± 0.87 months for control animals and 8.41 ± 0.84 months for freeze lesion animals ($P > 0.05$ between groups). The location and orientation of the microelectrode array in relation to the S1 region is demonstrated in **Figure 4A** (left panel). DiI labeling was use to verify the location of the electrode track as demonstrated in **Figure 4A** (middle panel). A distinct microgyrus was observed in animals exposed to the neonatal freeze lesion injury (7/7 animals) as compared to the intact tissue of control animals (0/7 animals; **Figure 4A**, right panel). Using this technique, the electrode array was positioned in the iS1 cortex, within 0.5–3 mm of the microgyrus as verified from histological analysis of the tissue (Williams et al., 2016). Digital filtering of raw signals across defined frequency bands was used to evaluate presence of HFOs during B-S (**Figure 4B**). Visual inspection of B-S activity indicated that, in comparison to sham controls, freeze lesion animals exhibited an increase HFO activity above 100 Hz (up to 5,000 Hz) as indicated by transient increases in signal amplitude above baseline that was largely confined to the upper cortical layers (**Figure 4B**, channel 1 vs. 8). In total, only 9% (1/12) of controls exhibited increases in HFOs above 100 Hz as compared to 60% (12/20) of freeze lesion recordings during periods of B-S ($P < 0.05$ between groups, Fisher's Exact test) with a similar profile of activity across cortical level for the HFO frequency bands above 100 Hz as summarized in **Figure 4C**. Spectrograph analysis of each B-S event was also used to verify that the presence of HFOs was associated with subsequent increases in high-frequency spectral power as demonstrated in **Figure 5**. In all cases, the presence of HFOs and subsequent increases in high-frequency spectral power were only observed during periods of hyperexcitable burst activity and were not observed during the intermittent periods of signal suppression.

Spectral Disruption of Cortical S1 Circuitry in Freeze Lesion Brain

Quantitative analysis of changes in the spectral architecture of the malformed cortex was evaluated by spectral analysis of control and freeze lesion animals during periods of B-S (**Figure 6**). Overall, B-S events typically presented across all layers of the S1 cortex in both control and freeze lesion animals (**Figure 6A**). Significant differences in average PSD values were measured across both frequency and electrode for both control and freeze lesion animals ($P < 0.05$, multivariate ANOVA, **Figure 6B**). In general, both experimental groups exhibited a similar expression pattern of PSD values with strongest increases in the upper cortical layers and the majority

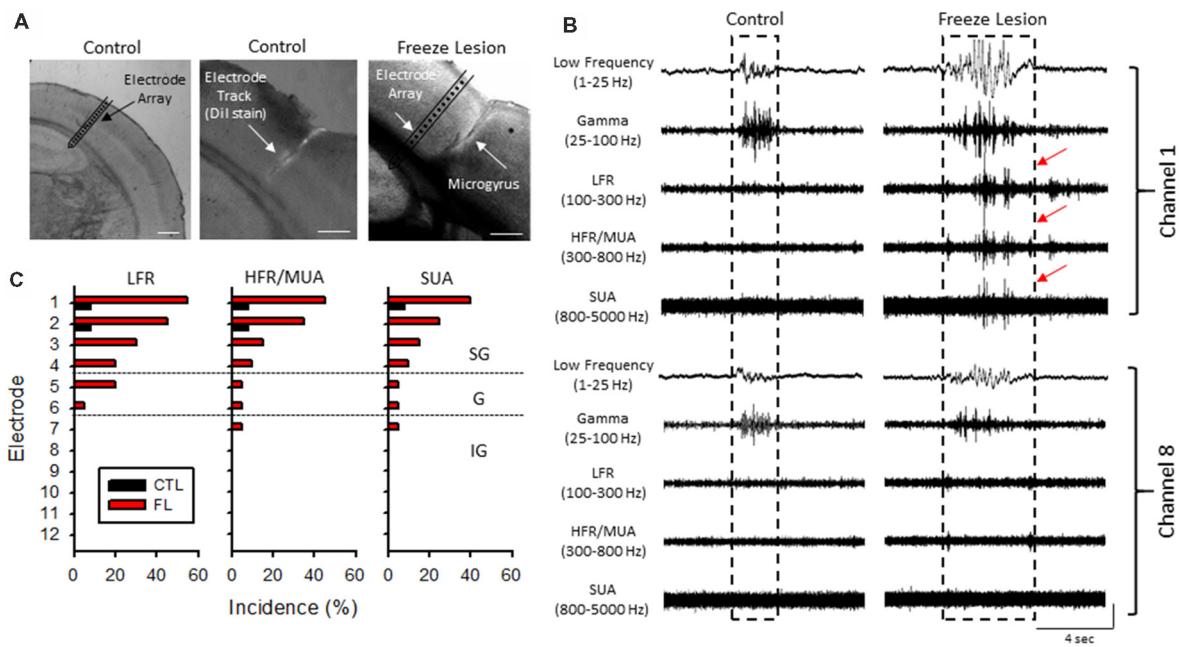

FIGURE 4 | Band-pass filter analysis of linear array recordings indicated an increase in HFOs during periods of B-S in freeze lesion animals in the upper cortical layers of the malformed cortex. **(A)** Representative coronal sections from the S1 cortical region of control and freeze lesion animals. Left panel indicates orientation of the linear micro-electrode array in comparison to the S1 cortex. The first 12 electrodes spanned the vertical extent of the cortex. Middle panel indicates the micro-electrode recording track as indicated by fluorescent DiI labeling of the linear array. Right panel demonstrates a freeze lesion induced microgyrus as compared to the position of a micro-electrode array. White scale bars = 400 μm. **(B)** Representative samples of B-S events recorded from channels 1 and 8 of a control and freeze lesion animal. The waveforms were digitally filtered to evaluate spectral changes across defined bandwidth ranges; low-frequency, gamma, low-frequency ripple (LFR), HFR, and multi-unit activity (MUA). Increases in HFOs above 100 Hz were largely confined to the upper cortical layers near the site of the freeze lesion injury (red arrows). Amplitude scale bar = 0.4 mV (unfiltered signals) and 0.04 mV (filtered signals). Amplitude of filtered signals was increased to show detail of high-frequency events. **(C)** Percent of recordings exhibiting increases in HFOs between control and freeze lesion animals across three frequency bands. Electrodes 1–12 represent recordings from the upper to lower regions of the cortex, respectively. SG, supragranular; G, granular; IG, infragranular.

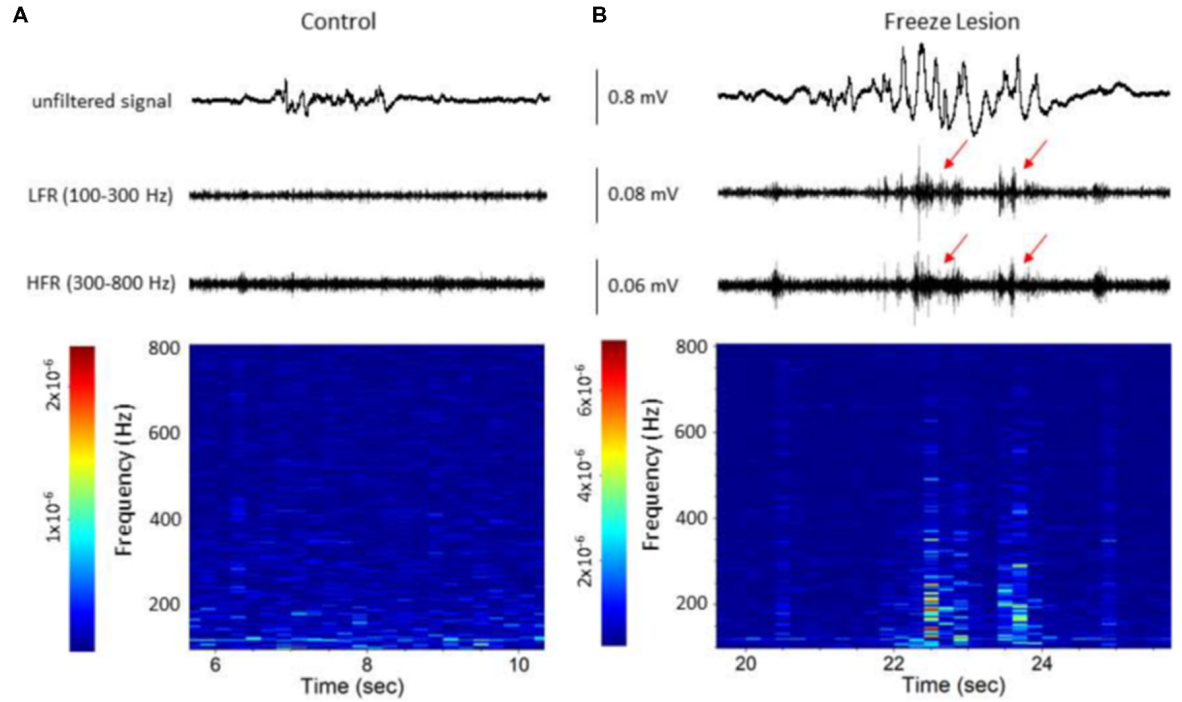

FIGURE 5 | Spectrograph analysis of B-S events demonstrating the increase in high-frequency spectral power that was observed during the HFOs. **(A)** B-S event from a control animal indicating a lack of HFOs (i.e., LFR and HFR, upper panel) and minimal change in high-frequency spectral power (spectrograph, lower panel). **(B)** B-S event from a freeze lesion animal indicating the presence of HFOs (red arrows, upper panel) and subsequent increase in high-frequency spectral power (spectrograph, lower panel). **(A,B)** The corresponding signal is presented above each spectrograph. Recordings are representative samples from the most superficial linear array electrode (CH01) of both a control and freeze lesion animal. Scale bar represents the PSD (dB) level for each spectrotemporal subunit.

of spectral power confined to frequencies below 30 Hz (**Figure 6B**, upper two panels). However, comparison across groups (i.e., control vs. freeze lesion) indicated that freeze lesion animals exhibited significant increases in PSD of up to 6 dB predominately below 80 Hz but extending up to 800 Hz, particularly in the upper cortical layers ($P < 0.05$, Holm-Sidak *post hoc* analysis, **Figure 6B**, lower panel). In freeze lesioned animals, peak PSD increases were observed in the alpha band (8–12 Hz; **Figure 6B**, black arrow, lower panel), a peak frequency range increase also observed during SWDs in this model thought to be associated with seizure generalization and synchronization across brain regions and hemispheres (Sun et al., 2016).

The LFP coherence of each recorded signal (referenced to channel 1) was used to evaluate the similarity in waveform patterns across cortical lamina. Channel 1 was chosen as the reference channel as is represents the upper most cortical layer that would dominate cortical EEG recordings and also indicated the most robust B-S activity in both control and freeze lesion animals (i.e., **Figure 6A**). Results indicated significant differences in LFP coherence across both frequency and electrode position for both control and freeze lesion animals ($P < 0.05$, multivariate ANOVA, **Figure 6C**). Both experimental groups exhibited a similar pattern of LFP coherence with a gradual drop in coherence values as the distance between the electrodes increased (i.e., lowest values for the deepest cortical layers) along with a sharp drop in coherence values above 50 Hz (**Figure 6C**, upper two panels). However, comparison of LFP coherence across groups (i.e., control vs. freeze lesion) indicated a differential change dependent on frequency and electrode depth. In comparison to controls, freeze lesion animals exhibited a significant increase in LFP coherence in the supragranular layer for signals above 50 Hz (50–200 Hz) and contrasting drop in LFP coherence in the lower granular and infragranular layers for signals lower than 70 Hz (15–70 Hz; $P < 0.05$, Holm-Sidak *post hoc* analysis, **Figure 6C** lower panel) suggesting an altered communication network between cortical layers of the malformed cortex (see "Discussion" section).

Laminar Profile of Spontaneous Single-Unit Activity Induced by Neonatal Freeze Lesions

Multi-units like spike activities (MUA, >300 Hz) were recorded from multiple sites in 7/7 sham treated animals (three males and four females, age = 7 ± 2 months, weight = 34 ± 2 g) and 12/12 FL animals (six males and six females, age = 8 ± 2 months, weight = 35 ± 2 g) during the spontaneous B-S period. The MUA in each animal were numerous and were not able to be separated for further analysis (e.g., **Figure 5**). Therefore, well isolated single-units (Sirota et al., 2008; Reyes-Puerta et al., 2016)

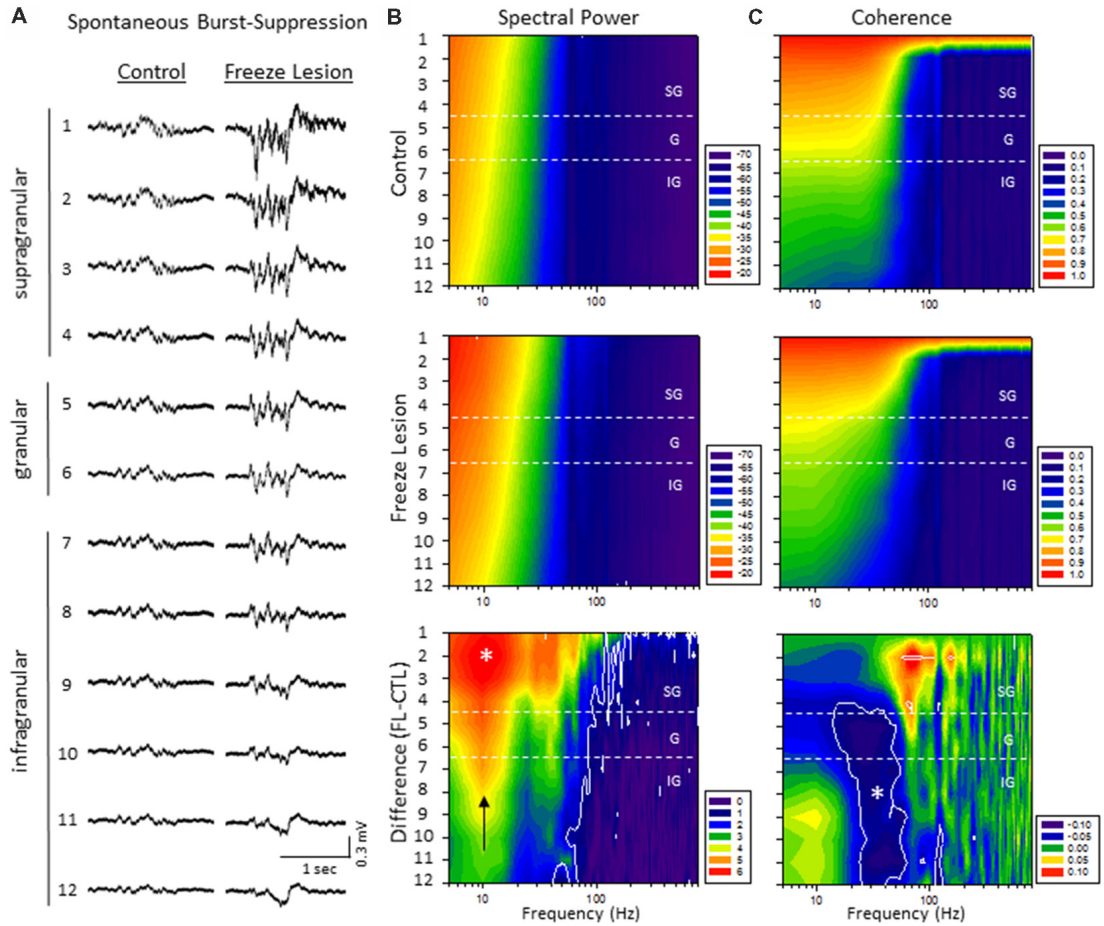

FIGURE 6 | A significant increase in spectral power and altered spectral coherence pattern were observed in the malformed cortex of freeze lesion animals as indicated from spectral analysis of linear electrode array recordings of anesthesia induced B-S. **(A)** Representative micro-electrode recordings of B-S events across cortical lamina from a control and freeze lesion animal under general anesthesia (2% isoflurane). **(B)** Average spectral power maps of control, freeze lesion, and the difference between each map. Black arrow indicates peak 10 Hz increase in PSD values from freeze lesion vs. control animals. **(C)** Average spectral LFP coherence maps of control, freeze lesion, and the difference between each map. **(B,C)** Values represent the group means from control (n = 12) and freeze lesion (n = 20) recordings. The topographic lines (solid white) indicate the $P < 0.05$ cutoff threshold and the white asterisks designate regions significantly different between groups (Holm-Sidak *post hoc* analysis). See "Results" section for additional statistical analysis.

were used to classify and map the location of spontaneously firing cells that occurred during periods of B-S across cortical lamina. Overall, detection of spontaneous unit activity was rare in the S1 region of control as compared to freeze lesion animals and no single-units were isolated from any of the control recordings (11 recordings, seven animals) while 17 well isolated single-units were recorded from the S1 region of freeze lesion animals (20 recordings, 12 animals). As such, all subsequent analysis was based on single-units isolated from freeze lesion animals. Single-units were classified as either putative excitatory (n = 9) or putative inhibitory (n = 8) cells based on their waveform pattern (**Figure 7**) using a previously published classification protocol (Reyes-Puerta et al., 2016). The isolated excitatory (EXC) and inhibitory (INH) single-units were validated with principal component analysis and shows (**Figure 8A**) complete separation as expected in both the same recordings from the same animals (e.g., **Figure 7**) or all animals (**Figure 8B**). Although all isolated single-units were confined to the upper cortical layers of the malformed cortices (electrodes 1–6), a differential distribution of excitatory vs. inhibitory cells was observed across cortical lamina (**Figure 8C**). The majority of excitatory cells (78%, 7/9 cells) were recorded from the upper cortical layers (channels 1–3) while the majority of inhibitory cells (75%, 6/8 cells) were recorded from deeper cortical structures including the granular layer (channels 4–6).

Phase-Locking of Putative Inhibitory Cells to HFOs

The plot of spike rates of individual units in most animals indicated an enhanced spiking during the LFP bursts (**Figures 7C**, **9A**). Next, SFC analysis was used to assess if single-unit firing patterns correlated to specific frequencies within the LFP including HFOs up to 1 kHz. Single-unit SFC values were averaged across electrodes 1–2, 3–4, and

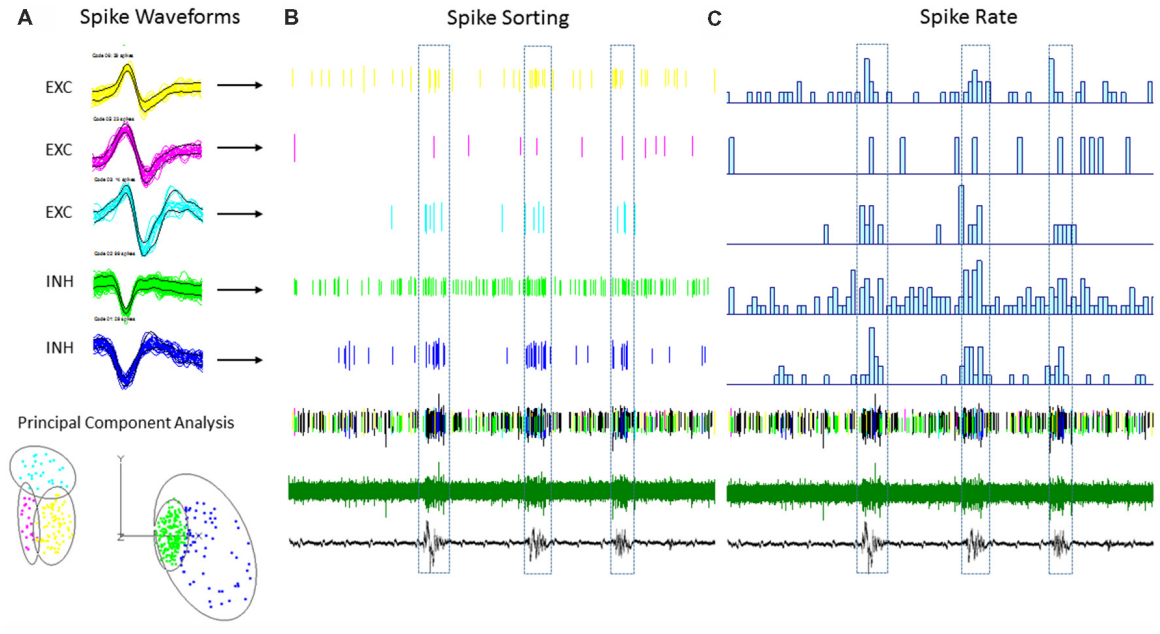

FIGURE 7 | An example of single-unit activities (SUAs) sorting during the B-S activities in a FL mouse. **(A)** Five (SUAs, three EXCs and two INHs) were shown from a single linear electrode recording. The spike amplitude and duration of these SUAs formed two separate large clusters using principal component analysis, INHs and EXCs are clustered together. **(B)** Raster plot showing the spike time of each spike aligned to the B-S LFPs. **(C)** The spike rate plotted on top of the LFPs. The spike rates are higher for all SUAs during the bursts activities.

5–6 to evaluate laminar differences. Significant increases in SFC values were observed in cells from the deeper cortical regions as compared to the most superficial electrodes; 188–468 Hz (electrodes 3–4) and 344–531 Hz (electrodes 5–6) as compared electrodes 1–2 (Holm-Sidak *post hoc* analysis). A Pearson's correlation analysis also indicated a significant increase in maximum SFC values across recording electrode depth (**Figure 8D**). Given the differential laminar distribution across cell type, a subset analysis was used to compare SFC values between the upper excitatory cells recorded from channel 1 (n = 5) and the lower inhibitory cells recorded from channel 4 (n = 4) that represent the cortical location of the highest percentage of cells recorded for each cell type (i.e., **Figure 8C**). Results indicated only weak SFC for the excitatory cells located in the superficial cortical layers as compared to the significantly higher values measured from the deeper inhibitory cells, specifically for frequencies above 250 Hz (**Figure 8E**).

To further address the correlation between unit firing and HFOs a firing phase analysis was used to evaluate possible phase-locking of unit activity across different frequency bandwidths. Both EXC (CH01) and INH (CH04) cells exhibited increases in firing rate during periods of B-S as demonstrated in **Figure 9A** (left column), however, only INH (CH04) cells indicated strong phase locking to HFO phase as demonstrated in **Figure 9A** (right column). Statistical analysis across groups indicated significant increases in firing probability in the higher HFO ranges (100–300 and 300–800 Hz, $P < 0.05$) but not for the lower gamma range (25–100 Hz, $P > 0.05$; multivariate ANOVA) although the results were dependent on cell type ($P < 0.05$, interaction between frequency × phase). *Post hoc* analysis indicated that the INH (CH04) cells had significantly higher firing probabilities across the 100–300 and 300–800 Hz oscillations, confined to the downward slope of the individual waveform (i.e., phase angles ranging between 250 and 350°, **Figure 9B**, left column). Polar plots are also presented to demonstrate the strong phase locking of the INH cells across the high-frequency range (>100 Hz) associated with ripple activity (**Figures 8F**, **9B**, right column).

In sham treated animals, well-isolated single-units were rare (2/7 mice), presumably because the suppression of activities associated with the anesthesia. To further validate if this was the case, we expressed channel-rhodopsin 2 (ChR2) in S1 of shame treated mice and examined the evoked single-units activities (SUAs; **Figure 10**). In 5/5 mice examined, blue laser (480 nm) delivered locally *via* a fiber optic positioned next to the recording site reliably evoked SUAs in 5/5 mice in majority of the electrode sites in the cortex (**Figure 10**) under all anesthesia levels (0.5%–2% isoflurane) thus the lack of the SUAs in sham-treated animals were unlikely to be caused by damage or some artifact.

DISCUSSION

In the current study, we evaluate the response of the malformed cortex to hyper-excitable activation due to anesthesia-induced B-S. Utilization of the B-S model represents a novel method

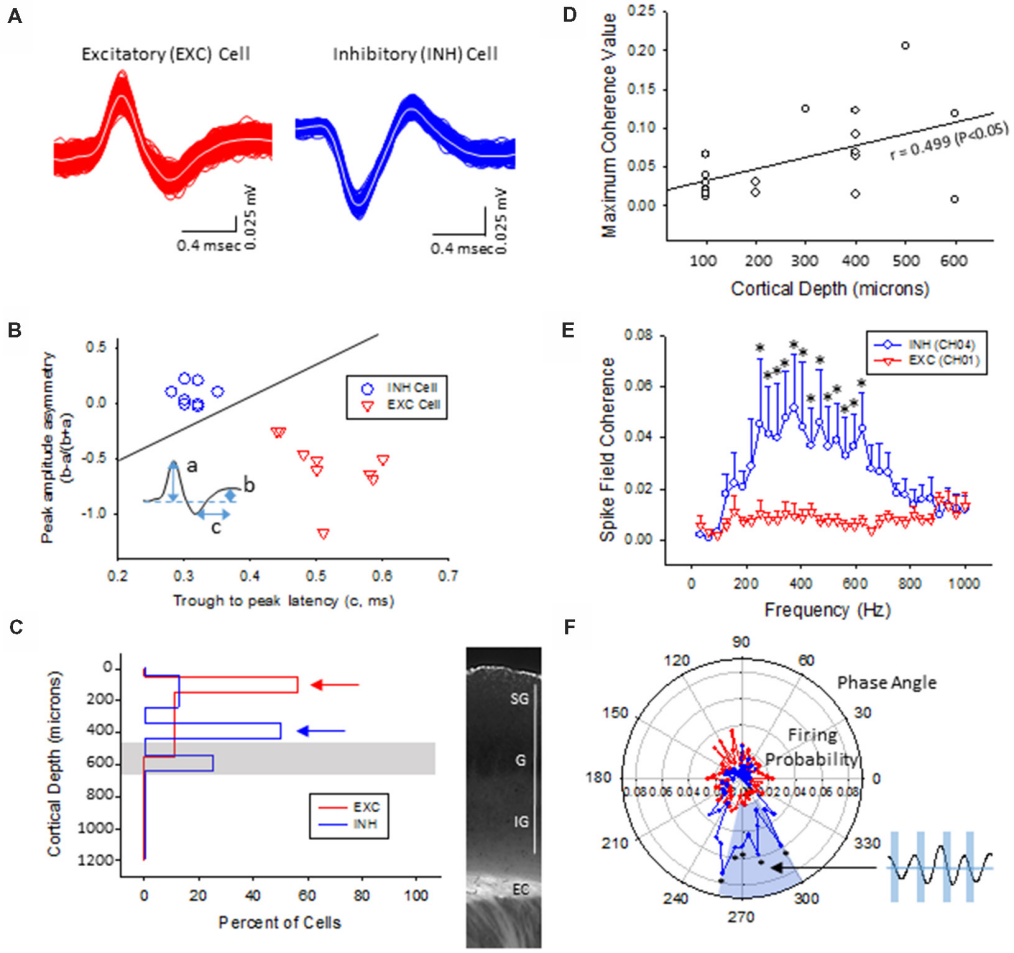

FIGURE 8 | Inhibitory cells from the lower supragranular layer were phase-locked to HFR oscillations in the malformed cortex of freeze lesion animals. **(A)** Spike sorting of a putative excitatory (red) and inhibitory (blue) cell, based on the associated waveform of each spike. White line in each trace represents the average of the multiple overlapping traces shown in color. **(B)** Three parameters were calculated from the average trace of each spike waveform (a–c as indicated from inset) to extract features used to classify neurons as either excitatory or inhibitory. Solid line represents the cutoff used to classify excitatory vs. inhibitory cells (Reyes-Puerta et al., 2016). **(C)** Distribution of isolated single-units across cortical depth. Value of 0 = cortical surface. Arrows indicate the cortical level that expressed the maximal number of excitatory vs. inhibitory neurons. Gray bar indicates level of the granular layer. Representative section of the S1 cortex is shown in the right panel for comparison. White bar = 1,000 μm. EC, external capsule. **(D)** Pearson's correlation between maximum spike field coherence (SFC) values and cortical depth. **(E)** Average SFC values between excitatory (CH01, $n = 5$) and inhibitory cells (CH04, $n = 4$) across frequency bin. $^*P < 0.05$, Holm-Sidak *post hoc* analysis between groups. **(F)** Polar plot of average firing probability of excitatory (CH01, $n = 5$, red) and inhibitory (CH04, $n = 4$, blue) units across phase angle of the HFR spectrum (300–800 Hz). Inhibitory cells indicated phase-locked responses (blue shaded region) to the downward phase of the corresponding ripple wave (i.e., see inset). $^*P < 0.05$, Holm-Sidak *post hoc* analysis between groups.

to explore neural hyperexcitability in epileptic brain and has recently been characterized in the neonatal freeze lesion model (Williams et al., 2016). B-S is a transitional brain state of induced hyper-excitability that occurs between signal suppression (deep anesthesia) and slow-wave activity (light anesthesia) that can be induced in both humans and animals by a variety of anesthetics with different modes of action (Kroeger and Amzica, 2007; Ferron et al., 2009). Previous studies have indicated that the incidence and spectral power of B-S events are significantly increased in freeze lesion animals, confined to the upper cortical layers, and often contain spike-and-wave components similar to the SWDs observed in unanesthetized animals (Williams et al., 2016). In the current study, we show that the upper cortical region of the malformed cortex is also associated with a significant increase in HFOs similar to that observed during SWDs in unanesthetized animals and are phase-locked to laminar-specific inhibitory cells within the deep supragranular layer.

The use of high-density linear micro-electrode arrays allowed for cross-laminar mapping of the S1 cortex and indicated distinct disruptions in spectrotemporal architecture near the site of the freeze lesion-induced microgyrus. In particular, a significant increase in spectral power was observed in the malformed cortex with peak increases near 10 Hz, a frequency dominated by SWDs in awake animals (Sun et al., 2016). In addition, the

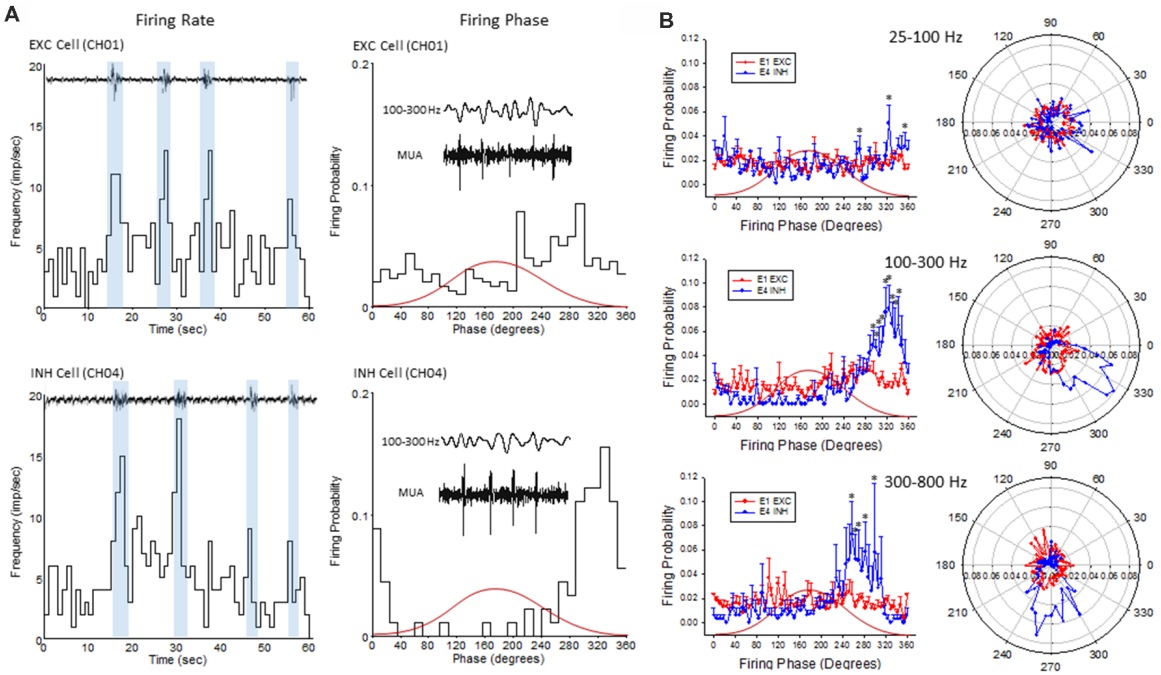

FIGURE 9 | Firing phase analysis between EXC units recorded from channel 1 (CH01) and INH units recorded from (CH04) across HFO bandwidths. **(A)** Firing rate (left column) of exemplar EXC (top) and INH (bottom) single-units in comparison to B-S activity. Blue bars indicate the increase in firing rate during B-S events. Firing phase (right column) of these same units in relation to HFOs (100–300 Hz). **(B)** Average firing phase (left column) of EXC (CH01, $n = 5$) and INH (CH04, $n = 4$) units across three frequency distributions. $^*P < 0.05$ between groups (Holm-Sidak *post hoc* analysis). The same data is presented in polar plots (right column) to demonstrate the relative phase-locking of average unit activity across each frequency spectrum. Red curves in **(A,B)** indicate the relative phase of the associated waveform.

increases in spectral power extended into the high frequency range (>100 Hz) along the upper cortical layers including an increase in MUA. Clinical evidence from epileptic patients with cortical dysplasia indicates that a hyperexcitable zone exists within the dysplastic cortex adjacent to the microgyric lesion though it can extend into nearby structurally intact tissues (Mattia et al., 1995; Palmini et al., 1995; Guerrini and Dobyns, 2014). Similar *in vitro* results have also been obtained in several experimental studies that have defined electrophysiological hyperexcitabilities in both dysplastic cortex and adjacent regions of normatopic tissue (Jacobs et al., 1996; Luhmann et al., 1998; Redecker et al., 1998). In particular, a study by Redecker et al. (2005) indicated a defined region of epileptogenicity that was strongest in the upper layers of the dysplastic cortex which then spread to adjacent regions through superficial cortical layers as determined from optical imaging of neuronal activity during induced epileptiform events in cortical slice preparations. The specific anatomical or physiological alterations that drive the induced hyper-excitability surrounding the freeze-lesion induced microgyrus is currently unknown though altered expression patterns of excitatory and inhibitory receptors within this region has been established (Zilles et al., 1998; Redecker et al., 2000), likely leading to shifts in the normal excitatory/inhibitory tone of the affected tissue. Neonatal freeze-lesions also disrupt cortical cell function likely due to a hyper-innervation of ascending input into dysplastic regions that originally targeted cells within the microgyrus (Jacobs et al., 1999c; Rosen and Galaburda, 2000; Jacobs and Prince, 2005; Zhou and Roper, 2010). However, additional circuit analysis will be necessary to define the specific cortical circuits that may be responsible for the induced hyper-excitability observed in the supra-granular layer of the dysplastic cortex.

The current study also revealed a distinct pattern of altered LFP coherence in the malformed cortex offering further evidence of disturbed columnar and laminar communication network within the S1 region. The role of brain oscillations and their effect on neural communication is an active area of research that suggests that the synchrony or coherence of specific frequency bands are linked to specific behavioral and cognitive processes (Buzsáki and Schomburg, 2015). Specifically, a significant increase in LFP coherence was observed in freeze lesion animals across the supragranular layer in the upper gamma frequency range (50–200 Hz). In general, gamma-band synchronization is thought to be involved in the entrainment of neural networks (Singer and Gray, 1995; Jensen et al., 2007; Buzsáki and Silva, 2012) and may be a consequence of the increase in spectral activity as observed in the upper cortical layers in the current study. In contrast, a drop in LFP coherence between the upper and lower cortical layers was measured across beta and lower gamma frequencies (15–70 Hz). Disruption of beta rhythms within the S1 region may distort normal somatosensory processing (Fransen et al., 2016)

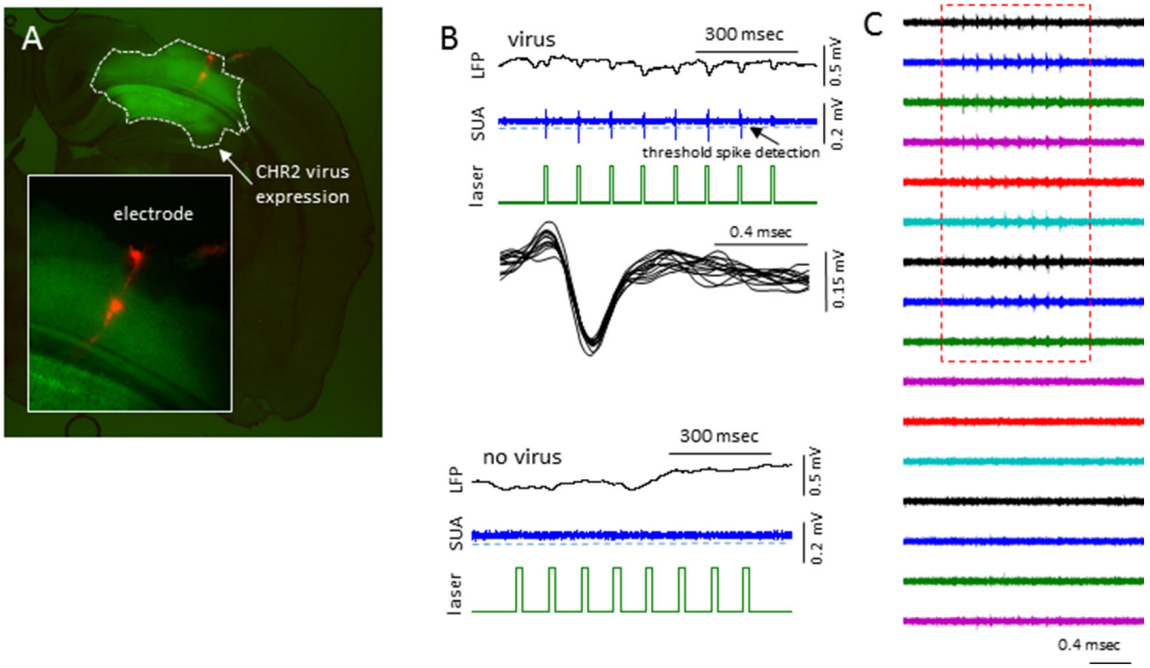

FIGURE 10 | Laser activation induces reliable SUAs in the sham-treated animals. **(A)** Photomicrograph of brain slice showing the channel-rhodopsin 2 (ChR2) transfected S1 region and location of linear electrodes across the center of the ChR2 transfected area. **(B)** In AAV-ChR2 transfected sham-treated animals, repeated exposure to short blue laser pulses (0.2 s), reliably and repeatedly induced SUAs in the S1 of ChR2 transfected brain but not in the slices without ChR2 expression. **(C)** The laser evoked SUA were distributed in the top 9/12 cortical sites.

and could lead to the observed behavioral changes that have been reported in this freeze lesion model (Sun et al., 2016).

Similar to the pattern of HFOs and increased spectral power observed across cortical lamina, spike sorting of spontaneous hyperexcitable unit activity in the malformed cortex was isolated to the upper half of the S1 region with a differential distribution of putative excitatory vs. inhibitory cells across layers. The majority of excitatory cells were recorded from the most superficial layers of the S1 cortex while inhibitory cells were mainly expressed in the deeper supragranular and granular layers. Although the highest incidence of HFO activity was observed in the most superficial cortical electrodes, the SFC of isolated single-units was strongest for deeper cortical layers, specifically for fast ripple frequencies ($>$250 Hz). The differential distribution of cell types and stronger SFC values within the deep supragranular and granular layers has not been previously reported in FCD models or in patients with cortical dysplasia. Further analysis of excitatory cells recorded from the most superficial cortical layers indicated only weak phase-locking to HFOs in comparison to the strong phase-locking of inhibitory cells located in the lower supragranular layer to fast ripple band frequencies (possibly emanating from cells within the granular layer). These data suggest that the deeper inhibitory cells may be the driving substrate of ripple waves near the site of the microgyric lesion. It should be noted that these results were obtained under isoflurane anesthesia and should be verified in awake animals as well. However, in line with these results, the concept of abnormal glutamatergic excitation as the driving force behind initiation of epileptic discharges has been challenged in favor of a possible role of GABAergic inhibition in shaping ictal activity (de Curtis and Avoli, 2016). It should also be noted that the classification of SUAs into excitatory and inhibitory cells type is based on waveforms recorded in extracellular field potentials. A limitation of this method vs. intracellular recording is that the waveform varies base on a number of factors, including the composition of the electrode, impedance, distance from the recorded neuron, and distance to different cellular compartment in which the extracellular signals were generated, etc. Given the diversity of interneurons and their different firing properties, it has been estimated that the present methods may cause upward of 30% misclassified cell types for INH cells and about 5% neurons identified as EXC cell types might be interneurons (Reyes-Puerta et al., 2016). Despite this confounding factor, our data still indicate robust differences in phase coupling between INH vs. EXC cell types. However, we would like to caution readers to use caution when they use this portion of our results. A more robust relationship requires larger set of experimental data.

AUTHOR CONTRIBUTIONS

Q-QS designed the experiments, co-wrote the manuscript. AW designed the experiments, performed data analysis and wrote the manuscript.

FUNDING

This research provided from National Institute of Neurological Disorders and Stroke (NINDS)/National Institute of General Medical Sciences (NIGMS, NIH) grant 5R01NS094550 and 5P20GM121310-02.

ACKNOWLEDGMENTS

We thank Sun lab members for assistance with the freeze lesion procedure and Chunzhao Zhang for maintenance of animal lines. We thank Chen Zhou for performing EEG recordings.

REFERENCES

Amzica, F. (2009). Basic physiology of burst-suppression. *Epilepsia* 50, 38–39. doi: 10.1111/j.1528-1167.2009.02345.x

Avoli, M., Bernasconi, A., Mattia, D., Olivier, A., and Hwa, G. G. (1999). Epileptiform discharges in the human dysplastic neocortex: *in vitro* physiology and pharmacology. *Ann. Neurol.* 46, 816–826. doi: 10.1002/1531-8249(199912)46:6<816::aid-ana3>3.0.co;2-o

Bragin, A., Azizyan, A., Almajano, J., and Engel, J. Jr. (2009). The cause of the imbalance in the neuronal network leading to seizure activity can be predicted by the electrographic pattern of the seizure onset. *J. Neurosci.* 29, 3660–3671. doi: 10.1523/JNEUROSCI.5309-08.2009

Brázdil, M., Halámek, J., Jurák, P., Daniel, P., Kuba, R., Chrastina, J., et al. (2010). Interictal high-frequency oscillations indicate seizure onset zone in patients with focal cortical dysplasia. *Epilepsy Res.* 90, 28–32. doi: 10.1016/j.eplepsyres.2010.03.003

Buzsáki, G., and Schomburg, E. W. (2015). What does γ coherence tell us about inter-regional neural communication? *Nat. Neurosci.* 18, 484–489. doi: 10.1038/nn.3952

Buzsáki, G., and Silva, F. L. (2012). High frequency oscillations in the intact brain. *Prog. Neurobiol.* 98, 241–249. doi: 10.1016/j.pneurobio.2012.02.004

Cepeda, C., André, V. M., Hauptman, J. S., Yamazaki, I., Huynh, M. N., Chang, J. W., et al. (2012). Enhanced GABAergic network and receptor function in pediatric cortical dysplasia Type IIB compared with Tuberous Sclerosis Complex. *Neurobiol. Dis.* 45, 310–321. doi: 10.1016/j.nbd.2011.08.015

Cuello-Oderiz, C., von Ellenrieder, N., Sankhe, R., Olivier, A., Hall, J., Dubeau, F., et al. (2018). Value of ictal and interictal epileptiform discharges and high frequency oscillations for delineating the epileptogenic zone in patients with focal cortical dysplasia. *Clin. Neurophysiol.* 129, 1311–1319. doi: 10.1016/j.clinph.2018.02.003

de Curtis, M., and Avoli, M. (2016). GABAergic networks jump-start focal seizures. *Epilepsia* 57, 679–687. doi: 10.1111/epi.13370

Dvorak, K., Feit, J., and Juránková, Z. (1978). Experimentally induced focal microgyria and status verrucosus deformis in rats—pathogenesis and interrelation. Histological and autoradiographical study. *Acta Neuropathol.* 44, 121–129. doi: 10.1007/bf00691477

Eichler, S. A., and Meier, J. C. (2008). E-I balance and human diseases—from molecules to networking. *Front. Mol. Neurosci.* 1:2. doi: 10.3389/neuro.02.002.2008

Fedele, T., van't Klooster, M., Burnos, S., Zweiphenning, W., van Klink, N., Leijten, F., et al. (2016). Automatic detection of high frequency oscillations during epilepsy surgery predicts seizure outcome. *Clin. Neurophysiol.* 127, 3066–3074. doi: 10.1016/j.clinph.2016.06.009

Ferrari-Marinho, T., Perucca, P., Dubeau, F., and Gotman, J. (2016). Intracranial EEG seizure onset-patterns correlate with high-frequency oscillations in patients with drug-resistant epilepsy. *Epilepsy Res.* 127, 200–206. doi: 10.1016/j.eplepsyres.2016.09.009

Ferrari-Marinho, T., Perucca, P., Mok, K., Olivier, A., Hall, J., Dubeau, F., et al. (2015). Pathologic substrates of focal epilepsy influence the generation of high-frequency oscillations. *Epilepsia* 56, 592–598. doi: 10.1111/epi.12940

Ferron, J. F., Kroeger, D., Chever, O., and Amzica, F. (2009). Cortical inhibition during burst suppression induced with isoflurane anesthesia. *J. Neurosci.* 29, 9850–9860. doi: 10.1523/JNEUROSCI.5176-08.2009

Fransen, A. M., Dimitriadis, G., van Ede, F., and Maris, E. (2016). Distinct α- and β-band rhythms over rat somatosensory cortex with similar properties as in humans. *J. Neurophysiol.* 115, 3030–3044. doi: 10.1152/jn.00507.2015

Frauscher, B., von Ellenrieder, N., Ferrari-Marinho, T., Avoli, M., Dubeau, F., and Gotman, J. (2015). Facilitation of epileptic activity during sleep is mediated by high amplitude slow waves. *Brain* 138, 1629–1641. doi: 10.1093/brain/awv073

Fujiwara, H., Greiner, H. M., Lee, K. H., Holland-Bouley, K. D., Seo, J. H., Arthur, T., et al. (2012). Resection of ictal high-frequency oscillations leads to favorable surgical outcome in pediatric epilepsy. *Epilepsia* 53, 1607–1617. doi: 10.1111/j.1528-1167.2012.03629.x

Guerrini, R., and Dobyns, W. B. (2014). Malformations of cortical development: clinical features and genetic causes. *Lancet Neurol.* 13, 710–726. doi: 10.1016/s1474-4422(14)70040-7

Ibrahim, G. M., Wong, S. M., Anderson, R. A., Singh-Cadieux, G., Akiyama, T., Ochi, A., et al. (2014). Dynamic modulation of epileptic high frequency oscillations by the phase of slower cortical rhythms. *Exp. Neurol.* 251, 30–38. doi: 10.1016/j.expneurol.2013.10.019

Jacobs, K. M., Gutnick, M. J., and Prince, D. A. (1996). Hyperexcitability in a model of cortical maldevelopment. *Cereb. Cortex* 6, 514–523. doi: 10.1093/cercor/6.3.514

Jacobs, K. M., Hwang, B. J., and Prince, D. A. (1999a). Focal epileptogenesis in a rat model of polymicrogyria. *J. Neurophysiol.* 81, 159–173. doi: 10.1152/jn.1999.81.1.159

Jacobs, K. M., Kharazia, V. N., and Prince, D. A. (1999b). Mechanisms underlying epileptogenesis in cortical malformations. *Epilepsy Res.* 36, 165–188. doi: 10.1016/s0920-1211(99)00050-9

Jacobs, K. M., Mogensen, M., Warren, E., and Prince, D. A. (1999c). Experimental microgyri disrupt the barrel field pattern in rat somatosensory cortex. *Cereb. Cortex* 9, 733–744. doi: 10.1093/cercor/9.7.733

Jacobs, J., Levan, P., Châtillon, C. E., Olivier, A., Dubeau, F., and Gotman, J. (2009). High frequency oscillations in intracranial EEGs mark epileptogenicity rather than lesion type. *Brain* 132, 1022–1037. doi: 10.1093/brain/awn351

Jacobs, K. M., and Prince, D. A. (2005). Excitatory and inhibitory postsynaptic currents in a rat model of epileptogenic microgyria. *J. Neurophysiol.* 93, 687–696. doi: 10.1152/jn.00288.2004

Jacobs, J., Staba, R., Asano, E., Otsubo, H., Wu, J. Y., Zijlmans, M., et al. (2012). High-frequency oscillations (HFOs) in clinical epilepsy. *Prog. Neurobiol.* 98, 302–315. doi: 10.1016/j.pneurobio.2012.03.001

Jensen, O., Kaiser, J., and Lachaux, J. P. (2007). Human γ-frequency oscillations associated with attention and memory. *Trends Neurosci.* 30, 317–324. doi: 10.1016/j.tins.2007.05.001

Kerber, K., LeVan, P., Dumpelmann, M., Fauser, S., Korinthenberg, R., Schulze-Bonhage, A., et al. (2013). High frequency oscillations mirror disease activity in patients with focal cortical dysplasia. *Epilepsia* 54, 1428–1436. doi: 10.1111/epi.12262

Kroeger, D., and Amzica, F. (2007). Hypersensitivity of the anesthesia-induced comatose brain. *J. Neurosci.* 27, 10597–10607. doi: 10.1523/JNEUROSCI.3440-07.2007

Lévesque, M., Salami, P., Gotman, J., and Avoli, M. (2012). Two seizure-onset types reveal specific patterns of high-frequency oscillations in a model of temporal lobe epilepsy. *J. Neurosci.* 32, 13264–13272. doi: 10.1523/JNEUROSCI.5086-11.2012

Luhmann, H. J. (2016). Models of cortical malformation—chemical and physical. *J. Neurosci. Methods* 260, 62–72. doi: 10.1016/j.jneumeth.2015.03.034

Luhmann, H. J., and Raabe, K. (1996). Characterization of neuronal migration disorders in neocortical structures: I. Expression of epileptiform activity in an animal model. *Epilepsy Res.* 26, 67–74. doi: 10.1016/s0920-1211(96)00041-1

Luhmann, H. J., Raabe, K., Qu, M., and Zilles, K. (1998). Characterization of neuronal migration disorders in neocortical structures: extracellular *in vitro* recordings. *Eur. J. Neurosci.* 10, 3085–3094. doi: 10.1046/j.1460-9568.1998.00311.x

Matsumoto, A., Brinkmann, B. H., Matthew Stead, S., Matsumoto, J., Kucewicz, M. T., Marsh, W. R., et al. (2013). Pathological and physiological

high-frequency oscillations in focal human epilepsy. *J. Neurophysiol.* 110, 1958–1964. doi: 10.1152/jn.00341.2013

Mattia, D., Olivier, A., and Avoli, M. (1995). Seizure-like discharges recorded in human dysplastic neocortex maintained *in vitro*. *Neurology* 45, 1391–1395. doi: 10.1212/wnl.45.7.1391

Moosa, A. N., and Gupta, A. (2014). Outcome after epilepsy surgery for cortical dysplasia in children. *Childs Nerv. Syst.* 30, 1905–1911. doi: 10.1007/s00381-014-2556-7

Ogren, J. A., Bragin, A., Wilson, C. L., Hoftman, G. D., Lin, J. J., Dutton, R. A., et al. (2009). Three-dimensional hippocampal atrophy maps distinguish two common temporal lobe seizure-onset patterns. *Epilepsia* 50, 1361–1370. doi: 10.1111/j.1528-1167.2008.01881.x

Palmini, A., Gambardella, A., Andermann, F., Dubeau, F., da Costa, J. C., Olivier, A., et al. (1995). Intrinsic epileptogenicity of human dysplastic cortex as suggested by corticography and surgical results. *Ann. Neurol.* 37, 476–487. doi: 10.1002/ana.410370410

Perucca, P., Dubeau, F., and Gotman, J. (2014). Intracranial electroencephalographic seizure-onset patterns: effect of underlying pathology. *Brain* 137, 183–196. doi: 10.1093/brain/awt299

Redecker, C., Hagemann, G., Köhling, R., Straub, H., Witte, O. W., and Speckmann, E. J. (2005). Optical imaging of epileptiform activity in experimentally induced cortical malformations. *Exp. Neurol.* 192, 288–298. doi: 10.1016/j.expneurol.2004.11.018

Redecker, C., Luhmann, H. J., Hagemann, G., Fritschy, J. M., and Witte, O. W. (2000). Differential downregulation of $GABA_A$ receptor subunits in widespread brain regions in the freeze-lesion model of focal cortical malformations. *J. Neurosci.* 20, 5045–5053. doi: 10.1523/JNEUROSCI.20-13-05045.2000

Redecker, C., Lutzenburg, M., Gressens, P., Evrard, P., Witte, O. W., and Hagemann, G. (1998). Excitability changes and glucose metabolism in experimentally induced focal cortical dysplasias. *Cereb. Cortex* 8, 623–634. doi: 10.1093/cercor/8.7.623

Reyes-Puerta, V., Yang, J. W., Siwek, M. E., Kilb, W., Sun, J. J., and Luhmann, H. J. (2016). Propagation of spontaneous slow-wave activity across columns and layers of the adult rat barrel cortex *in vivo*. *Brain Struct. Funct.* 221, 4429–4449. doi: 10.1007/s00429-015-1173-x

Roper, S. N., King, M. A., Abraham, L. A., and Boillot, M. A. (1997). Disinhibited *in vitro* neocortical slices containing experimentally induced cortical dysplasia demonstrate hyperexcitability. *Epilepsy Res.* 26, 443–449. doi: 10.1016/s0920-1211(96)01014-5

Rosen, G. D., and Galaburda, A. M. (2000). Single cause, polymorphic neuronal migration disorders: an animal model. *Dev. Med. Child Neurol.* 42, 652–662. doi: 10.1111/j.1469-8749.2000.tb00675.x

Singer, W., and Gray, C. M. (1995). Visual feature integration and the temporal correlation hypothesis. *Annu. Rev. Neurosci.* 18, 555–586. doi: 10.1146/annurev.ne.18.030195.003011

Sirota, A., Montgomery, S., Fujisawa, S., Isomura, Y., Zugaro, M., and Buzsáki, G. (2008). Entrainment of neocortical neurons and γ oscillations by the hippocampal theta rhythm. *Neuron* 60, 683–697. doi: 10.1016/j.neuron.2008.09.014

Sisodiya, S. M. (2000). Surgery for malformations of cortical development causing epilepsy. *Brain* 123, 1075–1091. doi: 10.1093/brain/123.6.1075

Sun, Q. Q., Zhou, C., Yang, W., and Petrus, D. (2016). Continuous spike-waves during slow-wave sleep in a mouse model of focal cortical dysplasia. *Epilepsia* 57, 1581–1593. doi: 10.1111/epi.13501

van Diessen, E., Hanemaaijer, J. I., Otte, W. M., Zelmann, R., Jacobs, J., Jansen, F. E., et al. (2013). Are high frequency oscillations associated with altered network topology in partial epilepsy? *Neuroimage* 82, 564–573. doi: 10.1016/j.neuroimage.2013.06.031

van Klink, N., Frauscher, B., Zijlmans, M., and Gotman, J. (2016). Relationships between interictal epileptic spikes and ripples in surface EEG. *Clin. Neurophysiol.* 127, 143–149. doi: 10.1016/j.clinph.2015.04.059

Williams, A. J., Zhou, C., and Sun, Q. Q. (2016). Enhanced burst-suppression and disruption of local field potential synchrony in a mouse model of focal cortical dysplasia exhibiting spike-wave seizures. *Front. Neural Circuits* 10:93. doi: 10.3389/fncir.2016.00093

Wu, C., Wais, M., Sheppy, E., del Campo, M., and Zhang, L. (2008). A glue-based, screw-free method for implantation of intra-cranial electrodes in young mice. *J. Neurosci. Methods* 171, 126–131. doi: 10.1016/j.jneumeth.2008.03.001

Zhou, F. W., and Roper, S. N. (2010). Altered firing rates and patterns in interneurons in experimental cortical dysplasia. *Cereb. Cortex* 21, 1645–1658. doi: 10.1093/cercor/bhq234

Zhu, W. J., and Roper, S. N. (2000). Reduced inhibition in an animal model of cortical dysplasia. *J. Neurosci.* 20, 8925–8931. doi: 10.1523/JNEUROSCI.20-23-08925.2000

Zijlmans, M., Jiruska, P., Zelmann, R., Leijten, F. S., Jefferys, J. G., and Gotman, J. (2012). High-frequency oscillations as a new biomarker in epilepsy. *Ann. Neurol.* 71, 169–178. doi: 10.1002/ana.22548

Zilles, K., Qu, M., Schleicher, A., and Luhmann, H. J. (1998). Characterization of neuronal migration disorders in neocortical structures: quantitative receptor autoradiography of ionotropic glutamate, $GABA_A$ and $GABA_B$ receptors. *Eur. J. Neurosci.* 10, 3095–3106. doi: 10.1046/j.1460-9568.1998.00322.x

Conflict of Interest Statement: The authors declare that the research was conducted in the absence of any commercial or financial relationships that could be construed as a potential conflict of interest.

frontiers in Neural Circuits

ORIGINAL RESEARCH
published: 22 February 2019
doi: 10.3389/fncir.2019.00012

Compensatory Neural Responses to Cognitive Fatigue in Young and Older Adults

*Immanuel Babu Henry Samuel[1], Chao Wang[1], Sarah E. Burke[2], Benzi Kluger[3] and Mingzhou Ding[1]**

[1] J. Crayton Pruitt Family Department of Biomedical Engineering, University of Florida, Gainesville, FL, United States, [2] Department of Neuroscience, University of Florida, Gainesville, FL, United States, [3] Department of Neurology, University of Colorado, Denver, Denver, CO, United States

Prolonged performance of a demanding cognitive task induces cognitive fatigue. We examined the behavioral and neural responses to fatigue-induced cognitive impairments in young and older adults. Particular emphasis was placed on whether the brain exhibited compensatory neural activity in response to cognitive fatigue. High-density EEG was recorded from a young (n = 16; 18–33 years of age) and an older (n = 18; 60–87 years of age) cohort who performed a Stroop task continuously for ∼2 h with no breaks. In the young cohort, behavioral performance declined as the experiment progressed, reflecting the deleterious effects of cognitive fatigue. Neurophysiologically, in addition to declining neural activity as cognitive fatigue developed, there is also evidence of region- and time-specific increase in neural activity, suggesting neural compensation. The compensatory activities followed patterns paralleling that of posterior-anterior shift in aging (PASA) and early to late shift in aging (ELSA) observed in cognitive aging and helped to moderate fatigue-induced behavioral deterioration. In the older cohort, behavioral performance did not decline as the experiment progressed, and neural activity either declined or stayed unchanged, showing no evidence of neural compensation, in contrast to the young. These results suggest that young and older adults coped with cognitive fatigue differently by exhibiting differential responses as a function of time-on-task at both the behavioral level and the neural level.

Keywords: mental fatigue, young, old, reactive cognitive control, brain compensation, EEG, Stroop

OPEN ACCESS

Edited by:
Fu-Ming Zhou,
The University of Tennessee Health Science Center (UTHSC), United States

Reviewed by:
Nicoletta Berardi,
National Research Council (CNR), Italy
Lijuan Hou,
Beijing Normal University, China

***Correspondence:**
Mingzhou Ding
mding@bme.ufl.edu

Received: *24 September 2018*
Accepted: *06 February 2019*
Published: *22 February 2019*

Citation:
Babu Henry Samuel I, Wang C, Burke SE, Kluger B and Ding M (2019) Compensatory Neural Responses to Cognitive Fatigue in Young and Older Adults. Front. Neural Circuits 13:12. doi: 10.3389/fncir.2019.00012

INTRODUCTION

Compared to the appropriate control groups, cognition is generally impaired in the aged population and in patients suffering from neurological diseases. For the aged population, the appropriate control group is healthy young adults, whereas for neurological patients, the appropriate control group is gender- and age-matched healthy individuals. Neurophysiologically, task-evoked neural responses in the aging or diseased brain are generally weaker, signifying impaired brain function (Carter et al., 2001; Lorist et al., 2005; Cader et al., 2006; Cheng and Hsu, 2011). However, studies have also found brain regions where the activation is stronger in aging and in neurological diseases, and these increased activities are thought to reflect neural compensation (Cabeza et al., 2002); the neural networks associated with these compensatory activities are termed

compensatory neural networks (Reuter-Lorenz and Cappell, 2008). When performing a task, these compensatory neural networks may get engaged when the primary task network is impaired, with this engagement yielding behavioral benefits (Anderer et al., 2003; Lum et al., 2009; Wang et al., 2016; Babu Henry Samuel et al., 2018).

Cognitive aging research has identified several general patterns of compensatory neural activity. For example, posterior-anterior shift in aging (PASA) reflects that impaired posterior sensory processing is associated with increased compensatory activity in higher-order anterior brain areas (Cabeza et al., 2004). Early to late shift in aging (ELSA), observed in age-related impairments during working memory tasks, reflects a reduction in brain activity during an early period of neural processing (e.g., memory retention), which is then followed by increase in brain activity in a later period of neural processing (e.g., memory retrieval) (Dew et al., 2012).

As alluded to earlier, most studies of neural compensation utilize a between-subject design, such as old-versus-young or diseased-versus-healthy. We have recently begun to examine neural compensation in a fatigue paradigm in which participants are asked to perform a demanding cognitive task for a prolonged period of time (Wang et al., 2014). This paradigm reliably induces cognitive fatigue. In young adults, with increasing cognitive fatigue, behavioral performance declined, and there is evidence of neural compensation that accompanies fatigue-induced cognitive impairments (Wang et al., 2016). To what extent the aforementioned patterns of compensatory neural activities typically associated with aging-related cognitive impairments can be generalized to neural responses to cognitive-fatigue induced impairments in the young population has not been studied. Addressing this problem is the first objective of this study.

For older adults, compensatory mechanisms are engaged at baseline, as the foregoing discussion suggests, to counteract the deleterious effects of cognitive decline in aging (Davis et al., 2008; Dew et al., 2012). Will older adults have the capacity to recruit additional resources to cope with the cognitive fatigue related impediments? Prior studies comparing young and older adults have found that, although older adults generally had slower reaction time at baseline, they did not show additional reaction time slowing during driving induced fatigue, in contrast to the young cohort who exhibited significant reaction time slowing with the development of fatigue (Philip et al., 1999). Similarly, older adults did not show any motor-related performance decline with increase in time-on-task, whereas the younger participants did (Bunce et al., 2004). These findings suggest that slower reaction time at baseline, possibly due to speed-accuracy tradeoff in aging (Smith and Brewer, 1995; Forstmann et al., 2011), is not followed by additional slowing with the onset of cognitive fatigue. How the brain responds to cognitive fatigue in the older population and whether neural compensation is behind the absence of performance deterioration has not been systematically studied. Addressing this problem is the second objective of this study.

We recruited participants in two age groups: a young cohort of n = 16 (18–33 years of age) and an older cohort of n = 18 (60–87 years of age). High-density EEG was recorded while participants performed a cued Stroop task continuously for ∼2 h without break. Neural responses evoked by target words were examined for time-on-task effects. Particular emphasis is placed on whether classical patterns of neural compensation can be observed in the young participants and whether additional neural compensation was possible in the older participants.

MATERIALS AND METHODS

Participants

The study was approved by the Institutional Review Board of the University of Florida. A cohort of 16 healthy young adults (18–33 years of age, 9 females) and a cohort of 18 healthy older adults (60–87 years of age, 7 females) provided written informed consent and participated in the study. Participants were right-handed, native English speakers, free from neurological disorders and with normal to corrected-to-normal vision. Participants were asked to refrain from consuming caffeine or nicotine on the day of testing. All experiments began at 9.00 AM. The experimental procedure and data analysis methods, to be detailed below, were exactly the same for the two cohorts.

Procedure

After a brief practice session to familiarize with a computerized cued Stroop task, the participants were fit with EEG electrodes and asked to perform the task continuously for 180 min (3 h). The recording was done in an electrically and acoustically shielded room to reduce contaminations by external sounds, electrical line noises and other electromagnetic interferences. Breaks for any purpose were taken only upon request and resulted in discontinuation of the experiment. In the young cohort, nine participants performed the entire 180 min of the task; 5 completed at least 160 min. One participant quit before 160 min; this subject was rejected. Another participant exhibited excessive body motion and was also rejected. The data from the 14 young subjects were analyzed here and the time-on-task varied from 0 to 160 min. In the older cohort, 11 participants performed the entire 180 min of the task; 6 completed at least 100 min. One participant quit before 100 min and was rejected. Another participant was also rejected due to poor EEG data quality. The data from the remaining 16 older subjects were analyzed here and the time-on-task varied from 0 to 100 min.

Experimental Paradigm

See **Figure 1**. Each trial began with a cue ('w' for word or 'c' for color) which lasted for 1 s. After a random cue-target interval of 1, 3, or 5 s, one of three target words ('red', 'blue,' or 'green') printed in different font colors (red, blue, or green) appeared on the screen. If the trial was cued for word (word trial), participants were instructed to read the word; if the trial was cued for color (color trial), participants were instructed to name the color of the font in which the word was printed. When the font color of the word and the meaning of the word matched, it is a congruent trial; otherwise, it is an incongruent trial. Reaction time (RT) was determined by a voice activated microphone and the pronounced

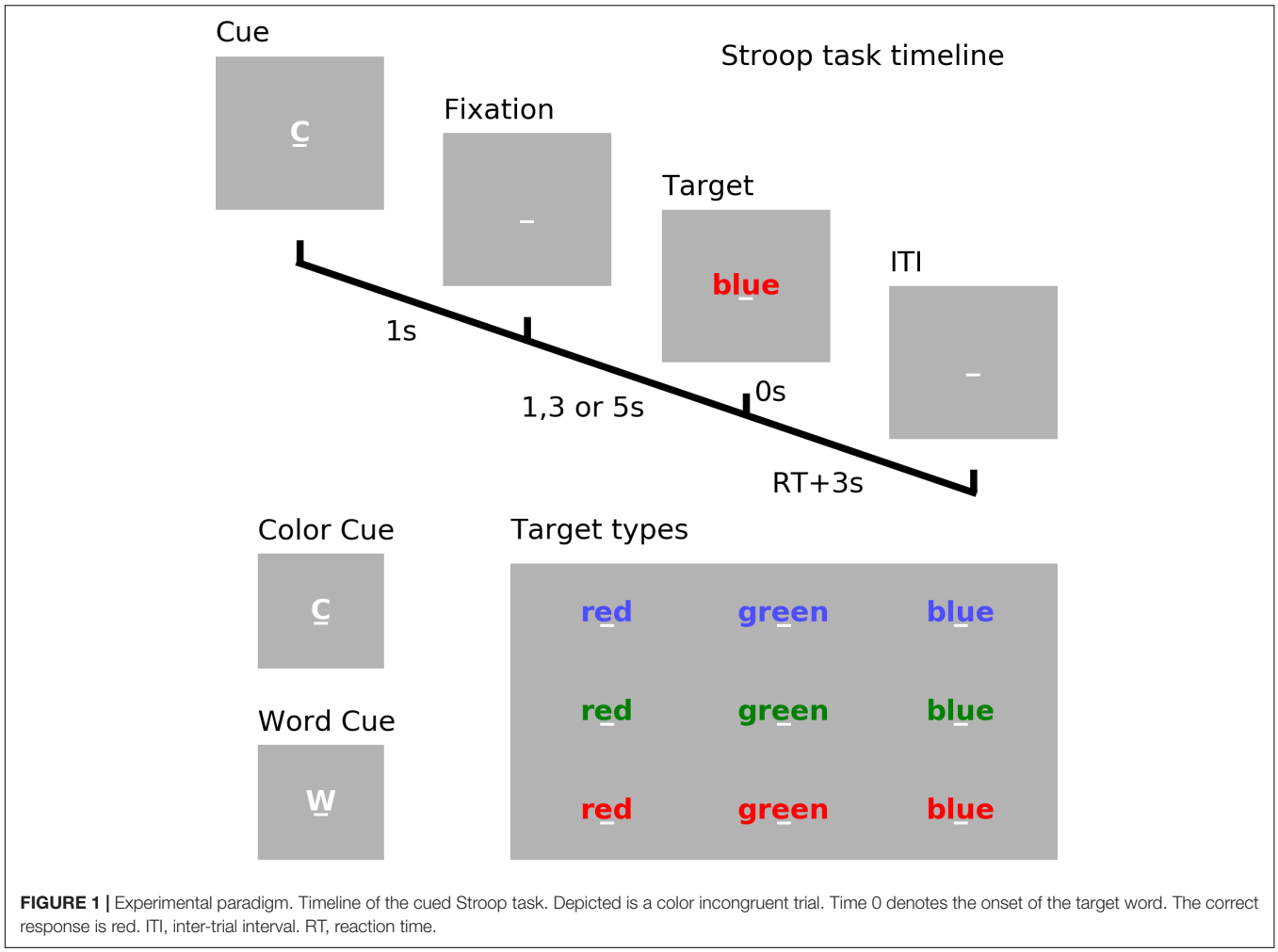

FIGURE 1 | Experimental paradigm. Timeline of the cued Stroop task. Depicted is a color incongruent trial. Time 0 denotes the onset of the target word. The correct response is red. ITI, inter-trial interval. RT, reaction time.

word was manually recorded by the experimenter. The next trial started 3 s after the voice response.

EEG Recording and Preprocessing

The EEG data was recorded using a 128-channel BioSemi Active Two System. Positions of the electrodes were obtained with a Polhemus spatial digitizer. Offline preprocessing was performed using BESA 5.3, EEGLAB and custom Matlab scripts. Data segments contaminated by movements were rejected. The remaining data was bandpass filtered between 0.1 and 83 Hz, down-sampled to 250 Hz, and epoched from −1.5 to 1 s relative to target word onset (0 s). After rejecting noisy trials, independent component analysis (ICA) was applied to remove artifacts resulting from eye movements, eye blinks, muscle activity, and line noise. After ICA, any epoch with incorrect behavioral response or with voltage exceeding 75 μV in any scalp channel was further rejected from analysis. Artifacts-corrected data was then re-referenced against the average reference. Inter-individual differences in electrode positioning were controlled for by using a spherical spline interpolation to project 128 channel preprocessed data onto the standard 81 channel montage (10–10 montage) implemented in BESA.

EEG Analysis and Interpretation

Similar to our previous paper on cue-related neural activity based on the young cohort data (Wang et al., 2016), we mainly focused on the more cognitively demanding incongruent trials where the word and its font color conflicted, thereby requiring more cognitive control to resolve the conflict and to suppress the irrelevant response. An example of such a trial was illustrated in **Figure 1**. Because of the high cognitive demand, these trials were more prone to the deleterious effects of cognitive fatigue, and were thus suited for analyzing the effects of cognitive fatigue on neural responses. The time period between −200 and 0 ms relative to target word onset was demeaned when calculating the event-related potentials (ERP).

Based on prior ERP studies of the Stroop task, we selected two times of interest (TOI) for analysis: (1) the Early Period (150–300 ms), in which sensory and early attentional processes are active (Weinstein, 1995; Atkinson et al., 2003); and (2) the Late Period (300–1000 ms), in which higher-order attention and conflict-related processing are active (West, 2003; Larson et al., 2004; Perlstein et al., 2006), along with response-related cognitive

adjustments and adaptation processes (Grune et al., 1993; Liotti et al., 2000).

As the experiment progressed (i.e., as time-on-task increased), the ERP responses in the early period and late period of stimulus processing were expected to undergo dynamic change due to increasing cognitive fatigue. To determine the time-on-task effect on ERP during each TOI, a moving-window approach across trials was adopted, in which the ERPs were estimated within a block of 40-min in duration and the block was stepped forward with a 10-min increment; there was a total of 13 blocks for the young cohort and a total of 7 blocks for the older cohort. These parameters were chosen for the following reasons. (1) 40-min time blocks allowed us to get a stable estimate of ERP with well-defined components. In fatigue paradigms, despite instructions telling the subjects not to move, they do move because cognitive fatigue makes them uncomfortable. Sufficient number of trials was needed to overcome the negative effects of movement and other noises. Compared to 40 min blocks, ERPs obtained from 10 min blocks were not stable, and the estimates of the ERP component amplitudes were too susceptible to noise contamination. (2) Using 40 min blocks without overlapping would reduce the temporal resolution needed to examine the detailed evolution of ERP responses with fatigue. Therefore, a 30 min overlap was used to achieve the best compromise between stable ERP estimation and good temporal resolution. For each EEG channel, a mixed-effects model was applied to examine whether ERP amplitudes during each TOI demonstrated significant time-on-task effects (thresholded at $p < 0.05$, controlling for multiple comparisons with false discovery rate). Channels were then grouped into regions of interest (ROIs) based on the time-on-task modulation patterns of the ERPs.

Event-related potentials' time-on-task effects were expected to fall broadly into three categories: (i) amplitude decreasing with time-on-task, (ii) amplitude increasing with time-on-task, and (iii) amplitude staying unchanged (Boksem et al., 2005). The first category was taken to signify impairment and the second category compensation. The relation between ERPs in different TOIs and ROIs and increasing time-on-task was subjected to a linear regression analysis and the slopes from such analysis gave the rates of ERP changes. The relationship between the compensation related increase and the impairment related decrease of ERPs in different TOIs and ROIs were examined using these rates of changes.

Relationship Between Compensatory Neural Response and Behavior

We quantified the time-on-task changes of RT, error rate and coefficient of variation of reaction time (CVRT) using the same moving block approach described above to be consistent with the ERP analysis. The change in these behavioral measures was tested using paired *t*-test between the values obtained in the first 40-min time-block and the values obtained in each consecutive 40-min time-block (corrected for multiple comparisons using False Discovery Rate – FDR). Although mean RT within each block is a well-established measure to quantify behavioral performance, it does not capture other aspects of the performance, such as RT variability. RT variability is reflective of attention fluctuations (Allcock et al., 2009), especially 'attention lapses' (Tamm et al., 2012), which are indicative of a fatigued mental state (Bruce et al., 2010). Our past work has shown that the CVRT, defined as the ratio of the standard deviation of reaction time to the mean of reaction time, was a suitable measure for characterizing fatigue-related behavioral change (Wang et al., 2014). Association of compensatory ERP change with change in behavioral performance was analyzed using a multiple regression model in which the independent variables were the rates of ERP changes in different TOIs and ROIs and the dependent variable was the rate of change of CVRT. Effect sizes, where appropriate, were reported to supplement statistical significance testing (Rosenthal and Rosnow, 1991).

RESULTS

Cognitive Fatigue and Behavioral/Neural Responses in Young Adults

Behavior

The 160 min of task performance was divided into 40-min time blocks stepped forward with 10 min increments. The RT and CVRT obtained for successive time blocks showed significant increase compared to the first time block (**Figures 2A,C**). Error rate showed an increasing trend but the increase did not reach statistical significance (**Figure 2B**). In the subsequent analysis we mainly focused on the change in CVRT because CVRT has been shown to be a good behavioral measure for characterizing cognitive fatigue (Wang et al., 2014). Linear regression model was fit to the CVRT across time-on-task blocks for each subject. The positive slopes in **Figure 2D** demonstrated the progressive deterioration of the task performance.

Neural Activity: Regions of Interest

The first 40 min, which was the first time block of the experiment, was defined as the baseline. During this baseline time block, the grand average ERPs evoked by the target word were shown for all electrodes in **Figure 3A**, where the two TOIs were marked using colored shading. ERPs from Fz and Pz were shown in **Figures 3B,C**. Stepping forward across time blocks, the time-on-task effect analysis on ERP amplitude, shown as scalp topographies in **Figures 3D,E**, revealed that there were two groups of electrodes for which the ERP amplitudes were systematically modulated by time-on-task for each of the two TOIs. These two groups of electrodes, located in the occipital-temporal sites and the central-frontal sites, formed the two ROIs (**Figure 3F**). ERPs from these two ROIs during the first block (baseline), the middle block (block 7), and the last block (block 13) are shown in **Figures 3G,H** to illustrate the time-on-task effect on ERP amplitude during the early and late period of stimulus (target word) processing. For early stimulus processing (early period), as time-on-task progressed, the ERP amplitudes decreased in both ROIs. For late stimulus processing (late period), the ERP amplitudes decreased in occipital-temporal

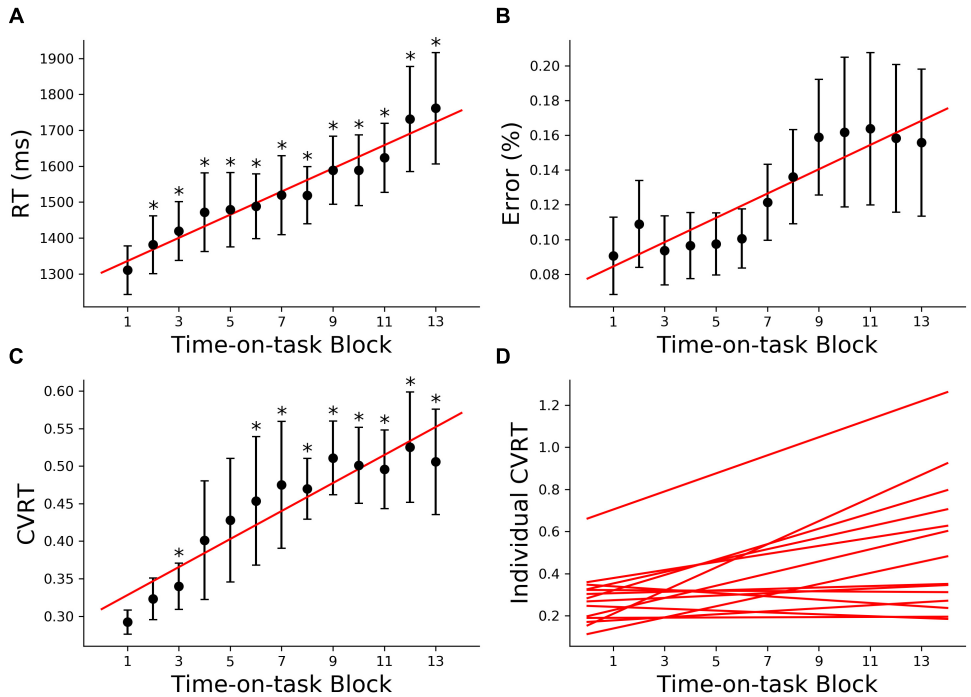

FIGURE 2 | Behavioral analysis (young adults). **(A)** Group average reaction time (RT), **(B)** group average error rate, **(C)** group average coefficient of variation of reaction time (CVRT), **(D)** individual regression fits to CVRT as a function of time-on-task blocks. The slopes of the regression lines denoted the rate of behavioral change with cognitive fatigue. *$p < 0.05$, corrected for multiple comparisons using False Discovery Rate (FDR).

ROI, but increased in central-frontal ROI (i.e., a negative ERP component became more negative).

Neural Activity: Effects of Cognitive Fatigue

Early period of stimulus processing

Neural activity during the early period of target word processing mainly reflects sensory processing and early attention-related activity (Hoffman, 1990; Luck, 1995; Nieuwenhuis et al., 2003). As shown in **Figure 4A**, with increase in time-on-task, ERP amplitude in the early period underwent steady decrease in both occipital-temporal and central-frontal ROI ($p < 0.05$, FDR corrected), suggesting progressive impairments of sensory, early attentional and target discrimination processes. Linear regression fit to the ERP amplitude changes were shown in **Figure 4C** to demonstrate individual variability.

Late period of stimulus processing

Neural activity during the late period of target word processing reflected higher-order processes including conflict detection/resolution and cognitive adjustments (Grune et al., 1993; Liotti et al., 2000). ERPs during the late period exhibited a more complex pattern of temporal dynamics in response to cognitive fatigue. In the occipital-temporal ROI, ERP amplitude decreased with time-on-task increase ($p < 0.05$, FDR corrected), whereas the central-frontal ERP amplitude increased with time-on-task increase ($p < 0.05$, FDR corrected), as shown in **Figure 4B**. This result suggests that while some regions underwent progressive impairment due to the onset and deepening of cognitive fatigue, reflected by decrease in ERP amplitude, other areas showed progressive recruitment of compensatory activities, reflected by the increase in ERP amplitudes. The individual slopes of the linear regression fit to ERP amplitude change were shown in **Figure 4D** to demonstrate individual variations.

Relation Between ERP Rates of Change

Relations between rates of ERP amplitude changes in different TOIs and ROIs were shown in **Figure 5A**. The rates of neural activity changes were generally significantly correlated ($p < 0.05$, FDR corrected). In particular, in **Figure 5B**, the decrease in early ERP amplitude and the increase in late ERP amplitude in the central-frontal ROI were shown to be significantly correlated ($r = 0.67$, $d = 1.79$, $p < 0.05$, FDR corrected, **Figure 5B**), demonstrating an ELSA-like compensation pattern observed in prior cognitive aging research (Davis et al., 2008; Dew et al., 2012). In **Figure 5C**, the rate of occipital-temporal ERP decrease (posterior decrease) and central-frontal ERP increase (anterior increase) during the late period was significantly correlated ($r = -0.81$, $d = -2.73$, $p < 0.05$, FDR corrected). This posterior decline followed by anterior increase is similar to the PASA compensation pattern observed in prior cognitive aging research (Davis et al., 2008).

Relation Between Neural Activity and Behavior

A multiple regression analysis was applied to examine the relation between neural changes and behavioral changes. The rate of

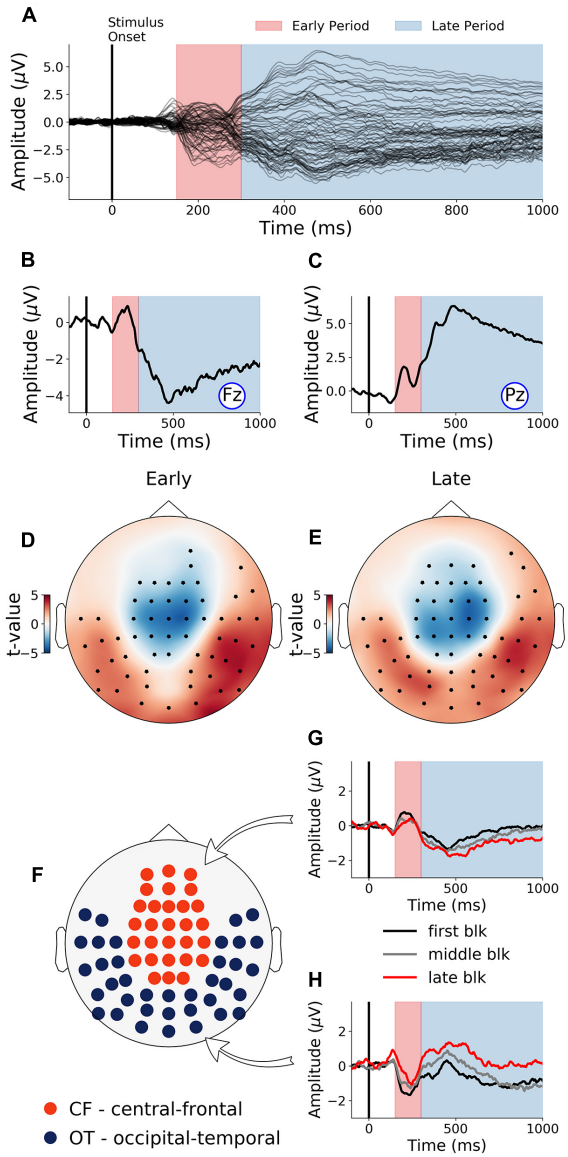

FIGURE 3 | Event-related potentials (ERP) and effects of time-on-task (young adults). **(A)** ERPs during baseline time block (first 40 min) from all channels. **(B,C)** Baseline ERPs from Fz and Pz. **(D,E)** Topographies showing channels where ERP amplitudes were significantly modulated by time-on-task ($p < 0.05$, FDR corrected) for the early period and the late period of stimulus processing. **(F)** ROIs defined based on analysis in **(D,E)**. **(G,H)** ERPs from first, middle, and last time-on-task blocks from central-frontal ROI and occipital-temporal ROI.

change of ERP over time-on-task across the two ROIs and two TOIs were treated as independent variables and the rate of change of CVRT as the dependent variable. As shown in **Figure 5D**, the rates of ERP changes predicted the rate of behavior change ($d = 1.24$, $r = 0.53$, $p = 0.05$), demonstrating functional significance of neural changes over the course of the experiment. To further characterize the effect of each ERP rate of change, the model coefficients were analyzed, and the results shown in **Figure 5E**. For both early ($d = 0.28$) and late ERPs ($d = 0.64$) in occipital-temporal ROI, the higher the rate of ERP amplitude decrease with time-on-task (signaling faster fatigue-related neural decline), the higher the rate of increase of CVRT (signaling faster fatigue-related behavioral decline). In contrast, for the late ERP in the central-frontal ROI ($d = 0.42$), the higher the rate of ERP amplitude change (signaling faster fatigue-related recruitment of compensatory neural resources), the slower the rate of increase of CVRT (signaling slower fatigue-related behavioral decline). The sizes of these effects (Cohen's d) were small to moderate. The change of the early central-frontal ERP did not have an effect on the change of CVRT ($d < 0.2$).

Cognitive Fatigue and Behavioral/Neural Responses in Older Adults

Behavior

Unlike the young cohort, the older cohort showed no significant change in RT, error rate or CVRT with increase in time-on-task, as shown in **Figures 6A–C**. This finding is in agreement with prior fatigue research showing that older adults were able to maintain a consistent level of performance over an extended period of time (Falkenstein et al., 2002). At the individual subject level, there was significant variability in the rate of behavioral change (**Figure 6D**), as expected.

Neural Activity: Effects of Cognitive Fatigue

Baseline ERPs (first 40 min) from all channels and from Pz and Fz were shown in **Figures 7A–C**. The early and late TOIs associated with stimulus processing were defined in the same way as the young for consistency and comparability. The two ROIs were also similarly defined (**Figure 7D**). ERPs from the two ROIs for three different time-on-task blocks were shown in **Figures 7E,F**. Statistical analysis revealed that ERP amplitudes from the early TOI declined significantly with increase in time-on-task in both ROIs ($p < 0.05$, FDR corrected, **Figure 7G**). ERP amplitudes from the late TOI showed no significant change as a function of time-on-task ($p = 0.36$, **Figure 7H**). Like the young cohort, early target-evoked response decreased with the development and deepening of cognitive fatigue, suggesting progressively impaired sensory and early attention-related processing. Unlike the young cohort, no increase in late target-evoked response was observed, suggesting a lack of compensatory neural activity in the older cohort. Individual variability in changes in neural responses can be seen in **Figures 7I,J**.

DISCUSSION

Prolonged performance of a cognitively demanding task can lead to cognitive fatigue. The adverse behavioral consequences of cognitive fatigue have been well studied in the literature (Akerstedt et al., 2004; Boksem et al., 2005; Boksem and Tops, 2008; Cheng and Hsu, 2011; Hopstaken et al., 2016). Here, we examined the behavioral and brain responses to cognitive fatigue in both young and older adults. Analyzing EEG data

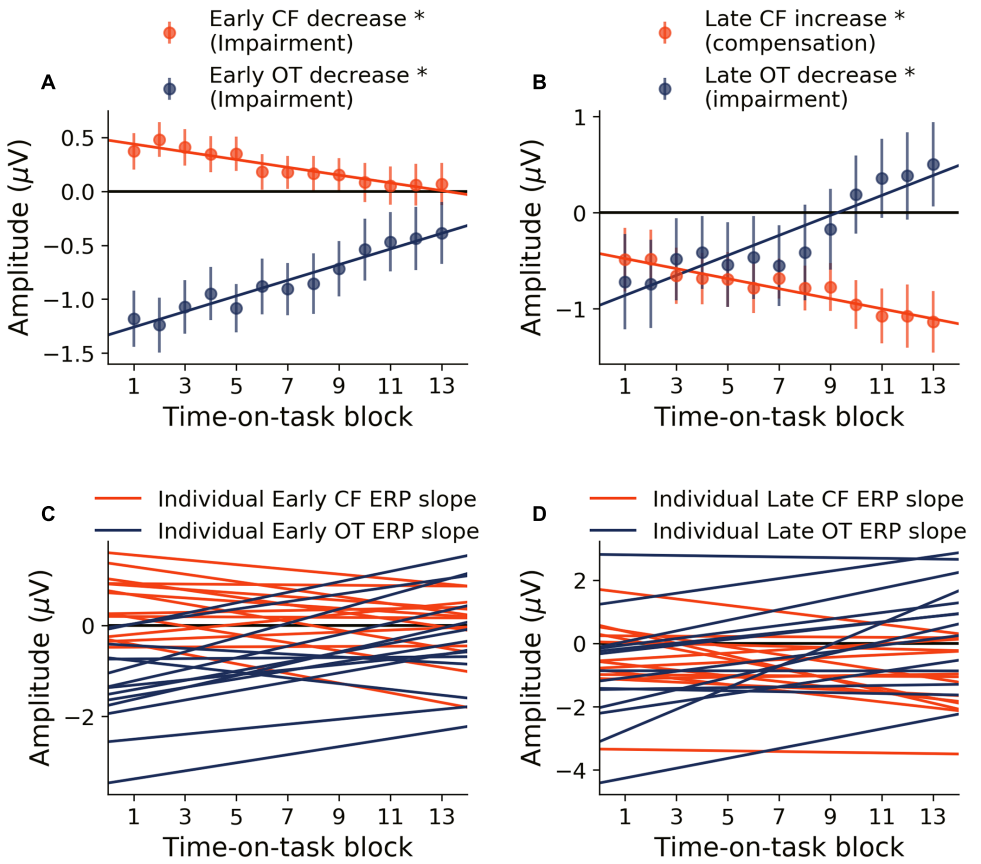

FIGURE 4 | Time-on-task effect on ERP (young adults). **(A)** ERP amplitude indexing the early processing of target words decreased in both central-frontal (CF) ROI and occipital-temporal (OT) ROI. **(B)** ERP amplitude indexing late target processing decreased for occipital-temporal ROI but increased in central-frontal ROI. **(C,D)** Linear regression lines were fit to ERP changes over time-on-task blocks for each participant. Slopes of these regression lines were taken as the rates of ERP changes with time-on-task. *$p < 0.05$, FDR corrected.

from the subjects performing a Stroop task continuously for at least 2 h and 40 min for young subjects and 1 h and 40 min for older subjects we reported the following findings. In the young cohort, performance declined with increase in time-on-task. Early ERP components in both the occipital-temporal and central frontal ROIs declined as well with increase in time-on-task, indicating fatigue-related impairments in sensory and early attentional processing. Whereas late ERP components in occipital-temporal ROI decreased with increase in time-on-task, late ERP components in the central-frontal ROI increased with increase in time-on-task, suggesting posterior impairments of neural processing that were accompanied by frontal neural compensation. The rates of amplitude changes of different ERP components over different TOIs and ROIs were related with one another, with the patterns being reminiscent of PASA and ELSA reported in cognitive aging (Cabeza et al., 2002, 2004). Importantly, these rates of ERP changes predicted the rate of change in behavioral performance (CVRT) over the whole experiment in a linear model, and an analysis of the model coefficients suggested that the declining ERPs (impairment) were detrimental for the maintenance of task performance whereas the increasing ERPs (compensation) were beneficial for the maintenance of task performance. In the older cohort, there was no significant change in behavioral performance across the entire experiment. While the early ERP components declined in both ROIs, the late ERP components exhibited no systematic change as a function of time-on-task; thus only neural impairment, but no compensatory neural increase, was observed in the older adults.

Patterns of Neural Decline and Neural Compensation

To separately examine the impact of cognitive fatigue on sensory and early attentional processes (Hoffman, 1990; Atkinson et al., 2003) and on higher order activities such as cognitive control and conflict processing (Botvinick et al., 2001), we separated target word evoked activity into two time periods, namely: (1) Early Period (150–300 ms) and (2) Late Period (300–1000 ms). In the healthy young cohort, during the early period, ERP topographies highlight the involvement of the occipital-temporal region (Patel and Azzam, 2005) and the central-frontal region (Huster et al., 2010). With the onset and deepening of cognitive fatigue, ERPs in the early period underwent a steady decrease, suggesting

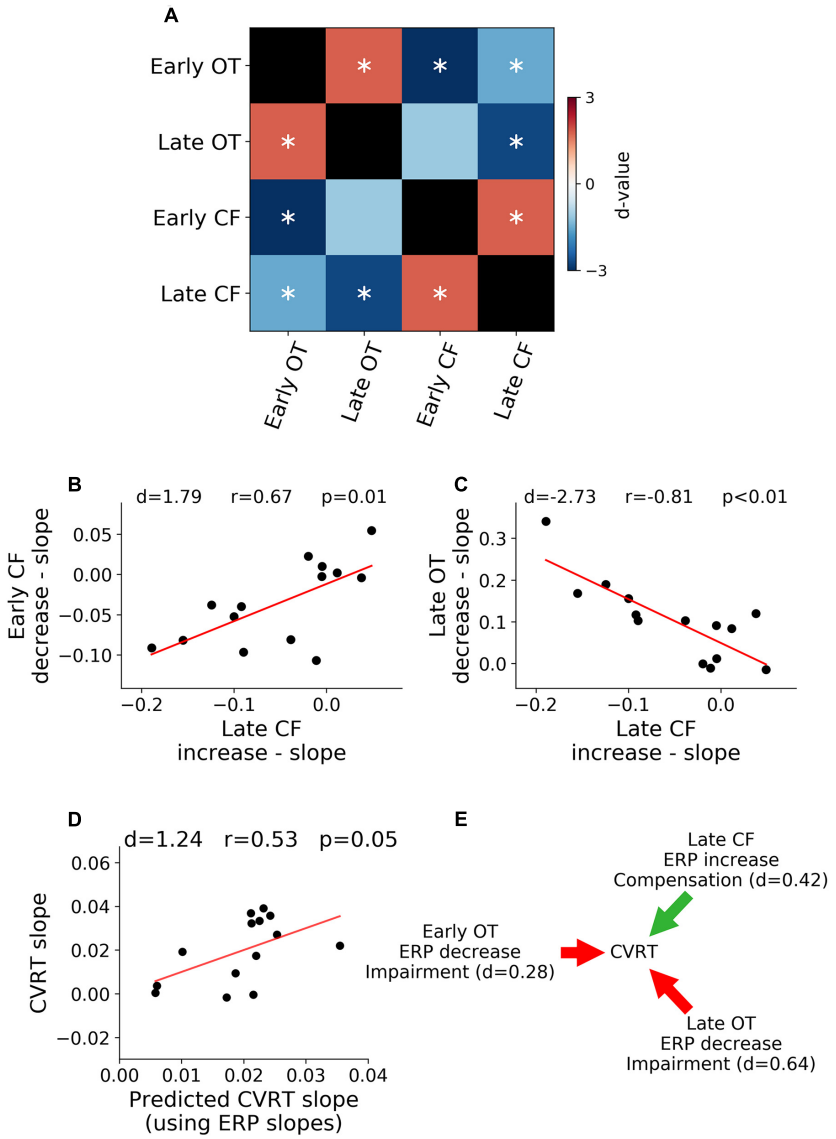

FIGURE 5 | Relation between neural activity changes and performance. **(A)** Pairwise correlation between ERP regression slopes across ROIs and TOIs. **(B)** Late ERP increase was correlated with early ERP decrease in central-frontal (CF) ROI (ELSA). **(C)** Late occipital-temporal (OT) ERP decrease was correlated with late central-frontal (CF) ERP increase (PASA). **(D)** Rates of ERP changes over time-on-task across different TOIs and ROIs predict the rate of behavioral change over time-on-task. **(E)** Illustration of functional contributions of each ERP rate of change to the rate of behavioral change. *$p < 0.05$, FDR corrected.

that sensory and early attentional processes were becoming increasingly impaired (**Figure 3D**). This is reminiscent of prior research showing that early visual processing is very susceptible to the effects of aging (Davis et al., 2008; Dew et al., 2012) and neuropathology (Uc et al., 2005; Armstrong, 2011; Weil et al., 2016). However, in these prior studies, aging and neuropathology related visual decline has other contributing factors such as corneal damage, decrease in vascular density and the reduced number of rods (Schneider and Pichora-Fuller, 2000). In subjects undergoing progressive cognitive fatigue over a short time scale (a few hours compared to a few decades), however, such anatomical changes are unlikely; therefore, the progressive decline of neural activities during the early period reflects neural impairments, free from the confounding influences of factors such as corneal/retinal changes. Late period ERPs are associated with higher-order cognitive processes such as conflict processing and response adjustments (Liotti et al., 2000; Atkinson et al., 2003; Larson et al., 2009). With the onset and deepening of cognitive fatigue, ERPs over the occipital-temporal region during the late period steadily decreased (**Figure 3E**), demonstrating the deleterious effects of cognitive fatigue on the underlying neural activities. In contrast to ERP decrease in both ROIs during the early period and in the occipital-temporal ROI during the late period, ERP amplitude increased with increase in time-on-task in the central-frontal region during the late period, indicating neural compensatory activity.

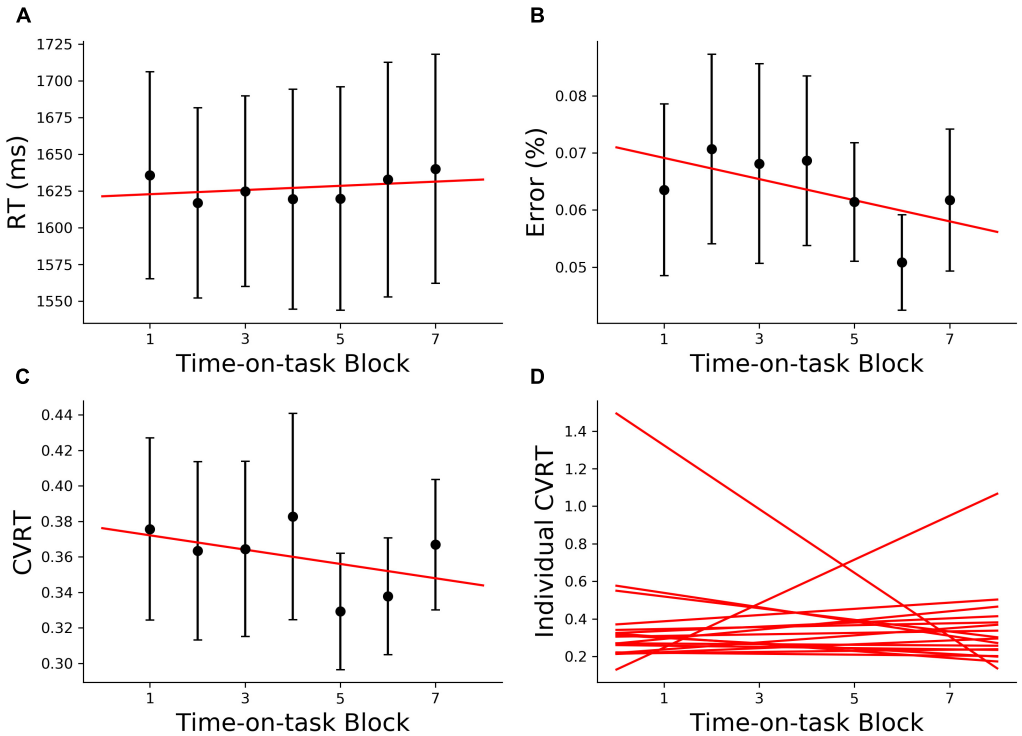

FIGURE 6 | Behavioral analysis (older adults). **(A)** Group average reaction time (RT), **(B)** group average error rate, **(C)** group average CVRT, **(D)** individual regression fits to CVRT as a function of time-on-task blocks. The slopes of the regression lines denoted the rate of behavioral change with cognitive fatigue. $^{*}p < 0.05$, corrected for multiple comparisons using False Discovery Rate (FDR).

Early to late shift in aging (ELSA) is a commonly observed pattern in cognitive compensation in aging and in neurological disorders (Dew et al., 2012). In ELSA, decline in early neural processing is compensated by increase in late neural processing. The data from the young cohort undergoing cognitive fatigue exhibited the ELSA pattern, namely, early period neural activity decline is accompanied by the late period neural activity increase. To test whether early neural processing impairments and late neural compensation is related, we compared the rate of increase and rate of decrease in ERP amplitudes across the two time periods, and found that within the central-frontal ROI, ERP decrease in early period were correlated with the ERP increase in late period, suggesting that the magnitude of compensation is proportional to the magnitude of impairments. Similar effects have been observed in a previous report on cognitive fatigue (Hopstaken et al., 2016), although in that report, the neural compensatory activity was not explicitly recognized.

Another form of compensatory response on cognitive aging is posterior-anterior shift in aging (PASA). In PASA, declined posterior processing is accompanied by increased anterior compensatory activity (Grady et al., 1994; Cabeza et al., 2004; Davis et al., 2008). The decrease in posterior/occipital activity is thought to reflect sensory decline as a function of age (Lindenberger and Baltes, 1994). Our results demonstrated that PASA can be observed in a cognitive fatigue paradigm as well, namely, the occipital-temporal ERP decrease was accompanied by a central-frontal ERP increase, and the rates of ERP decrease and increase in different regions of the scalp are correlated with one another, suggesting that sensory decline can occur acutely as a result of cognitive fatigue, and the frontal compensatory activity can be recruited acutely with the rate of recruitment being proportional to the rate of impairment of posterior neural activity (Davis et al., 2008).

In the older cohort, we only observe ERP decline in the early target evoked response period but no ERP increase in any time period or regions of interest, suggesting that cognitive fatigue caused further deterioration of sensory and early attentional processes but did not trigger neural compensatory response. It is worth noting that the decline in ERP amplitude in the older cohort is not as drastic as that seen in the young cohort, which along with the lack of performance decline, appears to suggest that the old subjects are better able to resist the impairing effects of cognitive fatigue (Falkenstein et al., 2002). Whether the lack of compensatory activity is due to capacity limitation or other factors such as the lack of necessity to compensate is difficult to ascertain in the current paradigm.

Relating Neural Changes and Behavioral Changes

Cognitive fatigue results in performance decline in young adults. This has been consistently reported in the literature (Hopstaken et al., 2016; Wang et al., 2016). In this paper, we further reported that concomitant with performance decline, neural changes also

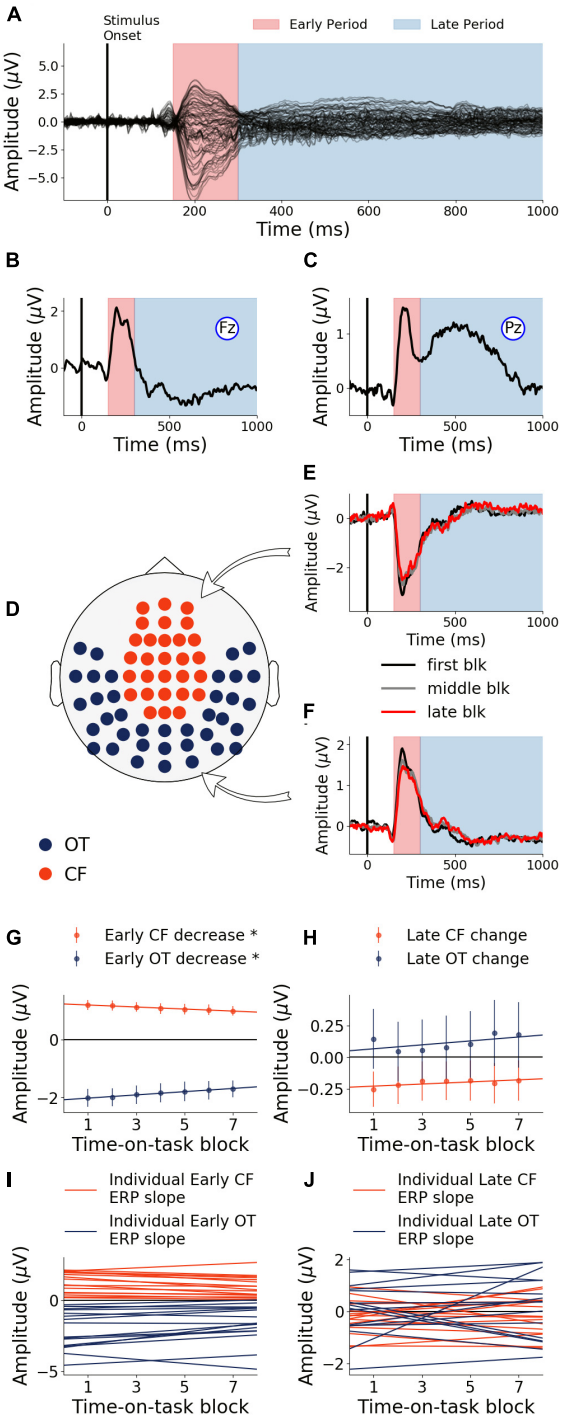

FIGURE 7 | Event-related potentials and effects of time-on-task (older adults). **(A)** ERPs during baseline (first 40 min) from all channels. **(B,C)** Baseline ERPs from Fz and Pz. **(D)** ROI definition. **(E,F)** ERPs from first, middle and last time-on-task blocks from central-frontal (CF) ROI and occipital-temporal (OT) ROI. **(G)** ERP amplitude during early target processing decreased in both central-frontal ROI and occipital-temporal ROI. **(H)** ERP amplitude in late target processing did not show significant change with time-on-task. **(I,J)** Linear regression lines were fit to ERP changes over time-on-task blocks for each participant. Slopes of these regression lines were taken as the rates of ERP changes with time-on-task. *$p < 0.05$, FDR corrected.

took place. To what extent neural changes and behavioral changes are related determines the functional significance of the observed neural activity changes. Past research has not always found a relationship between the two. Smith et al. (1999) showed that although the brain activity was significantly reduced for individuals with high risk for Alzheimer's disease compared to healthy controls, there were no performance differences in both visual naming and letter fluency tasks (Drummond et al., 2000). This may partly explain why we did not see performance decline in the older cohort despite impairment in neural responses. Moreover, increased neural activity in aging and in brain disorders, which were interpreted as compensatory activity, has been found to be associated with reduction in performance (Logan et al., 2002; Cabeza and Kingstone, 2006; Wingfield and Grossman, 2006), a finding at variance with the expectation that neural compensation should benefit behavioral performance. With these questions in mind, we performed a multiple regression analysis with neural changes as independent variables and behavioral change as dependent variables for the young cohort, given this cohort's rich impairment-versus-compensation dynamics. In addition to showing that neural changes predicted behavioral changes, our results further demonstrated that decreasing ERP amplitudes (impairments) are associated with worsening of task performance, whereas increasing ERP amplitude (compensation) helps to moderate performance decline.

Limitations

This study has a number of limitations. The first is the small sample size for both cohorts. Future studies will recruit larger numbers of participants to test the robustness of the findings reported here. The second is the different length of time-on-task used in the analysis for the two cohorts (at least 2:40 h for young adults and at least 1:40 h for older subjects). Although the task was designed to be performed for a maximum of 3 h for both cohorts, the participants in the old cohort had a higher tendency to quit earlier. The third is that the paradigm, designed to be more applicable to real world scenarios where people pace their responses based on their cognitive state, allowed self-pacing. To what extent self-pacing increased with the increase in time-on-task cannot be ascertained. The fourth is that the educational level of the participants was not acquired. Because education is known to contribute to cognitive reserve which in turn affects the brain response to cognitive fatigue (Jongen et al., 2012), without information on education, the relationship between cognitive reserve, cognitive fatigue and compensation cannot be addressed in this study. The fifth is that although both the young and older cohorts developed the sensation of cognitive fatigue as the experiment progressed, per post-experiment conversations, we did not have information to quantify the change of this sensation as a function of time-on-task (Burke et al., 2018).

SUMMARY

In this study we analyzed the behavioral and neural responses to cognitive fatigue induced impairment in young and older

adults. In young adults, we found that prolonged performance of a cognitively demanding task led to declined behavioral performance and was associated with both impaired neural responses as well as neural compensation. The spatial and temporal patterns of neural impairments and neural compensation were consistent with two widely reported patterns of neural compensation in the cognitive aging literature, namely, ELSA and PASA. In the older adults, behavioral performance did not decline, and there were only impaired neural responses but no compensatory neural activity.

Compensatory neural processes have been traditionally studied in cross-sectional designs where populations with advanced age or brain disorders are compared with young or gender- and age-matched healthy populations. In such comparisons it is difficult to determine whether neural compensation is developed over an extended period of time or can be recruited acutely. Our study suggests that the cognitive fatigue paradigm in healthy adults (both young and older) may be useful as a model to induce neural impairments and compensatory processes in a short period of time and provide an opportunity to study the functional roles of these processes in maintaining task performance.

ETHICS STATEMENT

This study was carried out in accordance with the recommendations of the NIH Protection of Human Research Subjects and HIPPA for research guidelines with written informed consent from all subjects. All subjects gave written informed consent in accordance with the Declaration of Helsinki. The protocol was approved by the University of Florida Gainesville Institutional Review Board.

AUTHOR CONTRIBUTIONS

MD and BK contributed conception and design of the study. CW and IBHS organized the database, performed the statistical analysis, and wrote the first draft of the manuscript. MD, BK, CW, and SB wrote sections of the manuscript. All authors contributed to manuscript revision, read and approved the submitted version.

FUNDING

This study was supported by NIH grant R21 AG044862.

REFERENCES

Akerstedt, T., Knutsson, A., Westerholm, P., Theorell, T., Alfredsson, L., and Kecklund, G. (2004). Mental fatigue, work and sleep. *J. Psychosom. Res.* 57, 427–433. doi: 10.1016/j.jpsychores.2003.12.001

Allcock, L. M., Rowan, E. N., Steen, I. N., Wesnes, K., Kenny, R. A., and Burn, D. J. (2009). Impaired attention predicts falling in Parkinson's disease. *Parkinsonism Relat. Disord.* 15, 110–115. doi: 10.1016/j.parkreldis.2008.03.010

Anderer, P., Saletu, B., Semlitsch, H. V., and Pascual-Marqui, R. D. (2003). Non-invasive localization of P300 sources in normal aging and age-associated memory impairment. *Neurobiol. Aging* 24, 463–479. doi: 10.1016/S0197-4580(02)00058-1

Armstrong, R. A. (2011). Visual symptoms in Parkinson's Disease. *Parkinson's Dis.* 2011:908306. doi: 10.4061/2011/908306

Atkinson, C. M., Drysdale, K. A., and Fulham, W. R. (2003). Event-related potentials to Stroop and reverse Stroop stimuli. *Int. J. Psychophysiol.* 47, 1–21. doi: 10.1016/S0167-8760(02)00038-7

Babu Henry Samuel, I., Barkley, C., Marino, S. E., Wang, C., Han, S., Birnbaum, A. K., et al. (2018). Brain's compensatory response to drug-induced cognitive impairment. *J. Clin. Exp. Neuropsychol.* 40, 1000–1012. doi: 10.1080/13803395.2018.1458822

Boksem, M. A., and Tops, M. (2008). Mental fatigue: costs and benefits. *Brain Res. Rev.* 59, 125–139. doi: 10.1016/j.brainresrev.2008.07.001

Boksem, M. A. S., Meijman, T. F., and Lorist, M. M. (2005). Effects of mental fatigue on attention: an ERP study. *Cogn. Brain Res.* 25, 107–116. doi: 10.1016/j.cogbrainres.2005.04.011

Botvinick, M. M., Braver, T. S., Barch, D. M., Carter, C. S., and Cohen, J. D. (2001). Conflict monitoring and cognitive control. *Psychol. Rev.* 108, 624–652.

Bruce, J. M., Bruce, A. S., and Arnett, P. A. (2010). Response variability is associated with self-reported cognitive fatigue in multiple sclerosis. *Neuropsychology* 24, 77–83. doi: 10.1037/a0015046

Bunce, D., MacDonald, S. W. S., and Hultsch, D. F. (2004). Inconsistency in serial choice decision and motor reaction times dissociate in younger and older adults. *Brain Cogn.* 56, 320–327. doi: 10.1016/j.bandc.2004.08.006

Burke, S. E., Samuel, I. B. H., Zhao, Q., Cagle, J., Cohen, R. A., Kluger, B., et al. (2018). Task-based cognitive fatigability for older adults and validation of mental fatigability subscore of pittsburgh fatigability scale. *Front. Aging Neurosci.* 10:327. doi: 10.3389/fnagi.2018.00327

Cabeza, R., Anderson, N. D., Locantore, J. K., and McIntosh, A. R. (2002). Aging gracefully: compensatory brain activity in high-performing older adults. *Neuroimage* 17, 1394–1402. doi: 10.3389/fnagi.2018.00327

Cabeza, R., Daselaar, S. M., Dolcos, F., Prince, S. E., Budde, M., and Nyberg, L. (2004). Task-independent and task-specific age effects on brain activity during working memory, visual attention and episodic retrieval. *Cereb. Cortex* 14, 364–375. doi: 10.1093/cercor/bhg133

Cabeza, R., and Kingstone, A. (2006). *Handbook of Functional Neuroimaging of Cognition*. Cambridge, MA: MIT Press. doi: 10.1093/cercor/bhg133

Cader, S., Cifelli, A., Abu-Omar, Y., Palace, J., and Matthews, P. M. (2006). Reduced brain functional reserve and altered functional connectivity in patients with multiple sclerosis. *Brain* 129, 527–537. doi: 10.1093/brain/awh670

Carter, C. S., MacDonald, A. W., Ross, L. L., and Stenger, V. A. (2001). Anterior cingulate cortex activity and impaired self-monitoring of performance in patients with schizophrenia: an event-related fmri study. *Am. J. Psychiatry* 158, 1423–1428. doi: 10.1176/appi.ajp.158.9.1423

Cheng, S.-Y., and Hsu, H.-T. (2011). *Mental Fatigue Measurement Using EEG, Risk Management Trends*. Available from: http://www.intechopen.com/books/risk-management-trends/mental-fatigue-measurement-using-eeg

Davis, S. W., Dennis, N. A., Daselaar, S. M., Fleck, M. S., and Cabeza, R. (2008). Que PASA? The posterior–anterior shift in aging. *Cereb. Cortex* 18, 1201–1209. doi: 10.1093/cercor/bhm155

Dew, I. T., Buchler, N., Dobbins, I. G., and Cabeza, R. (2012). Where is ELSA? The early to late shift in aging. *Cereb. Cortex* 22, 2542–2553. doi: 10.1093/cercor/bhr334

Drummond, S. P., Brown, G. G., Gillin, J. C., Stricker, J. L., Wong, E. C., and Buxton, R. B. (2000). Altered brain response to verbal learning following sleep deprivation. *Nature* 403, 655–657. doi: 10.1038/35001068

Falkenstein, M., Hoormann, J., and Hohnsbein, J. (2002). Inhibition-related ERP components: variation with modality, age, and time-on-task. *J. Psychophysiol.* 16, 167–175. doi: 10.1027//0269-8803.16.3.167

Forstmann, B. U., Tittgemeyer, M., Wagenmakers, E.-J., Derrfuss, J., Imperati, D., and Brown, S. (2011). The speed-accuracy tradeoff in the elderly brain: a structural model-based approach. *J. Neurosci.* 31, 17242–17249. doi: 10.1523/JNEUROSCI.0309-11.2011

Grady, C. L., Maisog, J. M., Horwitz, B., Ungerleider, L. G., Mentis, M. J., Salerno, J. A., et al. (1994). Age-related changes in cortical blood flow activation during visual processing of faces and location. *J. Neurosci.* 14, 1450–1462. doi: 10.1523/JNEUROSCI.14-03-01450.1994

Grune, K., Mecklinger, A., and Ullsperger, P. (1993). Mental comparison. *NeuroReport* 4, 1272–1274. doi: 10.1097/00001756-199309000-00016

Hoffman, J. E. (1990). "Event-related potentials and automatic and controlled processes," in *Event-Related Brain Potentials; Basic Issues and Applications*, eds J. Rohrbaugh, R. Parasuraman, and R. Johnsoneds (New York, NY: Oxford University Press).

Hopstaken, J. F., van der Linden, D., Bakker, A. B., Kompier, M. A., and Leung, Y. K. (2016). Shifts in attention during mental fatigue: evidence from subjective, behavioral, physiological, and eye-tracking data. *J. Exp. Psychol. Hum. Percept. Perform.* 42, 878–889. doi: 10.1037/xhp0000189

Huster, R. J., Westerhausen, R., Pantev, C., and Konrad, C. (2010). The role of the cingulate cortex as neural generator of the N200 and P300 in a tactile response inhibition task. *Hum. Brain Mapp.* 31, 1260–1271. doi: 10.1002/hbm.20933

Jongen, P. J., Ter, A. H., and Brands, A. M. (2012). Cognitive impairment in multiple sclerosis. *Minerva Medica* 103, 73–96.

Larson, M. J., Jones, V., Kelly, K. G., and Perlstein, W. M. (2004). "Dissociating components of cognitive control with high-density ERPs: Implementation of control, conflict processing, and error monitoring," in *32nd Annual Meeting of the International Neuropsychological Society*, Baltimore, MD.

Larson, M. J., Kaufman, D. A. S., and Perlstein, W. M. (2009). Neural time course of conflict adaptation effects on the Stroop task. *Neuropsychologia* 47, 663–670. doi: 10.1016/j.neuropsychologia.2008.11.013

Lindenberger, U., and Baltes, P. B. (1994). Sensory functioning and intelligence in old age: a strong connection. *Psychol. Aging* 9, 339–355. doi: 10.1037/0882-7974.9.3.339

Liotti, M., Woldorff, M. G., Perez, R., and Mayberg, H. S. (2000). An ERP study of the temporal course of the Stroop color-word interference effect. *Neuropsychologia* 38, 701–711. doi: 10.1016/S0028-3932(99)00106-2

Logan, J. M., Sanders, A. L., Snyder, A. Z., Morris, J. C., and Buckner, R. L. (2002). Under-recruitment and nonselective recruitment: dissociable neural mechanisms associated with aging. *Neuron* 33, 827–840. doi: 10.1016/S0896-6273(02)00612-8

Lorist, M. M., Boksem, M. A. S., and Ridderinkhof, K. R. (2005). Impaired cognitive control and reduced cingulate activity during mental fatigue. *Cogn. Brain Res.* 24, 199–205. doi: 10.1016/j.cogbrainres.2005.01.018

Luck, S. J. (1995). Multiple mechanisms of visual-spatial attention: recent evidence from human electrophysiology. *Behav. Brain Res.* 71, 113–123. doi: 10.1016/0166-4328(95)00041-0

Lum, P. S., Mulroy, S., Amdur, R. L., Requejo, P., Prilutsky, B. I., and Dromerick, A. W. (2009). Gains in upper extremity function after stroke via recovery or compensation: potential differential effects on amount of real-world limb use. *Top. Stroke Rehabil.* 16, 237–253. doi: 10.1310/tsr1604-237

Nieuwenhuis, S., Yeung, N., van den Wildenberg, W., and Ridderinkhof, K. R. (2003). Electrophysiological correlates of anterior cingulate function in a go/no-go task: effects of response conflict and trial type frequency. *Cogn. Affect. Behav. Neurosci.* 3, 17–26. doi: 10.3758/CABN.3.1.17

Patel, S. H., and Azzam, P. N. (2005). Characterization of N200 and P300: selected studies of the event-related potential. *Int. J. Med. Sci.* 2, 147–154. doi: 10.7150/ijms.2.147

Perlstein, W. M., Larson, M. J., Dotson, V. M., and Kelly, K. G. (2006). Temporal dissociation of components of cognitive control dysfunction in severe TBI: ERPs and the cued-Stroop task. *Neuropsychologia* 44, 260–274. doi: 10.1016/j.neuropsychologia.2005.05.009

Philip, P., Taillard, J., Quera-Salva, M. A., Bioulac, B., and Åkerstedt, T. (1999). Simple reaction time, duration of driving and sleep deprivation in young versus old automobile drivers. *J. Sleep Res.* 8, 9–14. doi: 10.1046/j.1365-2869.1999.00127.x

Reuter-Lorenz, P. A., and Cappell, K. A. (2008). Neurocognitive aging and the compensation hypothesis. *Curr. Direct. Psychol. Sci.* 17, 177–182. doi: 10.1111/j.1467-8721.2008.00570.x

Rosenthal, R., and Rosnow, R. L. (1991). *Essentials of Behavioral Research: Methods and data Analysis,* Chapter 12. New York, NY: McGraw-Hill Humanities Social.

Schneider, B. A., and Pichora-Fuller, M. K. (2000). "Implications of perceptual deterioration for cognitive aging research," in *The Handbook of Aging and Cognition*, eds F. I. M. Craik and T. A. Salthouse (Mahwah, NJ: Lawrence Erlbaum Associates Publishers), 155–219.

Smith, C. D., Andersen, A. H., Kryscio, R. J., Schmitt, F. A., Kindy, M. S., Blonder, L. X., et al. (1999). Altered brain activation in cognitively intact individuals at high risk for Alzheimer's disease. *Neurology* 53, 1391–1391. doi: 10.1212/WNL.53.7.1391

Smith, G. A., and Brewer, N. (1995). Slowness and age: speed-accuracy mechanisms. *Psychol. Aging* 10, 238–247. doi: 10.1037/0882-7974.10.2.238

Tamm, L., Narad, M. E., Antonini, T. N., O'Brien, K. M., Hawk, L. W., and Epstein, J. N. (2012). Reaction time variability in ADHD: a review. *Neurotherapeutics* 9, 500–508. doi: 10.1007/s13311-012-0138-5

Uc, E. Y., Rizzo, M., Anderson, S. W., Qian, S., Rodnitzky, R. L., and Dawson, J. D. (2005). Visual dysfunction in Parkinson disease without dementia. *Neurology* 65, 1907–1913. doi: 10.1212/01.wnl.0000191565.11065.11

Wang, C., Ding, M., and Kluger, B. M. (2014). Change in intraindividual variability over time as a key metric for defining performance-based cognitive fatigability. *Brain Cogn.* 85, 251–258. doi: 10.1016/j.bandc.2014.01.004

Wang, C., Trongnetrpunya, A., Samuel, I. B. H., Ding, M., and Kluger, B. M. (2016). Compensatory neural activity in response to cognitive fatigue. *J. Neurosci.* 36, 3919–3924. doi: 10.1523/JNEUROSCI.3652-15.2016

Weil, R. S., Schrag, A. E., Warren, J. D., Crutch, S. J., Lees, A. J., and Morris, H. R. (2016). Visual dysfunction in Parkinson's disease. *Brain* 139, 2827–2843. doi: 10.1093/brain/aww175

Weinstein, A. M. (1995). Visual ERPs evidence for enhanced processing of threatening information in anxious university students. *Biol. Psychiatry* 37, 847–858. doi: 10.1016/0006-3223(94)00249-3

West, R. (2003). Neural correlates of cognitive control and conflict detection in the Stroop and digit-location tasks. *Neuropsychologia* 41, 1122–1135. doi: 10.1016/S0028-3932(02)00297-X

Wingfield, A., and Grossman, M. (2006). Language and the aging brain: patterns of neural compensation revealed by functional brain imaging. *J. Neurophysiol.* 96, 2830–2839. doi: 10.1152/jn.00628.2006

Conflict of Interest Statement: The authors declare that the research was conducted in the absence of any commercial or financial relationships that could be construed as a potential conflict of interest.

frontiers in Neural Circuits

ORIGINAL RESEARCH
published: 16 April 2019
doi: 10.3389/fncir.2019.00026

Lower Posttraumatic α-Synuclein Level Associated With Altered Default Mode Network Connectivity Following Acute Mild Traumatic Brain Injury

Limei Ye[1,2], Danbin Zhang[1], Meihua Shao[3], Pinghui Zhao[1], Bo Yin[4], Jinfei Zhuang[5], Feifei Wang[6], Zhihan Yan[1] and Guanghui Bai[1]**

[1]Department of Radiology, The Second Affiliated Hospital and Yuying Children's Hospital of Wenzhou Medical University, Wenzhou, China, [2]Department of Radiology, Jinhua Municipal Central Hospital and Jinhua Hospital of Zhejiang University, Jinhua, China, [3]Department of Radiology, Tongde Hospital of Zhejiang Province, Hangzhou, China, [4]Department of Neurosurgery, The Second Affiliated Hospital and Yuying Children's Hospital of Wenzhou Medical University, Wenzhou, China, [5]Department of Rehabilitation, The Second Affiliated Hospital and Yuying Children's Hospital of Wenzhou Medical University, Wenzhou, China, [6]Department of MRI, The First Affiliated Hospital of Zhengzhou University, Zhengzhou, China

This study aimed to investigate the changes of α-synuclein in serum and its relationship with default mode network (DMN) connectivity after acute mild traumatic brain injury (mild TBI). Fifty-two patients with mild TBI at the acute phase and 47 matched healthy controls were enrolled in the study. All participants received resting-state functional magnetic resonance imaging (fMRI) and neuropsychological assessments. Relations between the levels of α-synuclein in serum and clinical assessments were obtained using multivariate linear regression. Results showed that the patients with lower α-synuclein presented more complaints on post-concussion symptoms and depression. Moreover, patients with high levels of α-synuclein exhibited significantly decreased functional connectivity in the left precuneus and increased functional connectivity in both the left anterior cingulate cortex and ventro-medial prefrontal cortex (MPFC) compared with patients with low levels of α-synuclein. These findings supported that α-synuclein may modulate the functional connectivity within the DMN and suggest the feasibility of using α-synuclein as an objective biomarker for diagnosis and prognosis of mild TBI.

Keywords: mild traumatic brain injury, α-synuclein, rs-fMRI, default mode network, functional connectivity

OPEN ACCESS

Edited by:
Tuo Zhang,
Northwestern Polytechnical University, China

Reviewed by:
Zhenyu Liu,
Institute of Automation (CAS), China
Lei Gao,
Wuhan University, China

****Correspondence:***
Zhihan Yan
zhihanyanwz@163.com
Guanghui Bai
bghu79@126.com

Received: *12 January 2019*
Accepted: *26 March 2019*
Published: *16 April 2019*

Citation:
Ye L, Zhang D, Shao M, Zhao P, Yin B, Zhuang J, Wang F, Yan Z and Bai G (2019) Lower Posttraumatic α-Synuclein Level Associated With Altered Default Mode Network Connectivity Following Acute Mild Traumatic Brain Injury. Front. Neural Circuits 13:26. doi: 10.3389/fncir.2019.00026

INTRODUCTION

Traumatic brain injury (TBI) is a major public health problem affecting approximately 1.6 million people every year in the United States. Most (about 80%) are diagnosed with mild TBI (mTBI; Langlois et al., 2006), among whom 10%–20% suffer from persistent headaches, difficulty of thinking, memory problems, attention deficits, mood swings, and frustration (McAllister, 2008; Zemek et al., 2013). However, mTBI diagnosis can be missed by conventional computed tomography and magnetic resonance imaging (Lee et al., 2008). Consequently, it is challenging to predict who will suffer from persistent symptoms after mTBI.

mTBI was recently found to probably cause progressive neurocognitive dysfunction (Mac Donald et al., 2017), leading to an increased risk of developing neurodegenerative and psychiatric diseases (Gardner and Yaffe, 2015), including Parkinson's disease (PD). However, the

pathophysiological mechanism underlying mTBI and its relationship with the risk of developing PD remain unclear. An evaluation of some 1,900 studies determined the plausibility of developing PD under moderate to severe TBI (Institute of Medicine, 2009). However, only "suggestive/limited evidence" was found relating mTBI with clinical diagnosis of PD (Institute of Medicine, 2009). Other studies have investigated the risk of developing PD from mTBI but obtained inconsistent findings (Gardner et al., 2015). Magnoni and Brody (2010) suggested that these results may partly be derived from the putative linkage between TBI and neurodegeneration, with the occurrence of TBI increasing the risk of neurodegenerative diseases.

Several biomarkers are available to diagnose and assess TBI, including imaging and fluid-based techniques (Kochanek et al., 2008). Supporting studies unveil some signatures of these biomarkers associated with TBI. Among these biomarkers, α-synuclein (α-syn) is the hallmark of a number of neurodegenerative diseases (Tokuda et al., 2010; Mollenhauer et al., 2011). Being a presynaptic protein activated by phosphorylation and other pathways, α-syn plays an important role in the circulation of synaptic vesicles. Cellular and genetic modification eventually leads to an overexpression of the total α-syn, and its accumulation has been proven to cause neuronal damages (Werner and Engelhard, 2007; Klein and Westenberger, 2012). In particular, the overexpression of α-syn may be a pathological link between TBI and the development of PD pathologies (Acosta et al., 2015). These results provide a reliable basis for us to investigate mTBI through the study of serum α-syn.

Resting-state functional magnetic resonance imaging (fMRI) has enabled the evaluation of brain networks without task-based fMRI experiments. The default mode network (DMN) is a well-recognized brain network activated during the resting states and suppressed during the execution of attention and decision-making tasks (Zhang and Raichle, 2010). The DMN typically comprises the posterior cingulate cortex (PCC), precuneus, inferior parietal, and medial prefrontal cortex (MPFC) areas (Ralchle and Snyder, 2007). Many studies have determined that several psychiatric disorders alter DMN functional connectivity (Buckner et al., 2008; Rocca et al., 2010; Slobounov et al., 2011). In addition, Zhou et al. (2012) verified significantly reduced connectivity in the PCC and parietal regions, and increased frontal connectivity around MPFC in the mTBI patients (Zhou et al., 2012). Likewise, Mayer et al. (2011) found decreased connectivity within the DMN and increased connectivity between its nodes and the lateral PFC in the mTBI patients (Mayer et al., 2011). However, few studies have addressed the mechanism of changes in the DMN functional connectivity in the mTBI patients. Despite being challenging, this type of study would be insightful for characterizing mTBI. Our main hypothesis was that serum α-syn concentration in the mTBI patients during acute phase will change, and that this inflammatory marker is correlated with clinical neurocognition and functional connectivity within the DMN in the brain.

MATERIALS AND METHODS

Participants

Acute head trauma patients from the local emergency department (ED) in August 2016 and June 2017, with non-enhanced head CT, consecutively became the initial patients in the present study. Inclusion criteria for the mTBI patients were based on guidelines from the World Health Organization's Collaborating Centre for Neurotrauma Task Force (Holm et al., 2005): (i) an initial Glasgow Coma Scale (GCS) score of 13–15; (ii) one or more of the following: loss of consciousness (LOC) <30 min, post-traumatic amnesia (PTA) <24 h, and/or other transient neurological abnormalities such as focal signs and seizure; and (iii) within 1 week after onset of mTBI. Exclusion criteria for mTBI patients included: (i) pre-TBI, pre-existing psychological disorders, Posttraumatic stress disorder (PTSD), substance abuse, and alcohol dependance; and (ii) a structural abnormality on neuroimaging (CT and MRI); (iii) manifestation of mTBI as complication from other injuries (e.g., systemic injuries, facial injuries, or spinal cord injury); and (iv) other problems (e.g., psychological trauma, language barrier, or coexisting medical conditions), or caused by penetrating craniocerebral injury. Overall, 52 patients with mTBI were enrolled in this study.

Healthy controls were recruited by the local imaging research facilities. Forty-seven age- and gender-matched healthy control participants without neurologic impairment or psychiatric disorders were enrolled.

All participants were right-handed according to the Edinburgh Handedness Inventory (Espírito-Santo et al., 2017). All subjects gave written, informed consent in person approved by the Research Ethics Committee of Second Affiliated Hospital of Wenzhou Medical University and conducted in accordance with the Declaration of Helsinki.

Serum α-Synuclein Collection

Serum samples for patients and controls were collected in the morning. All participants also did not take any medications. Samples were aliquoted and stored at −80°C until the time of assay after collection and centrifugation. The levels (pg/mL) of α-syn in serum were measured using reagents on a Luminex multiplex bead system (Luminex Corporation, Austin, TX, USA). Serum α-syn assay was performed at Covance using a commercially available ELISA Assay Kit (Covance, Dedham, MA, USA; Mollenhauer et al., 2013). A fluorescence detection laser optic system was used to analyze the binding of each individual protein on the microsphere simultaneously, which permits multiplexed analysis of each of the analytes in one sample. Immunoassays were performed according to manufacturer's protocols. Intra- and inter-assay coefficients of variation observed for Luminex quantification were less than 20 percent and 25 percent, respectively. Samples with levels that were undetectable by the assay were set to 0.0001 pg/mL. The levels of α-syn >3 standard deviations above and below the population mean within group were considered outliers and excluded for all analysis (Diamond et al., 2015).

Neuropsychological Tests

For all participants, comprehensive cognitive tests were performed within 48 h of blood sample collection and MRI acquisition. These tests included: (i) Trail-Making Test Part A and Digit Symbol Coding (DSC) score from the Wechsler Adult Intelligence Scale-III (WAIS-III), to examine cognitive information processing speed; (ii) Forward Digit Span (FDS) and Backward Digit Span from the WAIS-III, to assess working memory (Harman-Smith et al., 2013); (iii) Verbal Fluency Test, to assess verbal fluency including language ability, semantic memory, and executive function (Joy et al., 2004); (iv) Beck Depression Inventory-II (BDI-II), to assess depression severity (Reiland, 2017); (v) PTSD Checklist—Civilian Version (PCL-C; Weathers et al., 1991); and (vi) Fatigue Severity Scale (Krupp et al., 1989) and Insomnia Severity Index (ISI; Sadeghniiat-Haghighi et al., 2014). In addition, post-concussive symptoms (PCS) were measured with the Rivermead Post-Concussion Symptom Questionnaire (RPQ; King et al., 1995).

Image Acquisition

Following acute head injury, non-contrast CT scans were performed on all consecutive patients with a 64-row CT scanner (GE, Lightspeed VCT). MRI scans were acquired using a 3.0T MRI scanner (GE 750). A custom-built head holder was used to prevent head movements. All participants were instructed to remain in a relaxed state, to avoid engaging in any mental activities, and to keep their eyes closed. Alertness during the scan was confirmed immediately after the whole scan was completed. MRI protocols involved the high-resolution T1-weighted 3D MPRAGE sequence (echo time (TE) = 3.17 ms, repetition time (TR) = 8.15 ms, flip angle = 9°, slice thickness = 1 mm, field of view (FOV) = 256 mm × 256 mm, matrix size = 256 × 256), single-shot, gradient-recalled echo planar imaging (EPI) sequence with 54 slices covering the whole brain (TR = 2,000 ms, TE = 30 ms, slice thickness = 3 mm, flip angle = 90°, FOV = 216 mm × 216 mm, matrix size = 64 × 64, voxel size = 3 mm × 3 mm × 3 mm), and axial FLAIR (TR = 9,000 ms, TE = 95 ms, flip angle = 150°, thickness = 5 mm, slices = 20, FOV = 240 mm × 240 mm, matrix size = 173 × 256).

The presence of focal lesions and cerebral microbleeds was determined by an experienced clinical neuroradiologist (with 10 years' experience), who assessed multiple modalities of neuroimaging data (T1-weighted, SWI, FLAIR) for all subjects in random sequence. The neuroradiologist was blind to clinical information and group membership (patient or control).

Preprocessing of Resting-State fMRI Data

Data processing was performed using SPM12 (Statistical Parametric Mapping, University College of London, London, UK) on MATLAB platform (R2013a; MathWorks, Natick, MA, USA). Image preprocessing steps included anatomical segmentation, normalization to Montreal Neurological Institute (MNI) space, spatial smoothing (full-width at half-maximum, FWHM = 6 mm), band-pass filtering (0.01–0.1 Hz), and regressing out signal contributions from head motion, white matter, and cerebrospinal fluid (Thompson et al., 2016). We adopted a seed-based method to extract the DMN. Regions of interest (ROI) in the DMN were defined based on a previous task fMRI study (Duan et al., 2012). In our study, we selected only the PCC (MNI coordinates: 0, −52, 27) as the seed for brain network connectivity analysis. Next, for each subject, the time series of the mean BOLD signal of a 10-mm radius sphere centered at the peak coordinate of ROI was extracted to calculate the functional connectivity with each voxel of the whole brain. Prior to statistical analysis, the functional connectivity maps were transformed into *z*-values using Fisher transformation to improve normality. We then performed conjunction analyses to identify brain areas that were positively correlated with the PCC seed. A family-wise error (FWE) method with a threshold of $P < 0.05$ was set for multiple comparisons. A voxel-wise one-way analysis of variance (ANOVA) was used to test for network functional connectivity differences ($P < 0.05$, FWE correction) across three groups with gender as a nuisance covariate within DNM mask. We then used *post hoc* analyses to test for network functional connectivity differences ($P < 0.05$, FWE correction) across each of the two groups.

Statistical Analysis

All statistical analyses were performed using SPSS (version 19, IBM Corp, New York, NY, USA) and Prism (Version 7, GraphPad Software, San Diego, CA, USA). The Shapiro–Wilk W test was used to test for normality distribution in all continuous variables. The independent two-sample *t*-test and the Mann–Whitney test were used to compare group differences based on data normality. Chi-square analyses were applied to assess categorical variables. Multivariate linear regression analysis was used to determine the association between the levels of α-syn and neuropsychological testing. The levels of α-syn, age, gender, and education years were entered into the model as independent variables, with results of cognitive tests in the mTBI patients as dependent variables.

RESULTS

Participant Characteristics

Fifty-two patients with mTBI (27 males, age of 34.48 ± 13.32 years, education level of 9.31 ± 4.36 years) and 47 matched healthy controls (22 males, age of 35.43 ± 12.01 years, education level of 11.39 ± 5.66 years) were recruited for this study. No significant differences existed between the mTBI patients and healthy controls regarding age, education level, and gender ($p > 0.05$). The detailed demographic data and clinical characteristics of the participants are summarized in **Table 1**. Upon arrival at the emergency department, all patients with mTBI had an initial GCS of 15. The causes of injury included motor vehicle accidents (58%), assaults (25%), and falls (17%). All the mTBI patients had negative computed tomography findings.

We divided the mTBI patients into two groups according to the split criteria of whether the α-syn levels were above or below the mean plus one standard deviation α-syn level in the healthy controls. Therefore, patients with α-syn levels

TABLE 1 | Summary of demographic characteristic and neuropsychological test scores between patients and controls at acute phase.

	mTBI patients	Controls	*P*-value
Demographic			
Age	34.5 ± 13.3 (14–63)	35.4 ± 12.0 (14–60)	0.462
Gender (M/F)	27/25	22/25	0.258
Education	9.3 ± 4.4	11.4 ± 5.7	0.062
α-syn	536.9 ± 152.4	517.2 ± 86.3	0.470
Neuropsychological test			
TMT A	60.5 ± 43.5	46.3 ± 33.2	0.073
FDS	8.1 ± 1.6	8.5 ± 1.5	<0.001*
BDS	4.1 ± 1.5	4.6 ± 1.9	0.458
LF	17.3 ± 5.4	18.9 ± 5.9	0.280
DSC	37.9 ± 16.2	47.2 ± 16.9	0.007*
Self-report measures			
PCS	10.6 ± 7.1	2.1 ± 2.6	<0.001*
PCL-C	25.0 ± 6.3	17.0 ± 0.0	<0.001*
FSS	10.4 ± 5.7	9.0 ± 0.0	0.054
BDI	4.7 ± 3.7	0.1 ± 0.2	<0.001*
ISI	6.9 ± 6.2	1.9 ± 3.1	<0.001*
mTBI severity (N%)			
GCS = 15	52 (100%)		
GCS = 13, 14	0 (0%)		
Causes for mild TBI (N%)			
Motor vehicle accident	30 (58%)		
Assaults	13 (25%)		
Fall	9 (17%)		

*TMT A, Trail-Making Test Part A; FDS, Forward Digit Span Task; BDS, Backward Digit Span Task; LF, Language Fluency; DSC, Digit Symbol Coding; PCS, Postconcussive Symptoms Scale; PCL-C, Post-Traumatic Stress Disorder Checklist Civilian; FSS, Fatigue Severity Scale; BDI, Beck Depression Inventory; ISI, Insomnia Severity Index; GCS, Glasgow Coma Scale. *p < 0.05.*

TABLE 2 | Summary of demographic characteristic and neuropsychological test scores between patients and controls at acute phase.

	Patient-A	Patient-B	*P*-value
Demographic			
Age	33.9 ± 13.7 (17–60)	35.0 ± 13.2 (14–62)	0.479
Gender (M/F)	12/13	15/12	0.586
Education	9.4 ± 4.2	9.2 ± 4.6	0.941
α-syn	401.3 ± 66.3	662.5 ± 96.1	<0.001*
Neuropsychological test			
TMT A	62.0 ± 49.4	46.3 ± 33.2	0.679
FDS	8.2 ± 1.6	8.5 ± 1.5	0.718
BDS	4.2 ± 1.5	4.6 ± 1.9	0.652
LF	16.8 ± 5.9	18.9 ± 5.9	0.377
DSC	38.0 ± 14.5	47.2 ± 16.9	0.762
Self-report measures			
PCS	13.4 ± 8.3	2.1 ± 2.6	0.012*
PCL-C	25.6 ± 7.9	17.0 ± 0.0	0.612
FSS	12.0 ± 8.0	9.0 ± 0.0	0.026*
BDI	5.6 ± 4.2	0.1 ± 0.2	0.096
ISI	8.0 ± 6.7	1.9 ± 3.1	0.161
mTBI severity (N%)			
GCS = 15	25 (100%)	27 (100%)	
GCS = 13, 14	0 (0%)	0 (0%)	
Causes for mild TBI (N%)			
Motor vehicle accident	14 (56%)	16 (59%)	
Assaults	4 (16%)	9 (33%)	
Fall	7 (28%)	2 (8%)	

*TMT A, Trail-Making Test Part A; FDS, Forward Digit Span Task; BDS, Backward Digit Span Task; LF, Language Fluency; DSC, Digit Symbol Coding; PCS, Postconcussive Symptoms Scale; PCL-C, Post-Traumatic Stress Disorder Checklist Civilian; FSS, Fatigue Severity Scale; BDI, Beck Depression Inventory; ISI, Insomnia Severity Index; GCS, Glasgow Coma Scale. *p < 0.05.*

lower than 536.93 pg/mL were categorized into the Patient-A group, and those with α-syn levels higher than 536.93 pg/mL were divided into the Patient-B group. Patient-A consisted of 25 patients (12 male, age of 33.92 ± 13.67 years, education level of 9.40 ± 4.15 years), and Patient-B consisted of 27 patients (15 males, age of 35.00 ± 13.24 years, education level of 9.22 ± 4.62 years). No significant differences occurred between Patient-A and B in terms of age, education level, and gender ($p > 0.05$). The detailed demographic data and clinical characteristics of the patients per group were summarized in **Table 2**.

Neuropsychological Measures

Compared to the controls, the mTBI patients exhibited lower performance in terms of information processing speed while performing DSC task ($p = 0.007$), digit span forward ($p < 0.001$), and verbal fluency tasks rated by language fluency ($p = 0.013$). Moreover, the patients presented more complaints in the Post-Traumatic Stress Disorder Checklist (Civilian Version) compared to the controls ($p < 0.001$) and showed significant difference in the Post-Concussion Symptom Scale ($p < 0.001$), BDI ($p < 0.001$), and ISI ($p < 0.001$; **Table 1**).

Relationship of Serum α-Syn With Neuropsychological Characteristics

Multiple linear regression analysis showed that lower levels of α-syn in the mTBI patients are associated with severer outcomes from the Post-Concussion Symptom Scale ($\beta = -0.333$, $p = 0.013$, overall model: $F_{(3,48)} = 3.259$, $p = 0.019$, adjusted $R^2 = 0.217$, **Figure 1A**) and severer depression according to the BDI ($\beta = -0.311$, $p = 0.022$, overall model: $F_{(3,48)} = 2.840$, $p = 0.034$, adjusted $R^2 = 0.195$, **Figure 1B**).

The α-syn levels in Patient-A were significantly different compared with Patient-B ($p < 0.001$), and the α-syn levels in controls were significantly different compared to both Patient-A ($p < 0.001$) and B ($p < 0.001$; **Figure 2B**). The significant differences persisted after multiple corrections.

The α-syn in serum of Patient-A patients was significantly lower than those of Patient-B patients ($p = 0.012$) and controls ($p < 0.001$). Meanwhile, the α-syn in the serum of Patient-B patients was significantly higher than that of controls ($p < 0.001$; **Figure 2A**).

Default Mode Network Results

The results of the one-sample *t*-test used to identify brain regions within the DMN mask with functional connectivity differences ($p < 0.05$, FWE corrected) in the participants are shown in **Figure 3**. We also compared the changes in the DMN between the two groups, and Patient-B presented a prominently higher functional connectivity in the left anterior cingulate cortex and ventral MPFC ($p < 0.05$, FWE corrected), and a significantly lower functional connectivity in the precuneus ($p < 0.05$, FWE corrected) compared with Patient-A (**Figure 4**). There was also no significant correlation between functional connectivity and serum α-syn.

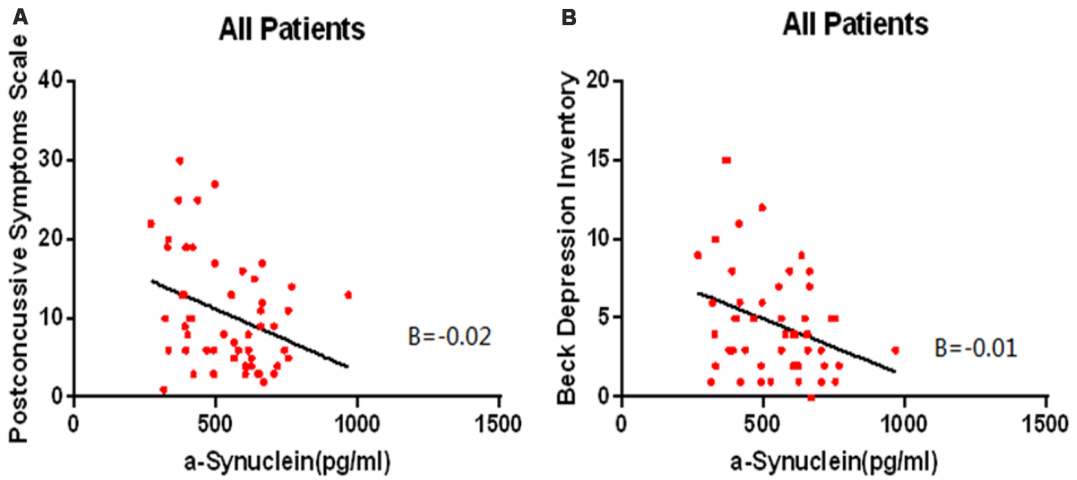

FIGURE 1 | The lower levels of α-syn are associated with severer outcomes from the Post-Concussion Symptom Scale (β = –0.333, p = 0.013, overall model: $F_{(3,48)}$ = 3.259, p = 0.019, adjusted R^2 = 0.217, **A**) and severer depression according to the Beck Depression Inventory (BDI; β = –0.311, p = 0.022, overall model: $F_{(3,48)}$ = 2.840, p = 0.034, adjusted R^2 = 0.195, **B**) in the mTBI patients.

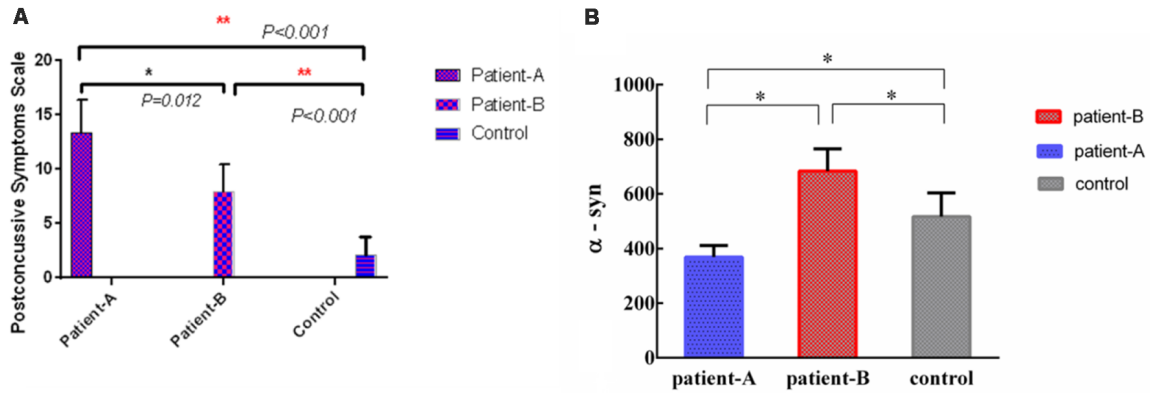

FIGURE 2 | The levels of serum α-syn of Patient-A was significantly different with Patient-B (p = 0.012) and controls ($p < 0.001$), meanwhile, the levels of serum α-syn of Patient-B was significantly different with controls ($p < 0.001$; **A**). The levels of serum α-syn in Patient-A were significantly different compared with Patient-B ($p < 0.001$), the levels of serum α-syn in controls were also significantly different compare with Patient-A ($p < 0.001$) and Patient-B ($p < 0.001$; **B**). *$p < 0.05$, **$p < 0.001$.

DISCUSSION

In this study, we explored α-syn as candidate biomarker and combined it with brain imaging data for both diagnosis and prognosis of patients suffering from mTBI. Compared with the healthy control group, the mTBI patients had lower scores for FDS and DSC, and higher scores for PCS, PCL-C, BDI and ISI. These results were consistent with neuropsychiatric symptoms of the mTBI patients: persistent headaches, difficulty thinking, memory deficits, inattention, emotional instability, and brief frustration after injury. We found that patients with lower α-syn levels exhibited severe post-concussion and depressive symptoms. Moreover, patients with higher α-syn levels, compared to those with lower α-syn levels, showed significantly increased functional connectivity in the left anterior cingulate cortex and ventral MPFC, and a significantly decreased connectivity in the precuneus. To the best of our knowledge, this is the first study to examine α-syn level and its association with the DMN during the early acute phase of mTBI, and explore the relationship between α-syn levels and cognitive function, which are major determinants of poor prognosis in mTBI.

The presynaptic terminals have plenty of neuronal proteins, one being α-syn (Vekrellis et al., 2011), which is the main component of Lewy bodies. The accumulation of α-syn aggregates is also found in Lewy body dementia and multiple system atrophy (Spillantini et al., 1998). Although several studies have examined the levels of α-syn in cerebrospinal fluid (Mollenhauer et al., 2011, 2013) or serum (Lin et al., 2017) of the mTBI patients, their results were inconsistent.

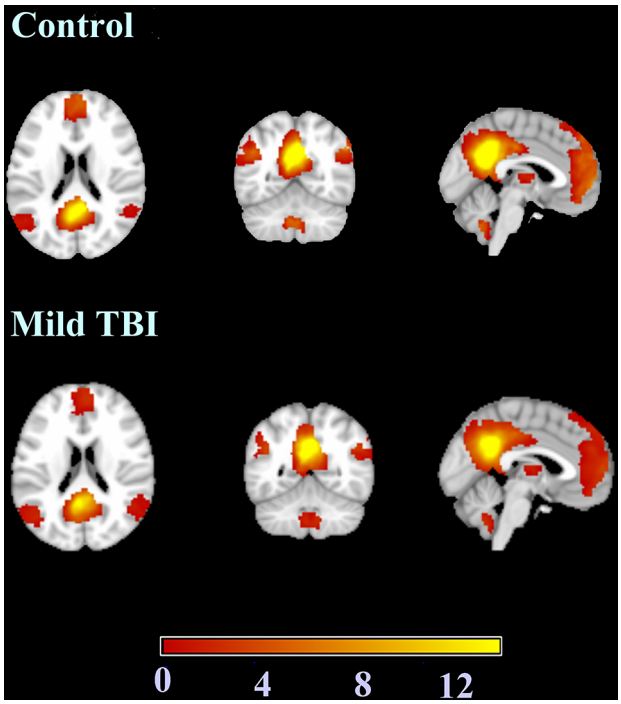

FIGURE 3 | The results of the one-sample *t*-test used to identify brain regions within the default mode network (DMN) mask with functional connectivity differences.

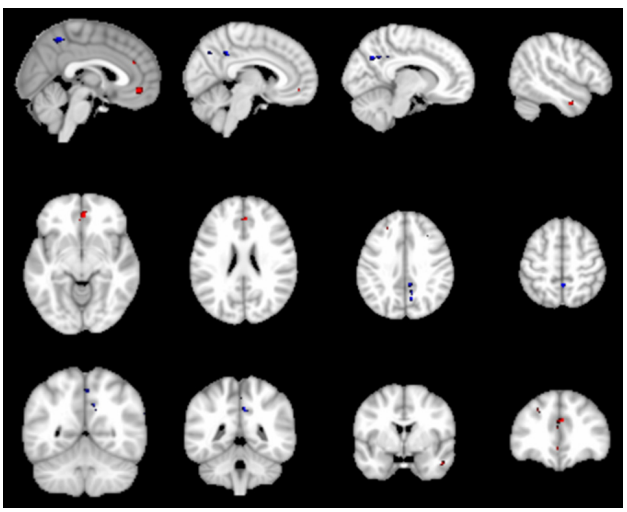

FIGURE 4 | The red represent regions of increased rs-FC in the Patient-B compared with Patient-A and the blue represent regions of reduced rs-FC. Cluster extent threshold of *p*-value of 0.05 using a family-wise error (FWE) correction for multiple comparisons.

Subsequently, reduction of costs, development of noninvasive techniques, and methodological advances have enabled more intensive and deep serum studies (Lin et al., 2017; Singh et al., 2018). Prior studies have investigated the relationship between TBI and the risk of developing PD (Kenborg et al., 2015; Perry et al., 2016; Taylor et al., 2016). It has been reported that mTBI is associated with a 56% increased risk of developing PD, even after adjusting for demographics and medical comorbidities among military veterans (Gardner et al., 2018). In this study, we found that patients with lower α-syn in serum exhibited severer post-concussion and depressive symptoms during the early acute phase of mTBI. Although past research on animals found that overexpression of α-syn may constitute a pathological link between TBI and development of pathologies similar to PD (Stewart et al., 2014), that study adopted male rats, whose brain function and structure notably differ from those of humans. In addition, the subjects of our study were recruited within the 1st week after suffering mTBI. We hypothesized that during the acute phase of mTBI, elevated α-syn is a product of compensatory mechanisms, which means lower α-syn patients may be unable to compensate these levels after mTBI, leading to severer post-concussion and depressive symptoms. Schilbach et al. (2008) suggested that decreased levels of cerebrospinal fluid α-syn in early stage PD may be the result of cellular compensatory mechanisms for pathological soluble α-syn, thus obtaining lower levels of α-syn compared with controls (Schilbach et al., 2008).

The DMN is a task-negative network involving self-reference processes, such as introspection and experiential memory (Schilbach et al., 2008; Fingelkurts and Fingelkurts, 2011). The essential nodes of the DMN include the PCC, bilateral angular gyri, precuneus, ventro-MPFC, and dorsal-MPFC. The functional connectivity within the DMN has been related to performance in higher cognitive functions such as attention and memory (Hampson et al., 2006; Buckner et al., 2008; Leech et al., 2011); meanwhile, cognitive dysfunctions are the most commonly reported consequences of mTBI (van der Naalt et al., 1999; Smith-Seemiller et al., 2003). In addition, fMRI-based studies have illustrated the DMN dysfunction after mTBI (Palacios et al., 2013; Nathan et al., 2015), and its relation to several diseases such as Alzheimer's disease, attention-deficit/hyperactivity disorder, and schizophrenia (Whitfield-Gabrieli et al., 2009; Koch et al., 2012).

Few studies have explored the causes of connectivity dysfunction within the DMN. Our results showed decreased functional connectivity between the anterior cingulate cortex and ventro-MPFC in patients with lower α-syn in serum compared to those with higher α-syn in serum. In addition, patients with lower levels of α-syn suffered significantly severer post-concussive and depressive symptoms. The brain regions involved in the DMN are related to high-level cognitive functions and decision-making. For instance, the precuneus is involved in learning and memory (Price, 2000). The anterior cingulate cortex has been associated with the anxiety disorder, post-traumatic stress disorder (Kennis et al., 2015), while MPFC has been found to participate in self-relevance, rapid error identification, and social functions. Moreover, changes in functional connectivity may be due to spontaneous seizures of neuronal ensembles, changes in blood flow, oxidative metabolism, or combinations of these factors (Fox and Raichle, 2007). Furthermore, α-syn is a presynaptic protein activated by various processes such as phosphorylation and contributes to the synaptic vesicle cycle (Acosta et al., 2015). These findings suggest that α-syn in

serum can modulate the connectivity of the DMN in patients with mTBI.

Several limitations of our study remain to be addressed. First, we only explored changes in the DMN functional connectivity within the 1st week post-injury. However, the considered post-injury period should be longer to accurately observe the functional connectivity evolution, and longitudinal analyses need to be conducted using follow-up data. Second, while α-syn concentration in serum changed significantly during the acute phase, the 1-week period post-injury provided limited information for observing the dynamic changes of α-syn in the acute phase. Third, we only considered resting-state fMRI, and the results did not exclude the possibility of structural changes, which can be measured by diffusion tensor imaging. Future research must explore the relationship between structural and functional network defects and their clinical significance.

CONCLUSION

We found that mTBI may involve a chronic, progressive, neurodegenerative process, and may be closely associated with the occurrence of PD. As biomarker of PD, α-syn in serum also exhibits significant changes in the mTBI patients. Specifically, patients with higher levels of α-syn in serum exhibited increased functional connectivity in the left anterior cingulate cortex and ventro-MPFC and decreased functional connectivity in the precuneus. Therefore, α-syn in serum may be considered as one of the modulations of the DMN connectivity in patients with mTBI. These results suggest the plausibility of using the α-syn in serum as objective biomarker for the prognosis of mTBI and early intervention to prevent adverse sequels in patients with this type of injury.

ETHICS STATEMENT

All the subjects gave written, informed consent in person approved by a local institutional review board and conducted in accordance with the Declaration of Helsinki.

AUTHOR CONTRIBUTIONS

LY, ZY, and GB contributed to the conception of the study. LY contributed significantly to analysis and manuscript preparation. LY, DZ, PZ, and MS performed the data analyses and wrote the manuscript. CG, BY, JZ, and FW helped perform the analysis with constructive discussions.

FUNDING

This research was supported by the Natural Science Foundation of Zhejiang Province (nos. LY19H180003, LY16H180009 and LY15H090016).

REFERENCES

Acosta, S. A., Tajiri, N., de la Pena, I., Bastawrous, M., Sanberg, P. R., Kaneko, Y., et al. (2015). α-synuclein as a pathological link between chronic traumatic brain injury and Parkinson's disease. *J. Cell. Physiol.* 230, 1024–1032. doi: 10.1002/jcp.24830

Buckner, R. L., Andrews-Hanna, J. R., and Schacter, D. L. (2008). The brain's default network: anatomy, function, and relevance to disease. *Ann. N Y Acad. Sci.* 1124, 1–38. doi: 10.1196/annals.1440.011

Diamond, M. L., Ritter, A. C., Failla, M. D., Boles, J. A., Conley, Y. P., Kochanek, P. M., et al. (2015). IL-1β associations with posttraumatic epilepsy development: a genetics and biomarker cohort study. *Epilepsia* 56, 991–1001. doi: 10.1111/epi.13100

Duan, X. J., Liao, W., Liang, D. M., Qiu, L. H., Gao, Q., Liu, C. Y., et al. (2012). Large-scale brain networks in board game experts: insights from a domain-related task and task-free resting state. *PLoS One* 7:e32532. doi: 10.1371/journal.pone.0032532

Espírito-Santo, H., Pires, C. F., Garcia, I. Q., Daniel, F., da Silva, A. G., and Fazio, R. L. (2017). Preliminary validation of the portuguese edinburgh handedness inventory in an adult sample. *Appl. Neuropsychol. Adult* 24, 275–287. doi: 10.1080/23279095.2017.1290636

Fingelkurts, A. A., and Fingelkurts, A. A. (2011). Persistent operational synchrony within brain default-mode network and self-processing operations in healthy subjects. *Brain Cogn.* 75, 79–90. doi: 10.1016/j.bandc.2010.11.015

Fox, M. D., and Raichle, M. E. (2007). Spontaneous fluctuations in brain activity observed with functional magnetic resonance imaging. *Nat. Rev. Neurosci.* 8, 700–711. doi: 10.1038/nrn2201

Gardner, R. C., Burke, J. F., Nettiksimmons, J., Goldman, S., Tanner, C. M., and Yaffe, K. (2015). Traumatic brain injury in later life increases risk for Parkinson disease. *Ann. Neurol.* 77, 987–995. doi: 10.1002/ana.24396

Gardner, R. C., Byers, A. L., Barnes, D. E., Li, Y. X., Boscardin, J., and Yaffe, K. (2018). Mild TBI and risk of Parkinson disease: a chronic effects of neurotrauma consortium study. *Neurology* 90, E1771–E1779. doi: 10.1212/wnl.0000000000005522

Gardner, R. C., and Yaffe, K. (2015). Epidemiology of mild traumatic brain injury and neurodegenerative disease. *Mol. Cell. Neurosci.* 66, 75–80. doi: 10.1016/j.mcn.2015.03.001

Hampson, M., Driesen, N. R., Skudlarski, P., Gore, J. C., and Constable, R. T. (2006). Brain connectivity related to working memory performance. *J. Neurosci.* 26, 13338–13343. doi: 10.1523/JNEUROSCI.3408-06.2006

Harman-Smith, Y. E., Mathias, J. L., Bowden, S. C., Rosenfeld, J. V., and Bigler, E. D. (2013). Wechsler adult intelligence scale-third edition profiles and their relationship to self-reported outcome following traumatic brain injury. *J. Clin. Exp. Neuropsychol.* 35, 785–798. doi: 10.1080/13803395.2013.824554

Holm, L., Cassidy, J. D., Carroll, L. J., and Borg, J. (2005). Summary of the WHO collaborating centre for neurotrauma task force on mild traumatic brain injury. *J. Rehabil. Med.* 37, 137–141. doi: 10.1080/16501970510027321

Institute of Medicine. (2009). *Gulf War and Health: Volume 7: Long-Term Consequences of Traumatic Brain Injury*. Washington, DC: The National Academies Press.

Joy, S., Kaplan, E., and Fein, D. (2004). Speed and memory in the WAIS-III Digit Symbol—Coding subtest across the adult lifespan. *Arch. Clin. Neuropsychol.* 19, 759–767. doi: 10.1016/j.acn.2003.09.009

Kenborg, L., Rugbjerg, K., Lee, P. C., Ravnskjær, L., Christensen, J., Ritz, B., et al. (2015). Head injury and risk for Parkinson disease Results from a Danish case-control study. *Neurology* 84, 1098–1103. doi: 10.1212/WNL.0000000000001362

Kennis, M., Rademaker, A. R., van Rooij, S. J. H., Kahn, R. S., and Geuze, E. (2015). Resting state functional connectivity of the anterior cingulate cortex in veterans with and without post-traumatic stress disorder. *Hum. Brain Mapp.* 36, 99–109. doi: 10.1002/hbm.22615

King, N. S., Crawford, S., Wenden, F. J., Moss, N. E., and Wade, D. T. (1995). The Rivermead Post Concussion Symptoms Questionnaire: a measure of symptoms commonly experienced after head injury and its reliability. *J. Neurol.* 242, 587–592. doi: 10.1007/bf00868811

Klein, C., and Westenberger, A. (2012). Genetics of Parkinson's disease. *PLoS One* 2:a008888. doi: 10.1101/cshperspect.a008888

Koch, W., Teipel, S., Mueller, S., Benninghoff, J., Wagner, M., Bokde, A. L. W., et al. (2012). Diagnostic power of default mode network resting state fMRI in the detection of Alzheimer's disease. *Neurobiol. Aging* 33, 466–478. doi: 10.1016/j.neurobiolaging.2010.04.013

Kochanek, P. M., Berger, R. P., Bayir, H., Wagner, A. K., Jenkins, L. W., and Clark, R. S. B. (2008). Biomarkers of primary and evolving damage in traumatic and ischemic brain injury: diagnosis, prognosis, probing mechanisms, and therapeutic decision making. *Curr. Opin. Crit. Care* 14, 135–141. doi: 10.1097/mcc.0b013e3282f57564

Krupp, L. B., LaRocca, N. G., Muir-Nash, J., and Steinberg, A. D. (1989). The fatigue severity scale. Application to patients with multiple sclerosis and systemic lupus erythematosus. *Arch. Neurol.* 46, 1121–1123. doi: 10.1001/archneur.1989.00520460115022

Langlois, J. A., Rutland-Brown, W., and Wald, M. M. (2006). The epidemiology and impact of traumatic brain injury: a brief overview. *J. Head Trauma Rehabil.* 21, 375–378. doi: 10.1097/00001199-200609000-00001

Lee, H., Wintermark, M., Gean, A. D., Ghajar, J., Manley, G. T., and Mukherjee, P. (2008). Focal lesions in acute mild traumatic brain injury and neurocognitive outcome: CT versus 3T MRI. *J. Neurotrauma* 25, 1049–1056. doi: 10.1089/neu.2008.0566

Leech, R., Kamourieh, S., Beckmann, C. F., and Sharp, D. J. (2011). Fractionating the default mode network: distinct contributions of the ventral and dorsal posterior cingulate cortex to cognitive control. *J. Neurosci.* 31, 3217–3224. doi: 10.1523/JNEUROSCI.5626-10.2011

Lin, C. H., Yang, S. Y., Horng, H. E., Yang, C. C., Chieh, J. J., Chen, H. H., et al. (2017). Plasma α-synuclein predicts cognitive decline in Parkinson's disease. *J. Neurol. Neurosurg. Psychiatry* 88, 818–824. doi: 10.1136/jnnp-2016-314857

Mac Donald, C. L., Barber, J., Jordan, M., Johnson, A. M., Dikmen, S., Fann, J. R., et al. (2017). Early clinical predictors of 5-year outcome after concussive blast traumatic brain injury. *JAMA Neurol.* 74, 821–829. doi: 10.1001/jamaneurol.2017.0143

Magnoni, S., and Brody, D. L. (2010). New perspectives on amyloid-β dynamics after acute brain injury moving between experimental approaches and studies in the human brain. *Arch. Neurol.* 67, 1068–1073. doi: 10.1001/archneurol.2010.214

Mayer, A. R., Mannell, M. V., Ling, J., Gasparovic, C., and Yeo, R. A. (2011). Functional connectivity in mild traumatic brain injury. *Hum. Brain Mapp.* 32, 1825–1835. doi: 10.1002/hbm.21151

McAllister, T. W. (2008). Neurobehavioral sequelae of traumatic brain injury: evaluation and management. *World Psychiatry* 7, 3–10. doi: 10.1002/j.2051-5545.2008.tb00139.x

Mollenhauer, B., Locascio, J. J., Schulz-Schaeffer, W., Sixel-Döring, F., Trenkwalder, C., and Schlossmacher, M. G. (2011). α-Synuclein and tau concentrations in cerebrospinal fluid of patients presenting with parkinsonism: a cohort study. *Lancet Neurol.* 10, 230–240. doi: 10.1016/S1474-4422(11)70014-X

Mollenhauer, B., Trautmann, E., Taylor, P., Manninger, P., Sixel-Döring, F., Ebentheuer, J., et al. (2013). Total CSF α-synuclein is lower in de novo Parkinson patients than in healthy subjects. *Neurosci. Lett.* 532, 44–48. doi: 10.1016/j.neulet.2012.11.004

Nathan, D. E., Oakes, T. R., Yeh, P. H., French, L. M., Harper, J. F., Liu, W., et al. (2015). Exploring variations in functional connectivity of the resting state default mode network in mild traumatic brain injury. *Brain Connect.* 5, 102–114. doi: 10.1089/brain.2014.0273

Palacios, E. M., Sala-Llonch, R., Junque, C., Roig, T., Tormos, J. M., Bargallo, N., et al. (2013). Resting-state functional magnetic resonance imaging activity and connectivity and cognitive outcome in traumatic brain injury. *JAMA Neurol.* 70, 845–851. doi: 10.1001/jamaneurol.2013.38

Perry, D. C., Sturm, V. E., Peterson, M. J., Pieper, C. F., Bullock, T., Boeve, B. F., et al. (2016). Association of traumatic brain injury with subsequent neurological and psychiatric disease: a meta-analysis. *J. Neurosurg.* 124, 511–526. doi: 10.3171/2015.2.jns14503

Price, D. D. (2000). Psychological and neural mechanisms of the affective dimension of pain. *Science* 288, 1769–1772. doi: 10.1126/science.288.5472.1769

Ralchle, M. E., and Snyder, A. Z. (2007). A default mode of brain function: a brief history of an evolving idea. *Neuroimage* 37, 1083–1090. doi: 10.1016/j.neuroimage.2007.02.041

Reiland, S. A. (2017). "Beck depression inventory," in *Encyclopedia of Personality and Individual Differences*, eds V. Zeigler-Hill and T. Shackelford (Cham: Springer), 1–3.

Rocca, M. A., Valsasina, P., Absinta, M., Riccitelli, G., Rodegher, M. E., Misci, P., et al. (2010). Default-mode network dysfunction and cognitive impairment in progressive MS. *Neurology* 74, 1252–1259. doi: 10.1212/WNL.0b013e3181d9ed91

Sadeghniiat-Haghighi, K., Montazeri, A., Khajeh-Mehrizi, A., Nedjat, S., and Aminian, O. (2014). The Insomnia Severity Index: cross-cultural adaptation and psychometric evaluation of a Persian version. *Qual. Life Res.* 23, 533–537. doi: 10.1007/s11136-013-0489-3

Schilbach, L., Eickhoff, S. B., Rotarska-Jagiela, A., Fink, G. R., and Vogeley, K. (2008). Minds at rest? Social cognition as the default mode of cognizing and its putative relationship to the "default system" of the brain. *Conscious. Cogn.* 17, 457–467. doi: 10.1016/j.concog.2008.03.013

Singh, A. P., Bajaj, T., Gupta, D., Singh, S. B., Chakrawarty, A., Goyal, V., et al. (2018). Serum mortalin correlated with α-synuclein as serum markers in Parkinson's disease: a pilot study. *Neuromolecular Med.* 20, 83–89. doi: 10.1007/s12017-017-8475-5

Slobounov, S. M., Gay, M., Zhang, K., Johnson, B., Pennell, D., Sebastianelli, W., et al. (2011). Alteration of brain functional network at rest and in response to YMCA physical stress test in concussed athletes: RsFMRI study. *Neuroimage* 55, 1716–1727. doi: 10.1016/j.neuroimage.2011.01.024

Smith-Seemiller, L., Fow, N. R., Kant, R., and Franzen, M. D. (2003). Presence of post-concussion syndrome symptoms in patients with chronic pain vs. mild traumatic brain injury. *Brain Inj.* 17, 199–206. doi: 10.1080/0269905021000030823

Spillantini, M. G., Crowther, R. A., Jakes, R., Cairns, N. J., Lantos, P. L., and Goedert, M. (1998). Filamentous α-synuclein inclusions link multiple system atrophy with Parkinson's disease and dementia with Lewy bodies. *Neurosci. Lett.* 251, 205–208. doi: 10.1016/s0304-3940(98)00504-7

Stewart, T., Liu, C. Q., Ginghina, C., Cain, K. C., Auinger, P., Cholerton, B., et al. (2014). Cerebrospinal fluid α-synuclein predicts cognitive decline in Parkinson disease progression in the DATATOP cohort. *Am. J. Pathol.* 184, 966–975. doi: 10.1016/j.ajpath.2013.12.007

Taylor, K. M., Saint-Hilaire, M. H., Sudarsky, L., Simon, D. K., Hersh, B., Sparrow, D., et al. (2016). Head injury at early ages is associated with risk of Parkinson's disease. *Parkinsonism Relat. Disord.* 23, 57–61. doi: 10.1016/j.parkreldis.2015.12.005

Thompson, W. H., Thelin, E. P., Lilja, A., Bellander, B. M., and Fransson, P. (2016). Functional resting-state fMRI connectivity correlates with serum levels of the S100B protein in the acute phase of traumatic brain injury. *Neuroimage Clin.* 12, 1004–1012. doi: 10.1016/j.nicl.2016.05.005

Tokuda, T., Qureshi, M. M., Ardah, M. T., Varghese, S., Shehab, S. A., Kasai, T., et al. (2010). Detection of elevated levels of α-synuclein oligomers in CSF from patients with Parkinson disease. *Neurology* 75, 1766–1772. doi: 10.1212/WNL.0b013e3181fd613b

van der Naalt, J., van Zomeren, A. H., Sluiter, W. J., and Minderhoud, J. M. (1999). One year outcome in mild to moderate head injury: the predictive value of acute injury characteristics related to complaints and return to work. *J. Neurol. Neurosurg. Psychiatry* 66, 207–213. doi: 10.1136/jnnp.66.2.207

Vekrellis, K., Xilouri, M., Emmanouilidou, E., Rideout, H. J., and Stefanis, L. (2011). Pathological roles of α-synuclein in neurological disorders. *Lancet Neurol.* 10, 1015–1025. doi: 10.1016/S1474-4422(11)70213-7

Weathers, F. W., Litz, B. T., Huska, J. A., and Keane, T. M. (1991). *PTSD Checklist—Civilian Version.* Boston, MA: National Center for PTSD, Behavioral Science Division.

Werner, C., and Engelhard, K. (2007). Pathophysiology of traumatic brain injury. *Br. J. Anaesth.* 99, 4–9. doi: 10.1093/bja/aem131

Whitfield-Gabrieli, S., Thermenos, H. W., Milanovic, S., Tsuang, M. T., Faraone, S. V., McCarley, R. W., et al. (2009). Hyperactivity and hyperconnectivity of the default network in schizophrenia and in first-degree relatives persons with schizophrenia. *Proc.*

Natl. Acad. Sci. U S A 106, 1279–1284. doi: 10.1073/pnas.0809141106

Zemek, R. L., Farion, K. J., Sampson, M., and McGahern, C. (2013). Prognosticators of persistent symptoms following pediatric concussion: a systematic review. *JAMA Pediatr.* 167, 259–265. doi: 10.1001/2013.jamapediatrics.216

Zhang, D. Y., and Raichle, M. E. (2010). Disease and the brain's dark energy. *Nat. Rev. Neurol.* 6, 15–28. doi: 10.1038/nrneurol.2009.198

Zhou, Y. X., Milham, M. P., Lui, Y. W., Miles, L., Reaume, J., Sodickson, D. K., et al. (2012). Default-mode network disruption in mild traumatic brain injury. *Radiology* 265, 882–892. doi: 10.1148/radiol.12120748

Conflict of Interest Statement: The authors declare that the research was conducted in the absence of any commercial or financial relationships that could be construed as a potential conflict of interest.

frontiers in Neural Circuits

ORIGINAL RESEARCH
published: 18 April 2019
doi: 10.3389/fncir.2019.00025

Aberrant Coupling Between Resting-State Cerebral Blood Flow and Functional Connectivity in Wilson's Disease

Sheng Hu[1†], Hongli Wu[1†], ChunSheng Xu[2], Anqin Wang[2], Yi Wang[1], Tongping Shen[1], Fangliang Huang[1], Hongxing Kan[1] and Chuanfu Li[2*]*

[1] Medical Information Engineering, Anhui University of Chinese Medicine, Hefei, China, [2] Laboratory of Digital Medical Imaging, Medical Imaging Center, The First Affiliated Hospital of Anhui University of Chinese Medicine, Hefei, China

Both abnormalities of resting-state cerebral blood flow (CBF) and functional connectivity in Wilson's disease (WD) have been identified by several studies. Whether the coupling of CBF and functional connectivity is imbalanced in WD remains largely unknown. To assess this possibility, 27 patients with WD and 27 sex- and age-matched healthy controls were recruited to acquire functional MRI and arterial spin labeling imaging data. Functional connectivity strength (FCS) and CBF were calculated based on standard gray mask. Compared to healthy controls, the CBF–FCS correlations of patients with WD were significantly decreased in the basal ganglia and the cerebellum and slightly increased in the prefrontal cortex and thalamus. In contrast, decreased CBF of patients with WD occurred predominately in subcortical and cognitive- and emotion-related brain regions, including the basal ganglia, thalamus, insular, and inferior prefrontal cortex, whereas increased CBF occurred primarily in the temporal cortex. The FCS decrease in WD patients was predominately in the basal ganglia and thalamus, and the increase was primarily in the prefrontal cortex. These findings suggest that aberrant neurovascular coupling in the brain may be a possible neuropathological mechanism underlying WD.

Keywords: neurovascular coupling, basal ganglia, arterial spin labeling, cerebral blood flow, functional magnetic resonance imaging

OPEN ACCESS

Edited by:
Lijun Bai,
Xi'an Jiaotong University, China

Reviewed by:
Alexey Brazhe,
Lomonosov Moscow State University, Russia
Lei Gao,
Wuhan University, China

****Correspondence:***
Hongxing Kan
984377701@qq.com
Chuanfu Li
13956078816@126.com

† These authors have contributed equally to this work

Received: *13 October 2018*
Accepted: *25 March 2019*
Published: *18 April 2019*

Citation:
Hu S, Wu H, Xu C, Wang A, Wang Y, Shen T, Huang F, Kan H and Li C (2019) Aberrant Coupling Between Resting-State Cerebral Blood Flow and Functional Connectivity in Wilson's Disease. Front. Neural Circuits 13:25. doi: 10.3389/fncir.2019.00025

INTRODUCTION

Wilson's disease (WD) is an inherited disorder of copper metabolism. The symptoms were first identified by Dr. Samuel Alexander Kinnier Wilson in 1912 (Wilson, 1912). The physical burden of the disease falls on the liver and the brain. Copper deposition in the brain affected by WD occurs primarily in the basal ganglia. In early stages of the disease, this results in neurological or psychiatric symptoms, such as mild cognitive deterioration, whereas late stages are characterized by dysarthria (de Bie et al., 2007), abnormal gait, risus sardonicus, dystonia, rigidity, and dyskinesia (Machado et al., 2006; Litwin et al., 2016). The neuropathological characteristics of WD are neuronal loss and atrophy in the bilateral basal ganglia, brainstem, cerebellum, and cerebral cortex (Page et al., 2004).

Resting-state functional connectivity (rsFC), which measures the temporal correlations of low-frequency fluctuations in the blood-oxygen-level-dependent (BOLD) signal across the brain regions (Biswal et al., 1995), has provided evidence that copper deposition profoundly impairs intrinsic brain activity (Hu et al., 2017). Seed-based FC analysis has been used to quantify FC changes in WD and has uncovered abnormal FC in the default mode network (DMN) (Han et al., 2016). Although these methods are conducive to quantifying functional dysconnectivity in the brain of individuals with WD, both rsFC and seed-based FC analysis have issues. Seed-based FC methods require *a priori* knowledge of the seed region. Thus, it is difficult to analyze data if the underlying pathology of a disease is unknown (Nair et al., 2014). Low-frequency BOLD signals are susceptible to physiological processes, such as respiratory and cardiac oscillations, which may lead to unreliable results when using rsFC methods (Biswal, 2012). Functional connectivity strength (FCS) analysis is a new data-driven method to measure average FC by calculating the correlation of each voxel with all other voxels in the brain (Liang et al., 2013). Brain regions with high FCS are identified as functional hubs, which have high connectivity to the remainder of the brain.

In the resting brain, cerebral blood flow (CBF) is closely related to glucose utilization, oxygen consumption, and aerobic glycolysis (Vaishnavi et al., 2010). Some studies have noted CBF deficits in WD. For example, positron emission tomography (PET) and single-photon emission computed tomography (SPECT) have revealed decreased metabolic rate of glucose consumption and hypoperfusion in the prefrontal cortex, occipital cortex, cerebellum, striatum, and thalamus (Hawkins et al., 1987; Kuwert et al., 1992). However, these two techniques are invasive, with a long acquisition time and low spatial resolution. Arterial spin labeling (ASL) MRI is a non-invasive technique for measuring CBF using an endogenous contrast (Roberts, 1994; Golay et al., 2004). Therefore, it has been widely used to evaluate cerebrovascular disease, including arterio-occlusive disease, and as a biomarker for neuronal metabolism in other disorders, such as Alzheimer's and Parkinsonism diseases (Telischak et al., 2015).

The human brain accounts for approximately 20% of the body's total energy demands (Raichle and Gusnard, 2002), which is more than any other organ. Brain metabolism, which consumes most of the glucose and produces most of the energy, is critical for supporting spontaneous brain activity (Raichle and Mintun, 2006). Brain regions with stronger neuronal activity tend to have greater brain metabolism, resulting in increased CBF (Kuschinsky, 1991; Venkat et al., 2016). The strength of neuronal activity in one brain region reflects the degree of functional connectivity with other brain regions (Zhu et al., 2017). Therefore, the degree of functional connectivity is related to brain metabolism, especially glucose utilization (Tomasi et al., 2013). Several studies have identified the relationship between functional networks and CBF. For instance, FCS analysis in healthy subjects and those with neurological diseases has suggested that brain FCS is coupled with CBF (Liang et al., 2013; Zhu et al., 2017).

Patients with WD experience copper accumulation in the brain, neuronal loss, and atrophy (Ala et al., 2007; Huster, 2010), possibly resulting in neurovascular imbalance. Therefore, we hypothesized that the coupling between CBF and brain FC would be abnormal in patients with WD relative to healthy subjects. To verify this hypothesis, we collected resting-state functional MRI (fMRI) data and ASL data from 27 patients with WD and 27 sex- and age-matched healthy controls to measure the brain FCS and CBF. Further, FCS–CBF correlations were compared between the groups.

MATERIALS AND METHODS

Subjects

Twenty-seven patients with WD with neurological symptoms (mean age, 22.42 years; SD, 3.66 years; 12 females) were recruited from the First Affiliated Hospital of Anhui University of Chinese Medicine (AUCM), and 27 age- and sex-matched healthy controls (mean age, 23.51 years; SD, 2.67 years; 12 females) were recruited from the local community. All patients were receiving drug treatment, including penicillamine and zinc salts. WD diagnosis was based on clinical symptoms (e.g., presentation of extrapyramidal and pyramidal symptoms and signs, and behavioral problems), the presence of the Kayser–Fleischer (KF) ring, and abnormal copper metabolism with serum ceruloplasmin (CP) less than 20 mg/dl and 24-h urinary excretion of copper of more than 1.6 μmol/day. The average CP was 6.28 ± 2.40 mg/dL (mean ± SD), and the average 24-h urinary copper excretion was 2.52 ± 1.44 μmol/day based on the WD group. There were no neurological diseases other than WD in the patients. Healthy controls had no history of head injury, neurological disorder, or concomitant medical disorder. All participants provided written informed consent. This study was approved by the Human Research Committee of the First Affiliated Hospital of AUCM. Detailed information regarding the subjects is presented in **Table 1**.

Data Acquisition

MRI data were acquired using a 3.0-Tesla MR system (Discovery MR750, General Electric) with an eight-channel high-resolution

TABLE 1 | Characteristics of the participants.

	WD (*N* = 27)	HC (*N* = 27)
Gender (male/female)	15/12	15/12
Age (years)	18–28 (22.42 ± 3.66)	19–31 (23.51 ± 2.67)
Education (years)	8–14 (10.21 ± 1.23)	9–15 (12.32 ± 2.55)
Handedness	27 right-handed	27 right-handed
WD duration (years)	4–10 (6.76 ± 1.38)	
WD types	Neurologic	
The KF ring	27 WD with the KF ring	
24-h urinary Cu (μmol/day)	1–6 (2.52 ± 1.44)	
CP (mg/dl)	3.52–13.24 (6.28 ± 2.40)	

WD, Wilson's disease; HC, healthy controls; N, number, KF, Kayser–Fleischer, Cu, copper, CP, ceruloplasmin.

radio-frequency head coil. Sagittal 3D T1-weighted images were acquired using a T1-3D BRAVO sequence with repetition time (TR)/echo time (TE) of 8.16 ms/3.18 ms, a flip angle (FA) of 12°, a 256 mm × 256 mm matrix, a field of view (FOV) of 256 mm × 256 mm, and a slice thickness of 1 mm, with 200 axial slices with no gap. Resting-state fMRI images were acquired using a gradient-echo single-shot echo planar imaging sequence with a TR/TE of 2,000/30 ms, an FOV of 220 mm × 220 mm, a 64 × 64 matrix, an FA of 90°, and a slice thickness of 3 mm, with 185 volumes. Functional ASL data were acquired using a pseudocontinuous arterial-labeling (pCASL) technique. Interleaved control and label images were acquired using a gradient echo EPI sequence with a TR/TE of 5,046/11 ms, an FA of 111°, 50 slices with 3-mm thickness, an FOV of 220 mm × 220 mm, a 128 × 128 matrix, three excitations, a post-label delay of 2,025 ms, and a spiral-in readout of 8 arms with 512 sample points. All participants were asked to keep their eyes closed, relax, move as little as possible, think of nothing, and stay awake during the scans.

Functional Magnetic Resonance Imaging Data Preprocessing

All fMRI data preprocessing was performed using SPM12[1] based on batch scripts. To account for magnetization equilibrium and subject's adaptation to the experimental environment, the first 10 volumes were removed. The remaining images underwent slice timing correction to address the time delay between different slices, and then all images were realigned to the first volume to correct for head motion. Subjects were excluded if head motion exceeded 1 mm of displacement or 1° of angular rotation. After head motion correction, the functional images were co-registered to the T1-weighted anatomical images, followed by removing white matter, and cerebrospinal fluid signals. Then, the functional images were normalized to the MNI152 standard brain. To reduce low-frequency drift ($0.008 < f < 0.1$) and Gaussian noise, all fMRI data were band-pass-filtered and spatially smoothed using a 6-mm full-width at half-maximum Gaussian kernel (FWHM).

Whole-Brain Functional Connectivity Strength Analysis

The FCS analysis was conducted using the Degree Centrality package of DPARSF[2]. For resting-state data, the BOLD time course of each voxel within gray matter (GM) was first extracted, and then correlation coefficients between all pairs of voxels within the GM were calculated. In order to eliminate weak correlations possibly arising from background noise, we restricted our analysis to positive correlations above a threshold of 0.25 (Liang et al., 2013; Wang et al., 2014; Liu et al., 2015). The correlation threshold was applied to FCS analysis to decrease the impact of false-positive connectivity on the data. The voxel was set to zero if its functional connectivity was smaller than the threshold. FCS at a given voxel x0 was calculated as the average of functional connectivity between x0 and all other voxels in the brain. Voxels with high FCS exhibited high connectivity to the remainder of the brain. The FCS maps were finally spatially smoothed using a 6-mm FWHM Gaussian kernel.

CBF Data Analysis

The ASL data were analyzed offline using the ASL Data Processing Toolbox (Wang et al., 2008). Perfusion-weighted image series were generated by subtraction of the label and control images, followed by conversion to absolute CBF images based on a single-compartment continuous ASL perfusion model (Wang et al., 2005). The CBF maps were first removed of non-brain tissue and co-registered to T1-weighted anatomical images. Then, the CBF image of each subject was normalized to the MNI152 standard brain and spatially smoothed using a 6-mm FWHM.

Cerebral Blood Flow – Functional Connectivity Strength Coupling Analysis

For each participant, both CBF and FCS values were standardized to *z* scores so that they could be averaged and compared across subjects. To quantitatively measure the coupling between CBF and FCS, we performed correlation analyses across voxels and subjects. Because neighboring voxels could be highly dependent, due to physiological correlations and spatial preprocessing, such as registration and spatial smoothing, the effective degrees of freedom (dfeff) in across-voxel correlation analysis was much smaller than the number of voxels used in the analysis. The dfeff of across-voxel correlations was estimated using the same method as proposed by Liang et al. (2013) in their CBF–FCS coupling study. The dfeff of across-voxel correlations was 1,342, and the number of voxels was 271,633 in this study. The CBF–FCS correlation coefficient value reflected the consistency of the spatial distribution between CBF and FCS.

Basal ganglia are directly or indirectly connected to the cerebellum, thalamus, and prefrontal cortex, and these connections may be mediated by the cortico-basal ganglia-thalamo-cortical circuit (CBGTC). Therefore, CBF–FCS coupling was also calculated in these regions, as extracted from the AAL template that was used widely by brain image researchers (Dimitriadis et al., 2017; Zou et al., 2018). Given the difference between the AAL template and the standard MNI template used in this study, we firstly co-registered the AAL template to the standard GM mask and further mask it with the standard GM mask. Finally, we extracted the mask for CBF–FCS coupling analysis.

Group Analysis

Across-subjects average CBF and FCS *z*-transformed maps were computed to demonstrate the spatial distribution patterns. A group-level two-sample *t* test was applied to identify the intergroup differences in CBF and FCS, and the whole brain correction was applied *via* Monte Carlo simulations (3dClusSim, AFNI package) at a voxel-wise height

[1] http://www.fil.ion.ucl.ac.uk/spm

[2] http://rfmri.org/DPARSF

threshold of $p < 0.001$ and a cluster size threshold of 30 contiguous voxels.

RESULTS

Spatial Distribution of Functional Connectivity Strength and Cerebral Blood Flow

The WD group and healthy controls showed similar spatial distributions of FCS and CBF (**Figure 1**). Higher CBF was primarily distributed among the posterior cingulate cortex, precuneus, prefrontal cortex, lateral temporal cortex, and DMN. Higher FCS was primarily observed in the visual cortex, prefrontal cortex, posterior cingulate cortex, and DMN.

Functional Connectivity Strength and Cerebral Blood Flow Changes in Wilson's Disease

Patients with WD showed decreased CBF in the bilateral insular and caudate, right cerebellum, left ventrolateral prefrontal cortex (VLPFC), precentral cortex, cingulate cortex, and thalamus, and increased CBF in the left middle temporal cortex (**Figure 2** and **Table 2**). Compared with healthy controls, patients with WD exhibited decreased FCS in the bilateral lentiform and caudate nuclei, left cuneus, and right thalamus, and increased FCS in the bilateral dorsolateral prefrontal cortex (DLPFC; **Figure 3** and **Table 3**).

Cerebral Blood Flow – Functional Connectivity Strength Coupling Changes in Wilson's Disease

CBF was significantly correlated with FCS within the whole GM, but the correlations in patients with WD were slightly lower than those in healthy controls (**Figure 1**). Patients with WD had significantly reduced CBF–FCS coupling in the basal ganglia and cerebellum, and increased CBF–FCS coupling in the thalamus relative to HC (**Figure 4**). There were no significant differences in CBF–FCS coupling in the prefrontal cortex.

DISCUSSION

To our knowledge, this is the first study to explore changed CBF–FCS coupling in WD by combining BOLD and ASL techniques. The whole GM CBF–FCS coupling in WD was slightly decreased compared to that of healthy controls. The WD group showed reduced CBF–FCS coupling in the basal ganglia and cerebellum, and increased coupling in the thalamus. Patients with WD exhibited decreased CBF and FCS in numerous brain regions, primarily the basal ganglia, and thalamus. These findings improve our understanding of the neural mechanisms underlying WD from the perspective of neurovascular coupling.

CBF Changes in WD

Decreased CBF was observed in the bilateral caudate nucleus, right thalamus, and cerebellum in WD. One possible explanation for this observation is neurovascular decoupling in these regions.

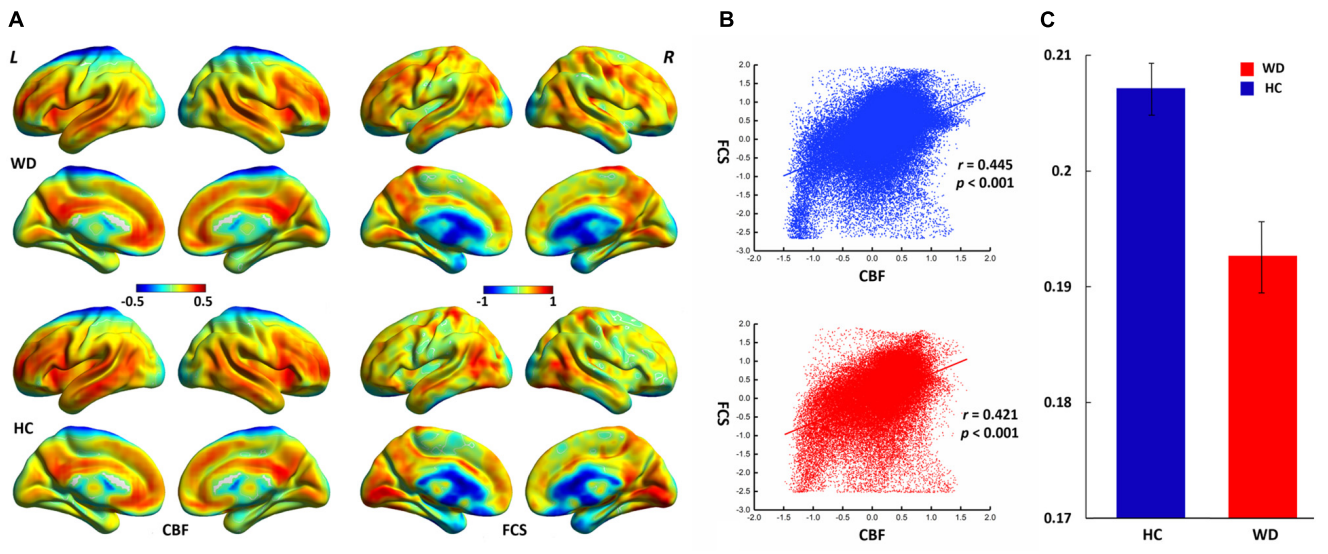

FIGURE 1 | Spatial distribution and neurovascular coupling in CBF and FCS. **(A)** Spatial distribution maps of CBF and FCS. **(B)** The whole-brain CBF–FCS coupling changes across voxel in the WD. **(C)** The whole-brain CBF–FCS coupling changes across subject in the WD. The FCS and CBF maps are normalized to *z* scores and averaged across subjects within groups. L, left; R, right. The right picture is whole gray matter (GM) level CBF–FCS coupling changes in WD. Scatter plots of the mean GM level spatial correlations across voxels between CBF and FCS in HC (blue) and WD (red), respectively. The mean CBF–FCS correlation across subjects in WD and HC. CBF, cerebral blood flow; FCS, functional connectivity strength; HC, healthy controls; WD, Wilson's disease.

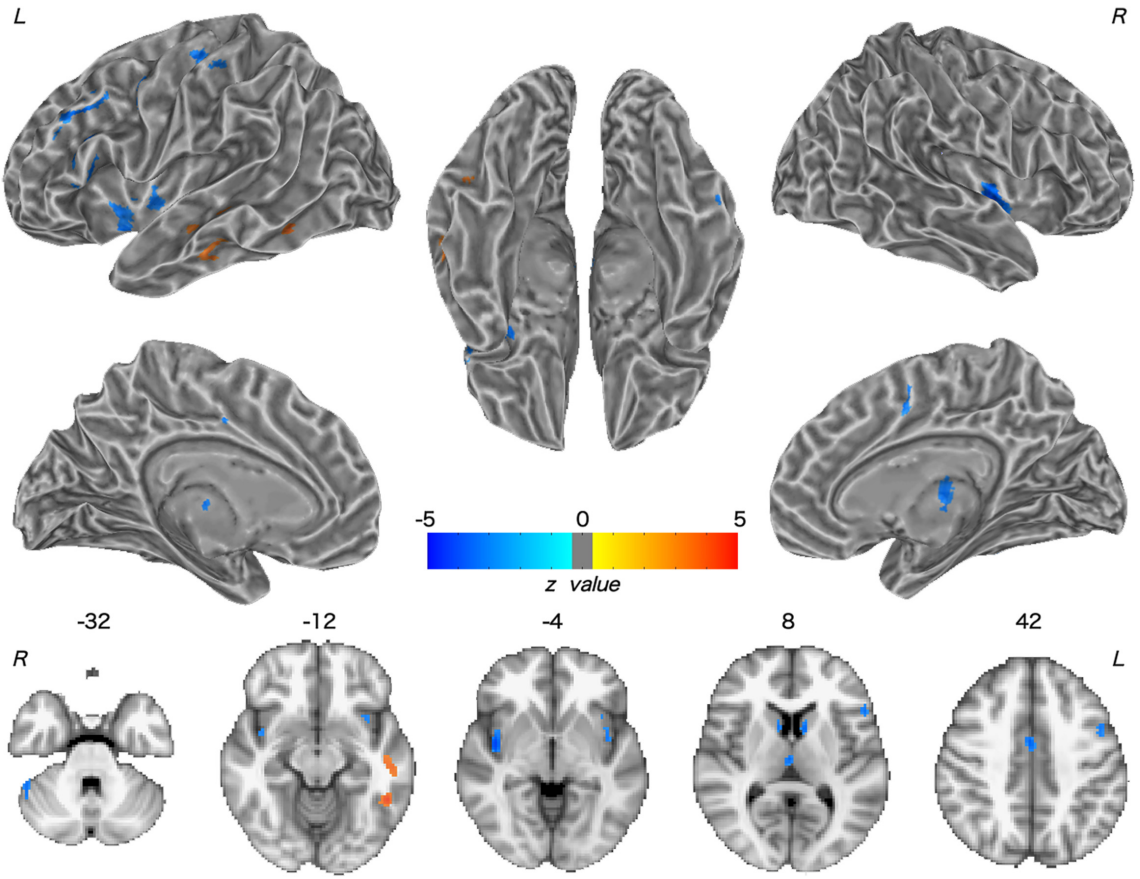

FIGURE 2 | Group difference in CBF between WD and HC. The warm and cold colors denote significantly increased and decreased CBF in WD patients, respectively. CBF, cerebral blood flow. L, left; R, right.

In the neurovascular coupling hypothesis (Kuschinsky, 1991), CBF changes are governed by neuronal activity and may reflect the altered neuronal activity in WD. For instance, brain regions with enhanced neuronal activity tend to have a greater brain metabolism, resulting in increased perfusion (Poornima et al., 2016). Because of the neuronal loss and atrophy in basal ganglia and thalamus, due to copper deposition in WD, the neuronal activity in these regions was reduced (Hu et al., 2017), which resulted in decreased CBF. These results are consistent with previous studies, which have identified decreased metabolic rate of glucose consumption and hypoperfusion in the putamen, caudate nucleus, thalamus, cerebellum, and frontal cortex (Piga et al., 2008; Huster, 2010; Ishida et al., 2012). Decreased CBF was also found in the left VLPFC and precentral cortex, right cingulate cortex, and bilateral insular cortex. The VLPFC is involved in executive functions and cognitive processes (Yang and Raine, 2009). The precentral cortex and insular are related to motor control (Fink et al., 1997; Meier et al., 2008) and multimodal sensory processing (Phan et al., 2002), whereas the cingulate cortex is involved in emotion formation and processing (Hadland et al., 2003). The basal ganglia and thalamus are highly interconnected with the cerebral cortex; for example, the prefrontal cortex is highly connected with the thalamus and parts of the basal ganglia (Silkis, 2001), and the cingulate cortex and insular directly receive inputs from the thalamus (Mcfarland and Haber, 2000; Ikemoto et al., 2015). All of these interconnections

TABLE 2 | Group difference in CBF between WD and HC.

Region	Side	MNI coordinate			Voxel	*z* value
		x	*y*	*z*		
VLPFC (45)	L	−50	22	18	330	−4.88
MiTG	L	−54	−24	−12	83	3.94
PrG	L	−40	−18	54	109	−4.13
MCC	R	2	−2	42	89	−4.41
CRB	R	50	−46	−32	55	−4.12
Insular	L	−30	12	−16	95	−4.29
	R	42	−4	−4	145	−5.45
Caudate	L	−8	8	6	51	−4.30
	R	10	8	12	50	−4.23
Thalamus	R	2	−16	8	52	−4.14

CBF, cerebral blood flow; VLPFC, ventrolateral prefrontal cortex; MiTG, middle temporal gyrus; PrG, precentral gyrus; MCC, middle cingulate cortex; CRB, cerebellum; L, left; R, right.

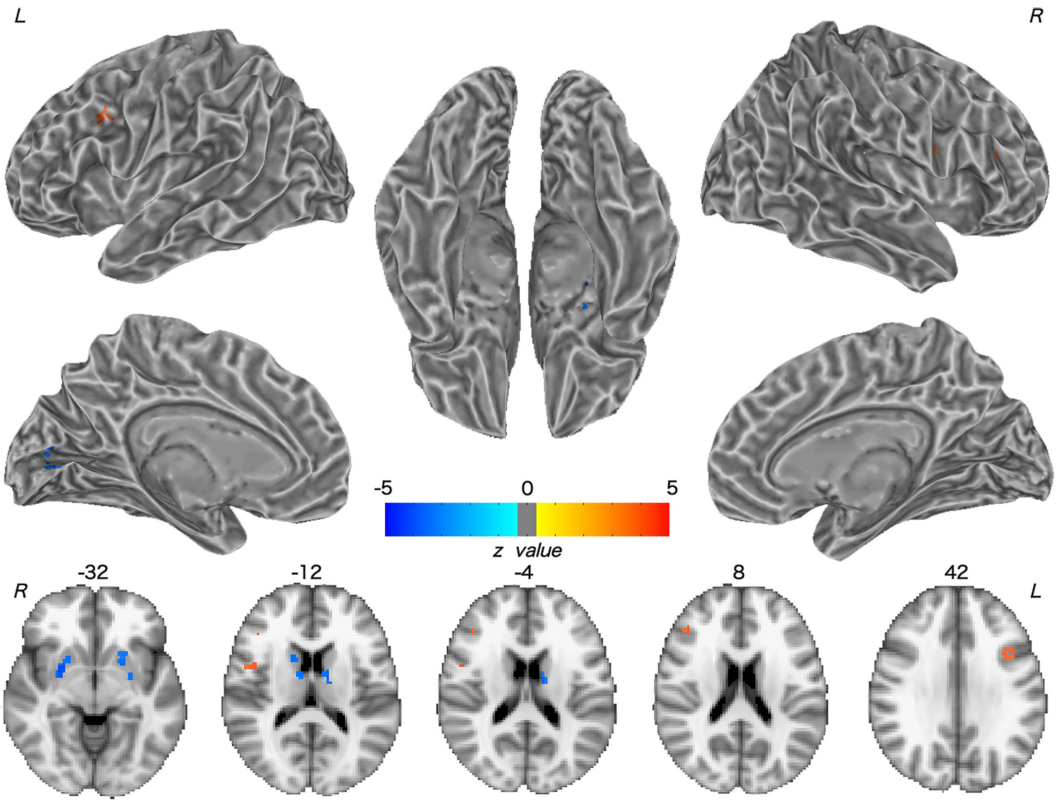

FIGURE 3 | Group difference in FCS between WD and HC. The warm and cold colors denote significantly increased and decreased FCS in WD patients, respectively. FCS, functional connectivity strength. L, left; R, right.

are mediated by the CBGTC (Silkis, 2001). CBF decreases in these regions may be the result of neurotransmitter (e.g., dopamine and GABA) changes in WD, because these chemicals also play a part in modulating vascular response (Cauli et al., 2004; Tayebati et al., 2011). The alterations in neurotransmitters may contribute to the disrupted CBGTC in WD, which results in imprecise regulation of CBF. In addition, patients with WD also exhibited a CBF increase in the left middle temporal cortex. One possible reason is that drug therapy may have effects on CBF in these regions. The increased CBF may be explained by the medication-induced dopamine turnover increase, resulting in CBF increase (Ala et al., 2007; Huster, 2010).

TABLE 3 | Group difference in FCS between WD and HC.

Region	Side	MNI coordinate			Voxel	*z* value
		x	*y*	*z*		
Lentiform	L	−22	10	−10	90	−3.99
	R	28	0	−6	122	−4.82
Caudate	L	−12	−6	18	32	−4.03
	R	12	20	6	50	−4.05
Thalamus	R	10	−4	14	21	−3.51
Ceneus	L	−14	−82	6	−3.96	−3.96
DLPFC (9)	L	−36	12	30	33	3.78
DLPFC (46)	R	42	32	20	21	3.81

FCS, functional connectivity strength; DLPFC, dorsolateral prefrontal cortex.

FCS Changes in WD

FCS decreased in patients with WD relative to healthy controls, including in the bilateral lentiform and caudate nuclei, left cuneus, and right thalamus. Structural damage, such as GM reduction and white matter alterations, may engender dysfunctional connectivity within the human brain (Hu et al., 2017; Wang et al., 2017), resulting in aberrant information transmission. The use of both traditional MRI and diffusion tensor imaging techniques has demonstrated brain gray and white matter structural abnormalities in the basal ganglia, thalamus, and cerebral cortex (Page et al., 2004; Piga et al., 2008; Jadav et al., 2013). FCS describes the whole-brain functional connectivity profile of each voxel from a global network perspective and reflects the role of each voxel in information transmission within the whole-brain network (Liang et al., 2013). The precise coordination of inter-regional functional synchronization may be impaired because of the loss of structural integrity (Honey et al., 2007; Mikail et al., 2009), thus giving rise to FCS decrease in WD. Moreover, patients with WD also showed increased FCS in the bilateral DLPFC. The DLPFC is associated with executive functions, such as working memory, cognitive

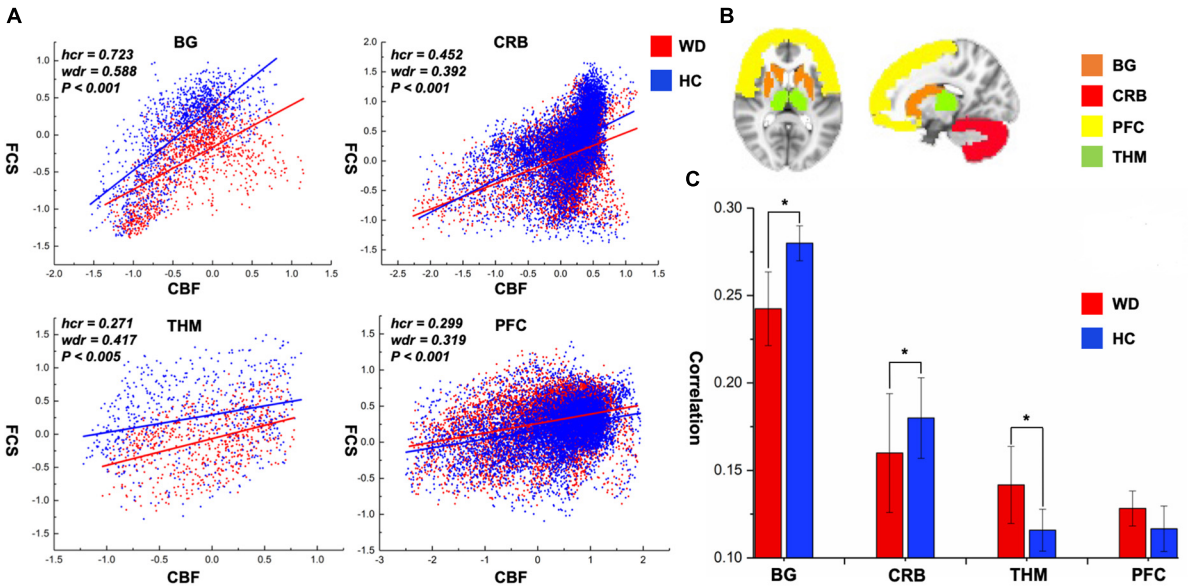

FIGURE 4 | CBF–FCS coupling changes of WD in basal ganglia, cerebellum, thalamus, and prefrontal cortex. **(A)** Scatter plots of mean GM level spatial correlations across voxels between CBF and FCS in HC (blue) and WD (red), respectively. **(B)** The GM regions of BG, CRB, THM, and PFC were extracted from AAL template. **(C)** The bar graph means CBF–FCS correlation across subjects in HC and WD. *Significant differences between both groups ($P < 0.05$). BG, basal ganglia; CRB, cerebellum; THM, thalamus; PFC, prefrontal cortex; hcr, the relationship between FCS and CBF in healthy controls; wdr, the relationship between FCS and CBF in patients with Wilson's disease.

flexibility, planning, and inhibition (Yang and Raine, 2009). The cognition problems (e.g., impulsivity, promiscuity, executive dysfunction, slow cognition, and memory loss) and psychiatric problems (e.g., depression, anxiety, and psychosis) in WD might result from the joint abnormal functions of the frontal cortex and subcortical regions, such as the basal ganglia (Hu et al., 2017). Although the regions with increased FCS in this study might not be the basis of the cognitive and psychiatric problems of WD, the functional connectivity increase in WD might be explained as a compensatory mechanism; the human brain tends to generate a compensatory response to structural impairments (Appel-Cresswell et al., 2010; Palmer, 2010; Palmer et al., 2010).

Neurovascular Abnormality in WD

The whole-brain correlation between CBF and FCS was computed in this study to identify the neurovascular coupling in WD. Neurovascular coupling depends on the integrity of neurovascular units, such as neurons, glial cells, and vascular components (Hawkins and Davis, 2005). The whole-brain CBF–FCS correlations in WD are slightly reduced relative to healthy controls, which may represent neurovascular decoupling in WD. Particularly, CBF–FCS correlations in the basal ganglia and cerebellum are significantly lower in WD than in healthy controls, possibly indicating neurovascular imbalance in WD. In the brain, astrocytes act as a bridge that links neural activity to the vascular response (Stobart and Anderson, 2013; Howarth, 2014). Abnormal astrocytes in the basal ganglia may reduce the connection between neural activity and vascular response, resulting in decreased CBF–FCS correlations. Interestingly, patients with WD exhibited a stronger CBF–FCS correlation in the thalamus than did healthy subjects. The increased CBF–FCS correlation may demonstrate that patients with WD improve synchronism between CBF and FCS in some brain regions, which is affected by the compensatory mechanism. However, this is the first time that CBF and FCS are used to study the neurovascular coupling in WD, and there is no literature on neurovascular coupling improving local brain regions. Therefore, the hypothesis here should be investigated in further studies.

CONCLUSION

In conclusion, aberrant coupling between resting-state CBF and functional connectivity in WD was revealed in this study. Specifically, we found that decreased FCS and CBF predominately occurred in subcortical regions involved in sensory processing and motor regulation, including the basal ganglia and thalamus, and increased CBF and FCS occurred in regions involved in cognitive control and emotional modulation, including the temporal cortex and DLPFC. These findings highlight the neurovascular imbalance in WD, which may be a potential neural mechanism underlying the pathophysiology of WD.

LIMITATIONS

In this study, we adopted CBF and FCS to investigate neurovascular coupling in patients with WD. Although the present study is meaningful, there are some limitations. Firstly, it is very important that the results are stable

over time in a repeated series of experiments. Therefore, another relatively larger data set should be collected for validating the present study. Secondly, because of the relatively small paramagnetism of copper, copper deposition might influence the MRI signal on the basal ganglia nucleus (Kanda et al., 2016). A patient group should be added in future studies, which would receive copper drainage treatment with the copper content close to normal levels, as a control group to minimize the influence of copper deposition on MRI signals. Thirdly, many studies associated neuroimaging results with clinical parameters, which can serve as neuroimaging indicators for some neurological disease. In the current study, we did not collect cognitive behavior and clinical parameters. Future studies must explore the relationship between functional network deficits and clinical implication. Finally, we used a standard gray mask to carry out the neurovascular coupling analysis, without taking the problem of incomplete coverage of individual image acquisition into consideration. In future studies, a common group-level mask on resting fMRI and the ASL should be used for the CBF–FCS coupling analysis.

ETHICS STATEMENT

This study was approved by the Human Research Committee in the First Affiliated Hospital of Anhui University of Chinese Medicine.

AUTHOR CONTRIBUTIONS

All authors listed have made a substantial, direct and intellectual contribution to the work, and approved it for publication.

FUNDING

This study was supported by Exploratory Science Research Project of Anhui University of Chinese Medicine (2016ts043), Natural Science Research Project of Anhui University of Chinese Medicine (2019zryb08), and Anhui Zhuokang Medical Equipment Limited Company (No. RD18200085).

REFERENCES

Ala, A., Walker, A. P., Ashkan, K., Dooley, J. S., and Schilsky, M. L. (2007). Wilson's disease. *Lancet* 369, 397–408. doi: 10.1016/S0140-6736(07)60196-2

Appel-Cresswell, S., De, L. F.-F. R., Galley, S., and Mckeown, M. J. (2010). Imaging of compensatory mechanisms in Parkinson's disease. *Curr. Opin. Neurol.* 23, 407–412. doi: 10.1097/WCO.0b013e32833b6019

Biswal, B., Yetkin, F. Z., Haughton, V. M., and Hyde, J. S. (1995). Functional connectivity in the motor cortex of resting human brain using echo-planar MRI. *Magn. Reson. Med.* 34, 537–541. doi: 10.1002/mrm.1910340409

Biswal, B. B. (2012). Resting state fMRI: a personal history. *Neuroimage* 62, 938–944. doi: 10.1016/j.neuroimage.2012.01.090

Cauli, B., Tong, X. K., Rancillac, A., Serluca, N., Lambolez, B., Rossier, J., et al. (2004). Cortical GABA interneurons in neurovascular coupling: relays for subcortical vasoactive pathways. *J. Neurosci.* 24, 8940–8949. doi: 10.1523/JNEUROSCI.3065-04.2004

de Bie, P., Muller, P., Wijmenga, C., and Klomp, L. W. (2007). Molecular pathogenesis of Wilson and Menkes disease: correlation of mutations with molecular defects and disease phenotypes. *J. Med. Genet.* 44, 673–688. doi: 10.1136/jmg.2007.052746

Dimitriadis, S. I., Drakesmith, M., Bells, S., Parker, G. D., Linden, D. E., and Jones, D. K. (2017). Improving the reliability of network metrics in structural brain networks by integrating different network weighting strategies into a single graph. *Front. Neurosci.* 11:694. doi: 10.3389/fnins.2017.00694

Fink, G. R., Frackowiak, R. S., Pietrzyk, U., and Passingham, R. E. (1997). Multiple nonprimary motor areas in the human cortex. *J. Neurophysiol.* 77, 2164–2174. doi: 10.1152/jn.1997.77.4.2164

Golay, X., Hendrikse, J., and Lim, T. C. (2004). Perfusion imaging using arterial spin labeling. *Top. Magn. Reson. Imaging* 15, 10–27. doi: 10.1097/00002142-200402000-00003

Hadland, K. A., Rushworth, M. F., Gaffan, D., and Passingham, R. E. (2003). The effect of cingulate lesions on social behaviour and emotion. *Neuropsychologia* 41, 919–931. doi: 10.1016/S0028-3932(02)00325-1

Han, Y., Cheng, H., Toledo, J. B., Wang, X., Li, B., Han, Y., et al. (2016). Impaired functional default mode network in patients with mild neurological Wilson's disease. *Parkinsonism Relat. Disord.* 30, 46–51. doi: 10.1016/j.parkreldis.2016.06.018

Hawkins, B. T., and Davis, T. P. (2005). The blood–brain barrier/neurovascular unit in health and disease. *Pharmacol. Rev.* 57, 173–185. doi: 10.1124/pr.57.2.4

Hawkins, R. A., Mazziotta, J. C., and Phelps, M. E. (1987). Wilson's disease studied with FDG and positron emission tomography. *Neurology* 37, 1707–1711. doi: 10.1212/WNL.37.11.1707

Honey, C. J., Kotter, R., Breakspear, M., and Sporns, O. (2007). Network structure of cerebral cortex shapes functional connectivity on multiple time scales. *Proc. Natl. Acad. Sci. U.S.A.* 104, 10240–10245. doi: 10.1073/pnas.0701519104

Howarth, C. (2014). The contribution of astrocytes to the regulation of cerebral blood flow. *Front. Neurosci.* 8:103. doi: 10.3389/fnins.2014.00103

Hu, X., Chen, S., Huang, C. B., Qian, Y., and Yu, Y. (2017). Frequency-dependent changes in the amplitude of low-frequency fluctuations in patients with Wilson's disease: a resting-state fMRI study. *Metab. Brain Dis.* 32, 685–692. doi: 10.1007/s11011-016-9946-3

Huster, D. (2010). Wilson disease. *Best Pract. Res. Clin. Gastroenterol.* 24, 531–539. doi: 10.1016/j.bpg.2010.07.014

Ikemoto, S., Yang, C., and Tan, A. (2015). Basal ganglia circuit loops, dopamine and motivation: a review and enquiry. *Behav. Brain Res.* 290, 17–31. doi: 10.1016/j.bbr.2015.04.018

Ishida, S., Doi, Y., Yamane, K., Sugino, M., Kimura, F., Hanafusa, T., et al. (2012). Resolution of cranial MRI and SPECT abnormalities in a patient with Wilson's disease following oral zinc monotherapy. *Intern. Med.* 51, 1759–1763. doi: 10.2169/internalmedicine.51.7341

Jadav, R., Saini, J., Sinha, S., Bagepally, B., Rao, S., and Taly, A. B. (2013). Diffusion tensor imaging (DTI) and its clinical correlates in drug naive Wilson's disease. *Metab. Brain Dis.* 28, 455–462. doi: 10.1007/s11011-013-9407-1

Kanda, T., Nakai, Y., Aoki, S., Oba, H., Toyoda, K., Kitajima, K., et al. (2016). Contribution of metals to brain MR signal intensity: review articles. *Jpn. J. Radiol.* 34, 258–266. doi: 10.1007/s11604-016-0532-8

Kuschinsky, W. (1991). Coupling of function, metabolism, and blood-flow in the brain. *Neurosurg. Rev.* 14, 163–168. doi: 10.1007/BF00310651

Kuwert, T., Hefter, H., Scholz, D., Milz, M., Weiß, P., Arendt, G., et al. (1992). Regional cerebral glucose consumption measured by positron emission tomography in patients with Wilson's disease. *Eur. J. Nucl. Med.* 19, 96–101. doi: 10.1007/BF00184123

Liang, X., Zou, Q., He, Y., and Yang, Y. (2013). Coupling of functional connectivity and regional cerebral blood flow reveals a physiological basis for network hubs of the human brain. *Proc. Natl. Acad. Sci. U.S.A.* 110, 1929–1934. doi: 10.1073/pnas.1214900110

Litwin, T., Dusek, P., and Czlonkowska, A. (2016). Neurological manifestations in Wilson's disease—possible treatment options for symptoms. *Expert Opin. Orphan Drugs* 4, 719–728. doi: 10.1080/21678707.2016.1188003

Liu, F., Zhu, C., Wang, Y., Guo, W., Li, M., Wang, W., et al. (2015). Disrupted cortical hubs in functional brain networks in social anxiety disorder. *Clin. Neurophysiol.* 126, 1711–1716. doi: 10.1016/j.clinph.2014.11.014

Machado, A., Chien, H. F., Deguti, M. M., Cancado, E., Azevedo, R. S., Scaff, M., et al. (2006). Neurological manifestations in Wilson's disease: report of 119 cases. *Mov. Disord.* 21, 2192–2196. doi: 10.1002/mds.21170

Mcfarland, N. R., and Haber, S. N. (2000). Convergent inputs from thalamic motor nuclei and frontal cortical areas to the dorsal striatum in the primate. *J. Neurosci.* 20, 3798–3813. doi: 10.1523/JNEUROSCI.20-10-03798.2000

Meier, J. D., Aflalo, T. N., Kastner, S., and Graziano, M. S. A. (2008). Complex organization of human primary motor cortex: a high-resolution fMRI study. *J. Neurophysiol.* 100, 1800–1812. doi: 10.1152/jn.90531.2008

Mikail, R., Olaf, S., Cees, V. L., and Michael, B. (2009). Symbiotic relationship between brain structure and dynamics. *BMC Neurosci.* 10:55. doi: 10.1186/1471-2202-10-55

Nair, A., Keown, C. L., Datko, M., Shih, P., Keehn, B., and Muller, R. A. (2014). Impact of methodological variables on functional connectivity findings in autism spectrum disorders. *Hum. Brain Mapp.* 35, 4035–4048. doi: 10.1002/hbm.22456

Page, R. A., Davie, C. A., MacManus, D., Miszkiel, K. A., Walshe, J. M., Miller, D. H., et al. (2004). Clinical correlation of brain MRI and MRS abnormalities in patients with Wilson disease. *Neurology* 63, 638–643. doi: 10.1212/01.WNL.0000134793.50831.C1

Palmer, S. J. (2010). *Compensatory Mechanisms in Parkinson's Disease*. Vancouver: The University of British Columbia.

Palmer, S. J., Li, J., Wang, Z. J., and Mckeown, M. J. (2010). Joint amplitude and connectivity compensatory mechanisms in Parkinson's disease. *Neuroscience* 166, 1110–1118. doi: 10.1016/j.neuroscience.2010.01.012

Phan, K. L., Wager, T., Taylor, S. F., and Liberzon, I. (2002). Functional neuroanatomy of emotion: a meta-analysis of emotion activation studies in PET and fMRI ??. *Neuroimage* 16, 331–348. doi: 10.1006/nimg.2002.1087

Piga, M., Murru, A., Satta, L., Serra, A., Sias, A., Loi, G., et al. (2008). Brain MRI and SPECT in the diagnosis of early neurological involvement in Wilson's disease. *Eur. J. Nucl. Med. Mol. Imaging* 35, 716–724. doi: 10.1007/s00259-007-0681-1

Poornima, V., Michael, C., and Chen, J. (2016). New insights into coupling and uncoupling of cerebral blood flow and metabolism in the brain. *Croat. Med. J.* 57, 223–228. doi: 10.3325/cmj.2016.57.223

Raichle, M. E., and Gusnard, D. A. (2002). Appraising the brain's energy budget. *Proc. Natl. Acad. Sci. U.S.A.* 99, 10237–10239. doi: 10.1073/pnas.172399499

Raichle, M. E., and Mintun, M. A. (2006). Brain work and brain imaging. *Ann. Rev. Neurosci.* 29, 449–476. doi: 10.1146/annurev.neuro.29.051605.112819

Roberts, D. A. (1994). *Magnetic Resonance Imaging of Perfusion in Humans Using Spin-Tagging of Arterial Water*. Dissertations available from ProQuest. AAI9427605.

Silkis, I. (2001). The cortico-basal ganglia-thalamocortical circuit with synaptic plasticity. II. Mechanism of synergistic modulation of thalamic activity via the direct and indirect pathways through the basal ganglia. *Biosystems* 59, 7–14. doi: 10.1016/S0303-2647(00)00135-0

Stobart, J. L., and Anderson, C. M. (2013). Multifunctional role of astrocytes as gatekeepers of neuronal energy supply. *Front. Cell. Neurosci.* 7:38. doi: 10.3389/fncel.2013.00038

Tayebati, S. K., Lokhandwala, M. F., and Amenta, F. (2011). Dopamine and vascular dynamics control: present status and future perspectives. *Curr. Neurovasc. Res.* 8, 246–257. doi: 10.2174/156720211796558032

Telischak, N. A., Detre, J. A., and Zaharchuk, G. (2015). Arterial spin labeling MRI: clinical applications in the brain. *J. Magn. Reson. Imaging* 41, 1165–1180. doi: 10.1002/jmri.24751

Tomasi, D., Wang, G. J., and Volkow, N. D. (2013). Energetic cost of brain functional connectivity. *Proc. Natl. Acad. Sci. U.S.A.* 110, 13642–13647. doi: 10.1073/pnas.1303346110

Vaishnavi, S. N., Vlassenko, A. G., Rundle, M. M., Snyder, A. Z., Mintun, M. A., and Raichle, M. E. (2010). Regional aerobic glycolysis in the human brain. *Proc. Natl. Acad. Sci. U.S.A.* 107, 17757–17762. doi: 10.1073/pnas.1010459107

Venkat, P., Chopp, M., and Chen, J. L. (2016). New insights into coupling and uncoupling of cerebral blood flow and metabolism in the brain. *Croat. Med. J.* 57, 223–228. doi: 10.3325/cmj.2016.57.223

Wang, A., Wu, H., Xu, C., Tang, L., Lee, J., Wang, M., et al. (2017). Study on lesion assessment of cerebello-thalamo-cortical network in Wilson's disease with diffusion tensor imaging. *Neural Plast.* 2017:7323121. doi: 10.1155/2017/7323121

Wang, J., Zhang, Y., Wolf, R. L., Roc, A. C., Alsop, D. C., and Detre, J. A. (2005). Amplitude-modulated continuous arterial spin-labeling 3.0 T perfusion MR imaging with a single coil: feasibility study. *Radiology* 235, 218–228. doi: 10.1148/radiol.2351031663

Wang, L., Dai, Z., Peng, H., Tan, L., Ding, Y., He, Z., et al. (2014). Overlapping and segregated resting-state functional connectivity in patients with major depressive disorder with and without childhood neglect. *Hum. Brain Mapp.* 35, 1154–1166. doi: 10.1002/hbm.22241

Wang, Z., Aguirre, G. K., Rao, H., Wang, J., Fernández-Seara, M. A., Childress, A. R., et al. (2008). Empirical optimization of ASL data analysis using an ASL data processing toolbox: ASLtbx. *Magn. Reson. Imaging* 26, 261–269. doi: 10.1016/j.mri.2007.07.003

Wilson, S. A. K. (1912). PROGRESSIVE lenticular degeneration: a familial nervous disease associated with cirrhosis of the liver. *Brain* 34, 1115–1119. doi: 10.1093/brain/34.4.295

Yang, Y., and Raine, A. (2009). Prefrontal structural and functional brain imaging findings in antisocial, violent, and psychopathic individuals: a meta-analysis. *Psychiatry Res. Neuroimaging* 174, 81–88. doi: 10.1016/j.pscychresns.2009.03.012

Zhu, J., Zhuo, C., Xu, L., Liu, F., Qin, W., and Yu, C. (2017). Altered coupling between resting-state cerebral blood flow and functional connectivity in schizophrenia. *Schizophr. Bull.* 43, 1363–1374. doi: 10.1093/schbul/sbx051

Zou, T. X., She, L., Zhan, C., Gao, Y. Q., and Chen, H. J. (2018). Altered topological properties of gray matter structural covariance networks in minimal hepatic encephalopathy. *Front. Neuroanat.* 12:101. doi: 10.3389/fnana.2018.00101

Conflict of Interest Statement: The authors declare that the research was conducted in the absence of any commercial or financial relationships that could be construed as a potential conflict of interest.

frontiers in Neural Circuits

ORIGINAL RESEARCH
published: 07 May 2019
doi: 10.3389/fncir.2019.00028

Longitudinal Changes in Diffusion Tensor Imaging Following Mild Traumatic Brain Injury and Correlation With Outcome

*Bo Yin[1,2], Dan-Dong Li[2], Huan Huang[3], Cheng-Hui Gu[2], Guang-Hui Bai[3], Liu-Xun Hu[2], Jin-Fei Zhuang[4] and Ming Zhang[1]**

[1] Department of Medical Imaging, The First Affiliated Hospital of Xi'an Jiaotong University, Xi'an, China, [2] Department of Neurosurgery, The Second Affiliated Hospital and Yuying Children's Hospital of Wenzhou Medical University, Wenzhou, China, [3] Department of Radiology, The Second Affiliated Hospital and Yuying Children's Hospital of Wenzhou Medical University, Wenzhou, China, [4] Department of Rehabilitation Medicine, The Second Affiliated Hospital and Yuying Children's Hospital of Wenzhou Medical University, Wenzhou, China

The chronic consequences of traumatic brain injury (TBI) may contribute to the increased risk for early cognitive decline and dementia, primarily due to diffusion axonal injury. Previous studies in mild TBI (mTBI) have been controversial in describing the white matter tract integrity changes occurring at acute and subacute post-injury. In this prospective longitudinal study, we aim to investigate the longitudinal changes of white matter (WM) using diffusion tensor imaging (DTI) and their correlations with neuropsychological tests. Thirty-three patients with subacute mTBI and 31 matched healthy controls were studied with an extensive imaging and clinical battery. Neuroimaging was obtained within 7 days post-injury for acute scans and repeated at 1 and 3 months post-injury. Using a region-of-interest-based approach, tract-based spatial statistics was used to conduct voxel-wise analysis on diffusion changes in mTBI and was compared to those of healthy matched controls, scanned during the same time period and rescanned with an interval similar to that of patients. We found decreased fractional anisotropy (FA) values in the left anterior limb of internal capsule (ALIC) and right inferior fronto-occipital fasciculus (IFOF) during the 7 days post-injury, which showed longitudinal evidence of recovery following 1 month post-injury. Increased FA values in these two tracts at 1 month post-injury were positively associated with better performance on cognitive information processing speed at initial assessment. By contrast, there were also some tracts (right anterior corona radiata, forceps major, and body of corpus callosum) exhibiting the continuing loss of integrity sustaining even beyond 3 months, which can predict the persisting post-concussion syndromes. Continuing loss of structural integrity in some tracts may contribute to the persistent post-concussion syndromes in mTBI patients, suggesting certain tracts providing an objective biomarker for tracking the pathological recovery process following mTBI.

Keywords: mild traumatic brain injury, diffusion tensor imaging, longitudinal changes, fractional anisotropy, neuropsychological test

OPEN ACCESS

Edited by:
Tuo Zhang,
Northwestern Polytechnical University, China

Reviewed by:
Yibin Xi,
Fourth Military Medical University, China
Jun Liu,
Central South University, China

****Correspondence:***
Ming Zhang
zhangming01@mail.xjtu.edu.cn

Received: *05 March 2019*
Accepted: *01 April 2019*
Published: *07 May 2019*

Citation:
Yin B, Li D-D, Huang H, Gu C-H, Bai G-H, Hu L-X, Zhuang J-F and Zhang M (2019) Longitudinal Changes in Diffusion Tensor Imaging Following Mild Traumatic Brain Injury and Correlation With Outcome. Front. Neural Circuits 13:28. doi: 10.3389/fncir.2019.00028

INTRODUCTION

The United States Centers for Disease Control and Prevention estimates that mild traumatic brain injury (TBI) is experienced in 70–90% of TBI-related emergency department (ED) visits (Taylor et al., 2017). The diagnosis of mild TBI (mTBI) still lacks an interdisciplinary consensus regarding what constitutes an mTBI, and its determination has been largely epidemiological in nature. Since the majority of patients always obtained negative results from both CT and conventional MRI, there is still limited information about the neurobiological changes that are associated with clinical recovery.

Despite the negative findings in conventional imaging assessments, distinctive white matter tracts (WMTs), also known as diffuse axonal injury (DAI), after mTBI have been confirmed in both human biopsies (Bigler, 2010) and animal models (Mac Donald et al., 2007; Spain et al., 2010). Diffusion tensor imaging (DTI) has gained wide acceptance in clinical-research-based detection of abnormalities in mTBI patients (Basser and Pierpaoli, 1998; Arfanakis et al., 2002; Bigler, 2010). Water molecules in brain tissue are influenced by cellular structures and macromolecules by promoting anisotropy diffusion due to its various disparities in different orientations. Detection of water molecule diffusion fractional anisotropy (FA) can indicate the integrity of a cellular structure (Beaulieu, 2002). Although consistent observations indicate decreased anisotropic diffusion at more chronic periods post-injury, considerable debate remains on the direction (i.e., increased or decreased) of diffusion metrics on the acute to semi-acute phase (usually less than 2 months after injury) of mTBI (Arfanakis et al., 2002; Bazarian et al., 2007; Lipton et al., 2009; Chu et al., 2010; Mayer et al., 2010; Henry et al., 2011; Messé et al., 2012). Mayer et al. (2010) investigated 22 adult patients with mTBI within weeks post-injury and found increased FA noted in the genu, left superior coronal radiation (CR), and left uncinate fasciculus (UF), while decreased radial diffusivity (RD) was noted only in the genu, left CR, and left UF. Wilde et al. (2008) indicated the increased FA in the entire corpus callosum (CC) in a sample of 10 pediatric mTBI patients scanned between 1 and 6 days post-injury. Another study presented decreased FA in the splenium and posterior CC in 20 adult mTBI patients between 1 and 10 days post-injury (Inglese et al., 2005). Some studies have reported null findings during the semi-acute stages of mTBI. In a study, 12 adult mTBI patients were scanned within 3 months of injury (Rutgers et al., 2008). There were no significant differences between mTBI patients and controls in the CC.

The existing data on diffusion measurements in mTBI patients have key limitations regarding experimental design and analysis methods, motivating further investigation of injury patterns. Acute effects of injury, particularly edema, can confound such analysis. Longitudinal studies documenting serial changes in DTI metrics following mild TBI have yet to be performed (Meier et al., 2016; Churchill et al., 2017). One of the studies demonstrated that concussed athletes had significantly increased FA in the superior longitudinal fasciculus (SLF) than healthy athletes both at acute (within 1 week) and chronic periods (1 month). Further analyses indicated that this increase of FA in the SLF was driven by the decrease in RD rather than an increase in axial diffusivity (RAD; Meier et al., 2016). Another study found regions showing reduced average FA for athletes at acute concussion and at return-to-play relative to controls, including right corona radiata and bilaterally in posterior limbs of the internal capsule (Churchill et al., 2017). In addition, some researchers have enrolled small numbers of patients (e.g., <20) or had highly variable between-scan intervals, making the interpretation of between-subject variability difficult. Furthermore, most studies have lacked appropriate control groups for a longitudinal investigation (Meier et al., 2015). This is essential for modeling normal time-related changes in the brain measurements and neuropsychological ratings.

In the present study, DTI was collected to measure regional (i.e., voxel-wise) changes in FA values in the initial 7 days post-injury and the 1- and 3-month follow-up phase in a sample of mild TBI patients. To our knowledge, no studies have prospectively examined serial DTI changes during the normal course of recovery that typifies patients with mild TBI from these time course phase. To control the between-scan intervals, we confined this at a narrow interval. We mainly focused on the main time effect of the structural integrity of white matter (WM) fibers and its relationship with the initial neuropsychological measures. We hypothesized that the structural integrity loss in some tracts would normalize in patients with mild TBI as they transitioned from the acute to subacute injury phase and predicted that these deficits would relate to outcome measures, while other tracts will have persistent injury even beyond the first 3 months.

MATERIALS AND METHODS

Participants

All consecutive patients with non-contrast head CT due to acute head trauma enrolled from the local ED formed the initial population. Inclusion criteria for all mild TBI patients were based on the World Health Organization's Collaborating Centre for Neurotrauma Task Force (Borg et al., 2004): (i) Glasgow Coma Scale (GCS) score of 13–15 on presentation to the ED; (ii) one or more/any of the following: loss of consciousness (LOC) for less than 30 min, posttraumatic amnesia (PTA) for 24 h or less, and/or other transient neurological abnormalities such as focal signs, seizure, and intracranial lesion not requiring surgery; (iii) within 1 week after onset of a mild TBI (concussion); and (iv) age 16 years or older. Mild TBI patients were excluded for the following: (1) a history of a previous brain injury, neurological disease, long-standing psychiatric condition, or concurrent substance or alcohol abuse; (2) a structural abnormality on neuroimaging (CT and MRI); (3) intubation and/or presence of a skull fracture and administration of sedatives; (4) the manifestation of mild TBI due to medications by other injuries (e.g., systemic injuries, facial injuries, or spinal cord injury); (5) other problems (e.g., psychological trauma, language barrier, or coexisting medical conditions); and (6) TBI caused by penetrating craniocerebral injury. All of the patients were also screened for litigation to avoid bias in the assessment of neuropsychological tests (NPTs).

Healthy controls (HCs) with no history of neurological or psychiatric disorder were also recruited via the local imaging research facilities. Thirty-three patients with mTBI and 31 sex-, age-, and education-matched HC participated in the study. All participants were right-handed according to the Edinburgh Handedness Inventory (Oldfield, 1971).

Standard Protocol

All the subjects gave written informed consent in person approved by a local institutional review board; the research procedures were approved by the Ethical Committee of the Second Affiliated Hospital of Wenzhou Medical University and conducted in accordance with the Declaration of Helsinki. MRI and neuropsychological assessments were performed on patients at both initial visit within 7 days post-injury (T1; median, 2 days; range, 0–5 days) and follow-up at both 1 month (T2; median, 37 days; range, 27–35 days) and 3 months (T3; median, 104 days; range 85–105 days). NPTs were performed within 48 h of MRI. The HCs received the first scanning within the same time range as the patients and follow-up 1 month (median, 35 days; range, 28–43 days) and 3 months (median, 108 days; range, 92–111 days) later. DTI and neuropsychological assessments were acquired in the full dataset of 33 patients and 31 HC at all three time points.

Image Acquisition

A non-contrast CT scan was performed on all consecutive patients following acute head injury with a 64-row CT scanner (GE, Lightspeed VCT). The MRI scans were acquired with the use of a 3.0-T MRI scanner (GE 750). A custom-built head holder was used to prevent head movements. The MRI protocol involved the following: the high-resolution T1-weighted 3D MPRAGE sequence [echo time (TE) = 3.17 ms, repetition time (TR) = 8.15 ms, flip angle = 9°, slice thickness = 1 mm, field of view (FOV) = 256 mm × 256 mm, matrix size = 256 × 256], axial FLAIR (TR = 9,000 ms, TE = 95 ms, flip angle = 150°, thickness = 5 mm, slices = 20, FOV = 240 mm × 240 mm, matrix size = 173 × 256), axial susceptibility weighted imaging (TR = 37.8 ms, TE = 25 ms, flip angle = 15°, thickness = 2 mm, slices = 70, FOV = 230 mm × 230 mm, matrix size = 512 × 512), and diffusion-weighted imaging (TR = 7,300 ms, TE = 99 ms, flip angle = 90°, thickness = 3 mm, slices = 50, FOV = 256 mm × 256 mm, matrix size = 128 × 128, two averages, voxel size = 2 mm × 2 mm × 3 mm). DTI scan (b = 1,000 s/mm^2) were acquired with 30 diffusion gradient orientations and the b = 0 repeated two times. The presence of focal lesions and cerebral microbleeds was independently determined by experienced clinical neuroradiologists (with 9 and 10 years' experience) who assessed multiple modalities of neuroimaging data acquired at baseline [T1-flair, T2-flair, T2, susceptibility weighted imaging (SWI)]. Any disagreement between these two observers was resolved by consensus. None of the patients were with visible contusion lesions using conventional neuroimaging techniques or exhibited cerebral microbleeds on SWI.

DTI Data Analysis

Preprocessing of the raw DTI data was performed using FSL software[1]. Motion and eddy current corrections were carried out by means of affine registration to the reference volume, and the corrected data were brain-extracted using FSL's Brain Extraction Tool (BET). FA images were then created by fitting a tensor model to the raw diffusion data using the FMRIB Diffusion Toolbox (FDT). Voxel-wise statistical analysis of the FA data was performed using tract-based spatial statistics (TBSS), a tool included in the FSL software to examine WM diffusion in a whole-brain voxel-based manner. All the subjects' diffusion metrics were subsequently aligned into a stereotactic coordinate system with the MNI152 template, using the FMRIB non-linear registration tool (FNIRT) with B-spline representation of the registration warp field. Next, all FA maps were averaged to produce a group mean FA image. The resultant mean FA map was then thinned to create a mean FA skeleton, representing the centers of all white-matter tracts in both study groups with a threshold FA value of 0.2. Statistical analysis was performed using the "randomize" command in FSL. The number of permutations was set to 10,000, and correction for multiple comparisons was achieved using threshold-free cluster enhancement (TFCE) with a family-wise error (FWE) rate of $P < 0.05$.

Effect of White Matter Hyperintensities on Diffusion Tensor Imaging Analysis

Automated lesion segmentation was performed using the T1-weighted and T2-FLAIR image modalities on LST (Lesion Segmentation Tool) software package implemented in SPM12. LST determines gray matter (GM), WM, and cerebrospinal fluid (CSF) segmentations from T1-weighted images and computes the FLAIR intensity distributions of these tissue classes. The amount of "hyperintensity" of each voxel in terms of distance from the mean intensity of the WM, GM, and CSF distributions in the FLAIR image is crucial for defining a conservative lesion belief map (obtained by thresholding the GM belief map, initial threshold kappa was set to κ = 0.15) and a liberal lesion belief map (consisting of the sum of the three lesion belief maps). Lesion growing is then performed iteratively between the conservative and the liberal belief maps, until no more voxels are added to the lesions (Valverde et al., 2015). Finally, the subject-specific WM mask, generated by FAST in FSL (Zhang et al., 2001), was used to calculate the volume of WM hyperintensity based on the lesion belief map. Then, we tested whether the between-group differences were influenced by the individual WM hyperintensities.

Neuropsychological Tests

Comprehensive NPTs were assessed: (i) Trail-making test part A (TMT-A) (Arnett and Labovitz, 1995) and WAIS-III Digit Symbol Coding score (DSC) (Wechsler et al., 1997) to examine cognitive information processing speed; (ii) forward digit span (FDS) and backward digit span (BDS) of the Wechsler Adult Intelligence Scale WAIS-III (Harman-Smith et al., 2013) to

[1] http://www.fmrib.ox.ac.uk/fsl/index.html

assess working memory; and (iii) verbal fluency test (VFT; Troyer et al., 1997) to assess verbal fluency including language ability, semantic memory, and executive function. Self-reported symptomatology included the following: the Rivermead post-concussion symptoms questionnaire (RPCS; King et al., 1995), Posttraumatic stress disorder Checklist – Civilian version (PCL-C) (Bliese et al., 2008), Beck Depression Inventory 2nd edition BDI-II (beck; Beck et al., 1996), Fatigue Severity Scale (FSS; Krupp et al., 1989), and Insomnia Severity Index (ISI; Bastien et al., 2001). We have conducted the "reliable change indices" analysis for all of NPTs in the present study. This method provides an estimate of the probability that a given difference score would not be obtained by chance; that is, the score would not be due to measurement error (Iverson, 2001; Baxendale and Thompson, 2005). The standard error of difference (S_{diff}) provides the clinician with an estimate of possible measurement error relating to test–retest scores.

Statistical Analyses

SPSS 19.0 software was used (IBM Corp., Armonk, NY, United States). The Shapiro–Wilk *W*-test was used to test for normality distribution of all continuous variables. The independent two-sample *t*-test and the Mann–Whitney test were used to compare group differences based on data normality, respectively. Chi-square analyses were applied to assess categorical variables. Effect sizes (Cohen's *d*) were computed to demonstrate the magnitude of observed differences. Longitudinal analysis, via repeated-measures ANOVA, was conducted to examine changes in both neuropsychological assessments and imaging FA metric as a function of recovery. This analysis only included the group and time as terms with no further control variables. Spearman's correlation coefficient was used to examine the association between FA metric of WMTs and neuropsychology test scores. The significance level was adjusted by using the Bonferroni correction with $P < 0.05$. None of the patients were with visible contusion lesions using neuroimaging techniques. Three patients exhibited cerebral microbleeds on SWI. All of the following analyses were also conducted in patients without microbleeds to investigate the influence of the presence of microbleeds on final results. We have also conducted the between-group difference in the TBSS analysis and used the individual WM hyperintensities observed in the T2-FLAIR sequence as regressors.

RESULTS

Demographic and Initial Neuropsychological Data

There were no significant differences in the age (Cohen's $d = 0.01$, $P = 0.956$), years of education (Cohen's $d = -0.49$, $P = 0.083$), or gender (Cohen's $d = 0.16$, $P = 0.36$) between the mTBI and control groups. The mTBI patients' NPT differed significantly from controls on a number of tests at initial admission (RPCS, PCL-C, beck, and ISI, all for Cohen's $d > 0.9$ and $P < 0.005$); however, some tests had no significant difference (TMT-A, DSC, FDS, BDS, VFT, and FSS all for $P > 0.05$). All demographic and clinical characteristics for patients with mild TBI and HC were presented in **Table 1**.

Neuropsychological Performance and Changes Over Time

Our results show that the majority of NPTs were sorted to the "most reliable" group, with the HCs having the most reliable change indices, given the relatively small practice effects (**Supplementary Figure S1**). However, only the Trail-making

TABLE 1 | Demographic and neuropsychological data for mTBI and control participants.

	mTBI mean (SD)	Controls mean (SD)	mTBI vs. controls *P*-value (Cohen's *d*)
Demographic			
Age	37.7(13.6)	37.5(12.2)	0.96(0.01)
Gender (M/F)	21/12	22/9	0.36(0.16)
Education	8.1(4.1)	10.5(5.9)	0.083(−0.49)
Neuropsychology			
TMT-A	64.1(31.7)	55.1(37.0)	0.30(0.26)
RPCS	11.0(7.3)	2.8(2.7)	< 0.001(1.48)
PCL-C	23.9(6.0)	17.0(0.0)	< 0.001(1.64)
DCS	31.8(15.0)	42.7(17.6)	0.010(−0.67)
FDS	7.6(1.7)	8.0(1.5)	0.34(−0.24)
BDS	3.6(1.4)	3.8(1.3)	0.56(−0.14)
VFT	17.3(5.1)	18.0(6.7)	0.62(−0.12)
Beck	4.4(4.7)	0.1(0.2)	< 0.001(1.31)
FSS	10.4(4.2)	9.0(0.0)	0.07(0.48)
ISI	7.3(6.0)	2.7(3.7)	0.001(0.92)

mTBI, mild traumatic brain injury; TMT-A, Trail-making test part A; RPCS, Rivermead post-concussion symptoms questionnaire; PCL-C, Posttraumatic Stress Disorder checklist – Civilian version; DSC, Wechsler Adult Intelligence Scale WAIS-III Digit Symbol Coding score; FDS and BDS, forward digit span and backward digit span of the Wechsler Adult Intelligence Scale WAIS-III; VFT, Verbal fluency test; Beck, Beck Depression Inventory 2nd edition BDI-II; FSS, Fatigue Severity Scale; ISI, Insomnia Severity Index. The results are thresholded at P < 0.05.

Test A presented the practice effects across the three time points. Thus, we were more cautious in explaining the corresponding changes in the Trail-making Test A in patients. For the tests with reliable change indices, the percentages of patients who demonstrated a significant improvement or decline were illustrated in **Supplemetary Figure S2**. For the DCS, about one-third of patients deteriorated and another one-third of patients improved between initial acute phase (T1) and follow-up 1 month post-injury (T2). For the FDS and BDS, one-third of patients presented improvement between T1 and T2. For the VFT, 20% of patients deteriorated and 15% of patients improved between T1 and T2.

Longitudinal analyses were first conducted to examine changes in the NPT as a function of recovery. A main effect of time was only observed in the DSC [$F(2,60) = 4.14$, $P = 0.018$]. For the DSC, scores were significantly improved at T2 and T3 relative to T1 ($P = 0.003$ and $P < 0.001$) and differences became non-significant at T2 and T3 following multiple comparison correction ($P > 0.1$). The main effect of group was significant for the RPCS, PCL-C, and beck (all for $P < 0.05$). Scores on the RPCS, PCL-C, and beck were significantly higher than HCs at T1 ($P < 0.001$), T2 ($P < 0.005$), and T3 ($P < 0.002$) following multiple comparison correction.

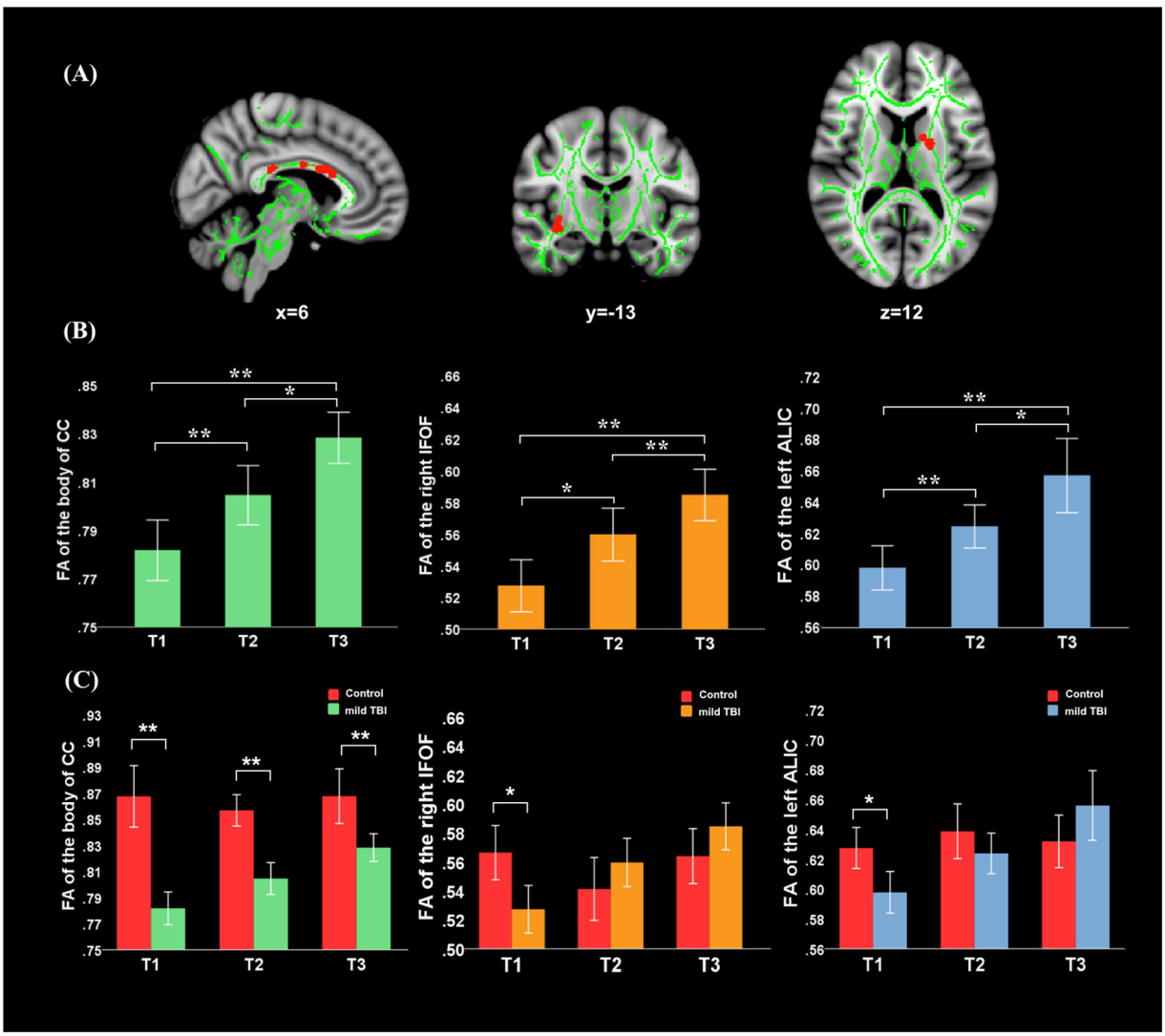

FIGURE 1 | Main effect of time and *post hoc* results in the fractional anisotropy (FA). **(A)** FA showed significant main effect of time in the body of CC, left anterior limb of internal capsule (ALIC), and right inferior fronto-occipital fasciculus (IFOF). **(B)** For these three tracts, *post hoc* analyses with Bonferroni correction revealed that FA values were significantly lower at T1 ($P < 0.001$) and T2 ($P < 0.005$) relative to the T3, and presented salient difference between T1 and T2 ($P < 0.005$). **(C)** Significant differences in the left ALIC and right IFOF FA values in patients relative to controls only at T1 ($P < 0.005$) but returned to the normal level at both T2 ($P > 0.1$ for all) and T3 ($P > 0.08$ for all). The body of CC exhibited the continuing loss of integrity at T1, T2, and T3 ($P < 0.001$) compared to healthy controls (HCs). Error bars represent 95% confidence intervals. *Significant Bonferroni corrected for multiple comparisons (*$P < 0.005$; **$P < 0.001$).

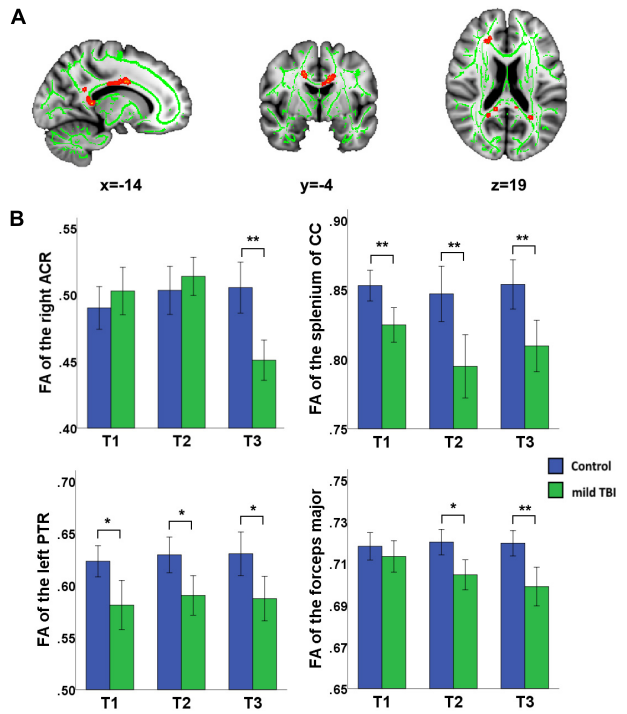

FIGURE 2 | Main effect of group and *post hoc* results in recovery of white matter tracts (WMTs). **(A)** Significant effect of group was presented in the right ACR, left posterior thalamic radiation (PTR), forceps major, body of corpus callosum (CC), and splenium of CC. **(B)** *Post hoc* analyses with Bonferroni correction further revealed that FA values in the left PTR, body of CC, and splenium of CC were reduced at T1, T2, and T3 relative to the HCs ($P < 0.005$ for all). The right ACR presents only loss of integrity at the later phase T3 rather than T1 and T2 ($P < 0.001$). For the forceps major, the reduced FA only presented at later phase at T2 ($P = 0.0012$) and T3 ($P < 0.001$) but not at T1. *Significant Bonferroni corrected for multiple comparisons (*$P < 0.005$; **$P < 0.001$).

Diffusion Metrics Differences and Recovery

There was no significant interaction effect (group × time) for the WMTs. A significant main effect of time was located in the left anterior limb of internal capsule (ALIC) [$F(1,61) = 9.49$; $P = 0.0023$], right inferior fronto-occipital fasciculus (IFOF) [$F(1,61) = 9.33$; $P = 0.0025$], and body of CC [$F(1,61) = 8.94$; $P = 0.0031$] (**Figure 1**). For these three tracts, *post hoc* analyses with Bonferroni correction revealed that FA values were significantly lower at T1 ($P < 0.001$) and T2 ($P < 0.005$) relative to T3 and presented salient difference between T1 and T2 ($P < 0.01$). Mild TBI data from the left ALIC, right IFOF, and body of CC were next compared with those of HCs using *post hoc* analyses with Bonferroni correction. We found significant differences in the left ALIC and right IFOF FA values in patients relative to controls only at T1 ($P < 0.005$) but presented no significant difference at both T2 ($P > 0.1$ for all) and T3 ($P > 0.08$ for all) compared with HCs. The body of CC exhibited persistent loss of integrity at T1, T2, and T3 ($P < 0.001$) compared to HCs.

Significant effect of group was presented in the right anterior corona radiata (ACR), left posterior thalamic radiation (PTR), forceps major, body of CC, and splenium of CC (**Figure 2**). *Post hoc* analyses with Bonferroni correction further revealed that FA values in the left PTR, body of CC, and splenium of CC were reduced at T1, T2, and T3 relative to the HCs ($P < 0.005$ for all). The right ACR presented loss of integrity only at T3 ($P < 0.001$) and not at T1 and T2. For the forceps major, the reduced FA only presented at T2 ($P = 0.0012$) and T3 ($P < 0.001$) and not at T1. The combination of multiple parameters (MD, RD, and AD) from DTI was very helpful to understand the possible physiopathology mechanism following mild TBI. We also supplemented other diffusion metrics that presented reduced FA in mild TBI patients, compared with controls (**Supplementary Table S1**). Our findings showed that most between-group differences were not influenced by the individual WM hyperintensities. Only the between-group difference in the left PTR at 1 month post-injury following mild TBI disappeared after regressing for the WM hyperintensities (**Supplementary Table S2**).

Relationship Between Outcome and Other Variables

The purpose of correlation analysis focused on the assessment of the relationship between the altered integrity of WMTs and neuropsychological performances within each time point and across time points. We were mainly concerned about both neuropsychological testing and WMTs showing the main effect of time. For the NPTs, a main effect of time was only observed in the DSC [$F(2,60) = 4.14$, $P = 0.018$]. For the fibers, a significant main effect of time was located only in the left ALIC [$F(1,61) = 9.49$; $P = 0.0023$], right IFOF [$F(1,61) = 9.33$; $P = 0.0025$], and body of CC [$F(1,61) = 8.94$; $P = 0.0031$]. The following analysis was conducted. Firstly, a correlation analysis between the clinical measure (DSC) and these three tracts for each time point was carried out. The FA value of these three tracts presented no significant associations with the DSC at any specific time points (all for $P > 0.2$). Additional analysis found that there was no significant correlation between altered DSC scores and FA values between T1 and T2, between T1 and T3, and between T2 and T3 in these three fibers (all for $P > 0.2$). Finally, considering that the left ALIC and right IFOF showed significant between-group differences at initial assessment but showed no significant difference at T2 and T3, we wanted to explore whether there was any association of the baseline DSC performance with the WM recovery in these two tracts. Exploratory analyses (Bonferroni correction at $P < 0.05$) were thus performed to assess the relationship between T1 clinical measure (DSC) with the left ALIC and right IFOF tracts at both T2 and T3, respectively. Results indicated that initial DSC performance can predict better recovery in the structural integrity of the left ALIC ($r = 0.48$, $P = 0.005$) and right IFOF ($r = 0.54$, $P = 0.0012$) at T2 after Bonferroni correction ($P < 0.05/2$, **Figure 3**). These findings may infer that an individual patient with better performance on the DSC at the acute phase can obtain better recovery in these two WMTs 1 month post-injury following mild TBI.

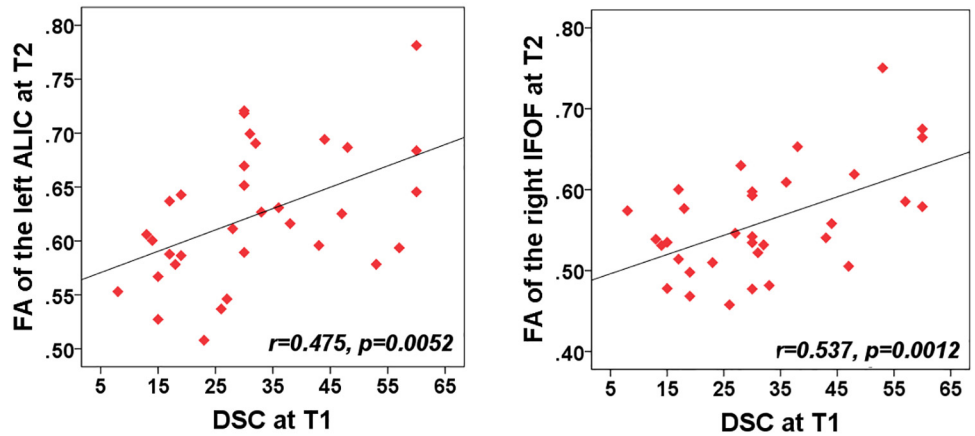

FIGURE 3 | Correlation between the FA of WMTs with clinical outcomes. Patient's cognitive information processing speed performance (rated by digit symbol coding, DSC) at T1 was positively related with FA value of the left anterior limb of internal capsule (ALIC) at T2 (r = 0.48, P < 0.005). Correlations of the DSC at T1 and FA value in the right IFOF at T2 (r = 0.5, P = 0.003) also showed significant positive values after Bonferroni correction.

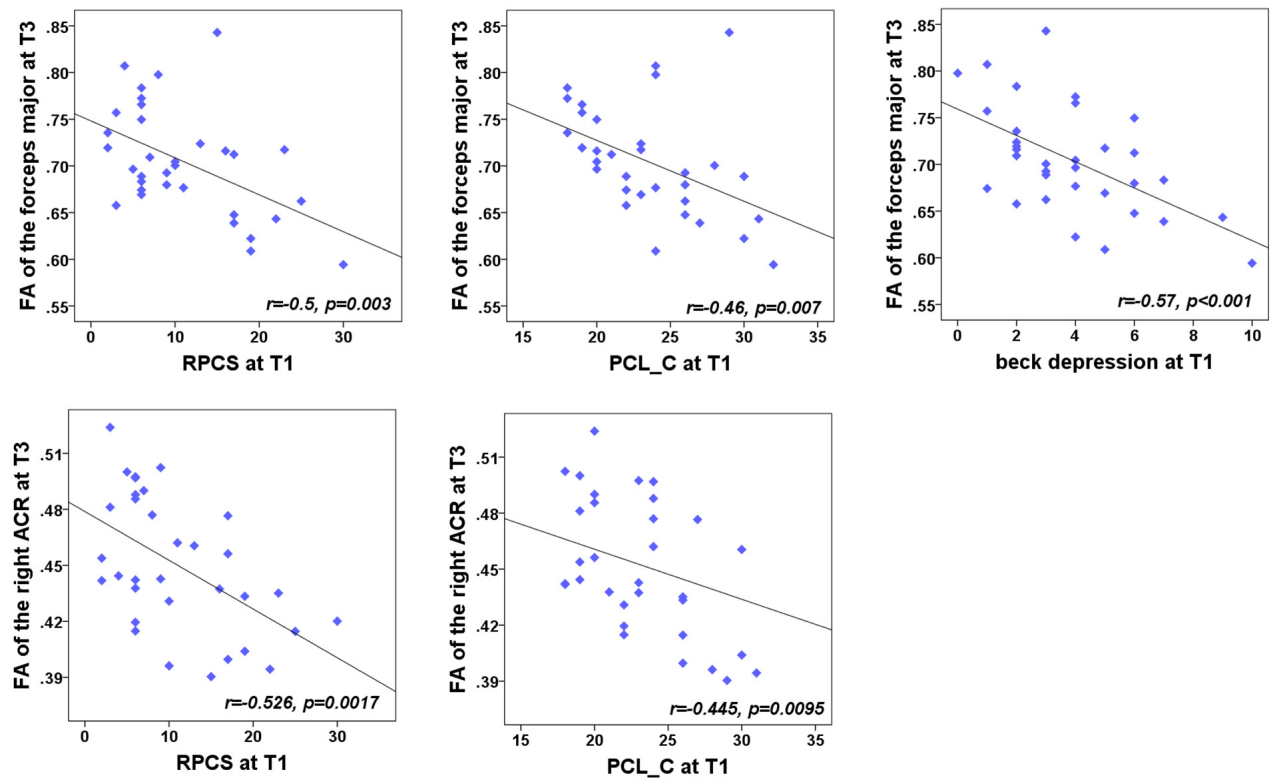

FIGURE 4 | Correlation between the FA of WMTs with clinical outcomes. At T3, the results indicated a negative relationship of the right anterior corona radiata (ACR) with both the post-concussion severity (rated by RPCS, r = -0.48, P < 0.005) and posttraumatic stress (PCL-C; r = -0.49, P = 0.0037). Correlations with the forceps major and RPCS, PCL-C, and Beck depression (r = -0.5, P = 0.003; r = -0.49, P = 0.0037; r = -0.57, P < 0.001) also showed significant negative values after Bonferroni correction.

We were also concerned with both neuropsychological testing and WMTs showing the main effect of group. For the NPTs, a main effect of time was only observed in the RPCS, PCL-C, and Beck depression (all for P < 0.05). For the fibers, a significant main effect of time was only located in the right ACR, left PTR, forceps major, body of CC, and splenium of CC. For each time point, correlation analyses showed that the FA value of these five tracts presented no significant correlations with these syndromes at any specific time point (P > 0.05). We also want to explore whether the baseline assessments of these NPTs were

associated with the later integrity of WMTs at T2 and T3 follow-up phases. Results showed that the significance only existed at T3 (**Figure 4**). Results indicated a negative relationship of the right ACR with both baseline post-concussion severity (rated by RPCS, r = -0.53, P = 0.0017) and posttraumatic stress (PCL-C) (r = -0.45, P = 0.0095) but did not survive correction for multiple comparisons ($P < 0.05/3 \times 5$). Correlations of the forceps major with RPCS and Beck depression (r = -0.5, P = 0.003; r = -0.57, $P < 0.001$) also showed significant negative values after Bonferroni correction. The loss of structural integrity in the forceps major also presented more complaints in the baseline PCL-C but did not survive correction for multiple comparisons (r = -0.46, P = 0.007). These findings inferred that patients with more complaints on the post-concussion syndromes at baseline have more loss of structural integrity in the right ACR and forceps major. Other correlations between baseline syndromes and later WM injury did not obtain significance.

DISCUSSION

To our knowledge, this is the first study to investigate longitudinal changes in WMTs from the acute through subacute phases to 3 months post-injury following mTBI. In a homogeneous sample of mTBI, we found decreased FA values in the left ALIC and right IFOF during the 7 days post-injury, which showed longitudinal evidence of recovery following 1 month post-injury. Increased FA values in these two tracts at 1 month post-injury were positively associated with better performance on cognitive information processing speed at initial assessment. By contrast, there were also some tracts (right ACR, forceps major, and body of CC) exhibiting the persistent loss of integrity sustaining even beyond 3 months, which can also predict the persisting post-concussion syndromes, posttraumatic stress, and depression even beyond 3 months post-injury. Crucially, the persistent loss of structural integrity in these tracts may contribute to the persistent post-concussion syndromes in mild TBI patients.

Diffusion tensor imaging is widely used *in vivo* studies on WM injury of TBI (Shenton et al., 2012). Among severe and chronic TBI patients, DTI scans can determine the altered FA values in fiber tracts, wherein the mechanism had been illustrated in previous studies with animal models or humans and was considered as the result of diffuse degenerative changes such as Wallerian degeneration, axonal collapse, and myelin degeneration (Albensi et al., 2000; Arfanakis et al., 2002; Inglese et al., 2005; Li et al., 2011). However, due to the preliminary nature of these studies, there is still controversy regarding the DTI metric changes in mild TBI patients. Indeed, there are several differences regarding the pathological changes between chronic and acute and subacute TBI patients (Povlishock and Katz, 2005; Newcombe et al., 2007). The cellular injury in the acute phase is volatile and may, in cases, stay the same, ameliorate gradually, or deteriorate; thus, it is thought to be a very dynamic process (Albensi et al., 2000; Povlishock and Katz, 2005). In addition to this characteristic of axon injury during the acute and subacute phases, the injuries of mTBI patients also differ from those of moderate to severe TBI patients. Until now, it is still unclear how these different neuropathological changes (individually or combined) affect the DTI test results. Indeed, many studies have reported differences in axial diffusivity and have been inconsistent, with some groups finding increases (Sidaros et al., 2008; Tasker et al., 2010), decreases (Henry et al., 2011), and no change (Mac Donald et al., 2007), and some regions showed axial diffusivity increases while others showed decreases (Farbota et al., 2012). Therefore, it is premature to suggest a physiopathology mechanism based on imaging data alone. This is a limitation for our study as well as most other current studies. These pathological changes occur at different points of time and have different effects on axons and neurons, which may explain the variable results of the FA values. To overcome these variabilities, all of the participants in the present study were evaluated using both neurological and imaging assessments at a narrow time interval.

The acute phase is thought to be a very dynamic process, and previous studies present bidirectional changes in FA of mTBI patients (Sidaros et al., 2008; Tasker et al., 2010; Henry et al., 2011). Histopathological studies with animal and human tissues show the acute stage of mTBI, and the pathological change of axon microstructure is a dynamic process with multiple variable effects. These inconsistencies may be partly due to the highly variable post-injury days for acute phase, such as 1–6 days (Chu et al., 2010; Yallampalli et al., 2013), within 72 h (Bazarian et al., 2007; Toth et al., 2013), and within 24 h (Arfanakis et al., 2002), or limited samples sizes, such as 5 patients in Arfanakis's study (Arfanakis et al., 2002), 6 in Bazarian's study (Bazarian et al., 2007), 10 in Chu's study (Chu et al., 2010), and 11 in Yallampalli's study (Yallampalli et al., 2013), making the interpretation of between-subject variability difficult. In the present study, decreased FA values were observed in the left ALIC and right IFOF within acute 7 days post-injury and no bidirectional changes were detected. The result presented in this report highlights the need of strictly standardized image acquisition time points for mTBI patients.

For mTBI injuries, partial pathological changes are usually transient, but may persist in some cases. The pathological changes at 1 month post-injury are, however, not the research focus in previous studies. We found that FA values of the right left ALIC and right IFOF in patients were firstly reduced at the initial acute phase but presented no significant difference after 1 month post-injury. Previously, Toth et al. (2013) found that the mTBI patients showed decreased FA values in nearly all the WMTs 72 h after injury; however, after 1 month of injury, the FA values remained decreased in some tracts. Similarly, in a homogeneous sample of collegiate athletes with sports-related mTBI, Meier et al. (2015) observed decreased CBF in the right dorsal middle insula cortex and superior temporal sulcus during the first week post-injury, which showed recovery at 1 month post-injury. Additionally, in athletes with concussion, Vagnozzi et al. (2010) demonstrated that a reduction in the ratios of *N*-acetylaspartate to creatine and choline is pronounced at 3 days post-concussion but fully recovered by 1 month. The recovery of FA could reflect reorganization within the WM, due to axonal recovery or even regrowth (Sidaros et al., 2008). We

found some support for this proposal by specifically examining the left ALIC and right IFOF, where the increased FA values at 1 month post-injury were positively associated with better performance on cognitive information processing speed at initial assessment. The ALIC connects the thalamus and prefrontal cortex, which conveys cognitive and corticothalamic fibers, and the right IFOF connects occipital, temporal, and frontal lobes, which has an important role in reading, attention, visual perception, processing and memory, and language; thus, such connections likely influence higher-order cognition (Martino et al., 2010). This result therefore provides support for the performance that 1 month post-injury is an important phase when the normalization of axial diffusivity in some WM occurs. Although statistical unification of neuroimaging data obtained acutely and subacutely (e.g., 1 month) after injury does not seem justifiable, these findings suggest that the MRI-detectable abnormality developing in the acute phase resolves dynamically in the first month after mild injury. Therefore, to determine whether the injuries obtained by complex and variable pathogenic mechanisms during the early stage might persist throughout the later stages of disease, 1 month post-injury was rather important.

By contrast, there were also some tracts (right ACR, forceps major, and body of CC) exhibiting the persistent loss of integrity sustaining beyond 3 months. Crucially, the correlations between FA and improved cognitive deficits at 3 months were positive: higher FA in right ACR and forceps major was associated with better outcomes. ACR connects to the internal capsule and forceps major connects to prefrontal and fronto-orbital regions, which may be related to perceptual and cognitive functions. Symptoms such as dizziness, fatigue, poor concentration, and memory problems experienced by chronic mTBI patients are thought to result from these lesions (Messé et al., 2011; Khong et al., 2016). Hence, the persistent loss of structural integrity in these tracts may contribute to the persistent post-concussion syndromes in mTBI patients, which can also predict the persisting post-concussion syndromes, posttraumatic stress, and depression even beyond 3 months post-injury. The identification of such predictive tracts (right ACR and forceps major) may help to better stratify patients early and to refine the concept of mTBI severity beyond traditional symptoms of alteration.

There were some limitations in the current study. Voxel-based analyses (i.e., TBSS) included the alignment of WMTs. In fact, such voxel-wise analysis is based on the assumption that clinically heterogeneous patients have a homogeneous (i.e., high degree of spatial overlap) spatial overlap pattern of WM abnormalities limited to detect the relative subtle diffuse "signals" influenced by the heterogeneity in injury location of mild TBI. Some studies adopted a new approach for quantifying diffusion abnormalities through a metric similar to lesion load (White et al., 2009; Ling et al., 2012). Specifically, clusters of abnormally high or low anisotropic diffusion were determined on a voxel-wise basis and then summed to represent total burden of distributed pathology. Further studies are needed to capture the individual-based "fine" diffuse patterns of WM abnormalities.

CONCLUSION

In conclusion, this study characterizes the dynamic variation rules of WM fibers within the first 3 months following mTBI. The results indicated that the pathological changes of fiber tracts at the acute phase were unstable and subject to a dynamic changing process. Therefore, we suggest a strict homogeneity of samples, and strictly standardized image acquisition time points for mTBI patients are required in subsequent studies. We found that FA values of the right left ALIC and right IFOF in patients were firstly reduced at the initial acute phase but presented no significant difference after 1 month post-injury compared with HCs. Hence, we suggest that 1 month post-injury is an important phase to determine whether the injuries obtained during the acute stage might persist throughout the chronic stages of mTBI. Finally, we also suggest that decreased FA values in right ACR and forceps major may help distinguish patients with posttraumatic stress disorder (PTSD) from mTBI patients at the acute and subacute stage.

DATA AVAILABILITY

All datasets generated for this study are included in the manuscript and/or the **Supplementary Files**.

ETHICS STATEMENT

All the subjects gave written, informed consent in person approved by a local institutional review board; the research procedures were approved by the Ethical Committee of The Second Affiliated Hospital of Wenzhou Medical University and conducted in accordance with the Declaration of Helsinki.

AUTHOR CONTRIBUTIONS

BY and MZ contributed to the conception and design of the study. D-DL and HH organized the database. L-XH performed the statistical analysis. D-DL and C-HG wrote the first draft of the manuscript. J-FZ and G-HB wrote the sections of the manuscript. All authors contributed to the manuscript revision, read, and approved the submitted version.

FUNDING

This research was supported by the National Natural Science Foundation of China under Grant No. 81571640, the Zhejiang Natural Science Foundation (Grant No. LY15H090016), and Wenzhou Municipal Sci-Tech Bureau (Y20140577).

SUPPLEMENTARY MATERIAL

The Supplementary Material for this article can be found online at: https://www.frontiersin.org/articles/10.3389/fncir.2019.00028/full#supplementary-material

REFERENCES

Albensi, B. C., Knoblach, S. M., Chew, B. G., O'Reilly, M. P., Faden, A. I., and Pekar, J. J. (2000). Diffusion and high resolution MRI of traumatic brain injury in rats: time course and correlation with histology. *Exp. Neurol.* 162, 61–72. doi: 10.1006/exnr.2000.7256

Arfanakis, K., Haughton, V. M., Carew, J. D., Rogers, B. P., Dempsey, R. J., and Meyerand, M. E. (2002). Diffusion tensor MR imaging in diffuse axonal injury. *AJNR Am. J. Neuroradiol.* 23, 794–802.

Arnett, J. A., and Labovitz, S. S. (1995). Effect of physical layout in performance of the trail making test. *Psychol. Assess.* 7:220. doi: 10.1037/1040-3590.7.2.220

Basser, P. J., and Pierpaoli, C. (1998). A simplified method to measure the diffusion tensor from seven MR images. *Magn. Reson. Med.* 39, 928–934. doi: 10.1002/mrm.1910390610

Bastien, C. H., Vallières, A., and Morin, C. M. (2001). Validation of the Insomnia Severity Index as an outcome measure for insomnia research. *Sleep Med.* 2, 297–307. doi: 10.1016/S1389-9457(00)00065-4

Baxendale, S., and Thompson, P. (2005). Defining meaningful postoperative change in epilepsy surgery patients: measuring the unmeasurable? *Epilepsy Behav.* 6, 207–211. doi: 10.1016/j.yebeh.2004.12.009

Bazarian, J. J., Zhong, J., Blyth, B., Zhu, T., Kavcic, V., and Peterson, D. (2007). Diffusion tensor imaging detects clinically important axonal damage after mild traumatic brain injury: a pilot study. *J. Neurotrauma* 24, 1447–1459. doi: 10.1089/neu.2007.0241

Beaulieu, C. (2002). The basis of anisotropic water diffusion in the nervous system—a technical review. *NMR Biomed.* 15, 435–455. doi: 10.1002/nbm.782

Beck, A. T., Steer, R. A., Ball, R., and Ranieri, W. F. (1996). Comparison of beck depression inventories-IA and -II in psychiatric outpatients. *J. Pers. Assess.* 67, 588–597. doi: 10.1207/s15327752jpa6703_13

Bigler, E. D. (2010). Neuroimaging in mild traumatic brain injury. *Psychol. Inj. Law* 3, 36–49. doi: 10.1007/s12207-010-9064-1

Bliese, P. D., Wright, K. M., Adler, A. B., Cabrera, O., Castro, C. A., and Hoge, C. W. (2008). Validating the primary care posttraumatic stress disorder screen and the posttraumatic stress disorder checklist with soldiers returning from combat. *J. Consult. Clin. Psychol.* 76, 272–281. doi: 10.1037/0022-006X.76.2.272

Borg, J., Holm, L., Cassidy, J. D., Peloso, P. M., Carroll, L. J., von Holst, H., et al. (2004). Diagnostic procedures in mild traumatic brain injury: results of the WHO collaborating centre task force on mild traumatic brain injury. *J. Rehabil. Med.* 36, 61–75. doi: 10.1080/16501960410023822

Chu, Z., Wilde, E. A., Hunter, J. V., McCauley, S. R., Bigler, E. D., Troyanskaya, M., et al. (2010). Voxel-based analysis of diffusion tensor imaging in mild traumatic brain injury in adolescents. *AJNR Am. J. Neuroradiol.* 31, 340–346. doi: 10.3174/ajnr.A1806

Churchill, N. W., Hutchison, M. G., Richards, D., Leung, G., Graham, S. J., and Schweizer, T. A. (2017). Neuroimaging of sport concussion: persistent alterations in brain structure and function at medical clearance. *Sci. Rep.* 7:8297. doi: 10.1038/s41598-017-07742-3

Farbota, K. D., Bendlin, B. B., Alexander, A. L., Rowley, H. A., Dempsey, R. J., and Johnson, S. C. (2012). Longitudinal diffusion tensor imaging and neuropsychological correlates in traumatic brain injury patients. *Front. Hum. Neurosci.* 6:160. doi: 10.3389/fnhum.2012.00160

Harman-Smith, Y. E., Mathias, J. L., Bowden, S. C., Rosenfeld, J. V., and Bigler, E. D. (2013). Wechsler adult intelligence scale—third edition profiles and their relationship to self-reported outcome following traumatic brain injury. *J. Clin. Exp. Neuropsychol.* 35, 785–798. doi: 10.1080/13803395.2013.824554

Henry, L. C., Tremblay, J., Tremblay, S., Lee, A., Brun, C., Lepore, N., et al. (2011). Acute and chronic changes in diffusivity measures after sports concussion. *J. Neurotrauma* 28, 2049–2059. doi: 10.1089/neu.2011.1836

Inglese, M., Makani, S., Johnson, G., Cohen, B. A., Silver, J. A., Gonen, O., et al. (2005). Diffuse axonal injury in mild traumatic brain injury: a diffusion tensor imaging study. *J. Neurosurg.* 103, 298–303. doi: 10.3171/jns.2005.103.2.0298

Iverson, G. L. (2001). Interpreting change on the WAIS-III/WMS-III in clinical samples. *Arch. Clin. Neuropsychol.* 16, 183–191. doi: 10.1093/arclin/16.2.183

Khong, E., Odenwald, N., Hashim, E., and Cusimano, M. D. (2016). Diffusion tensor imaging findings in post-concussion syndrome patients after mild traumatic brain injury: a systematic review. *Front. Neurol.* 7:156. doi: 10.3389/fneur.2016.00156

King, N. S., Crawford, S., Wenden, F. J., Moss, N. E., and Wade, D. T. (1995). The rivermead post concussion symptoms questionnaire: a measure of symptoms commonly experienced after head injury and its reliability. *J. Neurol.* 242, 587–592. doi: 10.1007/BF00868811

Krupp, L. B., LaRocca, N. G., Muir-Nash, J., and Steinberg, A. D. (1989). The fatigue severity scale: application to patients with multiple sclerosis and systemic lupus erythematosus. *Arch. Neurol.* 46, 1121–1123. doi: 10.1001/archneur.1989.00520460115022

Li, J., Li, X. Y., Feng, D. F., and Gu, L. (2011). Quantitative evaluation of microscopic injury with diffusion tensor imaging in a rat model of diffuse axonal injury. *Eur. J. Neurosci.* 33, 933–945. doi: 10.1111/j.1460-9568.2010.07573.x

Ling, J. M., Pena, A., Yeo, R. A., Merideth, F. L., Klimaj, S., Gasparovic, C., et al. (2012). Biomarkers of increased diffusion anisotropy in semi-acute mild traumatic brain injury: a longitudinal perspective. *Brain* 135, 1281–1292. doi: 10.1093/brain/aws073

Lipton, M. L., Gulko, E., Zimmerman, M. E., Friedman, B. W., Kim, M., Gellella, E., et al. (2009). Diffusion-tensor imaging implicates prefrontal axonal injury in executive function impairment following very mild traumatic brain injury. *Radiology* 252, 816–824. doi: 10.1148/radiol.2523081584

Mac Donald, C. L., Dikranian, K., Bayly, P., Holtzman, D., and Brody, D. (2007). Diffusion tensor imaging reliably detects experimental traumatic axonal injury and indicates approximate time of injury. *J. Neurosci.* 27, 11869–11876. doi: 10.1523/JNEUROSCI.3647-07.2007

Martino, J., Brogna, C., Robles, S. G., Vergani, F., and Duffau, H. (2010). Anatomic dissection of the inferior fronto-occipital fasciculus revisited in the lights of brain stimulation data. *Cortex* 46, 691–699. doi: 10.1016/j.cortex.2009.07.015

Mayer, A. R., Ling, J., Mannell, M. V., Gasparovic, C., Phillips, J. P., Doezema, D., et al. (2010). A prospective diffusion tensor imaging study in mild traumatic brain injury. *Neurology* 74, 643–650. doi: 10.1212/WNL.0b013e3181d0ccdd

Meier, T. B., Bellgowan, P. S., Singh, R., Kuplicki, R., Polanski, D. W., and Mayer, A. R. (2015). Recovery of cerebral blood flow following sports-related concussion. *JAMA Neurol.* 72, 530–538. doi: 10.1001/jamaneurol.2014.4778

Meier, T. B., Bergamino, M., Bellgowan, P. S., Teague, T. K., Ling, J. M., Jeromin, A., et al. (2016). Longitudinal assessment of white matter abnormalities following sports-related concussion. *Hum. Brain Mapp.* 37, 833–845. doi: 10.1002/hbm.23072

Messé, A., Caplain, S., Paradot, G., Garrigue, D., Mineo, J. F., Soto Ares, G., et al. (2011). Diffusion tensor imaging and white matter lesions at the subacute stage in mild traumatic brain injury with persistent neurobehavioral impairment. *Hum. Brain Mapp.* 32, 999–1011. doi: 10.1002/hbm.21092

Messé, A., Caplain, S., Pélégrini-Issac, M., Blancho, S., Montreuil, M., Lévy, R., et al. (2012). Structural integrity and postconcussion syndrome in mild traumatic brain injury patients. *Brain Imaging Behav.* 6, 283–292. doi: 10.1007/s11682-012-9159-2

Newcombe, V. F., Williams, G. B., Nortje, J., Bradley, P. G., Harding, S. G., Smielewski, P., et al. (2007). Analysis of acute traumatic axonal injury using diffusion tensor imaging. *Br. J. Neurosurg.* 21, 340–348. doi: 10.1080/02688690701400882

Oldfield, R. C. (1971). The assessment and analysis of handedness: the Edinburgh inventory. *Neuropsychologia* 9, 97–113. doi: 10.1016/0028-3932(71)90067-4

Povlishock, J. T., and Katz, D. I. (2005). Update of neuropathology and neurological recovery after traumatic brain injury. *J. Head. Trauma. Rehabil.* 20, 76–94. doi: 10.1097/00001199-200501000-00008

Rutgers, D. R., Fillard, P., Paradot, G., Tadié, M., Lasjaunias, P., and Ducreux, D. (2008). Diffusion tensor imaging characteristics of the corpus callosum in mild, moderate, and severe traumatic brain injury. *AJNR Am. J. Neuroradiol.* 29, 1730–1735. doi: 10.3174/ajnr.A1213

Shenton, M. E., Hamoda, H. M., Schneiderman, J. S., Bouix, S., Pasternak, O., Rathi, Y., et al. (2012). A review of magnetic resonance imaging and diffusion tensor imaging findings in mild traumatic brain injury. *Brain Imaging Behav.* 6, 137–192. doi: 10.1007/s11682-012-9156-5

Sidaros, A., Engberg, A. W., Sidaros, K., Liptrot, M. G., Herning, M., Petersen, P., et al. (2008). Diffusion tensor imaging during recovery from severe traumatic brain injury and relation to clinical outcome: a longitudinal study. *Brain* 131, 559–572. doi: 10.1093/brain/awm294

Spain, A., Daumas, S., Lifshitz, J., Rhodes, J., Andrews, P. J., Horsburgh, K., et al. (2010). Mild fluid percussion injury in mice produces evolving selective axonal

pathology and cognitive deficits relevant to human brain injury. *J. Neurotrauma* 27, 1429–1438. doi: 10.1089/neu.2010.1288

Tasker, R. C., Westland, A. G., White, D. K., and Williams, G. B. (2010). Corpus callosum and inferior forebrain white matter microstructure are related to functional outcome from raised intracranial pressure in child traumatic brain injury. *Dev. Neurosci.* 32, 374–384. doi: 10.1159/000316806

Taylor, C. A., Bell, J. M., Breiding, M. J., and Xu, L. (2017). Traumatic brain injury–related emergency department visits, hospitalizations, and deaths—United States, 2007 and 2013. *MMWR Surveill. Summ.* 66, 1–16. doi: 10.15585/mmwr.ss6609a1

Toth, A., Kovacs, N., Perlaki, G., Orsi, G., Aradi, M., Komaromy, H., et al. (2013). Multi-modal magnetic resonance imaging in the acute and sub-acute phase of mild traumatic brain injury: can we see the difference? *J. Neurotrauma* 30, 2–10. doi: 10.1089/neu.2012.2486

Troyer, A. K., Moscovitch, M., and Winocur, G. (1997). Clustering and switching as two components of verbal fluency: evidence from younger and older healthy adults. *Neuropsychology* 11, 138–146. doi: 10.1037/0894-4105.11.1.138

Vagnozzi, R., Signoretti, S., Cristofori, L., Alessandrini, F., Floris, R., Isgrò, E., et al. (2010). Assessment of metabolic brain damage and recovery following mild traumatic brain injury: a multicentre, proton magnetic resonance spectroscopic study in concussed patients. *Brain* 133, 3232–3242. doi: 10.1093/brain/awq200

Valverde, S., Oliver, A., Roura, E., Pareto, D., Vilanova, J. C., Ramió-Torrentà, L., et al. (2015). Quantifying brain tissue volume in multiple sclerosis with automated lesion segmentation and filling. *Neuroimage Clin.* 9, 640–647. doi: 10.1016/j.nicl.2015.10.012

Wechsler, D., Coalson, D. L., and Raiford, S. E. (1997). *WAIS-III: Wechsler Adult Intelligence Scale*. San Antonio, TX: NCS Pearson.

White, T., Schmidt, M., and Karatekin, C. (2009). White matter 'potholes' in early-onset schizophrenia: a new approach to evaluate white matter microstructure using diffusion tensor imaging. *Psychiatry Res.* 174, 110–115. doi: 10.1016/j.pscychresns.2009.04.014

Wilde, E. A., McCauley, S. R., Hunter, J. V., Bigler, E. D., Chu, Z., Wang, Z. J., et al. (2008). Diffusion tensor imaging of acute mild traumatic brain injury in adolescents. *Neurology* 70, 948–955. doi: 10.1212/01.wnl.0000305961.68029.54

Yallampalli, R., Wilde, E. A., Bigler, E. D., McCauley, S. R., Hanten, G., Troyanskaya, M., et al. (2013). Acute white matter differences in the fornix following mild traumatic brain injury using diffusion tensor imaging. *J. Neuroimaging* 23, 224–227. doi: 10.1111/j.1552-6569.2010.00537.x

Zhang, Y., Brady, M., and Smith, S. (2001). Segmentation of brain MR images through a hidden Markov random field model and the expectation-maximization algorithm. *IEEE Trans. Med. Imaging* 20, 45–57. doi: 10.1109/42.906424

Conflict of Interest Statement: The authors declare that the research was conducted in the absence of any commercial or financial relationships that could be construed as a potential conflict of interest.

frontiers in Neural Circuits

ORIGINAL RESEARCH
published: 08 May 2019
doi: 10.3389/fncir.2019.00031

Synaptic Failure Differentially Affects Pattern Formation in Heterogenous Networks

Maral Budak[1] *and Michal Zochowski*[1,2]*

[1] Biophysics Program, University of Michigan, Ann Arbor, MI, United States, [2] Department of Physics, University of Michigan, Ann Arbor, MI, United States

The communication of neurons is primarily maintained by synapses, which play a crucial role in the functioning of the nervous system. Therefore, synaptic failure may critically impair information processing in the brain and may underlie many neurodegenerative diseases. A number of studies have suggested that synaptic failure may preferentially target neurons with high connectivity (i.e., network hubs). As a result, the activity of these highly connected neurons can be significantly affected. It has been speculated that anesthetics regulate conscious state by affecting synaptic transmission at these network hubs and subsequently reducing overall coherence in the network activity. In addition, hubs in cortical networks are shown to be more vulnerable to amyloid deposition because of their higher activity within the network, causing decrease in coherence patterns and eventually Alzheimer's disease (AD). Here, we investigate how synaptic failure can affect spatio-temporal dynamics of scale free networks, having a power law scaling of number of connections per neuron – a relatively few neurons (hubs) with a lot of emanating or incoming connections and many cells with low connectivity. We studied two types of synaptic failure: activity-independent and targeted, activity-dependent synaptic failure. We defined scale-free network structures based on the dominating direction of the connections at the hub neurons: incoming and outgoing. We found that the two structures have significantly different dynamical properties. We show that synaptic failure may not only lead to the loss of coherence but unintuitively also can facilitate its emergence. We show that this is because activity-dependent synaptic failure homogenizes the activity levels in the network creating a dynamical substrate for the observed coherence increase. Obtained results may lead to better understanding of changes in large-scale pattern formation during progression of neuro-degenerative diseases targeting synaptic transmission.

Keywords: synaptic transmission failure, network dynamics, network synchrony, spatio-temporal pattern formation, scale-free networks

OPEN ACCESS

Edited by:
Tuo Zhang,
Northwestern Polytechnical University, China

Reviewed by:
Yimin Wang,
Shanghai University, China
Meng Li,
Harvard University, United States

***Correspondence:**
Michal Zochowski
michalz@umich.edu

Received: *13 August 2018*
Accepted: *11 April 2019*
Published: *08 May 2019*

Citation:
Budak M and Zochowski M (2019) Synaptic Failure Differentially Affects Pattern Formation in Heterogenous Networks. Front. Neural Circuits 13:31. doi: 10.3389/fncir.2019.00031

INTRODUCTION

Neurons transmit signals to communicate predominantly via synapses. The synapses may fail to transmit signals due to the depletion of neurotransmitters or external changes in membrane/ion channel activity. The examples of the latter, include interaction of oligomeric Aß or misfolded tau with cell surface receptors, intracellular signaling molecules or scaffold proteins, which leads to

the deterioration of synaptic structure and function causing Alzheimer's disease (AD) (Chen et al., 2019). Another example is an interaction of anesthetics with $GABA_A$ or NMDA receptors, or K^+ channels, causing hyperpolarization, glutamate desensitization or increase in K^+ conductance at the postsynaptic neuron, respectively (Franks, 2008).

Subsequently it is no surprise that synaptic failure can change functional network connectivity and consequently information processing leading to devastating outcomes. For instance, synaptic failure is part of the cause of most neurodegenerative diseases including AD, Huntington, ALS, and ischemic cerebral damage. In fact, it is the first pathologic event to occur in these diseases, even before the loss of neurons (Wishart et al., 2006). However, synaptic transmission failure may target different components of the network and lead to different consequences in terms of changes of spatio-temporal patterning in the network. Buckner et al. (2009) provided evidence that cortical hubs (i.e., regions that integrate and transmit information from/to many other parts of the brain) in humans are the most vulnerable areas to amyloid deposition, which results in atrophy and eventually AD. Moreover, another study on mice showed that amyloid deposition is caused by excessive neuronal and synaptic activity *in vivo* (Bero et al., 2011). de Haan et al. (2012) hypothesized that hubs are the most active regions in the brain, resulting in "activity dependent degeneration". Consequently, they showed that the hubs are the most active regions in the brain and activity dependent degeneration results in hub vulnerability as well as macro-scale disruption of brain connectivity, as observed in AD.

Another hypothetical consequence of synaptic failure is the loss of consciousness via application of anesthetics. Anesthetics are thought to act through ion channel blockage and/or changes in cellular membrane dynamics which lead to synaptic failure (Diao et al., 2014). One of the observed outcomes of anesthetics on a macro-network scale is a decrease in the large-scale functional connectivity between different parts of the brain. In particular, it was postulated that the hub regions of the brain are primarily affected by anesthetics and lead to the loss of the global functional connectivity which is followed by the loss of consciousness (Lee et al., 2013). In a similar spirit, another study investigated directionality of information flow in the network by simulating simple oscillatory models in a human anatomical network. They found the directionality of a network is determined by its topology (Moon et al., 2015). Since the hub nodes phase lag and peripheral nodes phase lead, they concluded that connections are from less to more degree nodes. Further, they perturbed the hub structure to simulate unconscious state, leading to the elimination of the directionality in the neuroanatomical network, which is consistent with anesthetic administered human data, where anterior (less hubs)-to-posterior (more hubs) directionality was lost.

Previously, a theoretical study was done to investigate how the topology of neuronal networks influences their dynamics when they suffer from synaptic loss. In this study, synapses were removed with a given probability, and they observed that bimodal networks are more robust than random ones (Mirzakhalili et al., 2017).

Here, we systematically studied the effects of gradual, stochastic synaptic failure on a functional network connectivity in scale-free networks. The aim of this study is to investigate the universal patterns of changes in functional connectivity based on the pattern and degree of synaptic failure. We specifically, wanted to know how the network responds when neurons having different number of connections (i.e., playing different roles in the network) are targeted. We investigate two modes of synaptic transmission loss: (1) in activity-independent case, transmission probability remains constant for all synapses in the network throughout the simulation, and (2) in activity-dependent case, synapses are more likely to fail, if the postsynaptic neuron has fired more recently. Further, we used both incoming (i.e., hubs predominantly receive the signals) and outgoing (i.e., hubs send signals) networks, since a recent study showed that direction of information flow is not always into the hubs, but can be bi-directional depending on the frequency of the signal (Hillebrand et al., 2016). We assessed the network-wide activity patterns through the degree of synchrony or coherence among the networks. We show that the two studied modes of synaptic failure can lead to non-trivial behavior of the network, which in turn can affect information processing.

MATERIALS AND METHODS

Network Structure and Connectivity

We used Barabasi – Albert algorithm (Barabasi et al., 1999) on a population of 1000 neurons to create a scale-free connectivity. We started with an all-to-all connected network of n neurons, and then expanded the network continuously by connecting new neurons to n pre-existing ones using preferential attachment principle: neurons with more connections have a higher chance to receive new connections. This results in a bidirectionally connected network with $\frac{n}{10}\%$ connectivity. Unless otherwise stated, we used $n = 16$ (1.6% connectivity) in our simulations. Then, we proceeded to make the connections unidirectional and defined two network transmission directions: incoming and outgoing. For that purpose, we first enumerated the neurons 1 to 1000 based on the time step they are added to the network. The earlier the neurons were added to the network, the higher chance they had to get new connections. Therefore, the neurons being assigned smaller numbers would eventually be more likely to have more connections. Then, we defined two different network structures according to the predominant directions of the connections at the hubs, i.e., nodes having a lot of connections to many other nodes (Boccaletti et al., 2006). We defined incoming networks as networks with hubs having majority of incoming connections. Therefore, we changed all bidirectional connections of the network into unidirectional connections from bigger to smaller-numbered neurons. Conversely, in outgoing networks, the hubs are dominated by outgoing connections. Therefore, the connections were directed from the neurons with smaller numbers to the ones with bigger numbers. Below, we will refer to these connectivity structures as "incoming" and "outgoing" networks, respectively (**Figure 1A**).

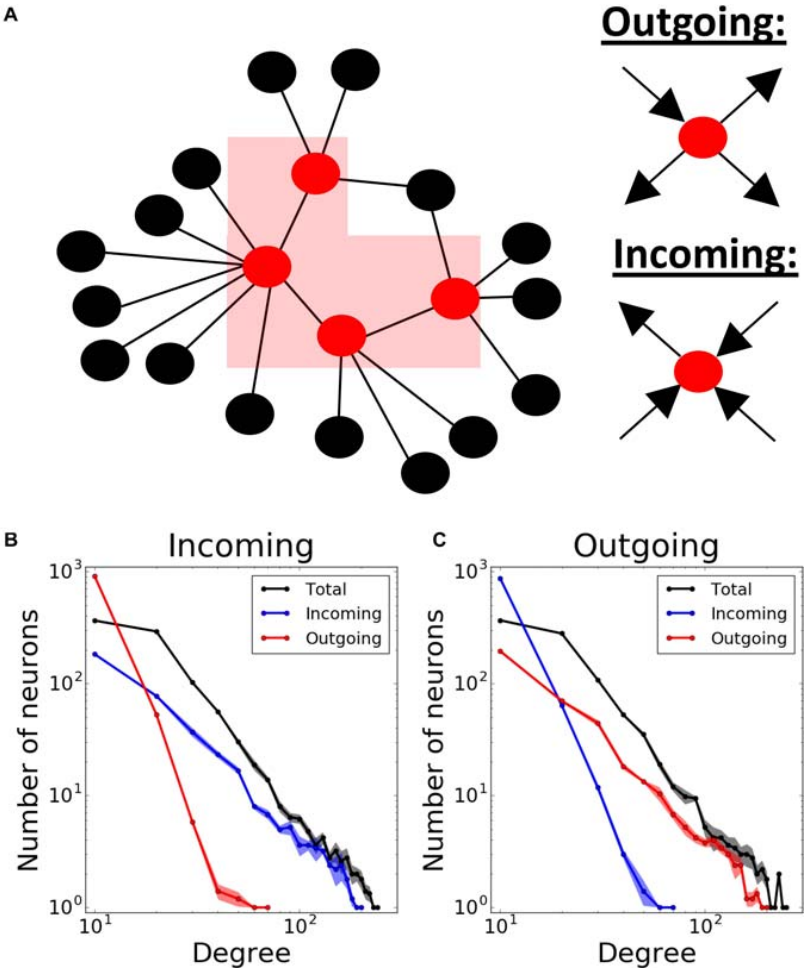

FIGURE 1 | Modeling different scale-free network structures depending on the directionality at the hubs. **(A)** Scale- free networks are defined as "outgoing," if the hubs have predominantly outgoing connections, and "incoming," if the hubs have predominantly incoming connections. Total, incoming and outgoing degrees in both **(B)** incoming and **(C)** outgoing networks exhibit power-law distributions. Degree distributions are averaged over 5 different network realizations.

Finally, to obtain feedback connectivity, we randomly chose m% of all connections to change their directions. We defined this proportion (m%) as "direction ratio" in the paper. As a result, each neuron has $\frac{100}{m} - 1$ times more incoming than outgoing connections on average in incoming networks, and vice versa in outgoing networks. Unless otherwise stated, we used 17% direction ratio in both network structures in our simulations. Consequently, the resulting networks have power-law degree distribution for their total, incoming and outgoing connections (**Figures 1B,C**).

We used integrate-and-fire excitatory neuron model to describe dynamics of each node. The current-balance equation of this neuron model for i-th neuron is

$$\frac{\partial V_i(t)}{\partial t} = -\alpha V_i(t) + \gamma \sum_j J_{ij} S_j(t, t_s) + \beta I_{rand}, \qquad (1)$$

where $V_i(t)$ is the membrane potential of the i-th neuron, J denotes the adjacency matrix, $\gamma = 0.25V/s$ is the synaptic strength, $\alpha = 0.3ms^{-1}$ is the inverse of the passive membrane time constant. The I_{rand} is a random term, which is a 0.1 ms-wide rectangular current with an amplitude of 1, perturbing the neuronal dynamics with 100 Hz frequency; $\beta = 6V/s$ is a term to modify the amplitude.

A neuron spikes when its membrane potential reaches $V_i(t) = 1$. At the time of the spike, the voltage of the spiking neuron is reset to 0, and the neuron enters the refractory period of 5 ms (t_{ref}). During this period, the neuron cannot receive any signals from its presynaptic connections (Burkitt, 2006).

There are no delays in the synaptic transmission. The postsynaptic signal arriving at each neuron is described by a double-exponential

$$S_i(t, t_s) = e^{\frac{-(t-t_{s_i})}{T_{decay}}} - e^{\frac{-(t-t_{s_i})}{T_{rise}}}, \qquad (2)$$

where t_s is the last spike time of the i-th presynaptic excitatory neuron, $T_{rise} = 0.3ms$ and $T_{decay} = 3ms$ are rise and decay time constants, respectively.

For one set of our simulations (**Figure 11**), we added a population of inhibitory neurons consisting of 1000 neurons to the network. This population is randomly and unidirectionally wired with the same mean connectivity as excitatory population (1.6%). Moreover, inhibitory population sends connections to the excitatory one with 1.6% random connectivity, and vice versa. All parameters governing dynamics of inhibitory neurons are the same, except the sign in signal S_i:

$$S_i(t, t_s) = -\left(e^{\frac{-\left(t-t_{s_i}\right)}{T_{decay}}} - e^{\frac{-\left(t-t_{s_i}\right)}{T_{rise}}}\right) \tag{3}$$

Implementation of Synaptic Transmission Failure

We defined a parameter, transmission probability p_{trans} that provides a probability of a synapse passing (or failing to transmit) the signal, i.e., each synapse independently can pass (or fail) a presynaptic spike to a postsynaptic neuron. Here, we studied two realizations of this process: (1) activity-independent one, where transmission probability is constant (and the same for every synapse), and (2) activity-dependent one, where the probability of the synapse to succeed or fail depends on the time elapsed from the last spike of the postsynaptic neuron:

$$p_{trans}(t) = 1 - p_{syn} \times e^{\frac{-\left(t-t_{last}-t_{ref}\right)}{T}}, \tag{4}$$

where p_{syn} is the base failure probability, T is the failure recovery time constant and t_{last} is the last spike time of that neuron. Therefore, the term $t - t_{last} - t_{ref}$ denotes for the time passed after the last spike time and its corresponding refractory period.

Measures and Statistics

For all realizations of the network and its dynamics, we measured the MPC (mean phase coherence) between the neurons and the degree of the synchrony. The first measure allows us to assess the stability of the spatio-temporal pattern irrespective whether it is synchronous or asynchronous. Briefly, the instantaneous phase between two neurons is defined as

$$\phi_k = 2\pi\left(\frac{t_{2,k} - t_{1,k}}{t_{1,k+1} - t_{1,k}}\right), \tag{5}$$

where $t_{1,\,k}$ is the time of the last spike of the neuron 1 before that of the neuron 2 $\left(t_{2,\,k}\right)$ and $t_{1,\,k+1}$ is the time of the first spike of the neuron 1 after $t_{2,\,k}$. Then the MPC between two neurons $\sigma_{1,2}$ is

$$\sigma_{1,2} = \left|\frac{1}{N}\sum_{k=1}^{N} e^{i\phi_k}\right|, \tag{6}$$

where N is the number of spike combinations at the two cells. The network measure of MPC, $\langle\sigma\rangle$, is the average of all pairs (Mormann et al., 2000).

The second measure indicates to what extent the neurons form synchronized pattern of activity. Here, the measure we used depends on the time-averaged fluctuations of the global voltage (σ_V) over an extended period of time, normalized to the average of N individual neurons' time-averaged fluctuations:

$$\lambda = \sqrt{\frac{[\sigma_v]^2}{\frac{1}{N}\sum_{i=1}^{N}[\sigma_{v_i}]^2}}. \tag{7}$$

It is in the range of (0,1), increasing with synchronous activity (Golomb and Rinzel, 1993). The simulations were repeated 5 times, we calculated mean and its standard error to establish significance of the obtained results.

RESULTS

We used scale-free network structures, which are thought to represent functional network connectivity in the brain (Bullmore and Sporns, 2009). Scale-free connectivity provides a power-law distribution of nodal degrees resulting in a heterogeneous population of interconnected cells (Barabasi et al., 1999). We further differentiated network types by establishing hub directionality, in the sense that the highly interconnected cells (the hubs) may predominantly receive inputs from other parts of the network, or send outputs to other cells (**Figure 1A**). The example statistics of the connectivity for both of these cases are provided on **Figures 1B,C**, where the direction ratio is being established at 17%.

First, to establish a baseline, we investigated pattern formation in the networks without failure, as a function of the mean connectivity (**Figures 2A,B**) and direction ratio (**Figures 2C,D**) in both incoming (**Figures 2A,C**), and outgoing (**Figures 2B,D**) networks. In incoming networks, the histograms of average MPC ($\langle\sigma\rangle$) as a function of neuron degrees, suggest that low degree neurons always have relatively lower MPC than the rest of the network, regardless of the connectivity and direction ratio of the network, because of the lack of common input they get. However, this difference is more pronounced for higher connectivities (**Figure 2A**). Generally, we observe that for low connectivity the network has relatively few connections and thus it remains less heterogeneous in terms of nodal degree. As the connectivity is increased, two competing mechanisms emerge – the networks become more heterogeneous, but at the same time stronger connectivity leads to more synchronous dynamics, as is commonly observed. However, even though nodal contributions exhibit different patterns for different connectivities, these differences are only minimal in incoming networks.

Connectivity has a bigger impact on outgoing networks (**Figure 2B**). Higher connectivities result in more significant increases in MPC for all degrees. That is not surprising as hubs are the synchronizing agent to the rest of the network when they drive network activity. Unlike incoming networks, outgoing ones have the highest MPC for the neurons with lowest degrees, for 0.8, and 1.6% connectivities. The reason is that in these type of networks, neurons with lowest degrees receive signals from hubs and form synchronized clusters. This trend disappears for 3.2% connectivity though, since the network is saturated and neurons with all degrees are coherent. The bigger fluctuations for highest

degrees at 3.2% connectivity might be due to the lower input they get from the network.

We then investigated how direction ratio (as defined in methods) affects network coherence. In incoming networks, MPC for all degrees is increased overall for lower direction ratios (more incoming connections at the hubs), although the change is not very significant (**Figure 2C**). However; there is a more substantial rise in the case of outgoing networks, when hubs send more outgoing connections (**Figure 2D**). These results point in the direction that the overall synchrony of the network is strongly dependent on the number of outgoing connections emanating from the hubs, rather than incoming ones. For the rest of our simulations, unless stated otherwise, we decided to use incoming and outgoing network structures with 1.6% connectivity, 17% direction ratio.

Finally, we varied the frequency of random external kick I_{rand}. In case all neurons are disconnected ($p_{trans} = 0.0$), spike frequency increases with increasing I_{rand} frequency, as expected. At the same time, as expected, the MPC decreases with more frequent I_{rand}. When all the connections are present $(p_{trans} = 1.0)$, both spike frequencies and MPCs are only minimally increased for higher frequencies of I_{rand}, since network connections dominate pattern formation. For the rest of our simulations, we chose the frequency as 100 Hz. This value results in a spike frequency lower than 200 Hz, the maximum frequency the network can fire due to the 5 ms refractory period, when $p_{trans} = 1.0$. Also, it introduces enough randomness to the network to make them spike less coherently when $p_{trans} = 0.0$. These results are briefly summarized in **Supplementary Figure S1**.

Activity – Independent Synaptic Failure

We first investigated the history-independent transmission probability, where p_{trans} is constant. We compared the pattern formation (i.e., the MPC and synchrony) for the outgoing and incoming networks as we gradually varied p_{trans} between 0 and 1 for both network types. We observed that outgoing networks are more sensitive to synaptic failure than incoming ones, as they become more coherent and synchronous with increasing synaptic transmission (**Figures 3A,B**).

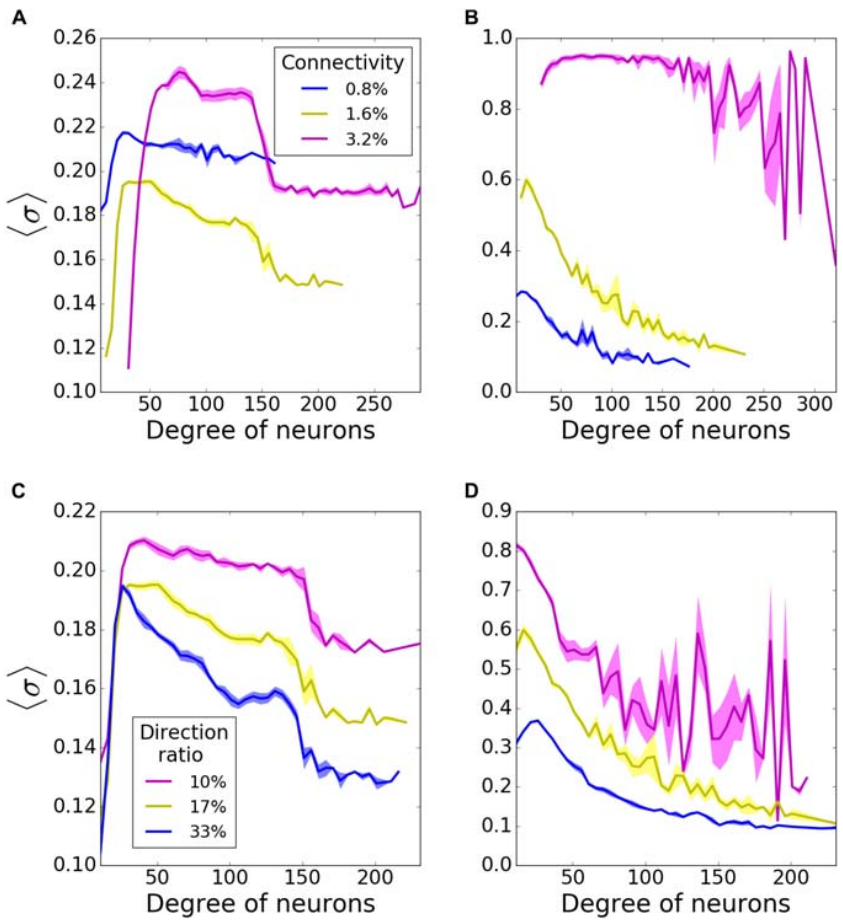

FIGURE 2 | Nodal contribution to network-wide mean phase coherence (MPC) as a function of its degree for incoming **(A,C)** and outgoing **(B,D)** networks for different connectivities **(A,B)**, and direction ratios at the hubs **(C,D)**. In incoming networks, **(A)** increasing connectivity causes a bigger gap between coherences of high- and moderate-degree neurons, whereas **(C)** increasing direction ratio decreases MPC of all degrees. In outgoing networks, MPC of all degrees increases with **(B)** increasing connectivity and **(D)** decreasing direction ratio. MPCs are averaged over 5 degrees and results are averaged over 5 randomized network realizations.

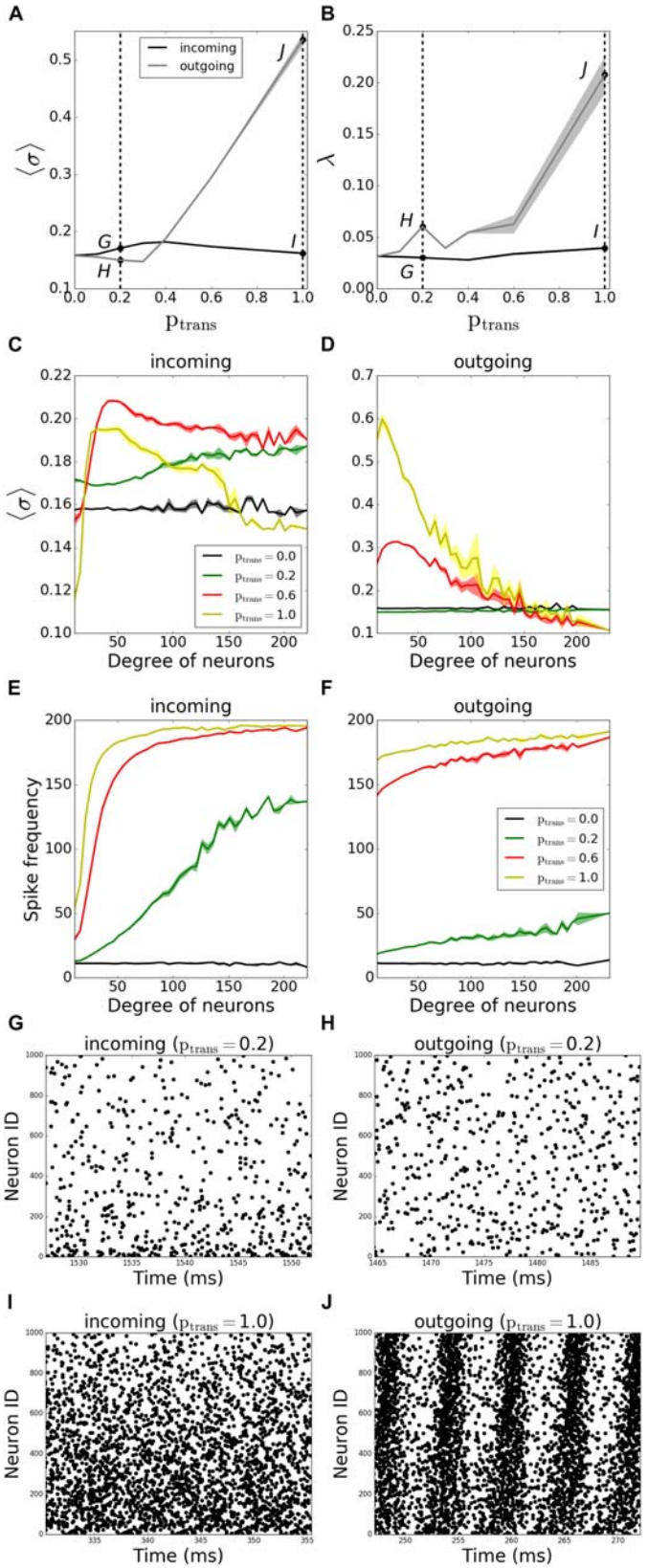

FIGURE 3 | Continued

FIGURE 3 | Pattern formation in the networks with activity-independent synaptic failure shows that outgoing networks become more coherent and synchronous due to a more uniform spike frequency distribution throughout the network. Signals are transmitted through synapses of a neuronal network with a constant probability p_{trans}. **(A)** MPC and **(B)** synchrony measure for incoming (black line) and outgoing (gray line) networks. **(C,D)** Participation in pattern formation as a function of nodal degree for activity-independent transmission failure. Histograms of MPC as a function of degree of neurons for incoming **(C)** and outgoing **(D)** networks, averaged over 5 degrees. **(E,F)** Spike frequencies of different degrees in incoming **(E)** and outgoing **(F)** networks, averaged over 5 degrees. Raster plots for incoming **(G,I)** and outgoing **(H,J)** networks for parameter values indicated on panels **(A)** and **(B)** [Points *G–J* correspond to panels **(G–J)**]. Lower neuron ID means higher degrees and vice versa (see **Figures 12A,E** for degrees corresponding to neuron IDs). Results are averaged over 5 simulations.

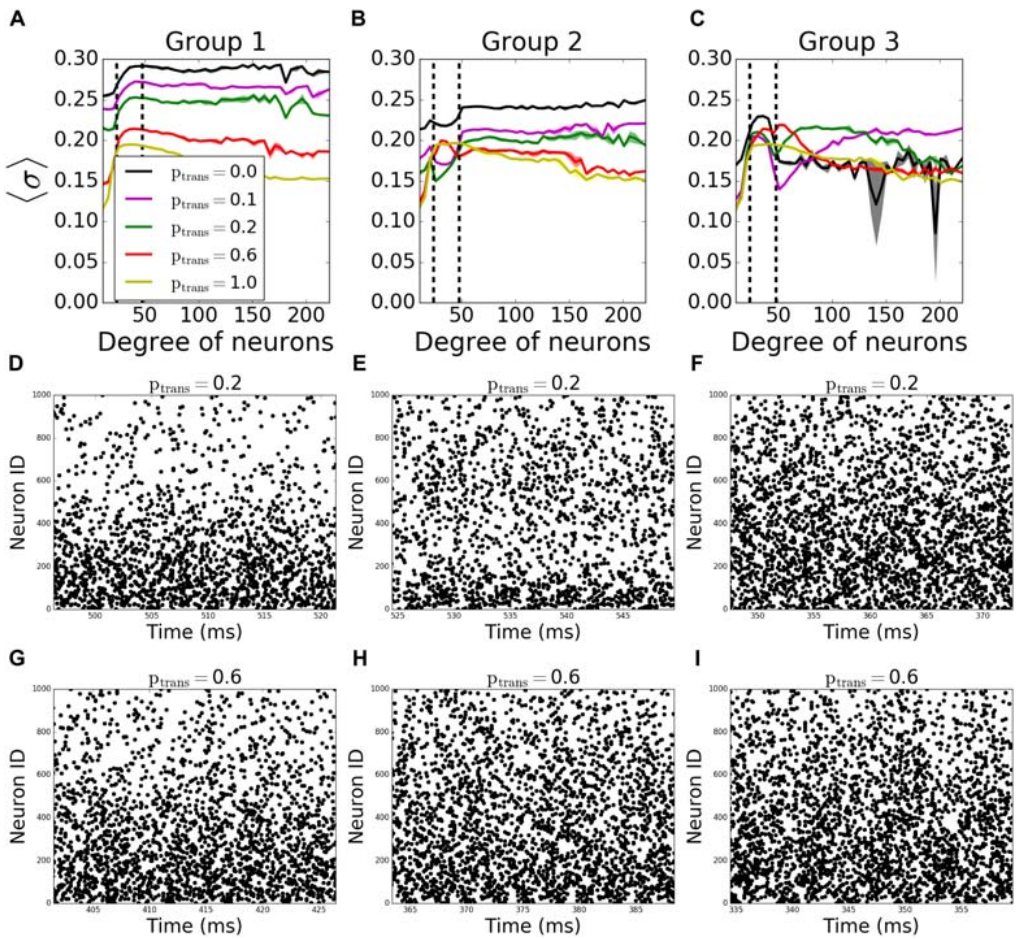

FIGURE 4 | Nodal contribution to network-wide MPC as a function of its degree for **incoming networks** show an increased coherence of hubs, when they fail to receive signals. Neurons in the network are grouped according to their degrees. Groups are assigned such that neurons in each group has equal total number of connections. Neurons with degrees 1–23 constitute group 1 [left of the first dashed line in panels **(A–C)**], neurons with degrees 24–47 constitute group 2 (between dashed lines), and neurons with degrees >48 constitute group 3 (right of the second dashed line). Signals are transmitted to group 1 **(A)**, group 2 **(B)**, and group 3 **(C)** with the probability p_{trans}, while the rest of the network receives signals without failure. Raster plots for the cases in **(A–C)** are shown in **(D–G)**, **(E–H)**, and **(F–I)**, respectively, for two values of p_{trans}. Lower neuron ID means higher degrees and vice versa (see **Figures 12A,E** for degrees corresponding to neuron IDs).

We then investigated how the MPC and synchrony forms within the network as a function of degree number of constituent neurons. The histogram of the average MPC constructed as a function of connection number for varying degrees of incoming networks (**Figure 3C**) suggests that, for full transmission $(p_{trans} = 1.0)$, moderate-degree neurons of incoming networks have higher average MPC values than low-degree or high-degree neurons. This seems intuitive as the neurons with very few connections don't get enough input to form stable patterns, whereas a few cells with a large number of inputs cannot synchronize with the rest of the population, as their frequency is significantly different due to widely varying number of excitatory inputs (**Figure 3E**). This trend is reversed for higher failure rate $(p_{trans} = 0.2)$, with hubs being more coherent than the rest of the network.

Moreover, for $p_{trans} = 0.6$, neurons fire more coherently than when $p_{trans} = 1.0$ for all degrees. This provides evidence that failure can promote more coherent behavior, as the input received by different degrees becomes more uniform with failure.

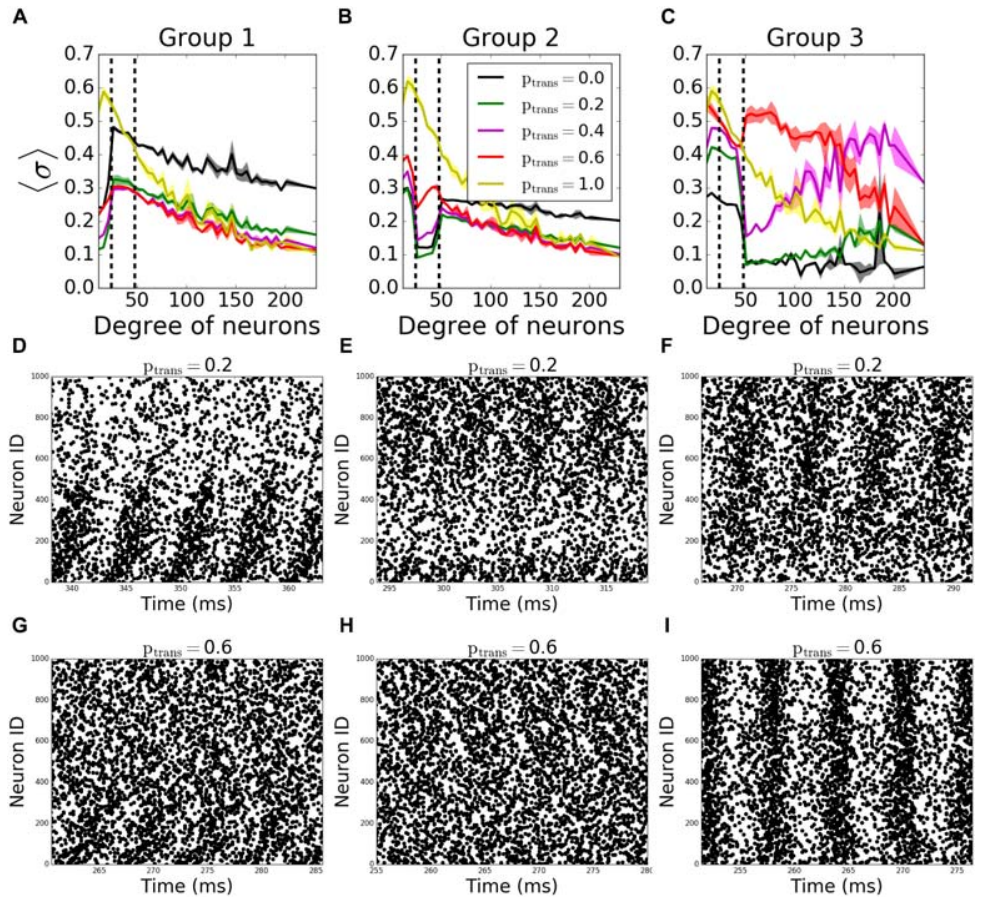

FIGURE 5 | Nodal contribution to network-wide MPC as a function of its degree for **outgoing networks** show an increased coherence of hubs for $p_{trans} \geq 0.4$ than when there's no failure. Neurons in the network are grouped according to their degree. Groups are assigned such that neurons in each group has equal total number of connections. Neurons with degrees 1–23 constitute group 1 [left of first dashed line in panels **(A–C)**], neurons with degrees 24–47 constitute group 2 (between dashed lines), and neurons with degrees >48 constitute group 3 (right of second dashed line). Signals are transmitted to group 1 **(A)**, group 2 **(B)**, and group 3 **(C)** with the probability p_{trans}, while the rest of the network receive signals without failure. Raster plots for the cases in **(A–C)** are shown in **(D–G)**, **(E–H)**, and **(F–I)**, respectively, for two values of p_{trans}. Lower neuron ID corresponds to cells with higher degrees (see **Figures 12A,E** for degrees corresponding to neuron IDs).

The same histogram for outgoing networks (**Figure 3D**) shows that, for the same p_{trans}, the average MPC values are higher than the incoming case. This is due to a more balanced input levels across the neurons in the network, i.e., a more balanced frequency distribution throughout different degrees (**Figure 3F**). In general, higher-degree neurons have lower average MPC in the outgoing case, and this effect is the most pronounced for higher values of p_{trans}. The example raster plots of the observed dynamics are presented on **Figures 3G–J**, with the corresponding values of p_{trans} marked on **Figures 3A,B**.

To assess better the specific role of neurons having different degree numbers (i.e., number of connections) on pattern formation, we divided the neurons in each network into 3 groups depending on their total degree (i.e., the sum of their incoming and outgoing connections). The groups were formed so that the total number of the connections in each group is equal. Thus, the number of neurons in each group is inversely proportional to the average degree of individual neurons in the groups, resulting in equal number of connections per group; neurons with degrees less than 24 are in "Group 1," between 24 and 48 degrees are in "Group 2", and with more than 48 degrees are in "Group 3." In terms of number of neurons, the groups consist on average of 533, 342, 125 neurons, respectively. The signals coming through the incoming connections to a given group are tested against different transmission probabilities p_{trans}, while the rest of the connections don't fail at all $(p_{trans} = 1.0)$, to see the individual effects of the failure of signals coming to different degrees on overall pattern formation.

In incoming networks, the response of MPC to the network manipulations is generally small. Interestingly we observe that the failing signals coming to Group 1 (**Figure 4A**, example raster plots on **Figures 4D,G**) and Group2 (**Figure 4B**, example raster plots on **Figures 4E,H**) result in an overall increase in MPC values of the unaffected groups, with Group 1 having a bigger effect than Group 2. The reason is that preventing lower degree groups from receiving signals make them fire only as a result of I_{rand}, decreasing their overall firing frequency as the synapses fail. Lowering the frequency in these two groups

reduced the frequency in all other groups leading to observable increase of coherence.

The progressive failure of incoming connections to Group 3 has a more complicated effect. We observe a higher coherence of that group than the rest of the network for $0.0 < p_{trans} < 1.0$ (**Figure 4C**, example raster plots on **Figures 4F,I**). This increase as a function of reduction of the transmission probability in the hub group brings the magnitude of the incoming signal to the hub cells to be similar to that of the intermediate group, increasing effectively the coherent backbone of the network. For $p_{trans} = 0.1$, we observe that the MPC of hubs are equal and higher than no failure case $\left(p_{trans} = 1.0\right)$, and this equalizing effect disappears with increasing p_{trans}. This effect is further confirmed through observation which neurons from Group 3 show increased synchronization as a function of increased failure – for lower transmission rates the neurons within that group with higher degrees exhibit increased coherence, whereas for higher transmission, the cells with lower degrees show increase of coherence.

In outgoing networks, even moderate increase in failure of Group 1 decreases Group 1 and Group 2's MPC significantly, but hubs (Group 3) are not affected. When $p_{trans} = 0.0$, we observe overall decrease in frequency which leads to increase in reported coherence (**Figure 5A**). The same holds for the case when Group 2 fails to receive signals (**Figure 5B**). However, when Group 3 is disconnected, the same reversal effect is observed as in incoming case (**Figure 5C**), but with significantly higher observed changes in MPC. This is again due to the homogenization of the received signals by neurons having different degree. As before, **Figures 5D–I** show example raster plots for two transmission values: $p_{trans} = 0.2$ and $p_{trans} = 1.0$.

Activity – Dependent Case

The second case we studied is when the transmission probability depends on the spiking history of the postsynaptic neurons, i.e., the signal coming to the postsynaptic neuron, which more recently fired, has a higher chance to fail due to the postsynaptic receptor sensitivity. This case may be biologically more relevant, since it is known that neurodegenerative diseases, such as AD and Parkinson's, have lower levels of postsynaptic ionotropic receptors (Dinamarca et al., 2012; Xu et al., 2012). As a result, this may cause a more effective desensitization of the neurotransmitter-gated ion channels in case of higher frequency stimulation via spiking presynaptic neurons (Rosenmund and Mansour, 2002; Papke et al., 2011). Moreover, higher activity is shown to result in regional vulnerability to amyloid-β deposition in AD, which causes synaptic failure (Bero et al., 2011).

In this case, we vary two parameters; the base failure probability p_{syn} and failure recovery time constant T. Here, $p_{syn} = 1$ indicates the possibility of complete failure of the synapse. We vary T between 0 ms and 5000 ms, with $p_{syn} = 1$ and $T = 5000ms$ being a disconnected network.

As before, we first assessed the overall degree of pattern formation in both types of networks. In incoming networks, we didn't see any significant changes in MPC and synchrony for various T and p_{syn} values (**Figures 6A,C**). However; for outgoing networks, we observed an overall decrease in the network coherence for increasing p_{syn}. For fast synaptic recovery, this decrease is significantly smaller (**Figures 6B,D**). Interestingly, however, for $T = 0.5ms$, we observed a dramatic increase of both MPC and synchrony as p_{syn} tends to unity.

A more systematic scan of time constants T reveals that for incoming networks, the network starts getting disconnected for $T > 5ms$. When $T = 5000ms$, the MPC and synchrony values are the same as activity-independent case, meaning that T is large enough that $p_{trans} \approx 1 - p_{syn}$ (**Figures 7A,B**; the corresponding raster plots are displayed on **Figures 7C,D**).

The behavior of outgoing networks is similar to the one described above except for $T = 0.5ms$, where we observed a

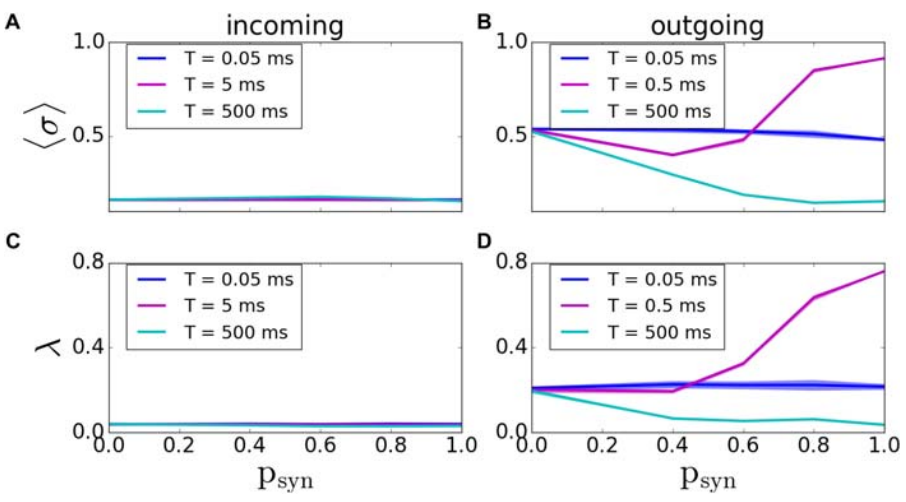

FIGURE 6 | Pattern formation in the incoming and outgoing networks with activity-dependent synaptic failure. **(A,B)** MPC and **(C,D)** synchrony for incoming **(A,C)**, and outgoing **(B,D)** networks as a function of p_{syn} for three different values of failure recovery time constants T. There is a dramatic increase in MPC and synchrony with increasing synaptic failure (p_{syn}) for a moderate T in outgoing networks.

large peak in both MPC and synchrony, as p_{syn} tends to one (**Figures 8A,B**; the corresponding raster plots are displayed on **Figures 8C–F**).

We then have investigated how synaptic failure interacts with neurons with specific nodal degree to form activity pattern within the network (**Figure 9**). For incoming networks and for large T (**Figures 9A–C**) the degree dependence is largely similar to that of constant p_{trans}, described in the previous section. The group with the largest coherence is the group having intermediate degree values. For small T, as expected, p_{syn} does not influence the overall coherence levels as the transmission probability rapidly recovers and $p_{trans} \approx 1.0$. For larger time constants, the overall level of coherence depends on the p_{syn}, as in the case of activity-independent case (**Figure 3C**). For a moderate time constant ($T = 5ms$), however, we observe that hubs have higher coherence when $p_{syn} \neq 0.0$ than when $p_{syn} = 0.0$, which means that failure of spikes results in a more coherent behavior of hubs, even though globally there's no significant change in the network's MPC. This is driven by synaptic failure capacity to equalize input to the cells across the network.

For outgoing networks, generally the same is true for low and high values of T (**Figures 9D,F**) as in incoming case. However, for the value $T = 0.5ms$ (**Figure 9E**), we observe a complete reversal of the overall network coherence, with the largest coherence happening for the largest p_{syn} and approaching to one. The MPC is then largely independent of the neuronal degrees, except the highest ones, where MPC starts dropping.

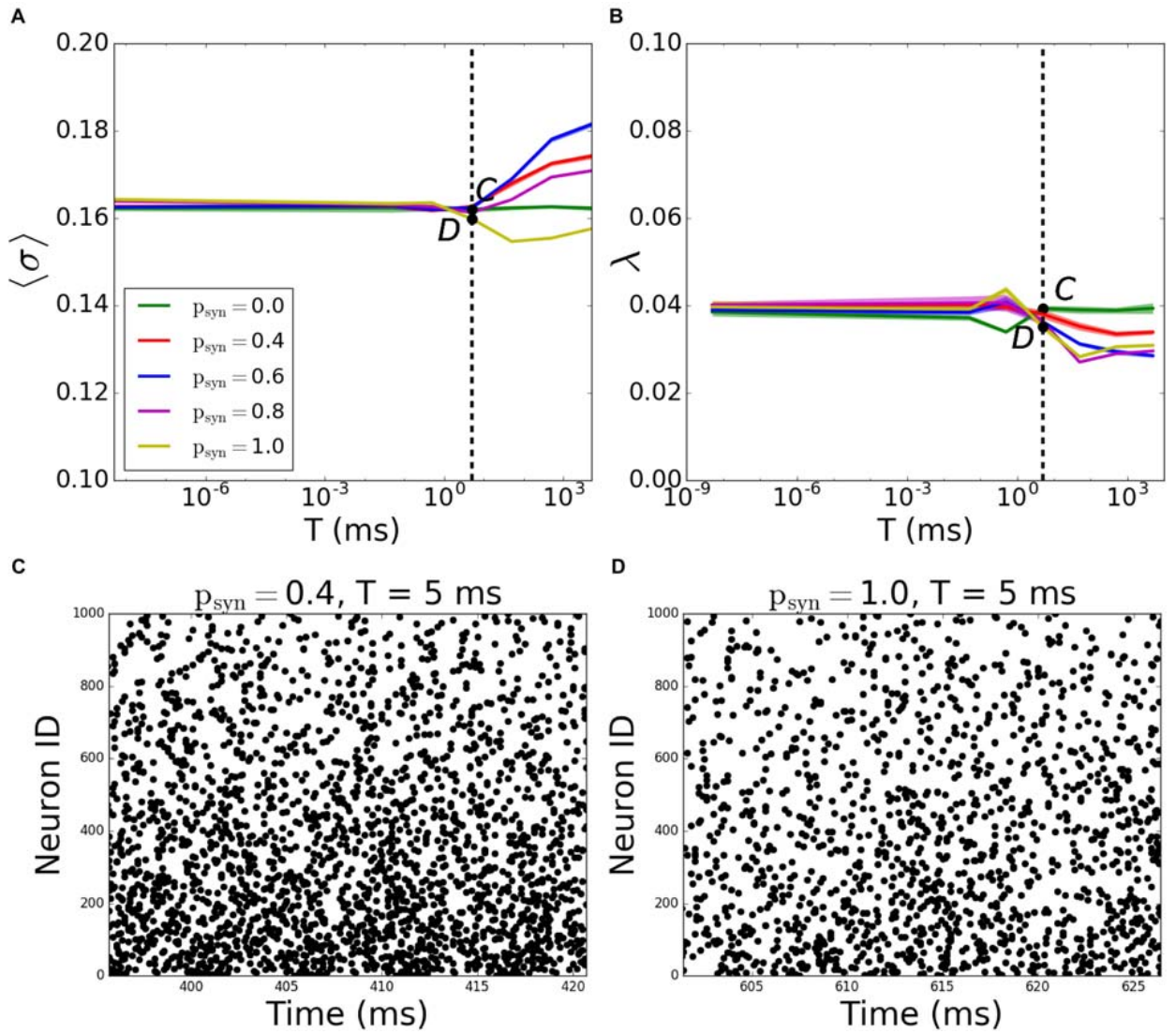

FIGURE 7 | Pattern formation in the incoming networks with activity-dependent synaptic failure as a function of failure recovery time constant T. **(A)** MPC and **(B)** synchrony as a function of time constant T for different values of p_{syn}. **(C,D)** Raster plots depicting network activity for parameter values marked on **(A,B)** [Points C and D correspond to panels **(C,D)**]. The specific parameter values of T and p_{syn} are listed on top of each raster plot. Lower neuron ID corresponds to cells with higher degrees (see **Figures 12A,E** for degrees corresponding to neuron IDs).

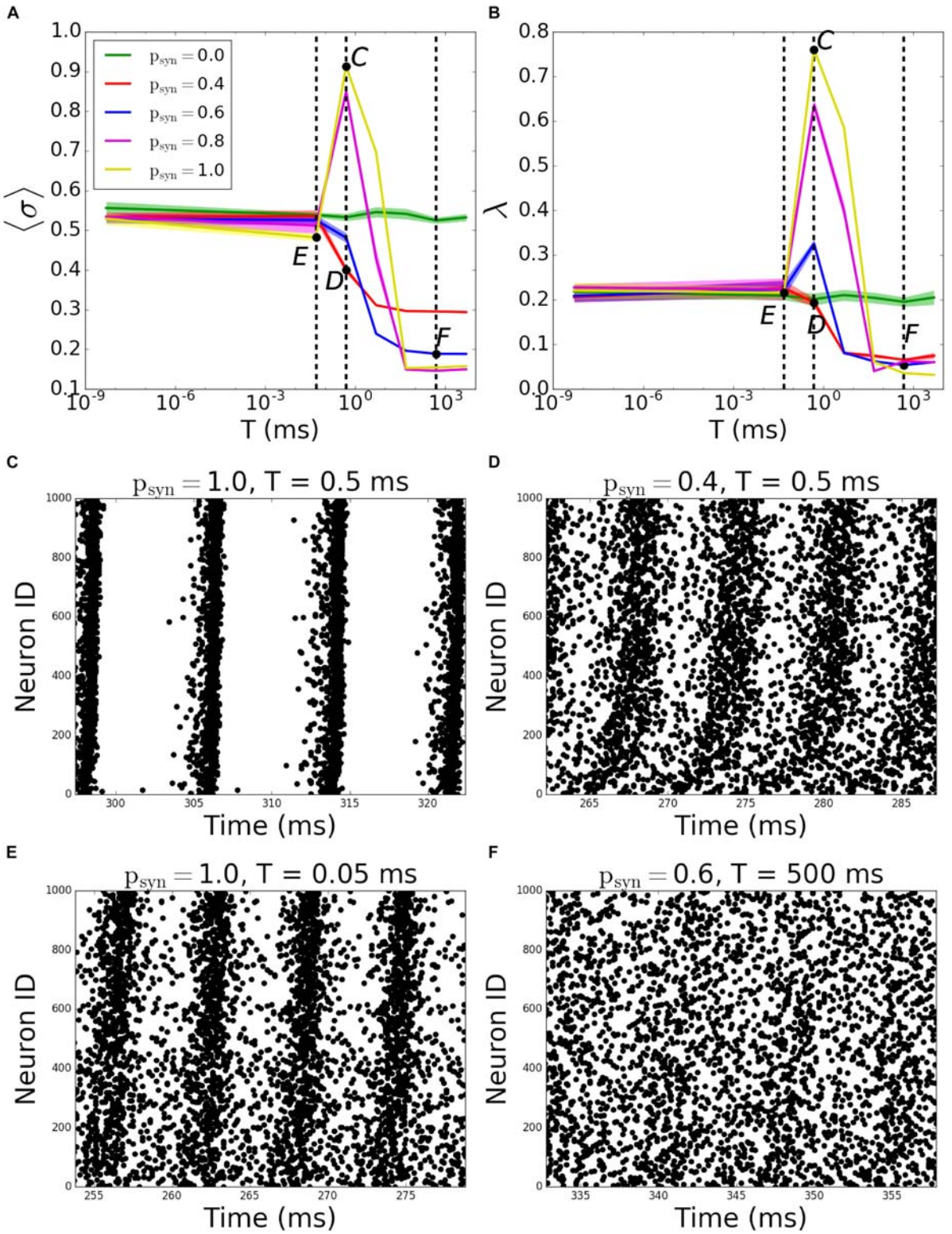

FIGURE 8 | Pattern formation in the outgoing networks with activity-dependent synaptic failure as a function of failure recovery time constant T. **(A)** MPC and **(B)** synchrony as a function of time constant T for different values of p_{syn}. **(C–F)** Raster plots depicting network activity for parameter values marked on **(A,B)** [Points *C–F* correspond to panels **(C–F)**]. The specific parameter values of T and p_{syn} are listed on top of each raster plot. Lower neuron ID corresponds to cells with higher degrees.

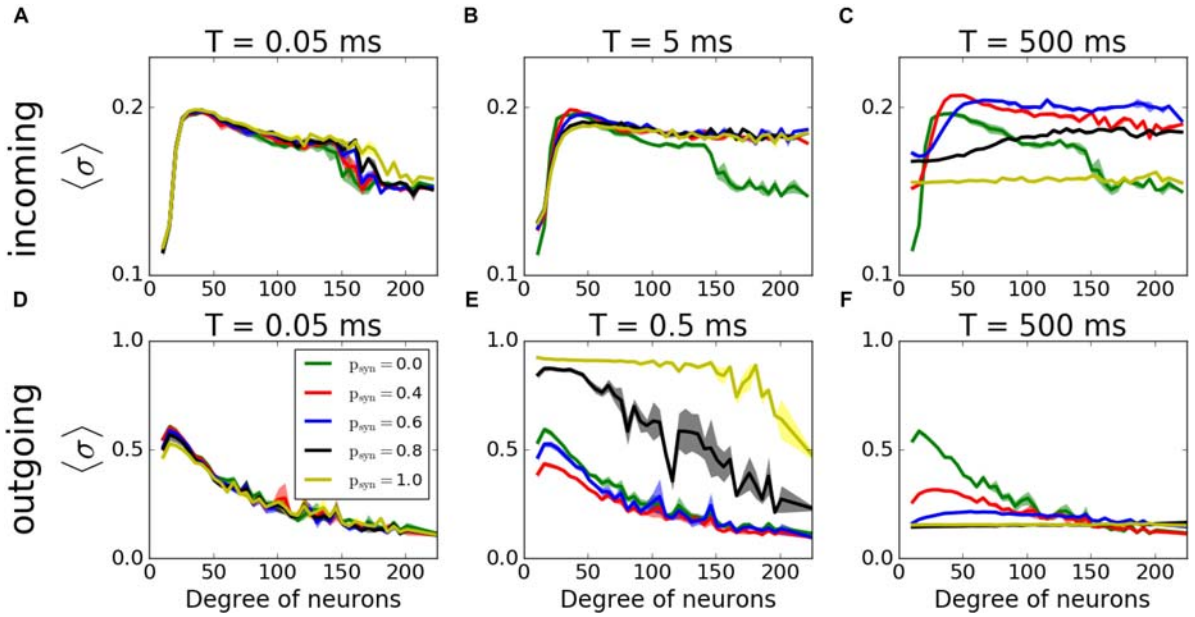

FIGURE 9 | Histograms of MPC as a function of degree of neurons of incoming **(A–C)** and outgoing **(D–F)** networks for varying failure recovery time constants T (denoted on top of each panel). Participation in pattern formation as a function of nodal degree for activity-dependent transmission failure shows an increased coherence with increased failure for moderate T in both networks.

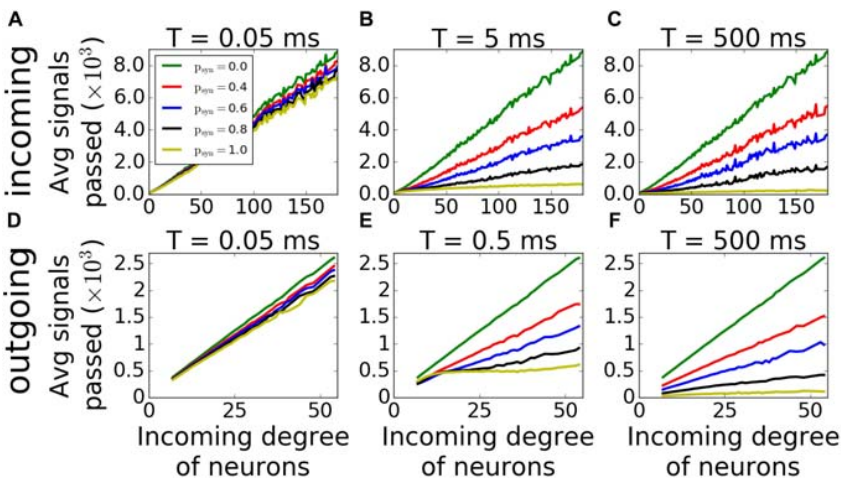

FIGURE 10 | Average input magnitude to a neuron as a function of nodal degree for activity-dependent synaptic failure. Histograms of average number of signals transmitted as a function of incoming degree of neurons of incoming **(A–C)** and outgoing **(D–F)** networks for varying failure recovery time constants T (denoted on top of each panel) show that for $T = 0.5ms$ and $p_{syn} = 1.0$, outgoing networks receive the same amount of signals, and independent from their degrees.

To understand the reason behind this sudden increase, we measured the average number of signals transmitted to each neuron as a function of its incoming degree. The histograms (**Figure 10**) suggest, that for low T, for both incoming and outgoing networks, there is a linear proportionality between the input and the incoming degree number (**Figures 10A,D**). For larger values of T, the signal curves depend directly on the value of p_{syn} and for large p_{syn} they saturate for large degree values (**Figures 10B,C,E,F**), making the amount of signal received by neurons largely independent of degree. However, only for outgoing networks and $T = 0.5ms$, all neurons, independent from their incoming degrees, receive the same number of the signals, which is significantly different from zero (**Figure 10E**). This suggest that at this specific T range, all cells in the network receive about the same input magnitude allowing them to synchronize across the entire system.

To see if similar results would be observed with different connectivities and direction ratios, we simulated various connectivity fractions and direction ratios for different time constants ($T = 0.05$, 5, $500ms$ for incoming networks and

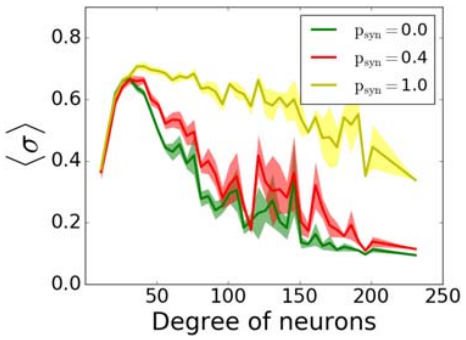

FIGURE 11 | Participation in pattern formation as a function of nodal degree for activity-dependent transmission failure for mixed excitatory-inhibitory networks. Histograms of MPC as a function of degree of neurons for $T = 0.5$ ms and varying p_{syn} levels show emergence of highly synchronous state for high values. The networks is composed of 1000 excitatory and 1000 inhibitory neurons. Excitatory neurons are wired as outgoing scale-free networks, while inhibitory neurons have random connections to both inhibitory and excitatory population with the same connectivity as the one within excitatory population (1.6%).

$T = 0.05$, 0.5, $500ms$ for outgoing networks). In incoming case, the reversal effect of MPC increase of hubs for higher p_{syn} at a moderate time constant ($T = 5ms$) is not observed for lower or higher connectivities (**Supplementary Figure S2**). However, increasing direction ratio makes this effect more pronounced, since increasing outgoing connections at hubs makes the network more balanced overall (**Supplementary Figure S3**). In outgoing networks, this dramatic increase of overall coherence is still observed, and it is more pronounced for higher connectivities (**Supplementary Figure S4**) and lower direction ratios (**Supplementary Figure S5**), since the amount of outgoing connections from hubs is increased in both cases, resulting in a more coherent network overall.

Lastly, we included inhibitory neurons to the network, since they are known to have significant effects on pattern formation in cortical networks (Vreeswijk and Sompolinsky, 1996). We simulated outgoing networks with an inhibitory population for $T = 0.5ms$ and various p_{syn}. Our results (**Figure 11**) suggest that there's still that reversal effect as we've seen in **Figure 9E**, i.e., increasing p_{syn} eventually increases the overall network coherence, when p_{syn} approaches to 1.

DISCUSSION

In this study, we systematically analyzed how synaptic failure affects two complementary (incoming and outgoing) scale-free network structures. We studied the cases when synaptic transmission probability is activity-independent and activity-dependent. In the first case, we have found that targeted synaptic failure to neuronal population having different nodal degrees, has differential effects on pattern formation in the network. When synaptic failure was activity dependent, we observed that structural features of networks don't map onto functional connectivity (**Figure 12**), but rather, synaptic

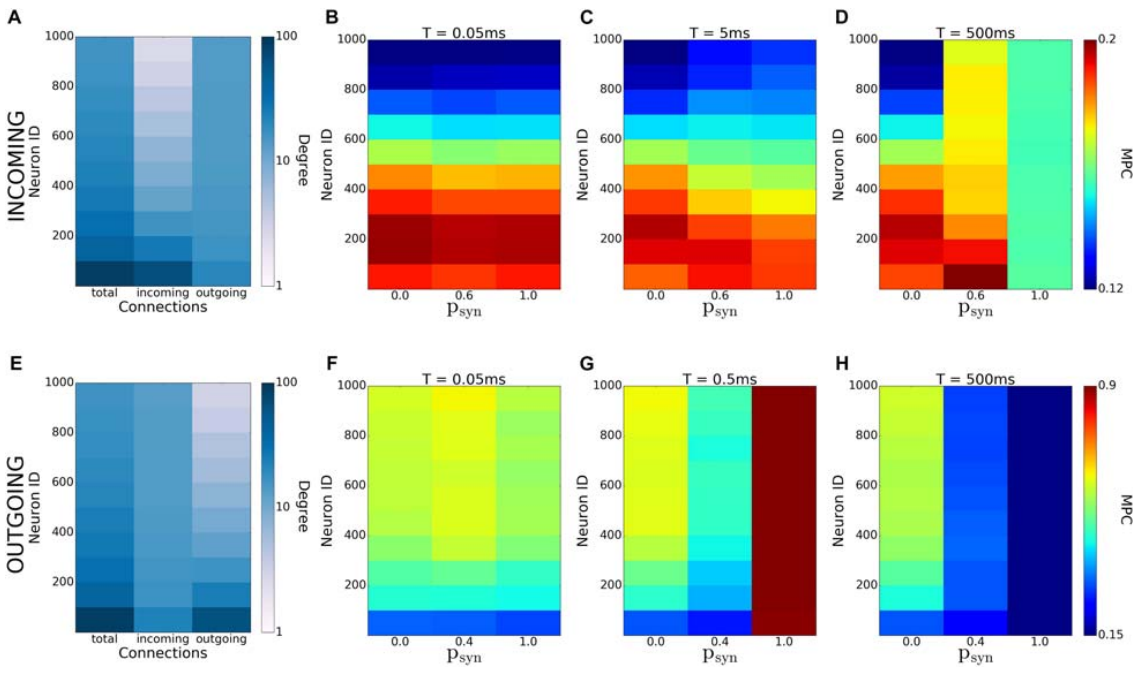

FIGURE 12 | Emergence of coherence patterns in scale-free networks. Heatmaps of degrees **(A,E)** and MPC [**(B–D)** and **(F–H)**] for incoming **(A–D)**, and outgoing **(E–H)** networks show dependence of network-wide pattern formation on parameters of activity-dependent synaptic failure (T and p_{syn}). Each color is an average of the values for 100 neurons.

failure may result in differential spatio-temporal patterning dependent on failure recovery time constant T and base failure probability p_{syn}. Moreover, the two network structures, (incoming and outgoing) behave differently, with outgoing networks displaying overall a larger degree of coherence/synchrony and a higher dependence on transmission probability. This is especially evident for the activity-dependent transmission probability, where the outgoing networks exhibit an increased level of coherence for a large base failure probability (p_{syn}) for a specific value of the failure recovery time constant ($T = 0.5ms$).

This abrupt increase in synchrony and coherence as a result of synaptic failure is unexpected and possibly paints a more complex picture of possible network interactions in the brain. It was hypothesized that anesthetics act predominantly on the network hubs and overall decrease the level of coherence across brain networks, leading to the loss of consciousness (Lee et al., 2013). Similarly, hubs are shown to be more vulnerable to amyloid deposition due to their high activity rate, causing the disruption of large-scale coherence in the brain and eventually AD (Buckner et al., 2009). In addition, numerical studies on scale-free networks suggest that they are robust against the random removal of nodes and the change in their synchronization process is insignificant in case 5% of their total nodes are randomly removed. However, when hubs are targeted, only the removal of 1% of the total nodes is enough to divide the network into subnetworks and to disrupt network synchronization (Albert et al., 2000; Jinhu and Guanrong, 2005; Boccaletti et al., 2006; Li et al., 2011). We, however, show that, depending on the network type, preferential deactivation of hubs and activity-dependent degeneration might lead to increased phase coherence and synchrony. Further investigation on human brain networks may be necessary to determine whether there's an overall increased coherence phase before the decrease of large-scale coherence in such cases as application of anesthetics or AD. That may be a useful biomarker for AD as well as a significant contribution to explain impact on anesthetics on human brain.

AUTHOR CONTRIBUTIONS

MZ designed the research, oversaw the execution, and participated in writing the manuscript. MB executed the research and wrote the manuscript.

FUNDING

The work was supported by NIBIB grant EB018297.

SUPPLEMENTARY MATERIAL

The Supplementary Material for this article can be found online at: https://www.frontiersin.org/articles/10.3389/fncir.2019.00031/full#supplementary-material

FIGURE S1 | Network spike frequency **(A,C)** and mean phase coherence **(B,D)** for various frequencies of random input I_{rand}, for incoming **(A,B)** and outgoing **(C,D)** networks. Results are averaged over 5 randomized network realizations.

FIGURE S2 | Nodal contribution to network-wide MPC as a function of its degree for incoming networks for different connectivities and failure recovery time constant T. The increase in MPC of hubs with higher failure cannot be observed for lower or higher connectivities for T = 5 ms. MPCs are averaged over 5 degrees and results are averaged over 5 randomized network realizations.

FIGURE S3 | Nodal contribution to network-wide MPC as a function of its degree for incoming networks for different direction ratios and failure recovery time constant T. Higher direction ratios result in a more obvious increase in MPC of hubs for T = 5 ms when there's more failure. MPCs are averaged over 5 degrees and results are averaged over 5 randomized network realizations.

FIGURE S4 | Nodal contribution to network-wide MPC as a function of its degree for outgoing networks for different connectivities and failure recovery time constant. Higher connectivities result in a bigger increase in MPC for T=0.5 ms with higher failure p_{syn}. MPCs are averaged over 5 degrees and results are averaged over 5 randomized network realizations.

FIGURE S5 | Nodal contribution to network-wide MPC as a function of its degree for outgoing networks for different direction ratios and failure recovery time constant T. For T = 0.5 ms, the increase in MPC values of $p_{syn} = 1.0$ is more pronounced for lower direction ratios. MPCs are averaged over 5 degrees and results are averaged over 5 randomized network realizations.

REFERENCES

Albert, R., Jeong, H., and Barabasi, A. L. (2000). Error and attack tolerance of complex networks. *Nature* 406, 378–382. doi: 10.1038/35019019

Barabasi, A. L., Albert, R., and Jeong, H. (1999). Mean-field theory for scale-free random networks. *Physica A* 272, 173–187. doi: 10.1016/S0378-4371(99)00291-5

Bero, A., Yan, P., Roh, J., Cirrito, J., Stewart, F., Raichle, M., et al. (2011). Neuronal activity regulates the regional vulnerability to amyloid-β deposition. *Nat. Neurosci.* 14, 750–756. doi: 10.1038/nn.2801

Boccaletti, S., Latora, V., Moreno, Y., Chavez, M., and Hwang, D. (2006). Complex networks: structure and dynamics. *Phys. Rep.* 424, 175–308. doi: 10.1016/j.physrep.2005.10.009

Buckner, R., Sepulcre, J., Talukdar, T., Krienen, F., Liu, H., Hedden, T., et al. (2009). Cortical hubs revealed by intrinsic functional connectivity: mapping, assessment of stability, and relation to Alzheimer's Disease. *J. Neurosci.* 29, 1860–1873. doi: 10.1523/jneurosci.5062-08.2009

Bullmore, E., and Sporns, O. (2009). Complex brain networks: graph theoretical analysis of structural and functional systems. *Nat. Rev. Neurosci.* 10, 186–198. doi: 10.1038/nrn2575

Burkitt, A. N. (2006). A review of the integrate-and-fire neuron model: II. inhomogeneous synaptic input and network properties. *Biol. Cybern.* 95, 97–112. doi: 10.1007/s00422-006-0082-8

Chen, Y., Fu, A., and Ip, N. (2019). Synaptic dysfunction in Alzheimer's disease: mechanisms and therapeutic strategies. *Pharmacol. Ther.* 195, 186–198. doi: 10.1016/j.pharmthera.2018.11.006

de Haan, W., Mott, K., van Straaten, E., Scheltens, P., and Stam, C. (2012). Activity dependent degeneration explains hub vulnerability in Alzheimer's Disease. *PLoS Comput. Biol.* 8:e1002582. doi: 10.1371/journal.pcbi.1002582

Diao, S., Ni, J., Shi, X., Liu, P., and Xia, W. (2014). Mechanisms of action of general anesthetics. *Front. Biosci. Landmark Ed.* 19, 747–757. doi: 10.2741/4241

Dinamarca, M. C., Rios, J. A., and Inestrosa, N. C. (2012). Postsynaptic receptors for amyloid-beta oligomers as mediators of neuronal damage in Alzheimer's Disease. *Front. Physiol.* 3:464. doi: 10.3389/fphys.2012.00464

Franks, N. (2008). General anaesthesia: from molecular targets to neuronal pathways of sleep and arousal. *Nat. Rev. Neurosci.* 9, 370–386. doi: 10.1038/nrn2372

Golomb, D., and Rinzel, J. (1993). Dynamics of globally coupled inhibitory neurons with heterogeneity. *Phys. Rev. E Stat. Phys. Plasmas Fluids Relat. Interdiscip. Topics* 48, 4810–4814. doi: 10.1103/physreve.48.4810

Hillebrand, A., Tewarie, P., van Dellen, E., Yu, M., Carbo, E., Douw, L., et al. (2016). Direction of information flow in large-scale resting-state networks is frequency-dependent. *Proc. Natl. Acad. Sci. U.S.A.* 113, 3867–3872. doi: 10.1073/pnas.1515657113

Jinhu, L., and Guanrong, C. (2005). A time-varying complex dynamical network model and its controlled synchronization criteria. *IEEE Trans. Automat. Contr.* 50, 841–846. doi: 10.1109/tac.2005.849233

Lee, H., Mashour, G. A., Noh, G. J., Kim, S., and Lee, U. (2013). Reconfiguration of network hub structure after propofol-induced unconsciousness. *Anesthesiology* 119, 1347–1359. doi: 10.1097/ALN.0b013e3182a8ec8c

Li, K., Fu, X., Small, M., and Ma, Z. (2011). Adaptive mechanism between dynamical synchronization and epidemic behavior on complex networks. *Chaos* 21:033111. doi: 10.1063/1.3622678

Mirzakhalili, E., Gourgou, E., Booth, V., and Epureanu, B. (2017). Synaptic impairment and robustness of excitatory neuronal networks with different topologies. *Front. Neural Circ.* 11:38. doi: 10.3389/fncir.2017.00038

Moon, J., Lee, U., Blain-Moraes, S., and Mashour, G. (2015). General relationship of global topology, local dynamics, and directionality in large-scale brain networks. *PLoS Comput. Biol.* 11:e1004225. doi: 10.1371/journal.pcbi.1004225

Mormann, F., Lehnertz, K., David, P., and Elger, C. E. (2000). Mean phase coherence as a measure for phase synchronization and its application to the EEG of epilepsy patients. *Physica D* 144, 358–369. doi: 10.1016/S0167-2789(00)00087-7

Papke, D., Gonzalez-Gutierrez, G., and Grosman, C. (2011). Desensitization of neurotransmitter-gated ion channels during high-frequency stimulation: a comparative study of Cys-loop, AMPA and purinergic receptors. *J. Physiol.* 589, 1571–1585. doi: 10.1113/jphysiol.2010.203315

Rosenmund, C., and Mansour, M. (2002). Ion channels: how to be desensitized. *Nature* 417, 238–239. doi: 10.1038/417238a

Vreeswijk, C., and Sompolinsky, H. (1996). Chaos in neuronal networks with balanced excitatory and inhibitory activity. *Science* 274, 1724–1726. doi: 10.1126/science.274.5293.1724

Wishart, T. M., Parson, S. H., and Gillingwater, T. H. (2006). Synaptic vulnerability in neurodegenerative disease. *J. Neuropathol. Exp. Neurol.* 65, 733–739. doi: 10.1097/01.jnen.0000228202.35163.c4

Xu, Y., Yan, J., Zhou, P., Li, J., Gao, H., Xia, Y., et al. (2012). Neurotransmitter receptors and cognitive dysfunction in Alzheimer's disease and Parkinson's disease. *Prog. Neurobiol.* 97, 1–13. doi: 10.1016/j.pneurobio.2012.02.002

Conflict of Interest Statement: The authors declare that the research was conducted in the absence of any commercial or financial relationships that could be construed as a potential conflict of interest.

frontiers in Neural Circuits

ORIGINAL RESEARCH
published: 08 May 2019
doi: 10.3389/fncir.2019.00033

Brain Structural Alterations in Left-Behind Children: A Magnetic Resonance Imaging Study

Yuchuan Fu[1†], Yuan Xiao[1,2†], Meimei Du[1], Chuanwan Mao[1], Gui Fu[1,2], Lili Yang[1], Xiaozheng Liu[1], John A. Sweeney[2,3], Su Lui[1,2] and Zhihan Yan[1]**

[1] Department of Radiology, The Second Affiliated Hospital and Yuying Children's Hospital of Wenzhou Medical University, Wenzhou, China, [2] Department of Radiology, Center for Medical Imaging, West China Hospital of Sichuan University, Chengdu, China, [3] Department of Psychiatry and Behavioral Neuroscience, University of Cincinnati, Cincinnati, OH, United States

Parental migration has caused millions of children left behind, especially in China and India. Left-behind children (LBC) have a high risk of mental disorders and may present negative life outcomes in the future. However, little is known whether there are cerebral structural alterations in LBC in relative to those with parents. This study is to explore the effect of parental migration on brain maturation by comparing gray matter volume (GMV) and fractional anisotropy (FA) of LBC with well-matched non-LBC. Thirty-eight LBC (21 boys, age = 9.60 ± 1.8 years) and 30 non-LBC (19 boys, age = 10.00 ± 1.95 years) were recruited and underwent brain scans in 3.0 T MR. Intelligence quotient and other factors including family income, guardians' educational level and separation time were also acquired. GMV and FA were measured for each participant and compared between groups using 2-sample *t*-tests with atlas-based analysis. Compared to non-LBC, LBC exhibited greater GMV in emotional and cortico-striato-thalamo-cortical circuits, and altered FA in bilateral superior occipitofrontal fasciculi and right medial lemniscus ($p < 0.05$, Cohen's $d > 0.89$, corrected for false-discovery rate). Other factors including family income, guardians' educational level and separation time were not associated with these brain changes. Our study provides empirical evidence of altered brain structure in LBC compared to non-LBC, responsible for emotion regulation and processing, which may account for mental disorders and negative life outcome of LBC. Our study suggests that absence of direct biological parental care may impact children's brain development. Therefore, public health efforts may be needed to provide additional academic and social/emotional supports to LBC when their parents migrate to seeking better economic circumstances, which has become increasingly common in developing countries.

Keywords: left-behind children, gray matter volume, fractional anisotropy, MRI, cognition

OPEN ACCESS

Edited by:
Lijun Bai,
Xi'an Jiaotong University, China

Reviewed by:
Wei Liao,
University of Electronic Science and Technology of China, China
Hengyi Cao,
Yale University, United States

***Correspondence:**
Su Lui
lusuwcums@hotmail.com
Zhihan Yan
yanzhihanwz@163.com

† These authors have contributed equally to this work

Received: *29 December 2018*
Accepted: *15 April 2019*
Published: *08 May 2019*

Citation:
Fu Y, Xiao Y, Du M, Mao C, Fu G, Yang L, Liu X, Sweeney JA, Lui S and Yan Z (2019) Brain Structural Alterations in Left-Behind Children: A Magnetic Resonance Imaging Study. Front. Neural Circuits 13:33. doi: 10.3389/fncir.2019.00033

INTRODUCTION

In recent years, migration has become a common phenomenon because of reduction in barriers to international trade and immigration, and rapid urbanization. These trends have lured hundreds of millions of laborers away from impoverished hometowns in rural areas of developing countries to seek better economic circumstances. It is estimated that up to 80% migrant worker in China to leave

away from impoverished hometown to developed countries or coastal cities, majorly southeast cities (Cheng and Sun, 2015). As a result, millions of children are left behind with friends and relatives, mostly grandparents (United Nations, 2009; Li et al., 2015). These children who stay at home with extended family members or boarding school when their parents migrate for at least 6 months are called "left-behind children" (LBC) (All-China Women's Federation, 2013). In China alone, there are more than 61 million LBC (All-China Women's Federation, 2013) – a population larger than California and New York combined.

Studies of LBC have shown increased levels of social anxiety and a lower quality of life (Zhao et al., 2014; Mazzucato et al., 2015). They also have increased rates of psychiatric syndromes later in life (Liu et al., 2009; Fan et al., 2010; Wang et al., 2015), particularly mood and anxiety disorders (Heim et al., 2010) and poor academic performance (Jingzhong and Lu, 2011). Accordingly, the phenomenon of LBC may represent a significant public health problem with long term consequences for society. However, there is not yet direct evidence for altered brain development in LBC in relative to non-LBC. There is evidence from previous studies of orphanages supporting lack of parents may lead to the alterations in brain, such as accelerated amygdala-mPFC development after maternal deprivation (Gee et al., 2013), widespread reductions of the cortical thickness especially in the prefrontal cortex (McLaughlin et al., 2014), smaller total gray matter volume (GMV) and larger amygdala volume (Mehta et al., 2009; Tottenham et al., 2010), and decreased fractional anisotropy (FA) in the body of the corpus callosum, the left and right external capsule and increased mean diffusivity and axial diffusivity in the right medial lemniscus (Bick et al., 2015b). The previous study also found that the length of time children experience orphanage rearing is associated with the alterations in GMV (Tottenham et al., 2010; Bick et al., 2015b). While the circumstances for orphanages were at times rather dire and extreme, it is quite difficult to answer whether such brain alterations occur in the less adverse circumstance of the millions of LBC world-wide raised by relatives rather than their biological parents who migrated for work opportunities.

Currently, magnetic resonance imaging (MRI) as a non-invasive technique has shown its value in objectively evaluating human brain *in vivo* (Lui et al., 2016). Especially, GMV reflected by voxel-based morphometry (VBM) has grown in popularity regarding the study of human brain at different age or under conditions. This automated voxel-based whole-brain analysis technique can comprehensively evaluate overall GMV differences between groups across all voxels (Ashburner and Friston, 2000; Good et al., 2001; Whitwell, 2009), preventing biases resulting from methods using liberal thresholds and region of interest (ROI) methods in neuroimaging studies. Meanwhile, Diffusion tensor imaging (DTI) is a MRI technique sensitive to the orientation of water diffusion restricted within the neuron sheath and myelination, provides measures of white-matter microstructure in the human brain. The orientation dependence of water diffusion – FA in DTI is thought to reflect anatomical features of neural fiber, such as axon caliber, fiber density, and myelination (Scholz et al., 2009). Our previous study has successfully revealed the white-matter microstructure changes of earthquake survivors (Chen et al., 2013). However, the brain of LBC individuals has not been well-characterized regarding both gray and white matter changes, which could unveil the neuropathological effects of being left-behind and expand our understanding of this group of individuals in developing countries.

Thus, the present cross-sectional study aimed to explore potential difference of brain GMV or FA of white matter between LBC and non-LBC. We hypothesized that: (1) LBC may exhibit changes of GMV in limbic-paralimbic system and prefrontal cortex which brain regions supporting emotion processing, as well as changes of FA values in related white matter tracts, and (2) that those brain differences would be related to the length of separation from parents and other factors.

MATERIALS AND METHODS

Participants

The study was approved by the research ethics committee of Second Affiliated Hospital and Yuying Children's Hospital of Wenzhou Medical University, and written informed consent was obtained from the participants and their guardians, before study participation. All participants attended the same local primary school in a town of southeastern China, and therefore had similar educational environments. Inclusion criteria for LBC were children who living with and taken care of by their grandparents because both of their parents had immigrated abroad for work for more than 6 months. In contrast, the non-LBC were children who living with their nuclear family throughout childhood. All subjects were evaluated by a child psychiatrist using the Chinese version of the SCID-I (Non-patient Edition) (Wang et al., 2009) to exclude any Axis I psychiatric diagnoses, and no first-degree relatives were known to have significant psychiatric illness. The exclusion criteria for both groups were as follows: (1) Neurological or psychiatric disorder; (2) Any systemic physical illness, such as hepatitis or diabetes; (3) Receiving medications known to affect brain function; (4) History of head trauma with significant loss of consciousness; (5) Premature or post-term birth; and (6) Malnutrition, mental deficiency or physical growth retardation.

Before MRI scanning, intelligence quotient was measured using the Chinese Wechsler Intelligence Scale for Children (C-WISC) (Gong and Cai, 1993) administered by an experienced child psychologist. Additionally, anxious and depression symptoms were assessed in the LBC group by Hamilton Anxiety Scale (HAMA) (Maier et al., 1988) and Hamilton Depression Scale (HAMD) (Hamilton, 1931), respectively. Originally, 76 children were recruited, of whom four children were excluded prior to MR imaging for the following reasons, i.e., two children were excluded because of fever, one child for lead poisoning and one child for precocious puberty. Another four subjects were excluded

because of excessive head motion during MRI scans. Thus, 68 subjects (38 LBC vs. 30 non-LBC) were included in analyses reported below.

Data Acquisition

High-resolution T1-weighted images were acquired using a 3.0T MRI system (Signa HDxt EXCITE, General Electric, Milwaukee) with a volumetric 3-dimensional spoiled gradient recall (SPGR) sequence (repetition time 9.2 ms, echo time 4.1 ms, flip angle 15°, slice thickness 1 mm) using an 8-channel phase array head coil. We used a field of view (FOV) of 240 mm × 240 mm, with an acquisition matrix 256 × 256 and left to right direction of phase-encoding to obtain 248 contiguous axial slices with a slice thickness of 1.0 mm and a voxel size of 0.94 mm × 0.94 mm × 1 mm.

Diffusion tensor imaging scans were acquired axially for the whole brain with TE/TR = 88.3 ms/8000 ms, *b*-value = 1000 s/mm^2, FOV = 220 mm × 220 mm, Matrix = 128 × 128, 34 slices, slice thickness = 4 mm, spacing between slices = 4 mm. One diffusion weighted image was acquired for each of 36 diffusion gradient directions. Two volumes with no diffusion encoding (b0) in alternate phase encoding directions were used to correct non-linear distortion corrections due to magnetic field inhomogeneity.

Image Processing

GMV

Image preprocessing and statistical analyses were performed with SPM8[1] using the VBM toolbox (VBM8). First, a customized tissue probability map was generated with the Template-O-Matic (TOM8) Toolbox (Wilke et al., 2008) using the matched-pairs approach to accurately reflect the specific brain morphometry for the age and gender of the children in our study. The anterior commissure was identified for each image and uniformly aligned for subsequent spatial normalization of native images that were segmented into gray matter, white matter and cerebrospinal fluid (CSF) according to the unified segmentation model. Then, the re-obtained gray matter images were subjected to Jacobian modulation (volume modulation) and smoothed with a 6 mm full-width at half-maximum Gaussian kernel.

DTI

The data were processed using the PANDA pipeline tool[2] for preprocessing and producing diffusion metrics. The preprocess steps were as follows: (1) data were converted from "DICOM" format to a "NIFTI" file; (2) Creation of brain mask, cropping raw images, correcting for eddy-current effects; (3) Calculation of diffusion tensor metrics. Automated atlas-based ROI analysis was used to identify differences of FA between the LBC and non-LBC groups. FSL software (FMRIB Software Library, FMRIB, Oxford, United Kingdom) was used to normalize FA images into MNI space and calculate regional diffusion metrics by averaging the values within each region of the ICBM DTI-81 atlas. Mean FA of all available white matter tracts was extracted and fed into SPSS for further data analysis.

[1]www.fil.ion.ucl.ac.uk/spm

[2]http://www.nitrc.org/projects/panda/

Statistical Analysis

GMV

The 2-sample *t*-tests and chi-square test were used to compare the demographic data. Global brain volume was extracted and compared between groups. Then, voxel-wise comparisons of GMV were performed between groups using 2-sample *t*-tests with age, gender and global brain volume as covariates. To control for multiple comparisons, all *t*-values comparing voxel-wise data were evaluated for significance using a threshold of $p < 0.05$ with false discovery rate (FDR) correction for multiple comparison.

FA

Independent sample *t*-tests was performed to compare the mean FA of all the 48 fibers within the brain between the two groups (thresholded as $p < 0.05$ after FDR correction) using age and gender as covariates (Mori and van Zijl, 1995; Bick et al., 2015b).

Then, GMV or FA in each region or fiber with significant differences between LBC and non-LBC was extracted for each subject. Correlation was performed between duration of each LBC's separation from parents and brain structure.

RESULTS

Demographic Data

Sixty-eight subjects were included in the statistical analyses for the study, including 38 subjects in the LBC group (21 boys, mean age = 9.60 ± 1.8 years, age range: 7–13 years; mean separation time = 7.00 ± 2.17 years, range: 2–11 years; mean age of separation = 22.53 ± 28.32 months, range: 1–84 months) and 30 subjects in the non-LBC group (19 boys, mean age = 10.00 ± 1.95 years, age range: 7–14 years). All subjects were right-handed. Demographic data, such as age, gender, IQ, weight, height, academic scores, special interests (such as singing, dancing as well as football), birth weight, delivery method, and annual family income did not differ between the two groups ($p > 0.05$; **Table 1**) except for the educational levels of the primary care givers, which was significantly lower in LBC relative to the non-LBC group ($p < 0.05$). Besides, only three LBC showed mild anxiety (HAMA score range 1∼3), no LBC presented depression symptom (see **Table 1**).

Altered GMV in LBC

There was no difference of global brain volume between the two groups ($p = 0.30$). Compared to non-LBC, LBC showed significantly greater GMV in the bilateral fusiform gyri, bilateral parahippocampal gyri, right superior parietal lobe, right thalamus, right superior occipital gyrus, left cuneus, right superior temporal gyrus, right medial prefrontal cortex, left postcentral gyrus, left middle occipital gyrus and left putamen (**Figure 1** and **Table 2**, with Cohen's $d > 0.89$). The clusters in parahippocampi were contiguous with those in the amygdala.

TABLE 1 | Demographic characteristics of left-behind children (LBC) and parentally reared children (non-LBC).

	Group				
	LBC		Non-LBC		
Characteristic	**Mean**	***SD***	**Mean**	**SD**	***p***
Age (years)	9.60	1.80	10.00	1.95	0.40
IQ-verbal	89.63	12.86	93.67	15.74	0.25
IQ-performance	97.39	13.14	99.00	14.53	0.64
IQ-full scale	92.76	13.05	95.67	14.70	0.39
Birth weight (Kg)	3.37	0.47	3.41	0.46	0.78
Height (cm)	140.34	12.18	139.53	12.80	0.79
Weight (kg)	35.85	9.88	35.62	12.51	0.93
Family income (10000 yuan/year)	16.50	9.96	15.33	9.09	0.62
Education of primary care givers (years)	4.26	2.45	7.92	3.26	0.01
Separation time (years)	7.00	2.17			
Age at parental departure (months)	22.53	28.32			
Reunion time (days/year)	26.7	16.4			
Communication time (minutes/week)	24.3	25.4			
HAMA	0.3 (range 0∼3)	0.8	–	–	
HAMD	0	0	–	–	
	N	**%**	***N***	**%**	***p***
Gender					
Girl	17	44.7	11	36.7	0.50
Boy	21	55.3	19	63.3	0.50
Delivery					
Labor	35	92.10	23	76.70	0.15
Cesarean	3	7.90	7	23.30	0.15
Special interest					
Singing/dancing	20	52.60	16	53.30	0.95
Football/Soccer	18	47.40	14	46.70	0.95

LBC, left-behind children; IQ, intelligence quotient; SD, standard deviation.

Altered FA in LBC

We used atlas-based ROI analysis to compare the mean FA values of all 48 fiber tracts between the LBC and the non-LBC groups. When controlling for age and gender as covariates, mean FA was increased in the left and right superior occipitofrontal fasciculi and decreased in right medial lemniscus in the LBC group (**Figure 2** and **Supplementary Table 1**).

Relationship of Rearing Environment With Brain Structure Measures

No significant correlation was observed between the guardian's educational level and family income and alterations of GMV in LBC.

Relationships of Time of Reunions, Time for Telephone Communication, and Length of Separation From Parents and the Brain Structure

Some LBC children had never even met their parents as they grew up. Other children had reunions (26.7 ± 16.4 days/year; max 60 days/year). They communicated with their parents abroad via telephone or internet audiovisual software (mean time = 24.3 ± 25.4 min/week; ranges = 0–70 min/week). No significant correlations between these parental contact parameters and GMV or FA were seen in LBC. To examine effects of early separation, comparison (using age and gender as covariates) of LBC subjects with parental separation before (25 cases) and after (13 cases) 1 year of age was conducted. There was no difference in GMV or FA between these subgroups of LBC ($p > 0.05$). Children separated from parents before (29 cases) and after (9 cases) 2 years of age also did not show difference ($p > 0.05$).

DISCUSSION

In this study, LBC demonstrated significantly greater GMV in limbic-paralimbic and other brain regions involved in emotion regulation and processing including parahippocampal gyri, amygdala, and medial prefrontal cortex (Cardinal et al., 2002; Lui et al., 2013). These processing have been reported to be disregulated in LBC (Liu et al., 2009; Fan et al., 2010; Wang

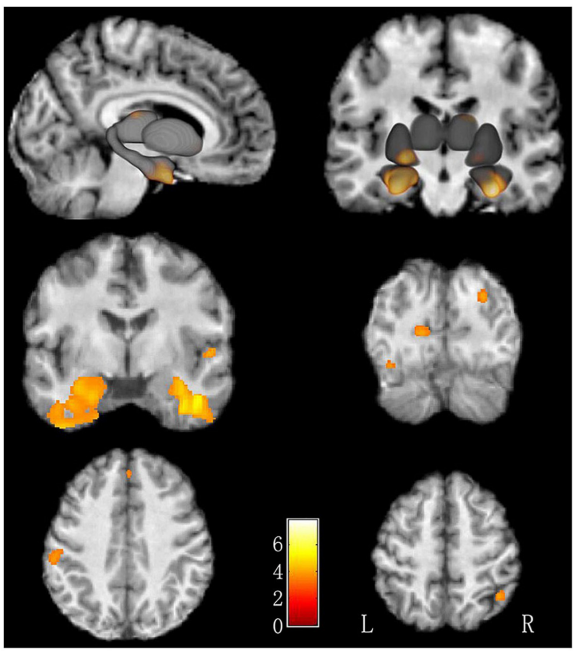

FIGURE 1 | Increased GMV in LBC relative to non-LBC. Increased gray matter volume was observed in the following regions (labeled in red-yellow): bilateral fusiform gyri, bilateral parahippocampal gyri, right superior parietal lobe, right thalamus, right superior occipital gyrus, left cuneus, right superior temporal gyrus, right medial prefrontal gyrus, left postcentral gyrus, left middle occipital gyrus, and left putamen in LBC relative to non-LBC.

et al., 2015). Other regions with group differences belong to cortico-striato-thalamo-cortical circuits, which are crucial for cognition (Metzger et al., 2013). Analysis of white matter tracts revealed mean FA value in the bilateral superior occipitofrontal fasciculi in LBC was increased when compared with non-LBC, but decreased in the right medial lemniscus. Thus, our findings provide empirical evidence in supporting of the hypothesis that direct biological parental rearing, relative to rearing by grandparents may affect brain development of children. Furthermore, these brain changes involving emotion circuit may represent antecedent alterations in brain development that contribute to the increased risk for psychiatric disorders in later life seen in LBC (McLaughlin et al., 2014). We also found no correlation between the time of reunion, time for telephone communication, or duration of separation from parents with GMV and FA, and no significant difference in GMV and FA between the subgroups of LBC with a parental departure before or after 1 or 2 years of age.

The previous studies found that the developmental trajectory of the normal brain GMV was inverted U-shaped trajectories, and the developmental curves for the frontal and parietal lobe peaking were at about age 12 and for the temporal lobe at about age 16 (Giedd et al., 1999; Gogtay et al., 2004). However, all subjects in our study were under the 12 years old, the "hyper-structural" pattern of GMV in LBC was interpreted to be "over-maturation." The main reason may be that the LBC couldn't gain the comfort and guidance from their parents in the process of self-development and socialization due to the long-term parental separation, it caused them have higher loneliness feeling and social anxiety, increased life stress (Zhao et al., 2014; Mazzucato et al., 2015; Wang et al., 2015). Stress activates the Limbic-Hypothalamic-Pituitary-Adrenal Axis and elevates levels of cortisol. Cortisol regulates the stress response system both in the hippocampus and medial prefrontal cortex, where it attenuates the stress response, and in the amygdala, where it promotes that response (Bellis and Zisk, 2014). Of note, larger amygdala volumes seen in our study have also been reported in orphans (Tottenham et al., 2010). Second, greater GMV in sensory, limbic-paralimbic and emotional-regulatory systems may result from increased dendritic branching, dendritic length and spine density (Muhammad and Kolb, 2011) or from neurogenesis (Kaplan, 2001). Such effects have been reported in studies of mammals and humans exposed to early-life maternal separation (Kaplan, 2001; Muhammad and Kolb, 2011).

In contrast to the results seen in the present study, previous study of children reared in public institutions showed reductions in cortical thickness and smaller the total GMV, decreased FA of superior occipitofrontal fasciculus (Mehta et al., 2009; McLaughlin et al., 2014; Bick et al., 2015b; Yang et al., 2015), and prolonged the length of time children experience orphanage rearing was associated with larger amygdala volume and reduced microstructural integrity of the body of the corpus callosum and tracts involved in limbic circuitry, and sensory processing (Tottenham et al., 2010; Bick et al., 2015b). Several possible reasons may explain these different observations. First, the living environment of children reared in institutions in some prior studies of orphans was quite extreme compared to those of LBC. The LBC are mostly taken care of by their grandparents and have relatively intact care giving support. What a more, in a typical Chinese culture, grandparents who are seeing their grandchildren as "only family treasure" express their love via indulge their grandchildren such as providing better physiological demands and protecting them from taking parts in household chores (Kelley et al., 2011; Williams, 2011). However, many of those institutionalized children grew up in a stunningly unstimulating and unresponsive environment (Marshall, 2014), which has been believed to cause dysmaturational effects resulting in regional reduction of gray matter (Mehta et al., 2009). In comparison to the institutionalized children, LBC typically lived in a more "open" and socially stimulating environment. Second, while the possibility that more modest socioemotional deprivation may lead to the opposite pattern of brain changes than is seen in more severe deprivation is most interesting.

The prior studies showed that decreased FA of superior occipitofrontal fasciculus was associated with spatial neglect in humans (Karnath et al., 2009; Yang et al., 2015). While the higher FA of superior occipitofrontal fasciculus seen in LBC may reflect increased myelination and neuronal remodeling (Beaulieu, 2002; Li et al., 2011) at a more molecular level, it is possible that a hyperattentiveness to the visual environment related to feelings of separation and concern about available social supports might be one factor leading to the overdevelopment of this tract. Though we did not test spatial abilities in this study, the evidence from prior rodent study has shown that spatial

TABLE 2 | Voxel-based analysis of gray matter volume (GMV) in LBC relative to non-LBC study participants.

	Cluster	Peak	*P*-value	Cohen's	Talairach coordinates
Cluster	**Size**	***t*-Value**	**(FDR-cor)**	***d***	**x, y, z (mm)**
Fusiform_R	848	5.26	0.015	1.29	45, −5, −30
Parahippocampus_R	575	4.95	0.015	1.22	23, −36, −9
Parahippocampus_L	872	4.86	0.015	1.20	−20, −42, −12
Parietal_Sup_R	137	4.58	0.015	1.13	42, −52, 57
Fusiform_L	601	4.33	0.015	1.07	−47, −57, −20
Thalamus_R	78	4.00	0.015	0.98	18, −22, 16
Occipital_Sup_R	57	4.00	0.015	0.98	26, −81, 27
Cuneus_L	88	3.94	0.015	0.97	−15, −81, 4
Temporal_Sup_R	56	3.86	0.016	0.95	54, −4, −0
Prefrontal_medial_R	107	3.86	0.016	0.95	2, 39, 42
Postcentral gyrus_L	121	3.77	0.016	0.93	−56, −28, 37
Middle occipital Gyrus_L	62	3.75	0.016	0.92	−35, −79, −17
Putamen_L	51	3.63	0.018	0.89	−21, 18, −8

GMV, gray matter volume; L, left; R, right; Sup, superior; FDR-cor, corrected for multiple comparisons with false discovery rate.

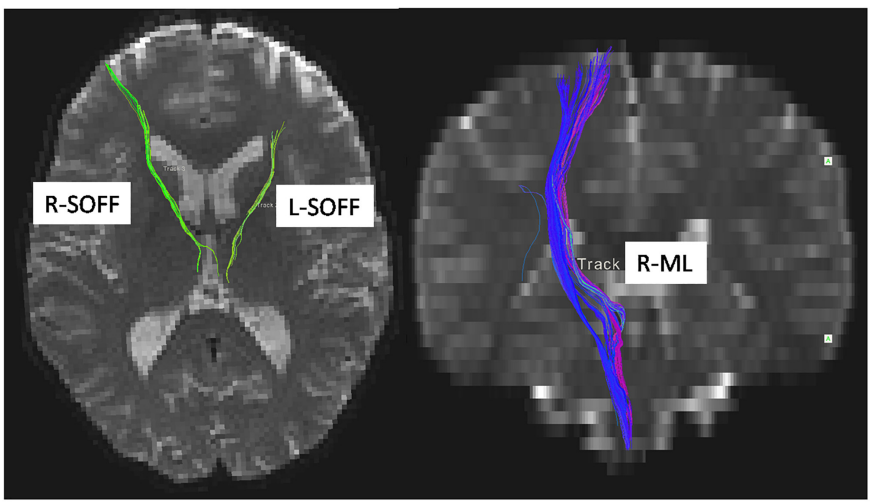

FIGURE 2 | Difference of white matter microstructure between LBC and non-LBC. Tracts with significantly increased mean fractional anisotropy (FA) in the left and right superior occipitofrontal fasciculi (labeled by green color) and decreased FA in right medial lemniscus (labeled by blue color) in LBC relative to parentally raised children. Age and gender were used as covariates. L, left; R, right; ML, medial lemniscus; SOFF, superior occipitofrontal fasciculus.

learning was improved after early life maternal deprivation (Loi et al., 2014). The current study also demonstrated decreased FA in the medial lemniscus in LBC. This is consistent with findings in institutionalized children (Bick et al., 2015a) as well as children neglected in early life (Hanson et al., 2013), which might result from insufficient sensory input experienced at critical points in neural development owing to reduction in maternal touch and other sensory stimulation. Previous studies pointed that, maternal touch had a positive relationship with the brain development, especially in the social brain (McGlone et al., 2014; Brauer et al., 2016), of which the medial lemniscus is a crucially relevant afferent pathway. Thus, the reduced integrity of the medial lemniscus in LBC observed here provides further evidence to support the role of parental care in brain development of brain, especially systems relevant for social and emotional processing.

The present study showed that no LBC suffered from obviously anxious or depression symptom, which suggests that the brain structural alteration may precede the occurrence of clinical symptom. The finding is consistent with a prior study (Luby et al., 2013). However, because of the limited sample size of the present study, more researches with a large sample size are needed. Additionally, longitudinal design is needed to explore such dynamic changes of brain development in LBC. While findings from our cross-sectional study are promising, it is possible that genetics or other factors in parents who decides to leave families for distant opportunities might be associated themselves with varying patterns of brain development. Longitudinal studies would contribute to resolving this possibility as well. Longitudinal studies might also clarify the reversibility of brain changes, as would studies

examining children after social enhancement programs were made available to LBC. Second, more extensive evaluation of behavioral, emotional, cognitive, and social development in future studies is needed to clarify the neurobehavioral significance of neuroanatomic changes seen in LBC. Nonetheless, while many questions remain to be answered, findings from our cross-sectional study of neuroanatomic differences in LBC relative to parentally raised children raised a concern that brain maturation may be altered less severe deprivation conditions than have been previously studied, and therefore in the many millions of children left by parents in the developing world to pursue better work opportunities.

CONCLUSION

Despite the limitations of this work, our study provides empirical evidence of altered cerebral structure in LBC, suggesting that absence of direct biological parental care may have a negative impact on children's brain development. From a public health perspective, our MRI study highlights the potential importance of limited parental rearing in LBC, which is known to have adverse cognitive and psychiatric sequelae. Thus, programs providing more emotional care and stimulation are needed for LBC in developing countries to reduce potential adverse long-term consequences on the individual children and for overall population health.

ETHICS STATEMENT

The study was approved by the research ethics committee of Second Affiliated Hospital and Yuying Children's Hospital of Wenzhou Medical University, and written consent was obtained from guardians and assent from children before study participation.

AUTHOR CONTRIBUTIONS

SL and ZY conceived the study and designed the protocol. YF, YX, LY, ZY, MD, SL, and CM did the experiments. YF, YX, GF, LY, and XL conducted the statistical analyses. JS, ZY, and SL interpreted the study findings and contributed to developing the manuscript. YF, YX, GF, and LY wrote the first draft of the manuscript that was revised by all authors.

FUNDING

This study was supported by the National Natural Science Foundation of China (Grant Nos. 81371527, 81671664, and 81621003), Zhejiang Provincial Natural Science Foundation (No. LY19H180003), Zhejiang Medical Health Science and Technology Program (Nos. 2017KY108 and 2017ZD024), Sichuan University Postdoctoral Interdisciplinary Fund (No. 55, 2018), and Postdoctoral Research Project, West China Hospital, Sichuan University. SL would like to acknowledge the support from Chang Jiang Scholars (Award No. Q2015154) of China and the National Program for Support of Top-notch Young Professionals (National Program for Special Support of Eminent Professionals, Organization Department of the Communist Party of China Central Committee, Award No. W02070140).

ACKNOWLEDGMENTS

We thank all members of the Wenzhou Overseas Chinese Federation, especially Xudong Xu, for their assistance with recruitment. We also thank Miss Anna Guo of the Department of Radiology, Second Affiliated Hospital & Yuying Children's Hospital of Wenzhou Medical University for her important advice during the revison.

SUPPLEMENTARY MATERIAL

The Supplementary Material for this article can be found online at: https://www.frontiersin.org/articles/10.3389/fncir.2019.00033/full#supplementary-material

REFERENCES

All-China Women's Federation (2013). *China Women's Federation. National Survey of Left-Behind Children in Rural areas and Migrant Children in Urban and Rural Areas*. Available at: http://acwf.people.com.cn/n/2013/0510/c99013-21437965.html (accessed on June 5, 2013).

Ashburner, J., and Friston, K. J. (2000). Voxel-based morphometry–the methods. *Neuroimage* 11, 805–821. doi: 10.1006/nimg.2000.0582

Beaulieu, C. (2002). The basis of anisotropic water diffusion in the nervous system - a technical review. *NMR Biomed.* 15, 435–455. doi: 10.1002/nbm.782

Bellis, M. D. D., and Zisk, A. (2014). The biological effects of childhood trauma. *Child Adolesc. Psychiatr. Clin. N. Am.* 23, 185–222. doi: 10.1016/j.chc.2014.01.002

Bick, J., Fox, N., Zeanah, C., and Nelson, C. A. (2015a). Early deprivation, atypical brain development, and internalizing symptoms in late childhood. *Neuroscience* 342, 845–853. doi: 10.1016/j.neuroscience.2015.09.026

Bick, J., Zhu, T., Stamoulis, C., Fox, N. A., Zeanah, C., and Nelson, C. A. (2015b). Effect of early institutionalization and foster care on long-term white matter development: a randomized clinical trial. *JAMA Pediatr.* 169, 211–219. doi: 10.1001/jamapediatrics.2014.3212

Brauer, J., Xiao, Y., Poulain, T., Friederici, A. D., and Schirmer, A. (2016). Frequency of maternal touch predicts resting activity and connectivity of the developing social brain. *Cereb. Cortex* 26, 3544–3552. doi: 10.1093/cercor/bhw137

Cardinal, R. N., Parkinson, J. A., Hall, J., and Everitt, B. J. (2002). Emotion and motivation: the role of the amygdala, ventral striatum, and prefrontal cortex. *Neurosci. Biobehav. Rev.* 26, 321–352. doi: 10.1016/S0149-7634(02)00007-6

Chen, L., Lui, S., Wu, Q. Z., Zhang, W., Zhou, D., Chen, H. F., et al. (2013). Impact of acute stress on human brain microstructure: an MR diffusion study of earthquake survivors. *Hum. Brain Mapp.* 34, 367–373. doi: 10.1002/hbm.21438

Cheng, J., and Sun, Y. H. (2015). Depression and anxiety among left-behind children in china: a systematic review.

Child Care Health Dev. 41, 515–523. doi: 10.1111/cch.12221

Fan, F., Su, L. F., Gill, M. K., and Birmaher, B. (2010). Emotional and behavioral problems of Chinese left-behind children: a preliminary study. *Soc. Psychiatry Psychiatr. Epidemiol.* 45, 655–664. doi: 10.1007/s00127-009-0107-4

Gee, D. G., Gabard-Durnam, L. J., Flannery, J., Goff, B., Humphreys, K. L., Telzer, E. H., et al. (2013). Early developmental emergence of human amygdala-prefrontal connectivity after maternal deprivation. *Proc. Natl. Acad. Sci. U.S.A.* 110, 15638–15643. doi: 10.1073/pnas.1307893110

Giedd, J. N., Blumenthal, J., Jeffries, N. O., Castellanos, F. X., and Rapoport, J. L. (1999). Brain development during childhood and adolescence: a longitudinal mri study. *Nat. Neurosci.* 2, 861–863. doi: 10.1038/13158

Gogtay, N., Giedd, J. N., Lusk, L., Hayashi, K. M., Greenstein, D., Vaituzis, A. C., et al. (2004). Dynamic mapping of human cortical development during childhood through early adulthood. *PNAS* 101, 8174–8179. doi: 10.1073/pnas.0402680101

Gong, Y., and Cai, T. (1993). *Manual of Chinese Revised Wechsler intelligence scale for children*. Changsha: Hunan Atlas Publishing House.

Good, C. D., Johnsrude, I. S., Ashburner, J., Henson, R., Friston, K. J., and Frackowiak, R. S. (2001). A voxel-based morphometric study of ageing in 465 normal adult human brains. *Neuroimage* 14, 21–36. doi: 10.1109/SSBI.2002.1233974

Hamilton, M. (1931). *Hamilton Depression Scale*. Zurich: Psychiatric University Hospital Zurich.

Hanson, J. L., Adluru, N., Chung, M. K., Alexander, A. L., Davidson, R. J., and Pollak, S. D. (2013). Early neglect is associated with alterations in white matter integrity and cognitive functioning. *Child Dev.* 84, 1566–1578. doi: 10.1111/cdev.12069

Heim, C., Shugart, M., Craighead, W. E., and Nemeroff, C. B. (2010). Neurobiological and psychiatric consequences of child abuse and neglect. *Dev. Psychobiol.* 52, 671–690. doi: 10.1002/dev.20494

Jingzhong, Y., and Lu, P. (2011). Differentiated childhoods: impacts of rural labor migration on left-behind children in China. *J. Peasant Stud.* 38, 355–377. doi: 10.1080/03066150.2011.559012

Kaplan, M. S. (2001). Environment complexity stimulates visual cortex neurogenesis: death of a dogma and a research career. *Trends Neurosci.* 24, 617–620. doi: 10.1016/S0166-2236(00)01967-6

Karnath, H. O., Rorden, C., and Ticini, L. F. (2009). Damage to white matter fiber tracts in acute spatial neglect. *Cereb. Cortex* 19, 2331–2337. doi: 10.1093/cercor/bhn250

Kelley, S. J., Whitley, D. M., and Campos, P. E. (2011). Behavior problems in children raised by grandmothers: the role of caregiver distress, family resources, and the home environment. *Child Youth Serv. Rev.* 33, 2138–2145. doi: 10.1016/j.childyouth.2011.06.021

Li, F., Huang, X., Yang, Y., Li, B., Wu, Q., Zhang, T., et al. (2011). Microstructural brain abnormalities in patients with obsessive-compulsive disorder: diffusion-tensor MR imaging study at 3.0 T. *Radiology* 260, 216–223. doi: 10.1148/radiol.11101971

Li, Q., Liu, G., and Zang, W. (2015). The health of left-behind children in rural China. *China Econ. Rev.* 36, 367–376. doi: 10.1016/j.chieco.2015.04.004

Liu, Z., Li, X., and Ge, X. (2009). Left too early: the effects of age at separation from parents on Chinese rural children's symptoms of anxiety and depression. *Am. J. Public Health* 99, 2049–2054. doi: 10.2105/AJPH.2008.150474

Loi, M., Koricka, S., Lucassen, P. J., and Joels, M. (2014). Age- and sex-dependent effects of early life stress on hippocampal neurogenesis. *Front. Endocrinol.* 5:13. doi: 10.3389/fendo.2014.00013

Luby, J., Belden, A., Botteron, K., Marrus, N., Harms, M. P., Babb, C., et al. (2013). The effects of poverty on childhood brain development: the mediating effect of caregiving and stressful life events. *JAMA Pediatr.* 167, 1135–1142. doi: 10.1001/jamapediatrics.2013.3139

Lui, S., Chen, L., Yao, L., Xiao, Y., Wu, Q. Z., Zhang, J. R., et al. (2013). Brain structural plasticity in survivors of a major earthquake. *J. Psychiatry Neurosci.* 38, 381–387. doi: 10.1503/jpn.120244

Lui, S., Zhou, X. J., Sweeney, J. A., and Gong, Q. (2016). Psychoradiology: the frontier of neuroimaging in psychiatry. *Radiology* 281, 357–372. doi: 10.1148/radiol.2016152149

Maier, W., Buller, R., Philipp, M., and Heuser, I. (1988). The Hamilton anxiety scale: reliability, validity and sensitivity to change in anxiety and depressive disorders. *J. Affect. Disord.* 14, 61–68. doi: 10.1016/0165-0327(88)90072-9

Marshall, E. (2014). An experiment in zero parenting. *Science* 345, 752–754. doi: 10.1126/science.345.6198.752

Mazzucato, V., Cebotari, V., Veale, A., White, A., Grassi, M., and Vivet, J. (2015). International parental migration and the psychological well-being of children in Ghana, Nigeria, and Angola. *Soc. Sci. Med.* 132, 215–224. doi: 10.1016/j.socscimed.2014.10.058

McGlone, F., Wessberg, J., and Olausson, H. (2014). Discriminative and affective touch: sensing and feeling. *Neuron* 82, 737–755. doi: 10.1016/j.neuron.2014.05.001

McLaughlin, K. A., Sheridan, M. A., Winter, W., Fox, N. A., Zeanah, C. H., and Nelson, C. A. (2014). Widespread reductions in cortical thickness following severe early-life deprivation: a neurodevelopmental pathway to attention-deficit/hyperactivity disorder. *Biol. Psychiatry* 76, 629–638. doi: 10.1016/j.biopsych.2013.08.016

Mehta, M. A., Golembo, N. I., Nosarti, C., Colvert, E., Mota, A., Williams, S. C. R., et al. (2009). Amygdala, hippocampal and corpus callosum size following severe early institutional deprivation: the english and romanian adoptees study pilot. *J. Child Psychol. Psychiatry* 50, 943–951. doi: 10.1111/j.1469-7610.2009.02084.x

Metzger, C. D., Vand, W. Y. D., and Walter, M. (2013). Functional mapping of thalamic nuclei and their integration into cortico-striatal-thalamo-cortical loops via ultra-high resolution imaging—from animal anatomy to in vivo imaging in humans. *Front. Neurosci.* 7:24. doi: 10.3389/fnins.2013.00024

Mori, S., and van, Zijl PC (1995). Diffusion weighting by the trace of the diffusion tensor within a single scan. *Magn. Reson. Med.* 33, 41–52. doi: 10.1002/mrm.1910330107

Muhammad, A., and Kolb, B. (2011). Maternal separation altered behavior and neuronal spine density without influencing amphetamine sensitization. *Behav. Brain Res.* 223, 7–16. doi: 10.1016/j.bbr.2011.04.015

Scholz, J., Klein, M. C., Behrens, T. E., and Johansen-Berg, H. (2009). Training induces changes in white-matter architecture. *Nat. Neurosci.* 12, 1370–1371. doi: 10.1038/nn.2412

Tottenham, N., Hare, T. A., Quinn, B. T., McCarry, T. W., Nurse, M., Gilhooly, T., et al. (2010). Prolonged institutional rearing is associated with atypically large amygdala volume and difficulties in emotion regulation. *Dev. Sci.* 13, 46–61. doi: 10.1111/j.1467-7687.2009.00852.x

United Nations (2009). *International Migration*. New York, NY: United Nations.

Wang, D., Yang, S., Jiang, C., and Michael, P. (2009). *Structured Clinical Interview for DSM-IV-TR Axis I Disorders, Research Version, Chinese Revision*. Beijing: Beijing Suicide Research and Prevention Center.

Wang, X., Ling, L., Su, H., Cheng, J., Jin, L., and Sun, Y. H. (2015). Self-concept of left-behind children in China: a systematic review of the literature. *Child Care Health Dev.* 41, 346–355. doi: 10.1111/cch.12172

Whitwell, J. L. (2009). Voxel-based morphometry: an automated technique for assessing structural changes in the brain. *J. Neurosci.* 29, 9661–9664. doi: 10.1523/jneurosci.2160-09.2009

Wilke, M., Holland, S. K., Altaye, M., and Gaser, C. (2008). Template-O-Matic: a toolbox for creating customized pediatric templates. *Neuroimage* 41, 903–913. doi: 10.1016/j.neuroimage.2008.02.056

Williams, M. N. (2011). The changing roles of grandparents raising grandchildren. *J. Hum. Behav. Soc. Environ.* 21, 948–962. doi: 10.1080/10911359.2011.588535

Yang, W., Liu, T. T., Song, X. B., Zhang, Y., Li, Z. H., Cui, Z. H., et al. (2015). Comparison of different stimulation parameters of repetitive transcranial magnetic stimulation for unilateral spatial neglect in stroke patients. *J. Neurol. Sci.* 359, 219–225. doi: 10.1016/j.jns.2015.08.1541

Zhao, X., Chen, J., Chen, M. C., Lv, X. L., Jiang, Y. H., and Sun, Y. H. (2014). Left-behind children in rural China experience higher levels of anxiety and poorer living conditions. *Acta Paediatri.* 103, 665–670. doi: 10.1111/apa.12602

Conflict of Interest Statement: The authors declare that the research was conducted in the absence of any commercial or financial relationships that could be construed as a potential conflict of interest.

frontiers in Neural Circuits

ORIGINAL RESEARCH
published: 15 May 2019
doi: 10.3389/fncir.2019.00036

Temporal Variability of Cortical Gyral-Sulcal Resting State Functional Activity Correlates With Fluid Intelligence

*Shimin Yang[1], Zhongbo Zhao[1], Han Cui[1], Tuo Zhang[2], Lin Zhao[2], Zhibin He[2], Huan Liu[2], Lei Guo[2], Tianming Liu[3], Benjamin Becker[1], Keith M. Kendrick[1] and Xi Jiang[1]**

[1] The Clinical Hospital of Chengdu Brain Science Institute, MOE Key Lab for Neuroinformation, School of Life Science and Technology, University of Electronic Science and Technology of China, Chengdu, China, [2] School of Automation, Northwestern Polytechnical University, Xi'an, China, [3] Department of Computer Science, Bioimaging Research Center, The University of Georgia, Athens, GA, United States

The human cerebral cortex is highly convoluted as convex gyri and concave sulci. In the past decades, extensive studies have consistently revealed substantial differences between gyri and sulci in terms of genetics, anatomy, morphology, axonal fiber connections, and function. Although interesting findings have been reported to date to elucidate the functional difference between gyri and sulci, the temporal variability of functional activity, which could explain individual differences in learning and higher-order cognitive functions, and as well as differences in gyri and sulci, remains to be explored. The present study explored the temporal variability of cortical gyral-sulcal resting state functional activity and its association with fluid intelligence measures on the Human Connectome Project dataset. We found that the temporal variance of resting state fMRI BOLD signal was significantly larger in gyri than in sulci. We also found that the temporal variability of certain regions including middle frontal cortex, inferior parietal lobe and visual cortex was positively associated with fluid intelligence. Moreover, those regions were predominately located in gyri rather than in sulci. This study reports initial evidence for temporal variability difference of functional activity between gyri and sulci, and its association with fluid intelligence measures, and thus provides novel insights to understand the mechanism and functional relevance of gyri and sulci.

Keywords: functional activity, temporal variability, cortical folding, gyri and sulci, resting state fMRI, fluid intelligence

OPEN ACCESS

Edited by:
Nicoletta Berardi,
Italian National Research Council (CNR), Italy

Reviewed by:
Jingxin Nie,
South China Normal University, China
Gang Li,
The University of North Carolina at Chapel Hill, United States

****Correspondence:***
Xi Jiang
xijiang@uestc.edu.cn;
superjx2318@gmail.com

Received: *17 November 2018*
Accepted: *02 May 2019*
Published: *15 May 2019*

Citation:
Yang S, Zhao Z, Cui H, Zhang T, Zhao L, He Z, Liu H, Guo L, Liu T, Becker B, Kendrick KM and Jiang X (2019) Temporal Variability of Cortical Gyral-Sulcal Resting State Functional Activity Correlates With Fluid Intelligence. Front. Neural Circuits 13:36. doi: 10.3389/fncir.2019.00036

INTRODUCTION

One of the most prominent organization principles of the human cerebral cortex lies in its highly convoluted folding patterns which are composed of convex gyri and concave sulci (Barron, 1950; Rakic, 1988; Zilles et al., 1988; Welker, 1990). The past decades have witnessed a variety of hypotheses regarding the complex gyrification process, including cortex area increase and compact wiring (Zilles et al., 2013), genetic regulation (Rakic, 2004), differential laminar growth (Richman et al., 1975), and axonal fiber tension (Van Essen, 1997). Although the precise mechanisms of gyrification process are still under debate, a growing number of studies suggests substantial

differences between gyri and sulci in terms of genetics (Stahl et al., 2013; Zeng et al., 2015), anatomy (Fischl and Dale, 2000; Li et al., 2015), morphology (Magnotta et al., 1999; Hilgetag and Barbas, 2005), and axonal fiber connections (Van Essen, 1997; Nie et al., 2012; Takahashi et al., 2012; Chen et al., 2013; Deng et al., 2014; Zhang et al., 2014; Li et al., 2015; Ge et al., 2018). For instance, cortical thickness is significantly larger in gyri than in sulci in both human developing infant (Li et al., 2015) and adult brains (Fischl and Dale, 2000). The axonal connectivity and gene expression patterns are significantly different between cerebellum gyri and sulci of rodent brains (Zeng et al., 2015). The diffusion weighted imaging derived axonal fibers concentrate significantly more on gyri than on sulci, which is developmentally and evolutionarily consistent across human fetus, human adult, chimpanzee, and macaque brains (Nie et al., 2012; Takahashi et al., 2012), and was supported by histology and dissection studies (Xu et al., 2010; Budde and Annese, 2013). The diffusion weighted imaging derived axonal fiber connection strength is strong between gyral–gyral regions, weak between sulcal–sulcal regions, and moderate between gyral-sulcal regions (Deng et al., 2014). Moreover, previous studies have reported that the morphological feature of gyri and sulci changes during aging (Magnotta et al., 1999) and development-related psychiatric disorders such as schizophrenia (White et al., 2003), reflecting a potential of gyral-sulcal indices as a biomarker for developmental and aging related disorders.

Given the close relationship between brain structure and function (Passingham et al., 2002; Zhang et al., 2011) and with the development of advanced *in vivo* functional neuroimaging such as functional MRI (fMRI) (Biswal et al., 1995; Logothetis, 2008; Friston, 2009), the functional characteristics of gyri and sulci has gained increasing interests in recent years (Deng et al., 2014; Jiang et al., 2015, 2018a,b; Liu et al., 2017, 2018; Zhang et al., 2018). A multi-modal diffusion tensor imaging (DTI) and fMRI study has reported that both structural fiber connectivity and functional connectivity are strong between gyral–gyral regions, weak between sulcal–sulcal regions, and moderate between gyral-sulcal regions in the whole-brain, suggesting that gyri represent a global functional hub and sulci a local function processing unit (Deng et al., 2014). The heterogeneous functional regions which are activated during multiple task conditions locate significantly more in gyri than in sulci under both temporal stationary (Jiang et al., 2015) and dynamics (Jiang et al., 2018a). The graph-theoretic characteristics of functional interaction (Liu et al., 2017) and functional signal reconstruction accuracy (Jiang et al., 2018b) are also different between gyri and sulci. In addition, recent studies using advanced deep learning methodologies have reported the frequency-specific pattern differences between gyri and sulci (Liu et al., 2018; Zhang et al., 2018).

In spite of these aforementioned interesting findings, the temporal variability of functional activity of gyri and sulci still remains to be explored. Instead of characterizing the static functional activity by simply averaging the fMRI blood-oxygen level-dependent (BOLD) signal, a growing number of recent studies have shown the temporal-varying dynamics of spontaneous neural activity within a single brain region as well as the functional connectivity/interaction between brain regions during both rest and task conditions (Gilbert and Sigman, 2007; Chang and Glover, 2010; Garrett et al., 2010; Protzner et al., 2010; Bassett et al., 2011, 2013, 2015; Smith et al., 2011; Calhoun et al., 2014; Li et al., 2014; Zhang et al., 2016; Vidaurre et al., 2017; Jiang et al., 2018a; Yuan et al., 2018). The temporal variability of functional activity reflected in neuroimaging fMRI signal could be related to the brain learning skill (Bassett et al., 2011, 2013, 2015; Zhang et al., 2016) and human intelligence (Saxe et al., 2018). Especially, fluid intelligence, as a measure of higher-order relational reasoning (Burgess et al., 2011), has been argued to be linked to specific functional outcomes and to variations in human neuronal structure and function (Duncan et al., 2000; Duncan, 2003, 2005). Previous studies have suggested that the higher temporal variability of brain functional activity might be closely linked with higher-order relational reasoning and learning (Bassett et al., 2011, 2013, 2015; Zhang et al., 2016; Saxe et al., 2018). Therefore, investigating the correlation between temporal variability in the resting state fMRI signal and fluid intelligence measures may allow to further determine whether intrinsic temporal variations in brain activity are related to individual variations in fluid intelligence. Taken together, investigating the temporal variability characteristics of functional activity as well as its associations with fluid intelligence on gyri and sulci could provide novel insights to understand the functional relevance of gyri and sulci.

To this end, the present study adopted 68 subjects with both resting state fMRI and fluid intelligence measures data in the publicly released Human Connectome Project (HCP) Q1 release (Barch et al., 2013; Smith et al., 2013) to test the hypothesized associations. We employed a previously evaluated approach to divide the fMRI BOLD signal into non-overlapping time segments in order to assess the temporal variability of functional activity on each gyral/sulcal region by means of calculating the variance of time series correlations among all time segments. To determine the behavioral relevance of the temporal variability we correlated the temporal variance with the available three fluid intelligence measures across subjects. Based on previous study (Duncan et al., 2000) reporting that frontal, parietal, and visual cortex were involved in intelligence-related cognitive tasks, we hypothesized that the temporal variability of functional activity in frontal, parietal, and visual cortex would positively correlate with the fluid intelligence measures. Furthermore, based on previous studies reporting the functional difference between gyri and sulci (Deng et al., 2014; Jiang et al., 2015, 2018a,b; Liu et al., 2017, 2018; Zhang et al., 2018), we hypothesized that the distribution of those brain regions would be different between gyri and sulci.

MATERIALS AND METHODS

Participants, Image Acquisition, and Data Preprocessing

We adopted all 68 subjects in the publicly released Human Connectome Project (HCP) Q1 data (Barch et al., 2013; Smith et al., 2013; Van Essen et al., 2013) to test our

hypotheses. There were 18 males and 50 females ranging from 22 to 35 years old. More demographic information was referred to Van Essen et al. (2013). The resting state fMRI (rsfMRI) BOLD signal was acquired using 3T "multiband" accelerated EPI when subjects were instructed to be relaxed, with eyes fixation on a white cross and not to fall asleep (Smith et al., 2013). The major acquisition parameters of rsfMRI data were as follows: 2 mm × 2 mm × 2 mm spatial resolution, TR = 0.72 s, TE = 33 ms, flip angle = 52°, 90 × 104 matrix, 72 slices, in-plane FOV = 208 mm × 180 mm, 1200 whole-brain volumes (14.4 min). The major preprocessing steps of rsfMRI data included skull removal, motion correction, slice time correction, and spatial smoothing (Smith et al., 2013).

Moreover, we adopted the preprocessed grayordinate rsfMRI data after the minimal preprocessing pipelines (Glasser et al., 2013) provided in the HCP datasets. The minimal preprocessing mainly included spatial artifacts and distortions removal, cortical surface generation, cross-subject registration to standard grayordinate space (Glasser et al., 2013). Specifically, the grayordinate space included both the cortical surface vertices and subcortical voxels of whole-brain gray matter in the MNI standard space. Each of the 60K grayordinate cortical surface vertices was associated with a set of geometric attributes and corresponding rsfMRI time series, and had correspondence across different subjects. Note that the grayordinate data had both high spatial and temporal resolution, thus can reliably differentiate gyri/sulci and map the fMRI signals on gyri/sulci. Therefore, it provided the prerequisite for the present study to investigate the temporal variability of cortical gyral-sulcal functional activity.

The fluid intelligence measures of the 68 subjects were also provided in the HCP dataset (Barch et al., 2013). The Penn Matrix Test was adopted to measure fluid intelligence via non-verbal reasoning using Form A of an abbreviated version of the Raven's Progressive Matrices as detailed in Bilker et al. (2012). Three measures were finally provided for each subject: number of correct responses, median reaction time for correct responses, and total skipped items (items not presented due to maximum errors allowed reached in the test) (Barch et al., 2013).

Cortical Surface Parcellation of Gyri and Sulci

To investigate the potential difference of BOLD signal temporal variability between cortical gyri and sulci, we first performed cortical surface parcellation to classify the cortical vertices into gyri and sulci. The average convexity (i.e., "sulc" map in FreeSurfer) of each cortical vertex, defined as the signed distance of the movement during inflation with the surface normal (Fischl et al., 1999; Destrieux et al., 2010; Fischl, 2012), was adopted to classify gyri and sulci in line with previous studies (Jiang et al., 2015, 2018a,b; Liu et al., 2018; Zhang et al., 2018). A single vertex with higher average convexity value would be more likely to be classified as gyri and vice versa, resulting in the highest convexity values in the crown of gyri and lowest values in the fundi of sulci. Moreover, there were transitional or intermixed areas between gyri crown and sulci fundi. To avoid any ambiguity and to ensure the accuracy of gyri/sulci parcellation, we set a threshold value q for the convexity values of all cortical vertices in line with previous studies (Liu et al., 2018; Zhang et al., 2018). The q% vertices with highest convexity values would be classified as gyri, and the q% vertices with lowest convexity values would be classified as sulci. The remaining (100-2q)% transitional vertices between gyri and sulci would be classified as "undefined" (which means not defined as gyri or sulci). As a consequence, the cortical surface was parcellated into three parts: gyri, sulci, and undefined (**Figure 1**). We tested different threshold values q ranging from 10 to 30 as shown in **Figures 1A,B** shows the parcellated cortical surface from different views when q = 30. The rsfMRI BOLD signal was then extracted for each vertex on gyri/sulci/undefined region. It is noted that our following temporal variability analyses were applied to the spectrum of qs.

Temporal Variability Assessment of Functional Activity on Cortical Gyri and Sulci

To assess the temporal variability of functional activity on cortical gyri and sulci, we divided the rsfMRI BOLD signal into non-overlapping windows in line with previous study (Zhang et al., 2016). The overlapping windows would introduce the common signal segments for two consecutive windows and could bias the correlation value of BOLD activity of the two consecutive windows. The detailed framework is presented in **Figure 2**. For a BOLD signal of gyri, sulci, or undefined region (**Figure 2A**), it was divided into n non-overlapping windows with size l (**Figure 2B**). We tested different window size l ranging from 25 to 200 to avoid arbitrary choice of window size. Within the time window i, the BOLD signal segment was annotated as S_i^G, S_i^S, and S_i^U for gyral, sulcal, and undefined vertex, respectively (**Figure 2B**). For any pair of signal segments in time window i and j ($i, j = 1, 2, 3, \ldots, n, i \neq j$), we assessed the similarity between the signal segments pair by means of calculating the Pearson's correlation coefficient (**Figure 2C**). Taking the gyral vertex as an example, the correlation $PCC_{i,j}^G$ of signal segments between time window i and j was defined as:

$$PCC_{i,j}^G = corrcoef\left(S_i^G, S_j^G\right),\ i, j = 1, 2, 3, \ldots, n,\ i \neq j \quad (1)$$

We then defined the temporal variability of BOLD signal by means of calculating the variance of all correlation values between time window pairs (**Figure 2D**):

$$Var\left(PCC^G\right) = \sum\left(PCC_{i,j}^G - \overline{PCC_{i,j}^G}\right)^2 /m,\ \ i, j = 1, 2, 3, \ldots, n,\ i \neq j,\ m = n(n-1)/2 \quad (2)$$

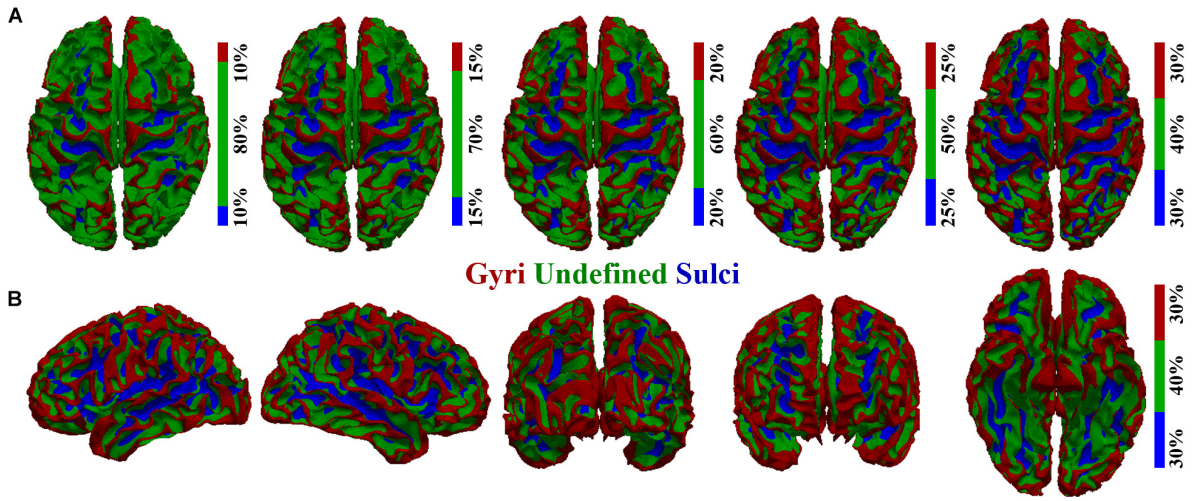

FIGURE 1 | Cortical surface parcellation of gyri, sulci, and undefined. **(A)** The parcellated cortical surface when the convexity threshold value *q* equals 10, 15, 20, 25, and 30, respectively. **(B)** The parcellated cortical surface when *q* equals 30 from another five different views.

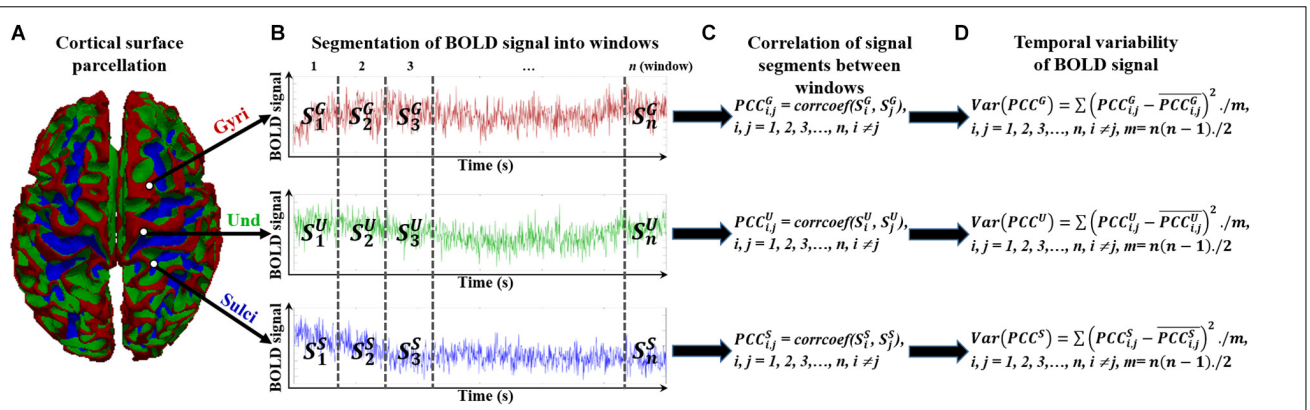

FIGURE 2 | Temporal variability assessment of functional activity in cortical gyri, sulci, and undefined regions. **(A)** The parcellated cortical surface of gyri, sulci, and undefined regions. **(B)** Segmented *n* non-overlapping time windows of each BOLD signal in gyri, sulci, and undefined regions. **(C)** Assessment of correlation between any pair of signal segments in time windows. **(D)** Assessment of variance of all correlation values between time window pairs.

where $\overline{PCC^{G}_{i,j}}$ is the mean correlation value. The potential difference of BOLD signal temporal variability among gyri, sulci, and undefined regions could then be assessed by means of comparing the mean temporal variance values of all vertices among the three groups. Since the fMRI signal represents the amplitude of BOLD oscillation, the correlation between different time windows of fMRI signals in Eq. (1) reflects the oscillation similarity of BOLD activity between different time windows. The Pearson's correlation coefficient is not 0 across time, indicating that there is oscillation association of BOLD activity between different time windows. And the temporal variance of the oscillation similarity of BOLD activity is finally calculated among all time window pairs to assess the oscillation change of BOLD activity during the entire period of the time series in Eq. (2). A previous study (Zhang et al., 2016) has demonstrated that the variability of a brain region is modulated by its BOLD activity, the α band power of its EEG, and the ratio of intra- to inter-community structural connections. The temporal variability of BOLD signal is also suggested to learning performance (Bassett et al., 2011, 2013, 2015; Zhang et al., 2016) and intelligence (Saxe et al., 2018). Taken together, the abovementioned method is reasonable to assess the temporal variance of BOLD activity.

Correlation of Gyral-Sulcal Temporal Variability With Fluid Intelligence Measures

To investigate the association between temporal variability of functional activity and the fluid intelligence, we performed correlation analysis of the variance value of each vertex with each of the three fluid intelligence measures. Specifically, since each vertex of the grayordinate data had correspondence across different subjects, we correlated the variance value of signal temporal variability with each of the three fluid intelligence

measures for each vertex. Those vertices with significant correlation values were counted for gyri, sulci, and undefined regions, respectively, in order to assess the distribution of those vertices on gyri, sulci, and undefined regions. The potential difference of significantly correlated vertex distribution among gyri, sulci, and undefined regions could then be compared across subjects. Note that we performed above-mentioned comparisons in both whole-brain scale and region of interest (ROI)-scale. The whole-brain scale comparison helped the assessment of averaged gyri-sulci-undefined regions difference across all brain regions, while the ROI-scale comparison enabled the assessment of gyri-sulci-undefined regions difference within the same brain region. Based on previous findings (Duncan et al., 2000), we adopted four ROIs provided in the used HCP dataset which are related to fluid intelligence: Rostral Middle Frontal, SupraMarginal, Inferior Parietal, and Lateral Occipital regions. Visualization of the four selected ROIs is in **Supplementary Figure 1**.

RESULTS

Temporal Variability Difference Between Gyri and Sulci

We found that the mean temporal variance of functional activity was significantly larger in gyri, smaller in sulci, and moderate in undefined regions across all brain regions within a single subject (independent sample t-test, $p < 0.001$, Bonferroni correction for multiple comparisons). Remarkably, this finding was consistent in thirty different combinations of six window size values (l = 25, 50, 75, 100, 150, and 200) and five convexity threshold values (q = 10, 15, 20, 25, and 30) shown in **Figures 3A–F**, respectively. More results of other subjects are provided in **Supplementary Figures 2 – 5**.

Moreover, we obtained similar findings in ROI-scale comparison. Within each of the four ROIs, the mean temporal variance of functional activity was significantly larger in gyri, smaller in sulci, and moderate in undefined regions (independent sample t-test, $p < 0.001$, Bonferroni correction for multiple comparisons). **Figures 4A–D** presents the mean temporal variance among gyri, sulci, and undefined regions in ten subjects within each of the four ROIs, respectively.

Reproducibility of Temporal Variability Difference via Permutation Test

We further assessed the reproducibility of temporal variability difference among gyral/sulcal/undefined vertices via permutation test. For each subject, we randomly assigned all vertices into 10% gyri, 10% sulci, and 80% undefined groups in line with the convexity threshold value 10, and compared the mean temporal variance of functional activity among the three groups. The procedure was repeated for 1000 times. We found that the mean temporal variance of functional activity was still significantly larger in gyri, smaller in sulci, and moderate in undefined regions (1000-time permutation

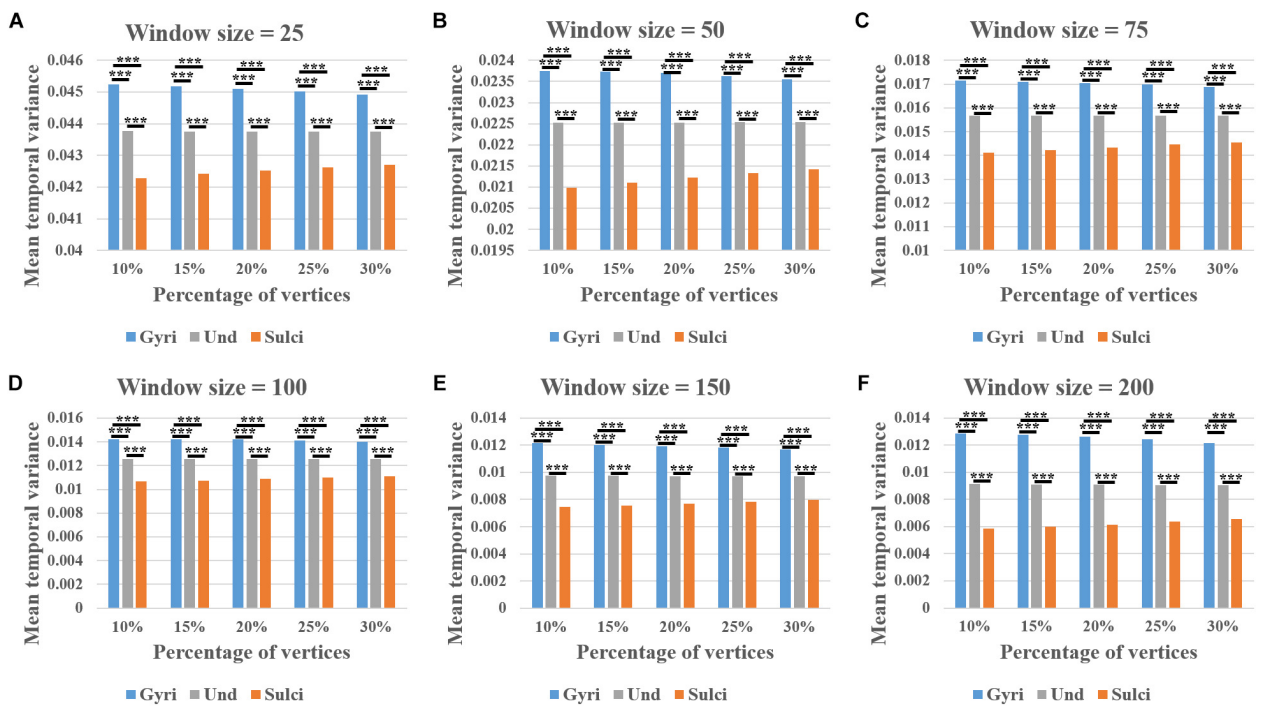

FIGURE 3 | Mean temporal variance difference of functional activity among gyri, sulci, and undefined regions across all brain regions in a single subject. **(A–F)** The mean temporal variance of gyri, sulci, and undefined regions when window size equals 25, 50, 75, 100, 150, and 200, respectively. Within each sub-figure, five convexity threshold values (10, 15, 20, 25, and 30) corresponding to five percentages of vertices (10, 15, 20, 25, and 30%) are tested. ***Indicates $p < 0.001$.

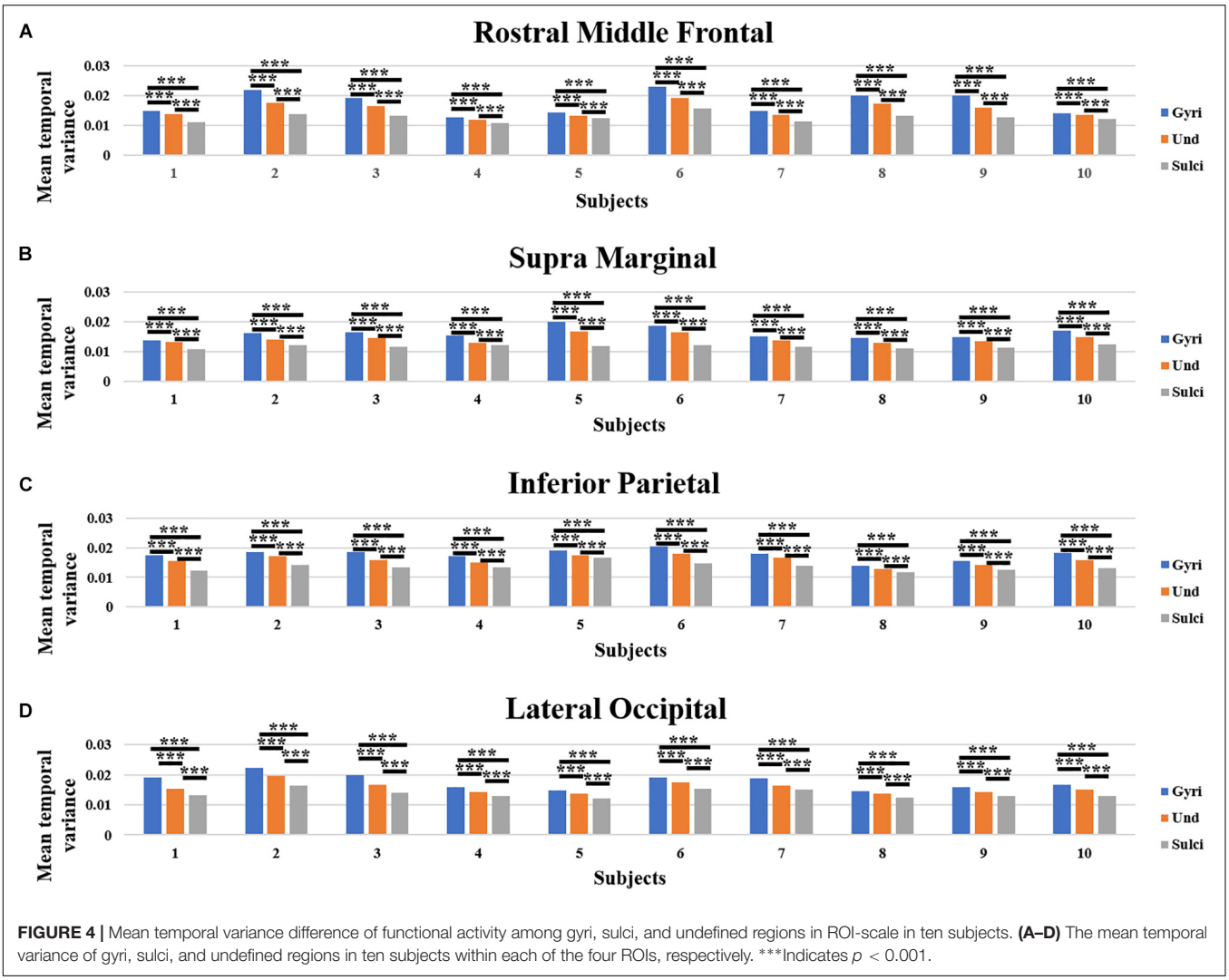

FIGURE 4 | Mean temporal variance difference of functional activity among gyri, sulci, and undefined regions in ROI-scale in ten subjects. **(A–D)** The mean temporal variance of gyri, sulci, and undefined regions in ten subjects within each of the four ROIs, respectively. ***Indicates $p < 0.001$.

independent sample *t*-test, $p < 0.05$, Bonferroni correction for multiple comparisons).

Correlation Between Temporal Variability and Fluid Intelligence Measures

We found that the temporal variability of functional activity in certain gyral/sulcal/undefined vertices had significant positive correlation with each of the three fluid intelligence measures ($r > 0.2$, $p < 0.05$, Bonferroni correction for multiple comparisons) across all brain regions. Taking the "number of correct responses" measure as an example, **Figures 5A–C** present the correlations between temporal variance and this measure across all 68 subjects of three example gyral vertices, three example sulcal vertices in **Figures 5D–F**, and three undefined vertices in **Figures 5G–I**. Moreover, those vertices which are significantly positively correlated with the "number of correct responses" measure are visualized on the cortical surface shown in **Figure 6** and are mainly located in the middle frontal cortex, inferior parietal lobe and visual cortex. More results of the other two fluid intelligence measures are provided in **Supplementary Figures 6–9**.

Moreover, we found that for those vertices with significant positive correlations between temporal variance and the "number of correct responses" measure across all brain regions, the percentage of vertices was significantly larger in gyri, smaller in sulci, and moderate in undefined regions across all 68 subjects as presented in **Figure 5J** (independent sample *t*-test, $p < 0.001$, Bonferroni correction for multiple comparisons). For the other two measures "median reaction time for correct responses" and "total skipped items," the percentage of vertices was significantly smaller in gyri, larger in sulci, and moderate in undefined regions across all 68 subjects as presented in **Supplementary Figures 6J**, **7J** (independent sample *t*-test, $p < 0.001$, Bonferroni correction for multiple comparisons).

For ROI-scale comparison, we obtained similar findings as the whole-brain comparison. Within each of the four ROIs, the temporal variability of functional activity in certain gyral/sulcal/undefined vertices had significant positive correlation with each of the three fluid intelligence

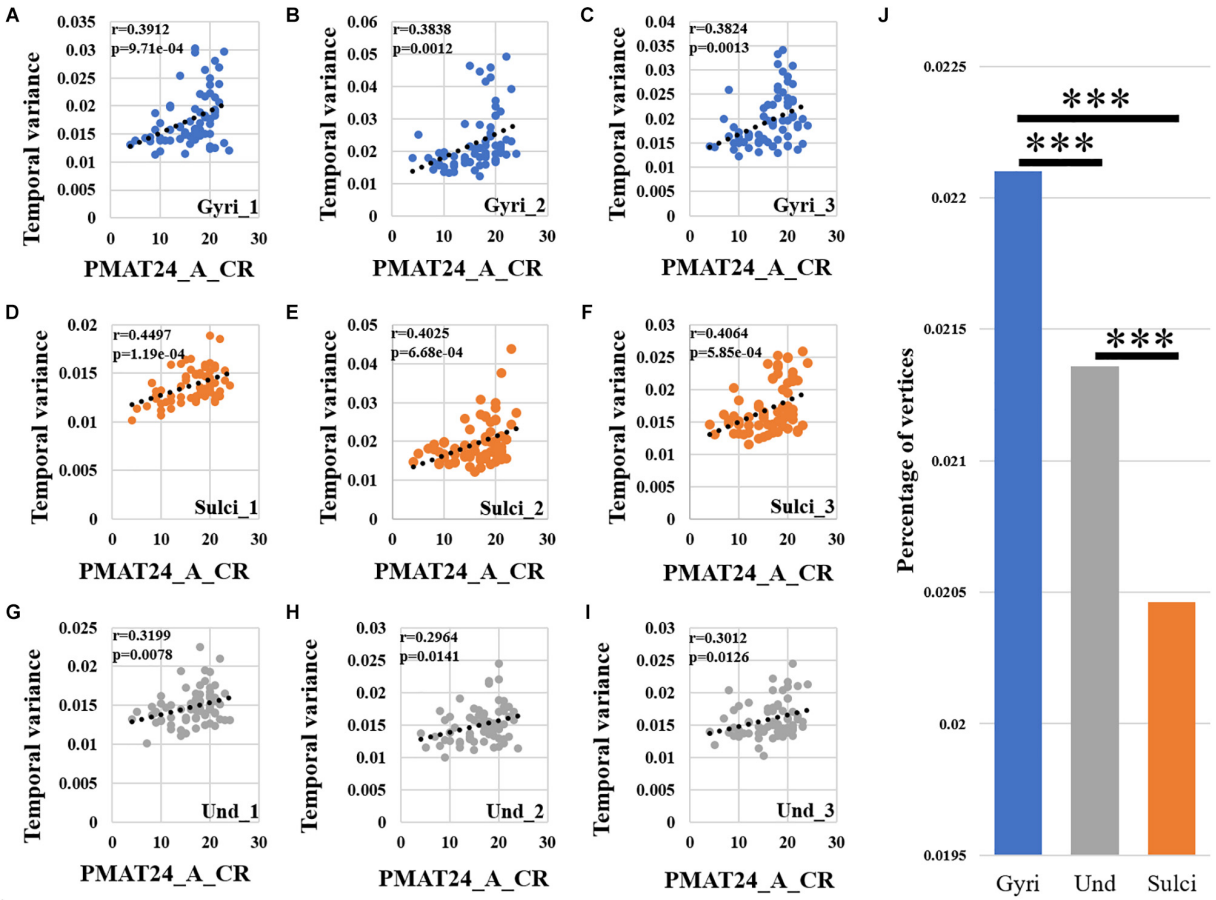

FIGURE 5 | Correlation between temporal variability of functional activity and fluid intelligence measure "number of correct responses" (PMAT24_A_CR) across all brain regions. **(A–C)** The correlations between temporal variance and "number of correct responses" measure across all 68 subjects of three example gyral vertices, respectively. **(D–F)** The correlations between temporal variance and "number of correct responses" measure across all 68 subjects of three example sulcal vertices, respectively. **(G–I)** The correlations between temporal variance and "number of correct responses" measure across all 68 subjects of three example undefined vertices, respectively. **(J)** The mean percentage of gyral/sulcal/undefined vertices with significant positive correlations with the "number of correct responses" measure across all 68 subjects. ***Indicates $p < 0.001$.

measures ($r > 0.2$, $p < 0.05$, Bonferroni correction for multiple comparisons) as illustrated in **Figures 7A–L** and **Supplementary Figures 10**, **11**. Those vertices which are significantly positively correlated with the three fluid intelligence measures within each of the four regions are visualized on the cortical surface shown in **Figure 8** and **Supplementary Figures 12**, **13**. Moreover, for those vertices with significant positive correlations between temporal variance and the "number of correct responses" measure within each of the four regions, the percentage of vertices was significantly larger in gyri, smaller in sulci, and moderate in undefined regions across all 68 subjects as presented in **Figures 7M–P** (independent sample *t*-test, $p < 0.001$, Bonferroni correction for multiple comparisons). For the other two measures "median reaction time for correct responses" and "total skipped items," the percentage of vertices was significantly smaller in gyri, larger in sulci, and moderate in undefined regions in three regions while no significant difference in middle frontal cortex as presented in **Supplementary Figures 10**, **11** (independent sample *t*-test, $p < 0.001$, Bonferroni correction for multiple comparisons).

Furthermore, we adopted all 12 temporal variance values of gyri/sulci/undefined regions in the four ROIs as independent variables to predict the fluid intelligence measure "number of correct responses." Specifically, we adopted linear regression model and leave-one-out cross validation implemented in Weka software. The result showed that the correlation coefficient value indicating how well the predictions are correlated with the actual value is as high as 0.41, suggesting that the temporal variance values of gyri/sulci/undefined regions in the four ROIs can predict the fluid intelligence.

DISCUSSION

We found that the temporal variance of resting state fMRI BOLD signal was significantly larger in gyri, smaller in sulci, and moderate in undefined regions. Since the undefined regions

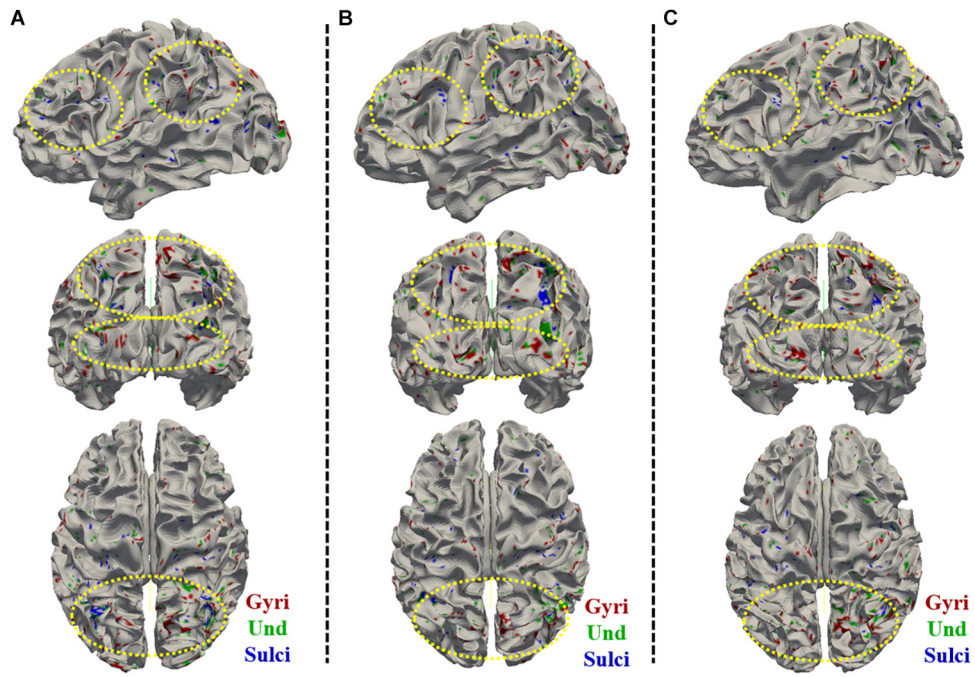

FIGURE 6 | Visualization of the vertices with significant positive correlation between temporal variance and the "number of correct responses" measure across all brain regions on cortical surface across three subjects. **(A–C)** shows the vertices distribution on cortical surface from three views across three subjects, respectively. The main locations of those vertices on cortical surface are highlighted by yellow dashed ovals.

were intermixed areas between gyri crown and sulci fundi, it was reasonable that their associated temporal variance of resting state fMRI BOLD signal was moderate between gyri and sulci. Notably, the current findings were consistent across different subjects, with a variety of combinations of time window size and convexity threshold values, and under different vertices selection strategies (convexity threshold and permutation test), demonstrating that gyri truly had significant larger temporal variance of resting state functional activity compared with sulci. This finding was supported by our recent study (Liu et al., 2018) showing that gyral resting state fMRI BOLD signals had lower frequency than sulcal signals. The fMRI BOLD signals with lower frequency tend to have more global temporal changes. Therefore, gyral resting state BOLD signals were more variable in global temporal changes represented as temporal variance than sulcal signals in this study.

We found that the temporal variability of functional activity in the middle frontal cortex, inferior parietal lobe, and visual cortex had significant positive correlation with the fluid intelligence measures. Previous studies have argued that fluid intelligence was linked to variations in human neuronal structure and function (Duncan et al., 2000; Duncan, 2003, 2005). The brain with higher variability of functional activity might be more easily for learning and higher-order relational reasoning of variable external environments (Bassett et al., 2011, 2013, 2015; Zhang et al., 2016; Saxe et al., 2018). Therefore, the identified positive correlation between temporal variability of functional activity and fluid intelligence measures was reasonable. The current finding was also consistent with previous studies reporting the correlation between fluid intelligence related networks and individual fluid intelligence scores (Santarnecchi et al., 2017), and that brain entropy measured by resting state fMRI was positively associated with intelligence (Saxe et al., 2018). Moreover, it was reported that in a spatial task with high Spearman's *g* (general intelligence) involvement, there were high-*g* activations occurred bilaterally in the prefrontal cortex, parietal lobe, and visual cortex (Duncan et al., 2000). The prefrontal cortex was recruited by different forms of cognitive demand such as working memory load, task novelty, response competition, and perceptual difficulty, etc. (Duncan and Owen, 2000) which were critical building blocks for fluid intelligence. The parietal lobe cortex was recruited in a variety of visuospatial task (Corbetta et al., 1995). The recruited visual cortex might presumably reflect more extensive visual analysis and/or the effects of eye movements (Duncan et al., 2000).

We found that the vertices with significant positive correlations between temporal variability and the fluid intelligence measure "number of correct responses" were predominately located in gyri, moderate in undefined regions, and less in sulci, while the other two measures "median reaction time for correct responses" and "total skipped items" generally showed reversed distributions, i.e., more in sulci, moderate in undefined regions, and less in gyri (**Supplementary Figures 6**, **7**, **10**, **11**). This is reasonable since higher fluid intelligence corresponded to more "number of correct responses," and less "median reaction time for

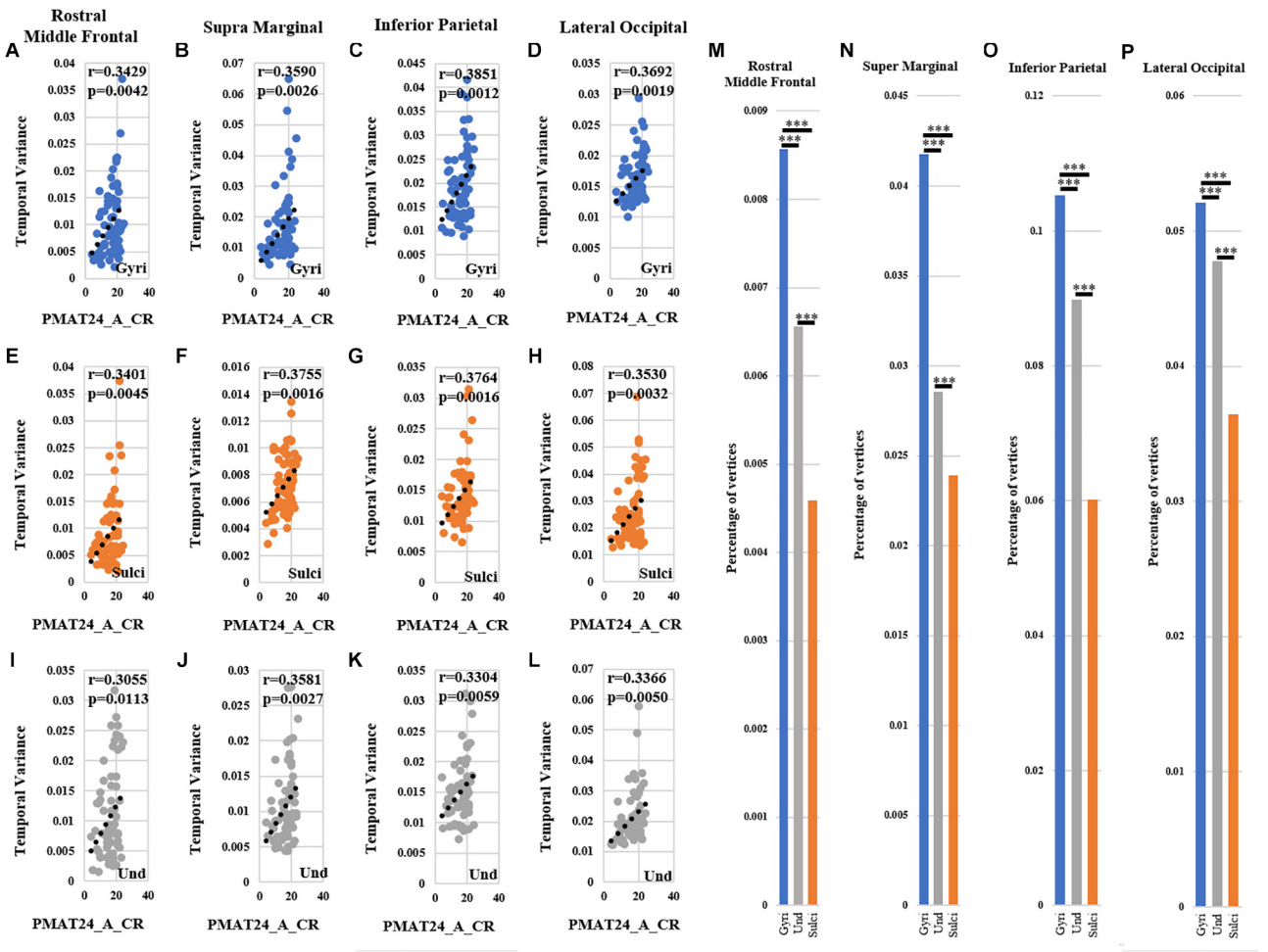

FIGURE 7 | Correlation between temporal variability of functional activity and fluid intelligence measure "number of correct responses" (PMAT24_A_CR) within each of the four ROIs. **(A–D)** The correlations between temporal variance and "number of correct responses" measure across all 68 subjects in one example gyral vertex within each of the four ROIs, respectively. **(E–H)** The correlations between temporal variance and "number of correct responses" measure across all 68 subjects in one example sulcal vertex within each of the four ROIs, respectively. **(I–L)** The correlations between temporal variance and "number of correct responses" measure across all 68 subjects in one example undefined vertex within each of the four ROIs, respectively. **(M–P)** The mean percentage of gyral/sulcal/undefined vertices with significant positive correlations with the "number of correct responses" measure across all 68 subjects. ***Indicates $p < 0.001$.

correct responses" and "total skipped items." As visualized in **Supplementary Figures 6**, **7**, **10**, **11**, a number of data points may qualify as outliers and thus potentially bias the correlation. Moreover, in **Supplementary Figures 7**, **11** there is a population of "no skipped item" subjects (26 out of 68 subjects) whose temporal variance spans almost the entire range of temporal variations in the sample, which may weaken the correlation. It is suggested that the "median reaction time for correct responses" and "total skipped items" measure of fluid intelligence may not have as strong correlations with temporal variations as the "number of correct responses" (**Figure 5**). Nevertheless, the positive correlation between the temporal variations and the first fluid intelligence measure "number of correct responses" is significant and supports our conclusion. This finding provided more evidence to elucidate the temporal variability difference of functional activity among gyri, sulci, and undefined regions. That is, gyri might participate more in the fluid intelligence than sulci and undefined regions. Our previous studies have demonstrated that gyri represent a global functional hub that performs neural communication among remote brain regions, and sulci a local function processing unit that directly communicates with neighboring gyri (Deng et al., 2014). The fluid intelligence might be more related to and supported by global neural communication among gyral regions in the whole brain.

This study assessed the temporal variability of functional activity using resting state fMRI signals in line with previous study (Zhang et al., 2016), since the resting state fMRI signals represent intrinsic functional brain activity without being affected by any external stimuli in task-based fMRI. Illustration of the temporal variability mapped on cortex with different time windows is in **Supplementary Figure 14**. Therefore, it would

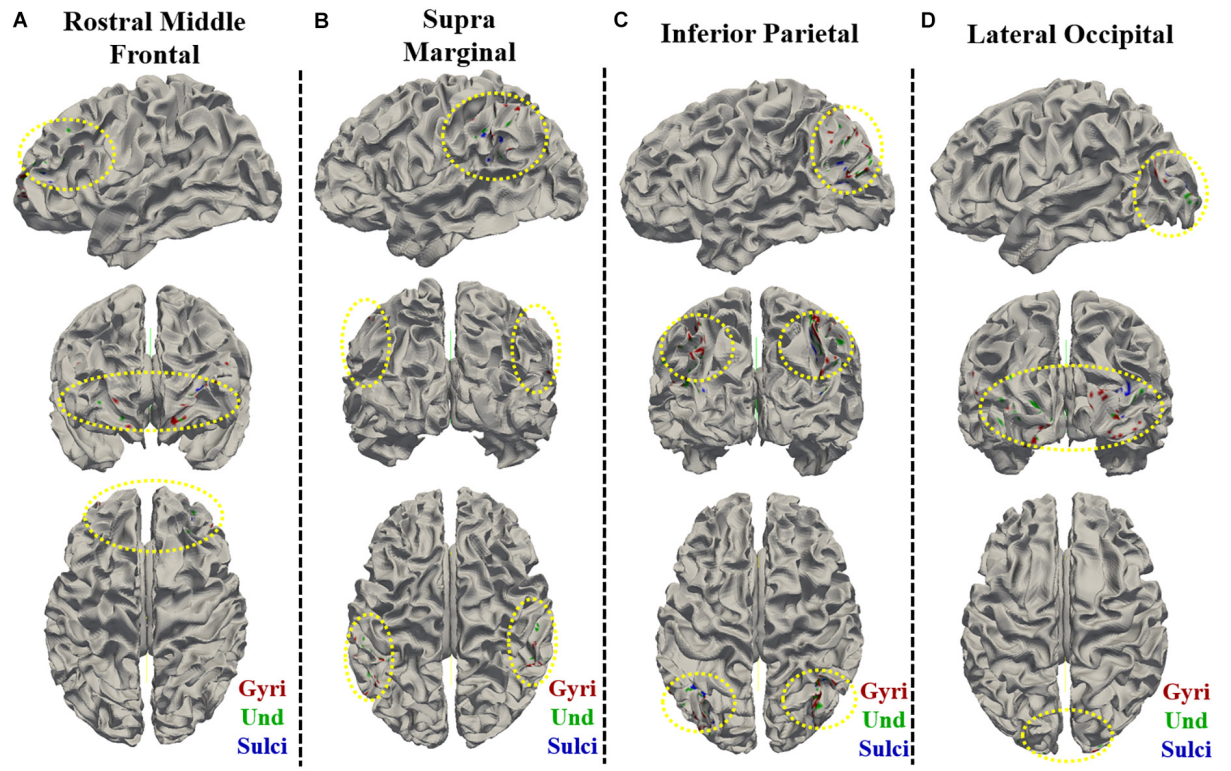

FIGURE 8 | Visualization of the vertices with significant positive correlation between temporal variance and the "number of correct responses" measure within single brain region on cortical surface of one subject. The vertices distribution on cortical surface are shown from three views within **(A)** Rostral Middle Frontal, **(B)** SupraMarginal, **(C)** Inferior Parietal, and **(D)** Lateral Occipital regions, respectively. The main locations of those vertices on cortical surface are highlighted by yellow dashed ovals.

be more suitable in the present study to assess the correlation between temporal variability of intrinsic functional activity and general human intelligence which is not related to specific task stimulus. In the future, it would be interesting to investigate the relationship between temporal variability of task-based fMRI signals and the in-task performance under specific task stimuli.

The present study has several limitations. First, the current study used average convexity (see section "Cortical Surface Parcellation of Gyri and Sulci") to define gyri/sulci within the brain regions. However, certain brain regions, e.g., insula, are hard to be defined as gyri/sulci merely based on the average convexity information. Although those brain regions were not identified to be related to fluid intelligence in the current study, more cautiousness is needed to study the gyral/sulcal characteristics of those regions in the future. Second, the current study adopted HCP grayordinate rsfMRI data to explore the temporal variability of BOLD signals on gyri/sulci. Due to the natural characteristics of fMRI imaging, more direct evidence in a finer-scale (e.g., neuron-level) is needed in the future to further validate the current findings of temporal variability difference between gyri and sulci.

In conclusion, the present study is one of the first studies to assess the temporal variability characteristics of resting state functional activity in gyri and sulci as well as its association with behavioral measures (fluid intelligence in this study). The findings could provide novel insights to understand the functional mechanisms of gyri and sulci and to demonstrate their functional relevance on the behavioral level. A future work would be applying the analysis framework on more subjects and to correlate with other behavioral measures which might be scientifically related to temporal variability. It would be also interesting to compare the temporal variability of functional activity between resting state and task-based fMRI signals in gyri and sulci and its association with behavioral measures.

ETHICS STATEMENT

This study used publicly released Human Connectome Project dataset.

AUTHOR CONTRIBUTIONS

SY analyzed part of the data, generated the figures, and wrote the manuscript draft. ZZ, HC, LZ, ZH, and HL analyzed part of the data. TZ interpreted part of the results and guided LZ and ZH on this study. LG guided LZ, ZH, and HL on this study. TL interpreted part of the results and revised the manuscript. BB and KK interpreted the results and revised the manuscript. XJ

designed the study, interpreted the results, and critically revised the figures and manuscript.

FUNDING

XJ was supported by the National Natural Science Foundation of China (NSFC 61703073) and the Fundamental Research Funds for the Central Universities (ZYGX2017KYQD165). KK was supported by the National Natural Science Foundation of China (NSFC 31530032) and the CNS Program of the University of Electronic Science and Technology of China. BB was supported by the National Natural Science Foundation of China (NSFC 91632117), the Fundamental Research Funds for the Central Universities (ZYGX2015Z002), and the Science, Innovation and Technology Department of the Sichuan Province (2018JY0001). TZ was supported by the National Natural Science Foundation of China (31671005 and 31500798). TL was supported by NIH R01 AG042599 and NSF ABI-1564736.

ACKNOWLEDGMENTS

The authors would like to thank the editor and the reviewers for their constructive comments.

SUPPLEMENTARY MATERIAL

The Supplementary Material for this article can be found online at: https://www.frontiersin.org/articles/10.3389/fncir.2019.00036/full#supplementary-material

REFERENCES

Barch, D. M., Burgess, G. C., Harms, M. P., Petersen, S. E., Schlaggar, B. L., Corbetta, M., et al. (2013). Function in the human connectome: task-fMRI and individual differences in behavior. *NeuroImage* 80, 169–189. doi: 10.1016/j.neuroimage.2013.05.033

Barron, D. (1950). An experimental analysis of some factors involved in the development of the fissure pattern of the cerebral cortex. *J. Exp. Zool.* 113, 553–581. doi: 10.1002/jez.1401130304

Bassett, D. S., Wymbs, N. F., Porter, M. A., Mucha, P. J., Carlson, J. M., and Grafton, S. T. (2011). Dynamic reconfiguration of human brain networks during learning. *Proc. Natl. Acad. Sci. U.S.A.* 108, 7641–7646. doi: 10.1073/pnas.1018985108

Bassett, D. S., Wymbs, N. F., Rombach, M. P., Porter, M. A., Mucha, P. J., and Grafton, S. T. (2013). Task-based core-periphery organization of human brain dynamics. *PLoS Comput. Biol.* 9:e1003171. doi: 10.1371/journal.pcbi.1003171

Bassett, D. S., Yang, M., Wymbs, N. F., and Grafton, S. T. (2015). Learning-induced autonomy of sensorimotor systems. *Nat. Neurosci.* 18, 744–751. doi: 10.1038/nn.3993

Bilker, W. B., Hansen, J. A., Brensinger, C. M., Richard, J., Gur, R. E., and Gur, R. C. (2012). Development of abbreviated nine-item forms of the Raven's standard progressive matrices test. *Assessment* 19, 354–369. doi: 10.1177/1073191112446655

Biswal, B., Zerrin Yetkin, F., Haughton, V. M., and Hyde, J. S. (1995). Functional connectivity in the motor cortex of resting human brain using echo-planar MRI. *Magn. Reson. Med.* 34, 537–541. doi: 10.1002/mrm.1910340409

Budde, M. D., and Annese, J. (2013). Quantification of anisotropy and fiber orientation in human brain histological sections. *Front. Integr. Neurosci.* 7:3. doi: 10.3389/fnint.2013.00003

Burgess, G. C., Gray, J. R., Conway, A. R., and Braver, T. S. (2011). Neural mechanisms of interference control underlie the relationship between fluid intelligence and working memory span. *J. Exp. Psychol. Gen.* 140, 674–692. doi: 10.1037/a0024695

Calhoun, V. D., Miller, R., Pearlson, G., and Adalı, T. (2014). The chronnectome: time-varying connectivity networks as the next frontier in fMRI data discovery. *Neuron* 84, 262–274. doi: 10.1016/j.neuron.2014.10.015

Chang, C., and Glover, G. H. (2010). Time–frequency dynamics of resting-state brain connectivity measured with fMRI. *Neuroimage* 50, 81–98. doi: 10.1016/j.neuroimage.2009.12.011

Chen, H., Zhang, T., Guo, L., Li, K., Yu, X., Li, L., et al. (2013). Coevolution of gyral folding and structural connection patterns in primate brains. *Cereb. Cortex* 23, 1208–1217. doi: 10.1093/cercor/bhs113

Corbetta, M., Shulman, G. L., Miezin, F. M., and Petersen, S. E. (1995). Superior parietal cortex activation during spatial attention shifts and visual feature conjunction. *Science* 270, 802–805. doi: 10.1126/science.270.5237.802

Deng, F., Jiang, X., Zhu, D., Zhang, T., Li, K., Guo, L., et al. (2014). A functional model of cortical gyri and sulci. *Brain Struct. Funct.* 219, 1473–1491. doi: 10.1007/s00429-013-0581-z

Destrieux, C., Fischl, B., Dale, A., and Halgren, E. (2010). Automatic parcellation of human cortical gyri and sulci using standard anatomical nomenclature. *Neuroimage* 53, 1–15. doi: 10.1016/j.neuroimage.2010.06.010

Duncan, J. (2003). Intelligence tests predict brain response to demanding task events. *Nat. Neurosci.* 6, 207–208. doi: 10.1038/nn0303-207

Duncan, J. (2005). Frontal lobe function and general intelligence: why it matters. *Cortex* 41, 215–217. doi: 10.1016/s0010-9452(08)70896-7

Duncan, J., and Owen, A. M. (2000). Common regions of the human frontal lobe recruited by diverse cognitive demands. *Trends Neurosci.* 23, 475–483. doi: 10.1016/s0166-2236(00)01633-7

Duncan, J., Seitz, R. J., Kolodny, J., Bor, D., Herzog, H., Ahmed, A., et al. (2000). A neural basis for general intelligence. *Science* 289, 457–460. doi: 10.1126/science.289.5478.457

Fischl, B. (2012). FreeSurfer. *Neuroimage* 62, 774–781. doi: 10.1016/j.neuroimage.2012.01.021

Fischl, B., and Dale, A. M. (2000). Measuring the thickness of the human cerebral cortex from magnetic resonance images. *Proc. Natl. Acad. Sci. U.S.A.* 97, 11050–11055. doi: 10.1073/pnas.200033797

Fischl, B., Sereno, M. I., and Dale, A. M. (1999). Cortical surface-based analysis: II: inflation, flattening, and a surface-based coordinate system. *Neuroimage* 9, 195–207. doi: 10.1006/nimg.1998.0396

Friston, K. J. (2009). Modalities, modes, and models in functional neuroimaging. *Science* 326, 399–403. doi: 10.1126/science.1174521

Garrett, D. D., Kovacevic, N., McIntosh, A. R., and Grady, C. L. (2010). Blood oxygen level-dependent signal variability is more than just noise. *J. Neurosci.* 30, 4914–4921. doi: 10.1523/JNEUROSCI.5166-09.2010

Ge, F., Li, X., Razavi, M. J., Chen, H., Zhang, T., Zhang, S., et al. (2018). Denser growing fiber connections induce 3-hinge gyral folding. *Cereb. Cortex* 28, 1064–1075. doi: 10.1093/cercor/bhx227

Gilbert, C. D., and Sigman, M. (2007). Brain states: top-down influences in sensory processing. *Neuron* 54, 677–696. doi: 10.1016/j.neuron.2007.05.019

Glasser, M. F., Sotiropoulos, S. N., Wilson, J. A., Coalson, T. S., Fischl, B., Andersson, J. L., et al. (2013). The minimal preprocessing pipelines for the human connectome project. *Neuroimage* 80, 105–124. doi: 10.1016/j.neuroimage.2013.04.127

Hilgetag, C. C., and Barbas, H. (2005). Developmental mechanics of the primate cerebral cortex. *Anat. Embryol.* 210, 411–417. doi: 10.1007/s00429-005-0041-5

Jiang, X., Li, X., Lv, J., Zhang, T., Zhang, S., Guo, L., et al. (2015). Sparse representation of HCP grayordinate data reveals novel functional architecture of cerebral cortex. *Hum. Brain Mapp.* 36, 5301–5319. doi: 10.1002/hbm.23013

Jiang, X., Li, X., Lv, J., Zhao, S., Zhang, S., Zhang, W., et al. (2018a). Temporal dynamics assessment of spatial overlap pattern of functional brain networks reveals novel functional architecture of cerebral cortex. *IEEE Trans. Biomed. Eng.* 65, 1183–1192. doi: 10.1109/TBME.2016.2598728

Jiang, X., Zhao, L., Liu, H., Guo, L., Kendrick, K. M., and Liu, T. (2018b). A cortical folding pattern-guided model of intrinsic functional brain networks in emotion processing. *Front. Neurosci.* 12:575. doi: 10.3389/fnins.2018.00575

Li, G., Liu, T., Ni, D., Lin, W., Gilmore, J. H., and Shen, D. (2015). Spatiotemporal patterns of cortical fiber density in developing infants, and their relationship with cortical thickness. *Hum. Brain Mapp.* 36, 5183–5195. doi: 10.1002/hbm.23003

Li, X., Zhu, D., Jiang, X., Jin, C., Zhang, X., Guo, L., et al. (2014). Dynamic functional connectomics signatures for characterization and differentiation of PTSD patients. *Hum. Brain Mapp.* 35, 1761–1778. doi: 10.1002/hbm.22290

Liu, H., Jiang, X., Zhang, T., Ren, Y., Hu, X., Guo, L., et al. (2017). Elucidating functional differences between cortical gyri and sulci via sparse representation HCP grayordinate fMRI data. *Brain Res.* 1672, 81–90. doi: 10.1016/j.brainres.2017.07.018

Liu, H., Zhang, S., Jiang, X., Zhang, T., Huang, H., Ge, F., et al. (2018). The cerebral cortex is bisectionally segregated into two fundamentally different functional units of gyri and sulci. *Cereb. Cortex* doi: 10.1093/cercor/bhy305 [Epub ahead of print].

Logothetis, N. K. (2008). What we can do and what we cannot do with fMRI. *Nature* 453, 869–878. doi: 10.1038/nature06976

Magnotta, V. A., Andreasen, N. C., Schultz, S. K., Harris, G., Cizadlo, T., Heckel, D., et al. (1999). Quantitative in vivo measurement of gyrification in the human brain: changes associated with aging. *Cereb. Cortex* 9, 151–160. doi: 10.1093/cercor/9.2.151

Nie, J., Guo, L., Li, K., Wang, Y., Chen, G., Li, L., et al. (2012). Axonal fiber terminations concentrate on gyri. *Cereb. Cortex* 22, 2831–2839. doi: 10.1093/cercor/bhr361

Passingham, R. E., Stephan, K. E., and Kötter, R. (2002). The anatomical basis of functional localization in the cortex. *Nat. Rev. Neurosci.* 3, 606–616. doi: 10.1038/nrn893

Protzner, A. B., Valiante, T., Kovacevic, N., McCormick, C., and McAndrews, M. P. (2010). Hippocampal signal complexity in mesial temporal lobe epilepsy: a noisy brain is a healthy brain. *Arch. Ital. Biol.* 148, 289–297.

Rakic, P. (1988). Specification of cerebral cortical areas. *Science* 241, 170–176. doi: 10.1126/science.3291116

Rakic, P. (2004). Genetic control of cortical convolutions. *Science* 303, 1983–1984. doi: 10.1126/science.1096414

Richman, D. P., Stewart, R. M., Hutchinson, J. W., and Caviness, V. S. (1975). Mechanical model of brain convolutional development. *Science* 189, 18–21. doi: 10.1126/science.1135626

Santarnecchi, E., Emmendorfer, A., Tadayon, S., Rossi, S., Rossi, A., and Pascual-Leone, A. (2017). Network connectivity correlates of variability in fluid intelligence performance. *Intelligence* 65, 35–47. doi: 10.1016/j.intell.2017.10.002

Saxe, G. N., Calderone, D., and Morales, L. J. (2018). Brain entropy and human intelligence: a resting-state fMRI study. *PLoS One* 13:e0191582. doi: 10.1371/journal.pone.0191582

Smith, S. M., Beckmann, C. F., Andersson, J., Auerbach, E. J., Bijsterbosch, J., Douaud, G., et al. (2013). Resting-state fMRI in the human connectome project. *Neuroimage* 80, 144–168. doi: 10.1016/j.neuroimage.2013.05.039

Smith, S. M., Miller, K. L., Salimi-Khorshidi, G., Webster, M., Beckmann, C. F., Nichols, T. E., et al. (2011). Network modelling methods for FMRI. *Neuroimage* 54, 875–891. doi: 10.1016/j.neuroimage.2010.08.063

Stahl, R., Walcher, T., De Juan Romero, C., Pilz, G. A., Cappello, S., Irmler, M., et al. (2013). Trnp1 regulates expansion and folding of the mammalian cerebral cortex by control of radial glial fate'. *Cell* 153, 535–549. doi: 10.1016/j.cell.2013.03.027

Takahashi, E., Folkerth, R. D., Galaburda, A. M., and Grant, P. E. (2012). Emerging cerebral connectivity in the human fetal brain: an MR tractography study. *Cereb. Cortex* 22, 455–464. doi: 10.1093/cercor/bhr126

Van Essen, D. C. (1997). A tension-based theory of morphogenesis and compact wiring in the central nervous system. *Nature* 385, 313–318. doi: 10.1038/385313a0

Van Essen, D. C., Smith, S. M., Barch, D. M., Behrens, T. E., Yacoub, E., Ugurbil, K., et al. (2013). The WU-Minn human connectome project: an overview. *Neuroimage.* 80, 62–79. doi: 10.1016/j.neuroimage.2013.05.041

Vidaurre, D., Smith, S. M., and Woolrich, M. W. (2017). Brain network dynamics are hierarchically organized in time. *Proc. Natl. Acad. Sci. U.S.A.* 114, 12827–12832. doi: 10.1073/pnas.1705120114

Welker, W. (1990). Why does cerebral cortex fissure and fold? A review of determinants of gyri and sulci. *Cereb. Cortex* 8, 3–136. doi: 10.1007/978-1-4615-3824-0_1

White, T., Andreasen, N. C., Nopoulos, P., and Magnotta, V. (2003). Gyrification abnormalities in childhood-and adolescent-onset schizophrenia. *Biol. Psychiatry* 54, 418–426. doi: 10.1016/s0006-3223(03)00065-9

Xu, G., Knutsen, A. K., Dikranian, K., Kroenke, C. D., Bayly, P. V., and Taber, L. A. (2010). Axons pull on the brain, but tension does not drive cortical folding. *J. Biomech. Eng.* 132:071013. doi: 10.1115/1.4001683

Yuan, J., Li, X., Zhang, J., Luo, L., Dong, Q., Lv, J., et al. (2018). Spatio-temporal modeling of connectome-scale brain network interactions via time-evolving graphs. *Neuroimage* 180, 350–369. doi: 10.1016/j.neuroimage.2017.10.067

Zeng, T., Chen, H., Fakhry, A., Hu, X., Liu, T., and Ji, S. (2015). Allen mouse brain atlases reveal different neural connection and gene expression patterns in cerebellum gyri and sulci. *Brain Struct. Funct.* 220, 2691–2703. doi: 10.1007/s00429-014-0821-x

Zhang, J., Cheng, W., Liu, Z., Zhang, K., Lei, X., Yao, Y., et al. (2016). Neural, electrophysiological and anatomical basis of brain-network variability and its characteristic changes in mental disorders. *Brain* 139, 2307–2321. doi: 10.1093/brain/aww143

Zhang, S., Liu, H., Huang, H., Zhao, Y., Jiang, X., Bowers, B., et al. (2018). Deep learning models unveiled functional difference between cortical gyri and sulci. *IEEE Trans. Biomed. Eng.* 66, 1297–1308. doi: 10.1109/TBME.2018.2872726

Zhang, T., Chen, H., Guo, L., Li, K., Li, L., Zhang, S., et al. (2014). Characterization of U-shape streamline fibers: methods and applications. *Med. Image Anal.* 18, 795–807. doi: 10.1016/j.media.2014.04.005

Zhang, T., Guo, L., Li, K., Jing, C., Yin, Y., Zhu, D., et al. (2011). Predicting functional cortical ROIs via DTI-derived fiber shape models. *Cereb. Cortex* 22, 854–864. doi: 10.1093/cercor/bhr152

Zilles, K., Armstrong, E., Schleicher, A., and Kretschmann, H. J. (1988). The human pattern of gyrification in the cerebral cortex. *Anat. Embryol.* 179, 173–179. doi: 10.1007/bf00304699

Zilles, K., Palomero-Gallagher, N., and Amunts, K. (2013). Development of cortical folding during evolution and ontogeny. *Trends Neurosci.* 36, 275–284. doi: 10.1016/j.tins.2013.01.006

Conflict of Interest Statement: The authors declare that the research was conducted in the absence of any commercial or financial relationships that could be construed as a potential conflict of interest.

frontiers in Neural Circuits

ORIGINAL RESEARCH
published: 18 June 2019
doi: 10.3389/fncir.2019.00042

Abnormal Interactions of the Salience Network, Central Executive Network, and Default-Mode Network in Patients With Different Cognitive Impairment Loads Caused by Leukoaraiosis

Hongyan Chen[1], *Yuexiu Li*[2,3,4,5,6], *Qi Liu*[7], *Qingli Shi*[2,3,4,5,6,7,8], *Jingfang Wang*[2,3,4,5,6,7,9], *Huicong Shen*[1], *Xuzhu Chen*[1], *Jun Ma*[1], *Lin Ai*[10] *and Yu Mei Zhang*[2,3,4,5,6,7]*

[1]*Department of Radiology, Beijing Tiantan Hospital, Capital Medical University, Beijing, China,* [2]*Department of Rehabilitation Medicine, Beijing Tiantan Hospital, Capital Medical University, Beijing, China,* [3]*Center of Stroke, National Clinical Research Center for Neurological Diseases, Beijing, China,* [4]*Beijing Institute for Brain Disorders, Beijing, China,* [5]*Beijing Key Laboratory of Translational Medicine for Cerebrovascular Disease, Beijing, China,* [6]*Beijing Key Laboratory of Central Nervous System Injury, Beijing, China,* [7]*Department of Neurology, Beijing Tiantan Hospital, Capital Medical University, Beijing, China,* [8]*Department of Neurology, Beijing Pinggu Hospital, Beijing, China,* [9]*Department of Neurology, General Hospital of The Yang Tze River Shipping, Wuhan Brain Hospital, Wuhan, China,* [10]*Department of Nuclear Medicine, Beijing Tiantan Hospital, Capital Medical University, Beijing, China*

OPEN ACCESS

Edited by:
Lijun Bai,
Xi'an Jiaotong University, China

Reviewed by:
Tao Liu,
Beihang University, China
Kai Wang,
Anhui Medical University, China
Xinyi Leng,
The Chinese University of Hong Kong, China

***Correspondence:**
Yu Mei Zhang
zhangyumei95@aliyun.com

Received: *19 March 2019*
Accepted: *28 May 2019*
Published: *18 June 2019*

Citation:
Chen H, Li Y, Liu Q, Shi Q, Wang J, Shen H, Chen X, Ma J, Ai L and Zhang YM (2019) Abnormal Interactions of the Salience Network, Central Executive Network, and Default-Mode Network in Patients With Different Cognitive Impairment Loads Caused by Leukoaraiosis. Front. Neural Circuits 13:42. doi: 10.3389/fncir.2019.00042

Leukoaraiosis (LA) is associated with cognitive impairment in the older people which can be demonstrated in functional connectivity (FC) based on resting-state functional magnetic resonance imaging (rs-fMRI). This study is to explore the FC changes in LA patients with different cognitive status by three network models. Fifty-three patients with LA were divided into three groups: the normal cognition (LA-NC; $n = 14$, six males), mild cognitive impairment (LA-MCI; $n = 27$, 13 males), and vascular dementia (LA-VD; $n = 12$, six males), according to the Mini Mental State Exam (MMSE) and Clinical Dementia Rating (CDR). The three groups and 30 matched healthy controls (HCs; 11 males) underwent rs-fMRI. The data of rs-fMRI were analyzed by independent components analysis (ICA) and region of interest (ROI) analysis by the REST toolbox. Then the FC was respectively analyzed by the default-mode network (DMN), salience networks (SNs) and the central executive network (CEN) with their results compared among the different groups. For inter-brain network analysis, there were negative FC between the SN and DMN in LA groups, and the FC decreased when compared with HC group. While there were enhanced inter-brain network FC between the SN and CEN as well as within the SN. The FC in patients with LA can be detected by different network models of rs-fMRI. The multi-model analysis is helpful for the further understanding of the cognitive changes in those patients.

Keywords: leukoaraiosis, resting-state MRI, functional connectivity, salience network, central executive network, default-mode network

INTRODUCTION

Leukoaraiosis (LA), also called white matter hyperintensities (WMH), was described as multifocal or diffuse periventricular or subcortical hyperintensity lesions of varying sizes (Hachinski et al., 1987). LA is found in 39% population and in 96% population above 60 years (Longstreth et al., 1996). The progression of LA is associated with cognitive impairments (Schmidt et al., 2007; O'Sullivan, 2008; Brickman et al., 2011; Chen et al., 2016).

Resting-state functional magnetic resonance imaging (rs-fMRI), including functional connectivity (FC), has been used in cognitive impairments (He et al., 2014; Cheng et al., 2017). FC has been identified as some robust intrinsic connectivity networks (ICNs), such as the default-mode network (DMN), central executive network (CEN) and salience network (SN; Seeley et al., 2007; Menon and Uddin, 2010; Menon, 2011; Chand et al., 2017). A triple network model made by DMN, CEN and SN has shown an explanatory power for psychiatric and neurological diseases (Seeley et al., 2007; Menon, 2011; Chand and Dhamala, 2016).

FC may be a potential predictor of cognitive impairments in patients with LA (Reijmer et al., 2015; Cheng et al., 2017; Li et al., 2017). Previous study has shown that the DMN, SN and CEN interact closely to control cognitive processes. Reijmer et al. (2015) reported the alternation of the DMN [the posterior cingulate cortex (PCC) and medial prefrontal cortex (MPFC)] in patients with WMH. Cheng et al. (2017) found an increased FC between the right insular region (an important area in SN) and the right superior orbital frontal gyrus and between the right calcarine cortex and the left PHG in LA patients. Chand et al.'s (2017) study showed the SN could modulate the interaction between DMN and CEN in healthy elderly controls but this modulation was disrupted in mild cognitive impairment MCI. However, the interactions of these brain networks associated with cognitive impairment loads in patients with LA are still undescribed. Therefore, our study aimed to investigate the connectivity patterns of DMN, SN and CEN by using rs-fMRI data in LA patients with different cognitive impairment.

MATERIALS AND METHODS

Participants

A total of 53 LA patients and 30 healthy control (HC) subjects in this study were consecutively recruited from the Beijing Tiantan Hospital. The inclusion criteria for the LA patients were as above: (1) age $\geq$50 years; (2) patients have LA lesions on MRI images according to the revised version of the scale of Fazekas; and (3) right-handed. The exclusion criteria were as above: (1) MRI contraindications; (2) severe systemic diseases; (3) related neurological diseases, such as epilepsy, traumatic brain injury, multiple sclerosis; (4) leukoencephalopathy of non-vascular origin; (5) dementia of non-vascular origin; and (6) inability to complete cognitive test and MRI exam. All of the LA patients have diffuse or confluent white matter hyperintensity lesions in periventricular or subcortical white matter on T2-weighted image (T2WI) and fluid-attenuated inversion recovery (FLAIR) MRI. HC subjects have the matched age, gender and education year with LA. All experimental protocols in our study were approved by the institutional review board of Beijing Tiantan Hospital, and all subjects signed informed consent forms. The flow chart of this study has been showed in **Figure 1**.

Clinical Assessment

The cognitive function of the four groups was evaluated by Mini Mental State Exam (MMSE) and their clinical diseases state was judged by the clinical dementia rating scale (CDR). All clinical scales were evaluated by two experienced neurologists.

Based on the MRI images and the scores of the MMSE, they were divided into four groups: LA patients with normal cognition (LA-NC; n = 14, MMSE scores range 28–30), LA patients with MCI (LA-MCI; n = 27, MMSE scores range 23–27), and LA patients with vascular dementia (VD; LA-VD; n = 12, MMSE scores less than 23). HC group (n = 30, MMSE scores range 28–30).

Image Acquisition

MR images were acquired using a 3T SIEMENS TIM whole-body MR system. We used a T2WI sequence with the following scan parameters: repetition time (TR) = 4,500 ms, echo time (TE) = 84 ms, flip angle (FA) = 120°, matrix = 256 × 256, field of view (FOV) = 220 × 220 mm^2, slice thickness = 5 mm, and slice gap = 1 mm, number of slices = 24. We used a T2WI-FLAIR sequence with the following scan parameters: TR = 11,000 ms, TE = 140 ms, FA = 90°, matrix = 256 × 256, FOV = 220 × 220 mm^2, slice thickness = 3.5 mm, and slice gap = 1.0 mm. The 3D MPRAGE sequence with the following scan parameters: TR = 2,300 ms, TE = 3.28 ms, FOV = 256 mm × 256 mm^2, matrix = 256 × 256, flip angle 9°, in plane resolution = 1 mm × 1 mm, slice thickness = 1 mm. rs-fMRI data were acquired using an echo planar imaging (EPI) sequence with the following scan parameters: TR = 2,000 ms, TE = 30 ms, flip angle (FA) = 90°, matrix = 64 × 64, FOV = 256 × 256 mm^2, slice thickness = 3.7 mm, and slice gap = 0 mm, number of slices 32. During the fMRI scans, all subjects were asked to keep their eyes closed, stay as motionless as possible, think of nothing in particular, and not fall asleep during the scan.

Pre-processing of Resting-State Data

All of the fMRI data were analyzed using SPM8[1]. The pre-processing steps include: slice-timing realignment and adjustment, motion correction, co-registration, normalization, spatial smoothing, delinearization and bandpass filtering. The first five volumes were discarded to eliminate T1 relaxation effects. Next, the head motion parameters of each volume were estimated and saved, and each volume was realigned to the mean map of the whole volumes to correct for geometric displacements using a six-parameter rigid-body transformation. Five subjects were excluded from further analysis because they had maximum displacements (>2 mm) in one or more of the orthogonal directions (x, y, z) or a maximum rotation (x, y, z) >2.0°. The

[1]http://www.fil.ion.ucl.ac.uk/spm/software/spm8

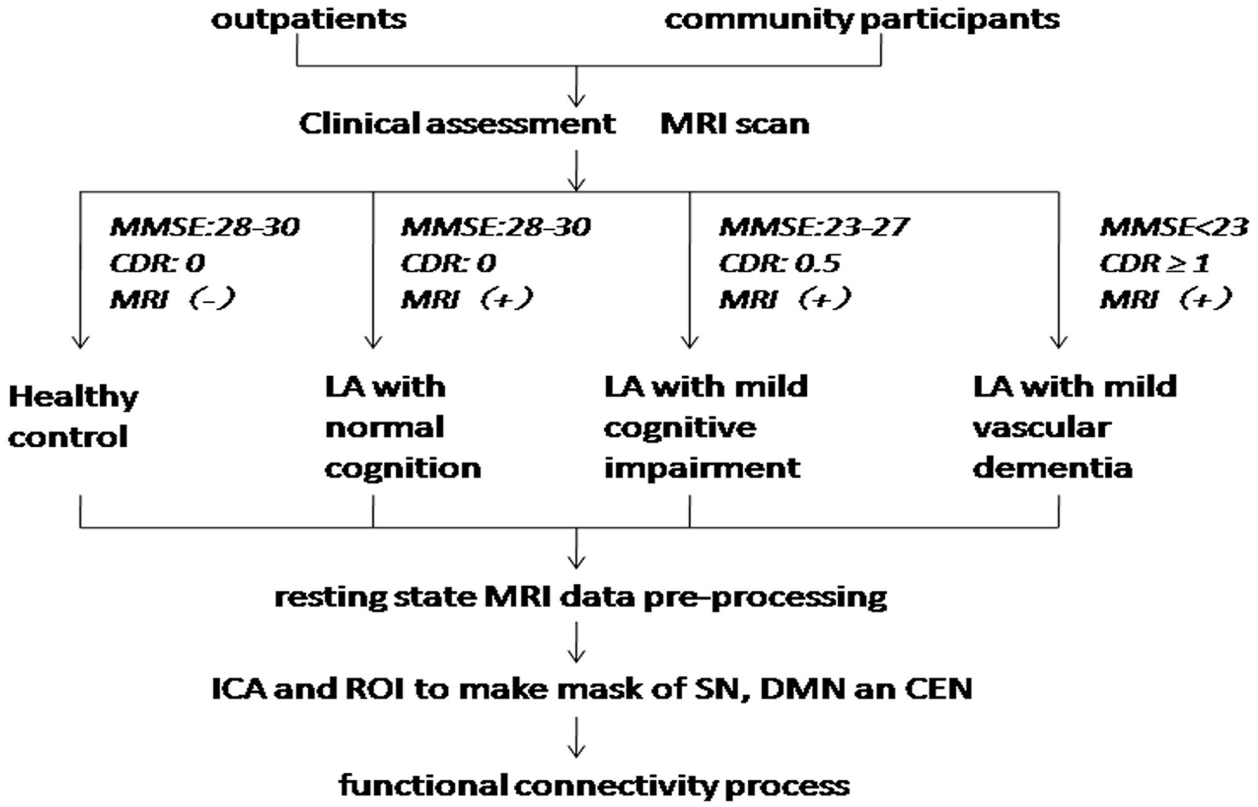

FIGURE 1 | Flow chart. MMSE, Mini Mental State Exam; CDR, Clinical Dementia Rating; LA, leukoaraiosis; ICA, independent components analysis; ROI, region of interest; SN, salience networks; DMN, default-mode network; CEN, central executive network.

data were spatially normalized to the standard EPI template and re-sampled to $2 \times 2 \times 2$ mm^3. The normalized data were smoothed using a 6-mm full width at half maximum.

Definition of the SN Mask by the ICA Method and Intra-Brain-Network FC

We applied group independent component analysis (gICA) to rs-MRI data with the Infomax algorithm implemented in Matlab (Calhoun et al., 2001) in order to identify the regions of interest (ROIs) for the SN. To ensure the stability of the ROIs, we performed gICA100 times. Twenty-five aggregate independent components (ICs) were identified using the GIFT toolbox[2], in which the number of components was determined by the minimum description length criterion. All aggregate ICs were visually inspected, and the IC representing SN was selected (Seeley et al., 2007). Then, the specify IC of all subjects regardless of group was entered into a random-effect one-sample *t*-test. We used a threshold of $P < 0.001$ [Family Wise Error (FWE) correction] to define the SN mask. The result was displayed on a brain surface template using the REST slice viewer[3]. Based on this result, the mask SN was made using MRIcro[4] and displayed on the brain surface template (**Figure 2**).

[2]http://icatb.sourceforge.net/groupica.htm
[3]http://www.restfmri.net/forum/REST
[4]http://mccauslandcenter.sc.edu/CRNL

In order to obtain the intra-brain-network FC of each group, we repeated the same group ICA test for each group. ICs representing the SN of each patient were selected and entered into a random-effect one-sample *t*-test. The result of the one-sample *t*-test was used to obtain the intra-brain-network FC for each ROI in the SN.

Definition of the DMN and CEN Masks by ROI and Intra-Brain-Network FC

The definitions of the ROIs of the DMN and CEN were based on a previous study (Duan et al., 2012). For the DMN, we defined three ROIs, including the ventromedial PFC (vmPFC, MNI coordinates: −2, 54, −6), left PCC (MNI coordinates: −6, −48, 32), and right PCC (MNI coordinates: 10, −52, 28). For the CEN, we defined four ROIs, including the left dorsolateral PFC (dlPFC; MNI coordinates: −48, 34, 34), right dlPFC (MNI coordinates: 48, 40, 30), left PPC (MNI coordinates: −36, −44, 46), and right PPC (MNI coordinates: 42, −42, 48). Then, a sphere mask of 10 mm in radius centered at each peak voxel was defined and the averaged time series for each of the defined ROIs was extracted. Then we used the averaged time series extracted from the SN template as the starting point, the FC measurement was performed for each voxel of the whole brain. Conjunction analysis was used to define the brain areas that were

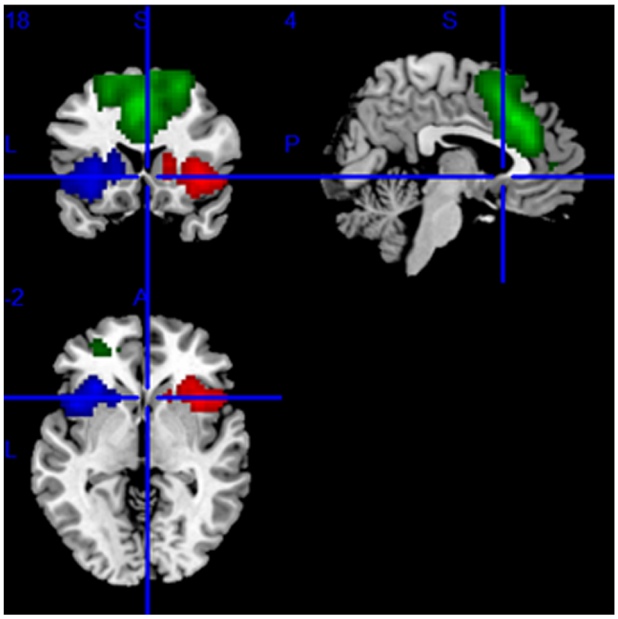

FIGURE 2 | The mask of the SN, mainly including the bilateral frontoinsular cortex (FIC) and anterior cingulate cortex (ACC). The red area is the right, the blue area is the left FIC, and the green area is ACC.

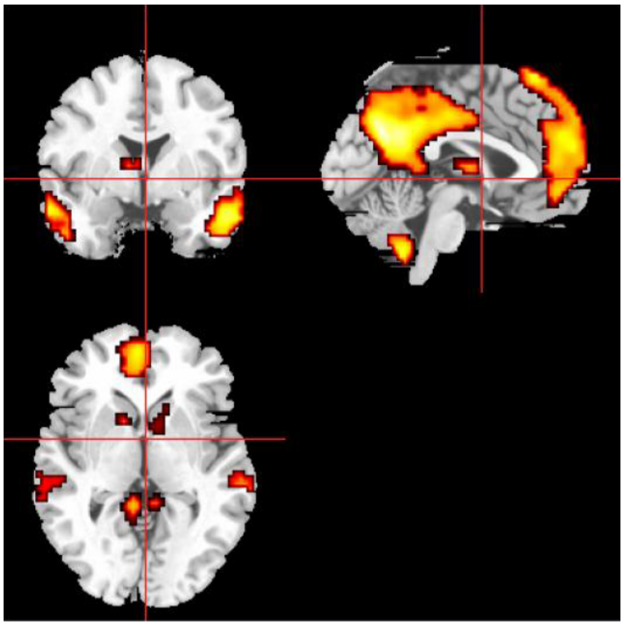

FIGURE 3 | The mask of the DMN, mainly including medial prefrontal cortex (MPFC), ACC, posterior cingulate cortex (PCC), and precuneus.

correlated with all of the ROIs of the specific functional networks. Then we used the FWE method with a threshold of $P < 0.05$ after multiple comparison corrections. Finally, the ROIs were selected as the masks capturing the key nodes within the DMN and CEN. The masks of DMN and CEN were shown on the MRIcrobrain surface template (**Figures 3**, **4**).

SN-Anchored FC Analysis

First, the right frontoinsular cortex (FIC) was selected as the seed region to calculate inter-brain-network FCs with the CEN and DMN because of its reported role in switching between the CEN and the DMN (Sridharan et al., 2008). We extracted the averaged time series of the right FIC to calculate its FC with each voxel across the whole brain. With the application of the DMN and CEN masks, the mean FCs of the core regions within the DMN and CEN were measured. ANOVA was used to determine the differences for both inter-brain-network and intra-brain-network FCs among these four groups. Between-group differences of the intra-brain-network FCs between the SN and DMN as well as between the SN and CEN were also compared.

Statistical Analyses

We used one-way ANOVA to compare the clinical features (age, education year, MMSE scores, CDR scores) and the FC across the four groups. Bonferroni correction and least significant difference (LSD) were used to *post hoc* comparisons.

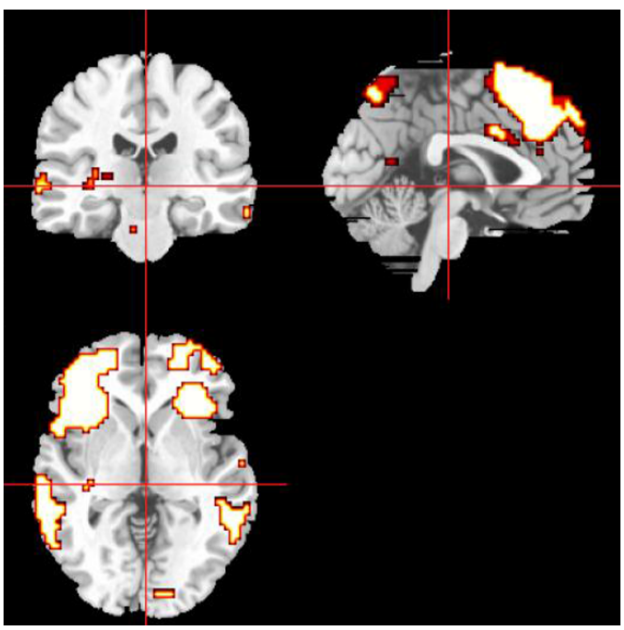

FIGURE 4 | The mask of the CEN, mainly including the ACC and bilateral dorsolateral PFC (dlPFC).

RESULTS

Participant Characteristics

In the present study, a total of 53 LA patients and 30 HCs were included in all the analyses. The demographic and behavioral statistics for the four groups are presented in **Table 1**. There were

TABLE 1 | Demographic and behavioral statistics for the four groups.

Items	HC	LA-NC	LA-MCI	LA-VD
Age (years)	54.3 ± 9.6	60.1 ± 5.3	62.0 ± 11.4	59.9 ± 12.8
Gender (M/F)	11/19	6/8	13/14	6/6
Education (years)	13.3 ± 3.0	12.0 ± 2.8	11.0 ± 3.2	11.1 ± 3.1
MMSE	28.9 ± 1.5	29.1 ± 1.0	27.2 ± 2.4	23.3 ± 3.4
CDR	0	0	0.5	≥1

CDR, clinical dementia rating; F, female; HC, healthy controls; LA, leukoaraiosis; M, male; MCI, mild cognitive impairment; MMSE, Mini Mental State Exam; VD, vascular dementia.

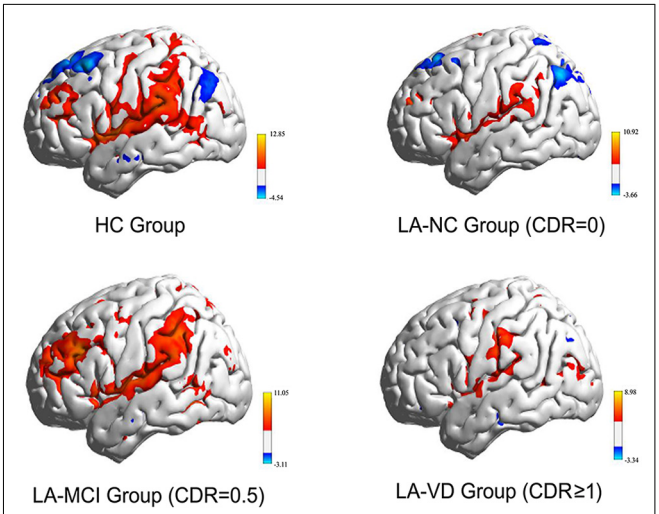

FIGURE 5 | The functional connectivity (FC) of the whole brain of each of the four study groups. The FC of the three LA groups is markedly weaker than that of the healthy control (HC) group. CDR, clinical dementia rating; MCI, mild cognitive impairment; VD, vascular dementia.

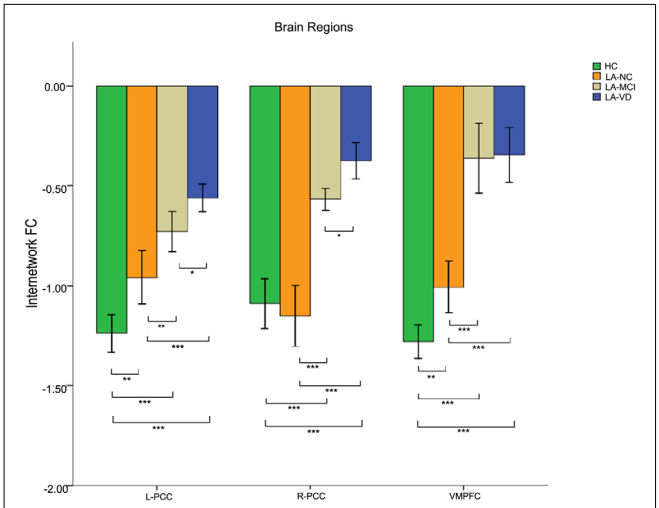

FIGURE 6 | The FC between anatomical brain regions in the DMN and SN. There was negative correlation between DMN and SN activity. The first group of bars is the left PCC, the second group of bars is the right PCC, the third group of bars is the ventromedial PFC (vmPFC). The overall connectivity trend from high to low was HC group, LA-normal cognition (NC) group, LA-MCI group, and LA-VD. Green bar, HC; yellow bar, LA-NC; gray bar, LA-MCI; and blue bar, LA-VD. *$P < 0.05$, LSD corrected; **$P < 0.05$, Bonferroni corrected; ***$P < 0.001$, Bonferroni corrected. Error bars represent standard error. Error bar: 95% confidence intervals (CIs).

no significant differences in age or education among the four groups ($P > 0.1$).

The FC of Whole Brain Based on Right FIC

Figure 5 showed the whole brain FC of the three LA groups and HC group based on the right FIC as the seed point. All the FC of LA groups were lower than HC, the next order was the LA-MCI, the LA-NC and the LA-VD.

The Relationship Between SN and DMN

The interaction between the SN and DMN was negatively correlated. The one-way ANOVA was used for inter-networks of SN and DMN.

We found differences in the bilateral PCC and bilateral vmPFC among the four groups, and we also found differences in the left AG and left inferior parietal lobe (IPL) among the HC group, LA-NC group and LA-MCI group (**Figure 6**). Within the left AG and left IPL, the number of negatively activated points in the LA-VD group was too small to be counted, so we only compared the FC of the HC group, the LA-NC group and the LA-MCI group (**Figure 7**).

This result showed that for the FC between the SN and DMN, the HC group has the highest connection, followed by LA-NC, LA-MCI and LA-VD.

The Relationship Between SN and CEN

The interaction between the SN and CEN was positively correlated. The overall connectivity trend was different from DMN, the HC group also has the highest FC, but its next order was LA-MCI, LA-VD and LA-NC. We found significant connectivity differences in the bilateral dlPFC, bilateral ventrolateral PFC (vlPFC), bilateral supplementary motor area (SMA), and bilateral IPL among the four groups (**Figures 8**, **9**).

The Relationship Within the SN

Nearly all the three components of SN showed significant differences across groups when used the one-way ANOVA, including the bilateral FICs and anterior cingulate cortex (ACC). The *post hoc* comparison of the intra-brain-network FC of the SN was positively correlated in terms of neural activity. The connectivity of HC also was the highest one, and the LA-VD/LA-MCI followed HC, the least one was LA-NC. We found significant FC in the ACC and the right FIC among the four groups (**Figure 10**).

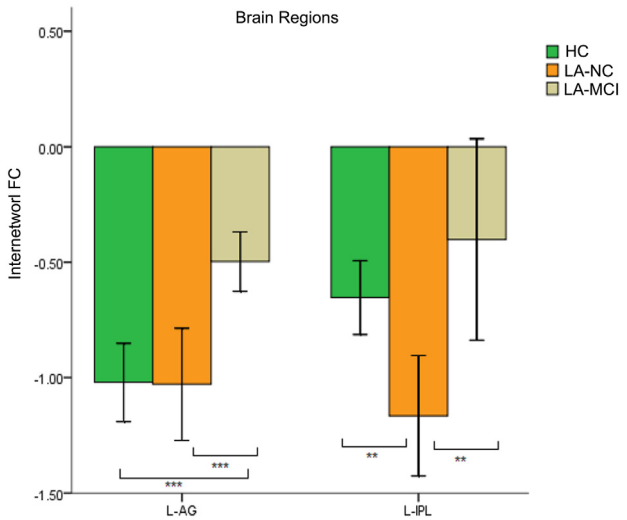

FIGURE 7 | The FC between anatomical brain regions in the DMN and SN. Within the left angular gyrus (AG) and left inferior parietal lobe (IPL), the number of negatively activated points in the LA-VD group was too small to be counted. The first group of bars is the left AG, the second group of bars is the left IPL. Green bar, HC; yellow bar, LA-NC; and gray bar, LA-MCI. $^{**}P < 0.05$, Bonferroni corrected; $^{***}P < 0.001$, Bonferroni corrected. Error bars represent standard error. Error bar: 95% CI.

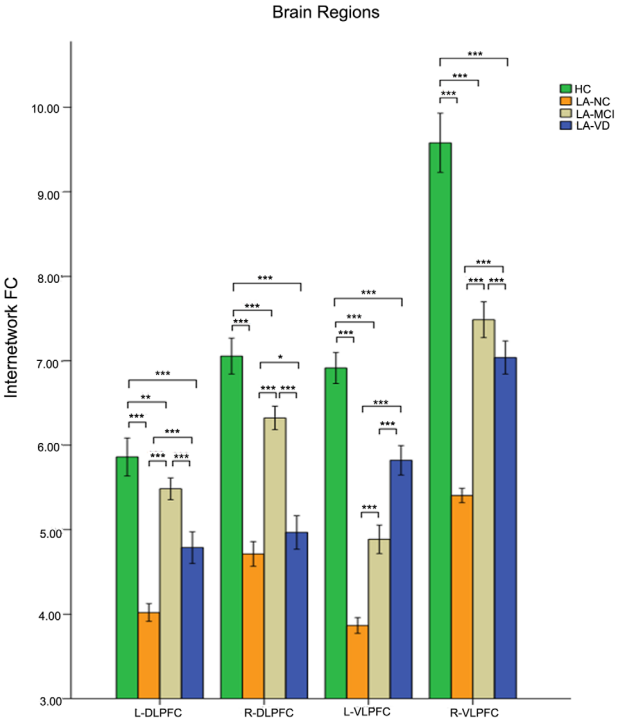

FIGURE 8 | The FC between anatomical brain regions in the CEN and SN. There was a positive correlation between CEN and SN activity. The first group of bars is the left dlPFC, the second group of bars is the right dlPFC, the third group of bars is the left ventrolateral PFC (vlPFC), and the fourth group of bars is the right vlPFC. The overall connectivity trend from high to low was HC group, LA-MCI group, LA-VD group, and LA-NC group. Green bar, HC; yellow bar, LA-NC; gray bar, LA-MCI; blue bar, LA-VD. $^{*}P < 0.05$, LSD corrected; $^{**}P < 0.05$, Bonferroni corrected; $^{***}P < 0.001$, Bonferroni corrected. Error bars represent standard error. Error bar: 95% CI.

DISCUSSION

In this study, we examined the FC of the SN, CEN, and DMN in LA patients with different cognitive impairment loads and HC participants. We found that different LA groups with different cognitive status presented differently in the ICNs compared to the HC group. There were four findings revealed in our study. First, the negative correlations between the SN and DMN were diminished as the cognitive impairment loads increased. As the load of cognitive, the decline of FC in LA groups was intensified. The FC between the SN and DMN provided a characterization of the cognitive load impairment of the LA. Second, with the increase in the severity of cognitive impairment, the positive correlation between the SN and CEN was increased. The FC between the SN and CEN provided a representation of LA's cognitive load compensation. Last, as the severity of LA cognitive impairment increased, the positive correlation within the SN was increasing. The intra-SN connection provided a representation of the cognitive burden compensation for LA.

In our study, the LA patients demonstrated decreased functional connectivity between the DMN and the right FIC in SN, especially in the bilateral PCC and vmPFC, consistent with previous studies (Menon and Uddin, 2010; Li et al., 2015; Reijmer et al., 2015; Atwi et al., 2018; Wang et al., 2019). It may indicate that LA leads to the decrease of FC between the SN and DMN, and the damage of connectivity between the DMN and SN. Wang et al. (2019) found that the PCC, precuneus and right inferior temporal gyrus showed significantly decreased ALFF values in LA patients. The researchers thought that the executive functional impairment of LA may be caused by the disruptions in the afferents of PCC. Although we used different method, we got the similar result. Atwi et al. (2018) found that older adults with WMH had lower activation in fronto-temporal and parietal cortices compared to the healthy older adults, so they got the conclusion WMH may contribute to the dysfunction of brain networks. Our result is consistent with this result. Reijmer et al. (2015) combined the structural and functional brain connectivity in WMH patients, and they found that the PCC and MPFC of the DMN were altered, as well as a significant correlation between the microstructural properties of the cingulum bundle and MPFC-PCC FC in patients with low WMH load. This decreased structural connectivity could explain the change in FC, and this result could explain our study. But more evidence of structural and FC is needed to ensure the physiological basis of LA patient's cognitive changes.

Our study showed that the CEN and the right FIC in SN were positively correlative, and the FC was decreased between the CEN and SN in LA patients regardless of the cognitive status. This may be explained by Wiggins research, since the LA contributed to the speeded and mental manipulation of executive function (Wiggins et al., 2018). Interestingly, the LA-MCI and LA-VD groups in our study showed higher FC between the CEN and SN, especially in the bilateral dlPFC, ventrolateral PFC, bilateral SMA, and IPL. This may due to the changes in functional compensation

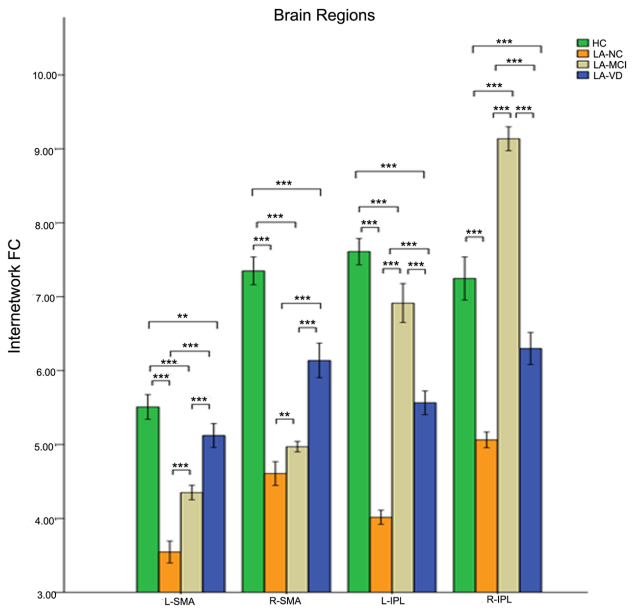

FIGURE 9 | The FC between anatomical brain regions in the CEN and SN. There was a positive correlation between CEN and SN activity. The first group of bars is the left supplementary motor area (SMA), the second group of bars is the right SMA, the third group of bars is the left IPL, the fourth group of bars is the right IPL. The overall connectivity trend from high to low was HC group, LA-MCI group, LA-VD group and LA-NC group. Green bar, HC; yellow bar, LA-NC; gray bar, LA-MCI; blue bar, LA-VD. $^{**}P < 0.05$, Bonferroni corrected; $^{***}P < 0.001$, Bonferroni corrected. Error bars represent standard error. Error bar: 95% CI.

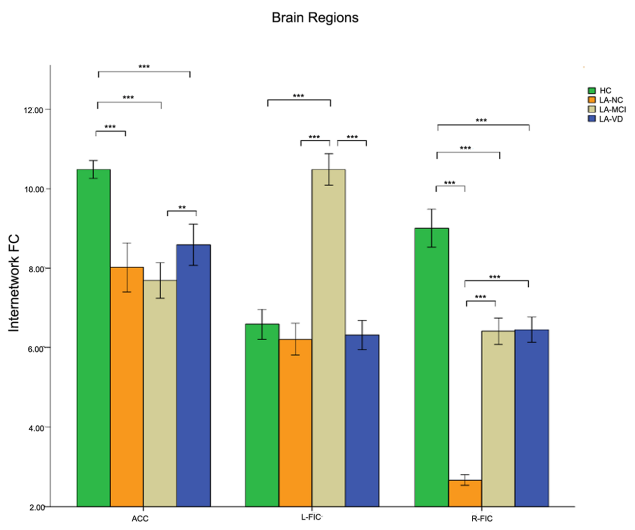

FIGURE 10 | The result of the intra-SN FC. There were positive correlations in neural activity. The first group of bars is the ACC, the second group of bars is the right FIC. The overall connectivity trend from high to low was HC group, LA-VD/MCI group, and LA-NC group. Green bar, HC; yellow bar, LA-NC; gray bar, LA-MCI; blue bar, LA-VD. $^{**}P < 0.05$, Bonferroni corrected; $^{***}P < 0.001$, Bonferroni corrected. Error bars represent standard error. Error bar: 95% CI.

in LA patients with cognitive dysfunction (Lockhart et al., 2015; Gold et al., 2017).

Our study also revealed decreased FC in the intra-SN at the ACC and right FIC in LA patients ignorance of their cognitive status. As an important part of the SN, FIC is a critical switcher between the CEN and DMN (He et al., 2014). He et al. (2014) found that the bilateral FIC showed decreased intra-SN FC in the AD group. The decrease of FC may indicate that the intra-SN connection has been damaged in LA groups, and it may be caused by LA. Furthermore, the LA-MCI and LA-VD group showed significant increase in intra-SN FC at the right FIC when compared with the LA-NC group. This mechanism may play a compensatory role in LA patients with MCI and VD, improving the efficiency of conversion. Since the FC in LA patients has changed and suggests a compensatory mechanism (Cheng et al., 2017) the intra-SN connection may provide a representation of the cognitive burden compensation for LA.

There are limitations of our study. First, the sample is not large enough. Second, this study did not contain a correlation analysis of the specific relationships among different cognitive functions and the three ICNs. Third, we did not analyze the relationship between the FC and the neuropsychological battery.

CONCLUSION

In our study, we evaluated the rs-fMRI by a triple network model in LA patients with different cognitive status. The multi-model analysis is helpful for further understanding of the cognitive changes in LA patients.

DATA AVAILABILITY

All datasets generated for this study are included in the manuscript.

ETHICS STATEMENT

This study was carried out in accordance with the recommendations of the institutional review board of Beijing Tiantan Hospital with written informed consent from all subjects. All subjects gave written informed consent in accordance with the Declaration of Helsinki. The protocol was approved by the institutional review board of Beijing Tiantan Hospital.

AUTHOR CONTRIBUTIONS

HC, QL, QS, YL, and JW performed the experiment. HC analyzed image data, drafted the manuscript and performed the statistical results. QL, QS, YL, and JW collected the data involved in the study. YZ designed the study. YZ, HS, JM, LA and XC gave critical comments on the manuscript.

FUNDING

This study was supported by the Beijing Municipal Administration of Hospitals Clinical Medicine Development

of Special Funding Support (ZYLX201836), National Key Technology Research and Development Program of China (2018YFC2002300, 2018YFC2002302 and 2015BAI12B02), the National Natural Science Foundation of China (NSFC: 81371201, 81772005), the National Key Technology Research and Development Program of the Ministry of Science and Technology of The People's Republic of China (2015BAI12B04), and the National Key Research and Development Program of China (2018YFC0115604).

REFERENCES

Atwi, S., Metcalfe, A. W. S., Robertson, A. D., Rezmovitz, J., Anderson, N. D., and MacIntosh, B. J. (2018). Attention-related brain activation is altered in older adults with white matter hyperintensities using multi-echo fMRI. *Front. Neurosci.* 12:748. doi: 10.3389/fnins.2018.00748

Brickman, A. M., Siedlecki, K. L., Muraskin, J., Manly, J. J., Luchsinger, J. A., Yeung, L. K., et al. (2011). White matter hyperintensities and cognition: testing the reserve hypothesis. *Neurobiol. Aging* 32, 1588–1598. doi: 10.1016/j.neurobiolaging.2009.10.013

Calhoun, V. D., Adali, T., Pearlson, G. D., and Pekar, J. J. (2001). A method for making group inferences from functional MRI data using independent component analysis. *Hum. Brain Mapp.* 14, 140–151. doi: 10.1002/hbm.1048

Chand, G. B., and Dhamala, M. (2016). The salience network dynamics in perceptual decision-making. *Neuroimage* 134, 85–93. doi: 10.1016/j.neuroimage.2016.04.018

Chand, G. B., Wu, J., Hajjar, I., and Qiu, D. (2017). Interactions of the salience network and its subsystems with the default-mode and the central-executive networks in normal aging and mild cognitive impairment. *Brain Connect.* 7, 401–412. doi: 10.1089/brain.2017.0509

Chen, Y., Wang, C., Liang, H., Chen, H., Bi, Y., Sun, H., et al. (2016). Resting-state-functional magnetic resonance imaging in patients with leukoaraiosis-associated subcortical-vascular cognitive impairment: a cross-sectional study. *Neurol. Res.* 38, 510–517. doi: 10.1080/01616412.2016.1177929

Cheng, R., Qi, H., Liu, Y., Zhao, S., Li, C., Liu, C., et al. (2017). Abnormal amplitude of low-frequency fluctuations and functional connectivity of resting-state-functional magnetic resonance imaging in patients with leukoaraiosis. *Brain Behav.* 7:e00714. doi: 10.1002/brb3.714

Duan, X., Liao, W., Liang, D., Qiu, L., Gao, Q., Liu, C., et al. (2012). Large-scale brain networks in board game experts: insights from a domain-related task and task-free resting state. *PLoS One* 7:e32532. doi: 10.1371/journal.pone.0032532

Gold, B. T., Brown, C. A., Hakun, J. G., Shaw, L. M., Trojanowski, J. Q., and Smith, C. D. (2017). Clinically silent Alzheimer's and vascular pathologies influence brain networks supporting executive function in healthy older adults. *Neurobiol. Aging* 58, 102–111. doi: 10.1016/j.neurobiolaging.2017.06.012

Hachinski, V. C., Potter, P., and Merskey, H. (1987). Leuko-araiosis. *Arch. Neurol.* 44, 21–23. doi: 10.1001/archneur.1987.00520130013009

He, X., Qin, W., Liu, Y., Zhang, S., Duan, Y., Song, J., et al. (2014). Abnormal salience network in normal aging and in amnestic mild cognitive impairment and Alzheimer's disease. *Hum. Brain Mapp.* 35, 3446–3464. doi: 10.1002/hbm.22414

Li, R., Lai, Y., Zhang, Y., Yao, L., and Wu, X. (2017). Classification of cognitive level of patients with leukoaraiosis on the basis of linear and non-linear functional connectivity. *Front. Neurol.* 8:2. doi: 10.3389/fneur.2017.00002

Li, C., Yang, J., Yin, X., Liu, C., Zhang, L., Zhang, X., et al. (2015). Abnormal intrinsic brain activity patterns in leukoaraiosis with and without cognitive impairment. *Behav. Brain Res.* 292, 409–413. doi: 10.1016/j.bbr.2015.06.033

Lockhart, S. N., Luck, S. J., Geng, J., Beckett, L., Disbrow, E. A., Carmichael, O., et al. (2015). White matter hyperintensities among older adults are associated with futile increase in frontal activation and functional connectivity during spatial search. *PLoS One* 10:e0122445. doi: 10.1371/journal.pone.0122445

Longstreth, W. T. Jr., Manolio, T. A., Arnold, A., Burke, G. L., Bryan, N., Jungreis, C. A., et al. (1996). Clinical correlates of white matter findings on cranial magnetic resonance imaging of 3301 elderly people. The cardiovascular health study. *Stroke* 27, 1274–1282. doi: 10.1161/01.str.27.8.1274

Menon, V. (2011). Large-scale brain networks and psychopathology: a unifying triple network model. *Trends Cogn. Sci.* 15, 483–506. doi: 10.1016/j.tics.2011.08.003

Menon, V., and Uddin, L. Q. (2010). Saliency, switching, attention and control: a network model of insula function. *Brain Struct. Funct.* 214, 655–667. doi: 10.1007/s00429-010-0262-0

O'Sullivan, M. (2008). Leukoaraiosis. *Pract. Neurol.* 8, 26–38. doi: 10.1136/jnnp.2007.139428

Reijmer, Y. D., Schultz, A. P., Leemans, A., O'Sullivan, M. J., Gurol, M. E., Sperling, R., et al. (2015). Decoupling of structural and functional brain connectivity in older adults with white matter hyperintensities. *Neuroimage* 117, 222–229. doi: 10.1016/j.neuroimage.2015.05.054

Schmidt, R., Petrovic, K., Ropele, S., Enzinger, C., and Fazekas, F. (2007). Progression of leukoaraiosis and cognition. *Stroke* 38, 2619–2625. doi: 10.1161/strokeaha.107.489112

Seeley, W. W., Menon, V., Schatzberg, A. F., Keller, J., Glarer, G. H., Kenna, H., et al. (2007). Dissociable intrinsic connectivity networks for salience processing and executive control. *J. Neurosci.* 27, 2349–2356. doi: 10.1523/jneurosci.5587-06.2007

Sridharan, D., Levitin, D. J., and Menon, V. (2008). A critical role for the right fronto-insular cortex in switching between central executive and default-mode networks. *Proc. Natl. Acad. Sci. U S A* 105, 12569–12574. doi: 10.1073/pnas.0800005105

Wang, J. F., Chen, H. Y., Liang, H. Z., Wang, W. M., Liang, Y., Liang, Y., et al. (2019). Low-frequency fluctuations amplitude signals exhibit abnormalities of intrinsic brain activities and reflect cognitive impairment in leukoaraiosis patients. *Med. Sci. Monit.* 25. doi: 10.12659/MSM.915528

Wiggins, M. E., Tanner, J., Schwab, N., Crowley, S. J., Schmalfuss, I., Brumback, B., et al. (2018). Regional leukoaraiosis cognition in non-demented older adults. *Brain Imaging Behav.* doi: 10.1007/s11682-018-9938-5 [Epub ahead of print].

Conflict of Interest Statement: The authors declare that the research was conducted in the absence of any commercial or financial relationships that could be construed as a potential conflict of interest.

frontiers in Neural Circuits

REVIEW
published: 06 August 2019
doi: 10.3389/fncir.2019.00050

Quantitative Susceptibility Mapping and Resting State Network Analyses in Parkinsonian Phenotypes—A Systematic Review of the Literature

Esther A. Pelzer[1,2]*, *Esther Florin*[1] *and Alfons Schnitzler*[1]

[1]*Institute of Clinical Neuroscience and Medical Psychology, Medical Faculty, Heinrich-Heine-University Duesseldorf, Düsseldorf, Germany,* [2]*Max-Planck Institute for Metabolism Research, Cologne, Germany*

An imbalance of iron metabolism with consecutive aggregation of α-synuclein and axonal degeneration of neurons has been postulated as the main pathological feature in the development of Parkinson's disease (PD). Quantitative susceptibility mapping (QSM) is a new imaging technique, which enables to measure structural changes caused by defective iron deposition in parkinsonian brains. Due to its novelty, its potential as a new imaging technique remains elusive for disease-specific characterization of motor and non-motor symptoms (characterizing the individual parkinsonian phenotype). Functional network changes associated with these symptoms are however frequently described for both magnetoencephalography (MEG) and resting state functional magnetic imaging (rs-fMRI). Here, we performed a systematic review of the current literature about QSM imaging, MEG and rs-fMRI in order to collect existing data about structural and functional changes caused by motor and non-motor symptoms in PD. Whereas all three techniques provide an effect in the motor domain, the understanding of network changes caused by non-motor symptoms is much more lacking for MEG and rs-fMRI, and does not yet really exist for QSM imaging. In order to better understand the influence of pathological iron distribution onto the functional outcome, whole-brain QSM analyses should be integrated in functional analyses (especially for the non-motor domain), to enable a proper pathophysiological interpretation of MEG and rs-fMRI network changes in PD. Herewith, a better understanding of the relationship between neuropathological changes, functional network changes and clinical phenotype might become possible.

Keywords: quantitative susceptibility mapping, magnetoencephallography (MEG), functional magnet resonance imaging (fMRI), motor, non-motor

OPEN ACCESS

Edited by:
Lijun Bai,
Xi'an Jiaotong University, China

Reviewed by:
Masanori Matsuzaki,
The University of Tokyo, Japan
Zang Hee Cho,
Advanced Institutes of Convergence Technology, South Korea

***Correspondence:**
Esther A. Pelzer
esther.pelzer@sf.mpg.de

Received: *12 November 2018*
Accepted: *17 July 2019*
Published: *06 August 2019*

Citation:
Pelzer EA, Florin E and Schnitzler A (2019) Quantitative Susceptibility Mapping and Resting State Network Analyses in Parkinsonian Phenotypes—A Systematic Review of the Literature. Front. Neural Circuits 13:50. doi: 10.3389/fncir.2019.00050

Abbreviations: AI, Anterior insula; ALFF, Amplitude of low frequency fluctuation; AR, Akinetic-rigidic; BOLD, Blood oxygen level dependent signal; CD, Caudate nucleus; CEN, Central execution network; dACC, Dorsal anterior cingulate cortex; DLPFC, Dorsal lateral prefrontal cortex; DMN, Default mode network; FC, Functional connectivity; FOG, Freezing of gait; GCA, Granger causality analysis; GP, Pallidum; GRE, Gradient echo; Hz, Herz; ICB, Impulsive control behavior; ICA, Independent component analysis; LFP, Local field potential; MCI, Mild cognitive impairment; MEG, Magnetoencephalography; MRI, Magnetic resonance imaging; PD, Parkinson's disease; PDD, Parkinson's disease dementia; PPC, Posterior parietal cortex; PUT, Putamen; QSM, Quantitative susceptibility mapping; ReHo, Regional Homogeneity; RN, Red nucleus; ROI, Region of interest; rs-MRI, Resting state functional magnetic resonance imaging; SMA, Supplementary motor area; SN, Substantia nigra; SNc, Substantia nigra, compact part; SNr, Substantia nigra, reticular part; STN, Subthalamic nucleus; TD, Tremor-dominant; THA, Thalamus; UPDRS, Unified Parkinson disease rating Scale.

INTRODUCTION

Quantitative susceptibility mapping (QSM) is a new technique for quantifying magnetic susceptibility (Haacke et al., 2015). It enables quantitative *in vivo* measurement of iron deposition in brain tissue of parkinsonian patients. Technically, QSM solves the deconvolution or inverse problem from a magnetic field to susceptibility source and thus maps the magnetic property of local tissue (de Rochefort et al., 2010). This local property is crucially different from the nonlocal property of traditional gradient echo (GRE) magnetic resonance imaging (MRI), including susceptibility-weighted imaging (SWI), the GRE magnitude T2*-weighted imaging and GRE phase imaging; additionally QSM and GRE MRI are considered to be sensitive to susceptibility (Wang and Liu, 2015). Iron likely stored in ferritin (Griffiths et al., 1999) is highly paramagnetic and can be sensitized in MR imaging by using relaxation contrast [such as T2-weighted imaging and R2 (1/T2) mapping] and susceptibility contrasts [such as T2*-weighted imaging and R2* (1/T2*) mapping; Liu et al., 2015]. R2* mapping has been used for a quantitative study of brain iron (Haacke et al., 2005). A recent postmortem correlation study in seven patients without signs of a neurological disorder has demonstrated that the relationship with R2* can be linear in regions of more uniform iron deposition (Langkammer et al., 2010). However, R2* mapping depends on field strength (Yao et al., 2009), contains substantial blooming artifacts that increase with echo time (Wang et al., 2013), and generally relates to iron concentration in a complex way (Liu et al., 2015). Physically meaningful regularizations, including the Bayesian approach, have been developed recently to enable accurate QSM to study iron distribution, calcification blood degradation, metabolic oxygen consumption, demyelination, and other pathophysiological susceptibility changes, as well as contrast agent bio-distribution in MRI (Wang et al., 2017). This latter development now opened the possibility to apply QSM to study iron distribution in movement disorders like Parkinson's disease (PD). Due to its novelty, its potential as a new imaging technique for disease-specific prediction of motor (Moustafa et al., 2016) and non-motor symptoms in PD (Chaudhuri et al., 2006) remains elusive. Here, we review the value of QSM imaging in the classification of different parkinsonian phenotypes and the possibility to predict parkinsonian subtypes in combination with well-established functional imaging techniques [resting state functional magnetic imaging (rs-fMRI) and magnetoencephalography (MEG)].

We propose that the combination of structural (QSM) and functional (MEG, rs-fMRI) imaging techniques may enable a more comprehensive view onto PD reflecting structural disease patterns and functional network changes characteristic for motor and non-motor subtypes in PD. These characteristic, disease-related changes measured by the proposed three imaging techniques might help to better classify individual patients with regards to their individual phenotypes. A better classification might then open the possibility for better prediction of disease course and more accurate treatment for the individual patient.

Medical electronic search engine (PubMed) was used to collect studies using QSM, MEG and rs-fMRI in patients suffering from PD (February, 2018). Mainly articles published after the year 2000 were included in the reviewing process; a few important articles, however, date back to the 1990s. The keywords used were: (Parkinson's disease OR Parkinson disease OR parkinsonian), (quantitative susceptibility mapping OR QSM), (magnetoencephalography OR MEG), (resting state functional magnetic resonance imaging OR functional connectivity in resting state functional magnetic resonance imaging OR resting state MRI). We listed all original studies in English that were retrieved with the search string.

QUANTITATIVE SUSCEPTIBILITY MAPPING

Numerous studies questioned if the QSM technique allows measuring the differences in susceptibility in Parkinsonian patients compared to controls. Langkammer et al. (2016) could extend the established finding of higher R2* rates in the SN in PD patients compared to controls by QSM showing superior sensitivity for PD-related tissue changes in nigro-striatal dopaminergic pathways including the pallidum (GP), thalamus (THA), SN and red nucleus (RN). QSM was additionally significantly correlated with the levodopa-equivalent dosage and disease severity. He et al. (2015) compared regional QSM and R2* values in patients with early-stage PD and questioned whether these techniques can be used as biomarkers for early diagnosis in PD. Here, QSM was more sensitive to pathological changes than R2* maps. In QSM measurements, bilateral SN and RN contralateral to the most affected limb showed significantly higher susceptibility values than controls, whereas R2* showed only in the SN contralateral to the most affected limb increased values in PD compared to controls. Furthermore, bilateral SN magnetic susceptibility positively correlated with disease duration and Unified Parkinson disease rating scale (UPDRS)-III scores in early PD. Murakami et al. (2015) also compared R2* measurements and QSM measurements in the following regions: THA, caudate nucleus (CD), GP, SN and RN. They only found significant differences between patients and controls in the SN and again QSM showed higher diagnostic performance than R2*. Barbosa et al. (2015) measured R2, R2* and QSM values in the SN, SNc (compact part), RN, GP, putamen (PUT), THA, white matter and gray matter and only found significant differences in the SN, predominantly in the SNc in comparison of patients with controls; again QSM was the most sensitive quantitative technique to measure iron deposition in the SN. Zhao et al. (2017) also found a significant difference in QSM values in the SN between 29 patients and 25 controls, but differently to the above presented studies, they described no significant differences between patients and controls in the R2* map. As regions of interest (ROIs) they additionally included the RN, GP, PUT and head of CD nucleus without reaching statistical significance. Additionally, they found no correlations of the UPDRS-III score and QSM or R2* values in the Parkinson

group. Azuma et al. (2016) performed an ROI analysis in the GP, RN, PUT CD, SN (anterior, medial and posterior part) and analyzed the asymmetry of mean susceptibility in PD compared to healthy controls. They worked out that QSM is useful for assessing the lateral asymmetry and spatial difference of iron deposition in the SN of patients with PD. This spatial difference of iron distribution has been considered in nigrosome-1 imaging, a subregion of the SNc that is specifically altered in PD (Kim et al., 2018). They found that high-spatial-resolution QSM combined with histogram analysis at 3 Tesla MRI could improve the diagnostic accuracy of early-stage idiopathic PD. Du et al. (2016) expanded the analyses to voxel-based midbrain (VBA-) analysis next to the above-described ROI analysis. By the application of midbrain-focused VBA, PD subjects displayed significantly higher QSM and R2* values in the SN. The total volume (cluster size) of significant QSM change was 106 mm^3 in the right and 164 mm^3 in the left midbrain, whereas the total volume of significant R2* change was 62 mm^3, distributed only in the left region of the SNc. In the ROI analysis, the QSM values and R2* values were significantly higher than in the control group with QSM being more sensitive. QSM values additionally correlated with disease duration, levodopa equivalent daily dosage (LEDD) and the UPDRS II. Acosta-Cabronero et al. (2017) performed a different approach. Besides structural analyses (subcortical volumetry, voxel-based morphometry, cortical thickness and tract-based DTI statistics), they performed a whole-brain QSM study to analyze the global distribution of iron accumulation in 25 PD compared to 50 controls. In addition to whole-brain analysis, a regional study including sub-segmentation of the SN into dorsal and ventral regions and qualitative assessment of susceptibility maps in single subjects were also performed. As already presented in the above studies, the most remarkable basal ganglia effect was an apparent magnetic susceptibility increase, which mirrors iron deposition, in the dorsal SN, though an effect was also observed in ventral regions. Increased susceptibility was also found in rostral pontine areas and in a cortical pattern consistent with known PD distributions of α-synuclein pathology: abnormalities were identified in the brainstem comprising the rostral pons (including pyramidal tracts and pontine tegmental areas co-localized with the site of the locus coeruleus), the superior cerebellar peduncle and caudal mesencephalon-seemingly spreading across pars compacta/ventral tegmental SN subregions and midbrain tegmental areas-, possibly also including dorsal raphe and oculomotor nuclei. Parts of the temporal paralimbic, prefrontal and occipito-parietal cortex and, less intensely, insular and cerebellar areas were also involved. In contrast, the striatum, as well as the primary motor and somatosensory fields, were relatively spared. The normally iron-rich cerebellar dentate nucleus (DN) had a susceptibility reduction suggesting a decrease of iron content. No significant changes were found for correlation analysis with the UPDRS-III and Mini Mental Status Examination (MMSE). Guan et al. (2017) analyzed the progressive accumulation of iron in PD patients at different stages of the disease. Forty-five patients with early PD had a Hoehn & Yahr (H&Y) stage of $\leq$2.5 and 15 patients were defined as late-stage PD with a H&Y stage $\geq$3. ROI's were drawn in SN pars reticulata (SNr), SNc, RN, PUT, GP, THA, CD (head) and DN. The SNc showed significantly increased QSM values in the early PD patients compared with the controls. In the late stage of PD regions with increased QSM values extended to the SNr, RN and GP, while the SNc continued to show increased QSM values compared with the controls. Guan et al. (2017) additionally found that the iron content in the SNc and GP was significantly correlated with the H&Y stage, and the SNc was also significantly correlated with the UPDRS-III motor scores. An et al. (2018) subdivided the patients' group according to clinical scores including the symptom severity (mild, advanced) and parkinsonian subtype [akinetic-rigidic (AR), tremor-dominant (TD) and mixed type (MT)]. In comparison to healthy controls, results redundantly showed significantly increased QSM values in the ROI region SN, whereas patients with more advanced PD showed even higher values. Both subtypes (AR and TD subtype) showed significantly enhanced values compared to controls. The iron content in the SN significantly correlated with the H&Y score, the UPDRS, the Montgomery Asberg Depression Rating Scale (MADRS) and Hamilton Anxiety scale (HAMA). In mildly affected patients, the significant correlation was only with MADRS and HAMA scores. When the disease progressed into advanced severity stage, all these clinical measures (H&Y stage, UPDRS-III, UPDRS total score, HAMA, and MADRS scores) showed a prominent correlation to SN iron content. In the three parkinsonian subtypes (AR, TD, MT), the correlation between iron content and MADRS, HAMA scores was exclusively found in AR subgroups, so that it seems that the AR subgroup was mostly affected by SN iron accumulation.

Next to the analysis of disease-specific Parkinson-related changes and the comparison to healthy controls, Sjöström et al. (2017) retrospectively compared QSM values of 15 patients with progressive supranuclear palsy, 11 multiple system atrophy and 62 PD and 14 healthy controls and found that susceptibility in the RN and GP was higher in progressive supranuclear palsy compared to PD, multiple system atrophy and HC. But susceptibility was higher in multiple system atrophy than in PD and controls and SN susceptibility was increased in PD compared to controls. These findings support that different parkinsonian disorders may have disease-specific topographical patterns of abnormal iron accumulation.

Alkemade et al. (2017) and Liu et al. (2013) could show that the calculation of QSM contrasts contributes to an improved visualization of the entire subthalamic nucleus (STN) and Ide et al. (2015) showed better differentiation between medial and lateral part of the GP and better depiction of medial GP in PD patients. All results are summarized in **Supplementary Table S1**.

Summing up, four main research questions were part of QSM analyses regarding PD: (1) ROI- analyses of basal ganglia regions (mainly comprising the region of the SN) with correlations to the motor domain; (2) only two studies found correlations with non-motor symptoms (UPDRS-II; MARDS, HAMA); (3) one whole-brain analysis of magnetic susceptibility perturbations in

PD exists; (4) QSM is applied for the improved visualization of the STN and the GP.

RESTING STATE NETWORKS IN MAGNETOENCEPHALOGRAPHY

MEG is a non-invasive modality for assessing cortical oscillatory activities with high temporal and spatial resolution; it mirrors the summed up excitatory postsynaptic potentials of neuronal populations (Hämäläinen et al., 1993). Neuronal oscillations can be classified into different frequency bands (delta: 1–3 Herz (Hz); theta: 4–7 Hz; alpha: 8–13 Hz; beta: 14–30 Hz; gamma: 30–80 Hz; fast: 80–200 Hz; ultra fast: 200–600 Hz). Functionally, oscillations are features of neuronal activity and the synchronization of oscillations, reflecting temporally precise interaction, is a likely mechanism for neuronal communication (Schnitzler and Gross, 2005). Under normal conditions in healthy subjects, increased synchrony in the beta frequency range accompanies movement preparation and disappears during the actual execution of movements (Schnitzler and Gross, 2005). In PD, synchronized oscillatory activity at beta frequency (13–30 Hz) in the basal ganglia loop is assumed to be anti-kinetic in nature and patho-physiologically relevant for the development of bradykinesia (Brown, 2006). The tremor-related network featuring oscillatory activity is harmonically related to the frequency of the tremor (Timmermann et al., 2003). Treatment with dopaminergic drugs and deep brain stimulation in the STN support the restoration of cortico-cortical interactions at the beta-frequency domain at rest with a reduction in cortical coupling (Silberstein et al., 2005; Hammond et al., 2007).

Regarding actual resting state analyses, some interesting findings have been described that show a slowing of resting state oscillatory activity. Bosboom et al. (2006) elucidated resting state oscillatory brain dynamics *via* MEG in PD patients at moderately advanced stages with and without dementia. They found in a spectral power analysis using Fast Fourier Transformation that in non-demented PD patients, relative theta power was diffusely increased and beta power concomitantly decreased, compared to controls. In central and parietal channels Gamma power was decreased. Dementia was associated with a slowing of resting state brain activity, involving delta and alpha bands, as well as a reduction in reactivity to eye-opening. In *de novo* PD patients compared to healthy controls, Stoffers et al. (2007) could confirm these findings. They applied the synchronization likelihood (SL) method (Montez et al., 2006). This measure is sensitive to both linear and nonlinear interdependencies between signals recorded over distributed brain regions. They further subdivided the alpha band in alpha1 (8–10 Hz) and alpha2 (10–13 Hz). Changes included a widespread increase in theta and low alpha power, as well as a loss of beta power overall but the frontal ROIs and a loss of gamma power overall but the right occipital ROI. Applying again the SL method in MEG, Stoffers et al. (2008a) questioned whether changes in resting-state cortico-cortical FC are a feature of early-stage PD and how functional coupling might evolve over the course of the disease and is related to clinical deficits. They found that drug-naive patients showed an overall increase in alpha1 range compared to controls. With disease progression, neighboring frequency bands were also altered. Alpha2 and beta frequency bands were positively associated with disease duration, whereas the severity of PD was associated with the theta and beta range. They were able to confirm the relationship between beta-band coupling and severity of parkinsonism, specifically bradykinesia, and found some evidence for a similar association between FC in the theta band and motor symptoms, in particular for the symptom tremor. In early-stage PD, cognitive perseveration was positively associated with increased interhemispheric FC in the 8–10 Hz range. They additionally found that the application of dopamine replacement therapy elevated SL in 4–30 Hz range in mild to moderate PD (Stoffers et al., 2008b). A strong motor response was associated with decreases in the local beta-band coupling; these results perfectly complement the findings of Silberstein et al. (2005).

Applying the SL method in MEG, Bosboom et al. (2008) compared 13 demented PD patients with 13 non-demented PD patients. Patients with PD related dementia (PDD) had lower fronto-temporal SL in the alpha range, lower intertemporal SL in delta, theta and alpha1 bands as well as decreased centro-parietal gamma-band synchronization. Moreover, higher parieto-occipital synchronization in the alpha2 and beta bands was found in PDD. Gómez et al. (2011) introduced the Lempel–Ziv complexity (LZC) method. LZC is a complexity measure for finite sequences related to the number of distinct substrings and the rate of their occurrence along the sequence (for further details please see Lempel and Ziv, 1976). They confirmed by this method that PD patients had less complex brain activity in 10 major cortical areas (frontal, central, temporal, parietal and occipital on the right and left hemisphere) and were able to distinguish patients from controls with an accuracy of 81.58%. In line with the above described studies, Pollok et al. (2012) found in an MEG study specifically focussing on S1/M1 region that patients with *de novo* PD have increased synchronized oscillatory activity within sensori-motor loops at beta frequency (13–30 Hz) during resting state modality as well as during isometric contraction compared to controls. The power of the contralateral hemisphere was significantly suppressed during isometric contraction in healthy controls. By contrast, in *de novo* patients both hemispheres were equally strongly activated. In medicated patients, the pattern was found to be reversed with a decrease of synchronized oscillatory activity within sensori-motor loops at beta-frequency. Contralateral beta power was significantly correlated with motor impairment during isometric contraction but not during rest. Pollok et al. (2012) suggested that the reduced ability of the primary motor cortex to disengage from increased synchronized beta-band oscillations during the execution of movements is an early marker of PD.

In a longitudinal study analyzing the cognitive decline in PD, Olde Dubbelink et al. (2013a) found that in contrast to healthy controls, PD patients showed a slowing of the dominant peak frequency. Additionally, analysis per frequency band showed an increase in theta power over time, along with decreases in alpha1 and alpha2 power. In PD patients, a decreasing cognitive

performance was associated with increases in delta and theta power, as well as decreases in alpha1, alpha2, and gamma power; increasing motor impairment, however, was associated with a theta power increase only.

A limitation of previous MEG studies (Bosboom et al., 2008; Stoffers et al., 2008a) is that the analyses were performed at the sensor level. Relating the functional sensor-based data to its underlying anatomical substrate is problematic, hampering the interpretation of these results. Additionally, FC calculated on sensor level may result in spurious connectivity due to volume conduction (Schoffelen and Gross, 2009). To overcome this problem, Hillebrand et al. (2012) proposed a new analysis technique, projecting sensor-based data onto an atlas-based source space using beamforming, providing a detailed anatomical mapping of cortical rhythms for 68 regions of interest corresponding to Brodmann areas. Additionally, the phase lag index (PLI) was introduced, because effects of volume conduction can be removed in either signal space or source space by estimating FC using the PLI, which is a measure that quantifies the consistency of non-zero phase differences between two signals (Stam et al., 2007). Olde Dubbelink et al. (2013b) implemented this atlas-based source-space method. To longitudinally investigate resting-state patterns FC in PD patients, eight cortical seed regions were selected: parahippocampal, inferior and middle temporal, temporal pole, orbitofrontal, precuneus, anterior cingulate and middle frontal regions. At baseline, early stage, untreated PD patients (n = 12) had lower parahippocampal and temporal delta band connectivity and higher temporal alpha1 band connectivity compared to controls. In a larger patient group (n = 43), longitudinal analyses over a 4-year period uncovered decreases in alpha1 and alpha2 band connectivity for multiple seed regions that were associated with motor or cognitive decline (alpha1: middle temporal cortex; alpha2: parahippocampal, inferior temporal, middle temporal, precuneus). Ponsen et al. (2013) applied the same method and compared 13 patients with PDD with 13 non-demented PD patients. Compared to PD patients, PDD patients had more delta and theta power in parieto-occipital and fronto-parietal areas. The PDD patients had less alpha and beta power in frontal and parieto-temporo-occipital areas. PDD patients had lower mean PLI values in the delta and alpha bands in fronto-temporal and parieto-temporo-occipital areas when compared to PD patients. Additionally, in PDD patients, connectivity between pairs of regions of interest (Brodmann areas) was stronger in the theta band and weaker in the delta, alpha and beta bands.

In order to examine large-scale structures of resting-state brain networks in PD, using concepts from graph theory, Olde Dubbelink et al. (2014) applied MEG measurements in 70 PD patients and 21 healthy controls in a longitudinal analysis over a 4-year period. They showed that impaired local efficiency (i.e., local clustering of connections) and network decentralization are very early features of PD that continue to progress over time, together with reduction of global efficiency (i.e., long-distance connections). By combining resting state MEG measurements with cognitive assessments, Olde Dubbelink et al. (2014) was able to predict dementia in PD better than with one factor alone (hazard factor: 27, 3; $p < 0.001$). Heinrichs-Graham et al. (2014) examined resting-state neurophysiological activity before and after dopamine replacement therapy in the motor network of patients with PD; they then compared this data to a group of matched controls without neurological diseases. They found that untreated patients with PD exhibited significantly decreased beta oscillations compared to controls in the bilateral motor regions and that this difference is almost normalized following dopamine replacement. Despite decreased beta oscillatory activity in the primary cortices, they found that patients with PD exhibited higher synchronicity between the left and right motor cortex, which was limited to the beta frequency and was partially normalized by dopamine replacement therapy. Boon et al. (2017) analyzed *via* MEG the pathophysiological mechanisms underlying PD cognitive decline and conversion to PD dementia. Preferential beta band information outflow was significantly higher in PD patients compared to controls for the basal ganglia and fronto-temporal cortical regions, and significantly lower for parieto-occipital regions. Additionally, in patients, low information outflow from occipital regions correlated with poor global cognitive performance. Boon et al. (2017) introduced the hypothesis that in the PD brain, a shift in balance towards a more anterior-to-posterior beta band information flow takes place and is associated with poorer cognitive performance.

But also in DBS resting state MEG becomes more and more applicable. Cao et al. (2015) investigated the effect of STN-DBS on spontaneous cortical oscillations of patients with PD, which were detected non-invasively with whole head MEG. Without surgery, a prominent slowing of resting oscillatory activities compared with healthy controls was found, consistently with previous studies (Bosboom et al., 2006). With STN-DBS switched-on, an improvement of the PD symptoms was found by suppressing the synchronization of alpha rhythm in the somato-motor region. Oswal et al. (2016) performed simultaneously MEG and intracranial local field potential (LFP) recordings and compared differences in STN-cortical coherence topographies at rest and during clinically effective high-frequency stimulation of the STN. Within the STN, DBS suppressed synchronized neuronal activity, preferentially at low beta (13–21 Hz) rather than high beta frequencies (21–30 Hz). Suppression in the low beta band correlated with motor improvement. In contrast, DBS suppressed the coupling of STN to cortical motor regions across the whole beta frequency band; this did not correlate with clinical improvement. The effect of STN DBS on coupling with cortex was spatially selective and restricted to mesial cortical areas, reflecting that coupling mediated predominantly by the hyperdirect and indirect pathways to STN (Alexander and Crutcher, 1990; Nambu et al., 2002). All results are summarized in **Supplementary Table S2**.

Summing up, three key findings from the MEG literature should be mentioned: (1) In PD, we can find a slowing of resting state oscillatory activity compared to controls, which increases during disease progression and is especially enhanced during cognitive decline. (2) The increased synchronization of beta-band activity is a pathognomic feature for the deficient motor action in PD and administration of dopamine decreases

beta-band synchronicity with an improvement of motor output. (3) Methodologically, a combination of whole-head-MEG and basal ganglia LFP recordings are nowadays possible.

RESTING STATE NETWORKS IN FUNCTIONAL MAGNETIC RESONANCE IMAGING

Spontaneous fluctuations in brain activity, as they have been described for rs-fMRI, have been detected *via* functional MRI (Fox and Raichle, 2007). The blood oxygen level dependent signal (BOLD) is an indirect measure of changes in neuronal activity. Examinations of rs-fMRI provide a non-invasive method that focuses on low-frequency spontaneous fluctuations (i.e., below 0.1 Hz) in the BOLD signal, which occurs when individuals are at rest. Numerous methods have been developed and used to study resting state FC like: (1) seed-based FC; (2) hierarchical clustering; (3) graph theory; (4) independent component analysis (ICA); (5) regional homogeneity (ReHo); (6) amplitude of low frequency fluctuation (ALFF); (7) Granger causality analysis (GCA; for a detailed overview see e.g., Prodoehl et al., 2014). A number of studies have consistently reported the formation of functionally linked resting-state networks during rest; these studies—although using different groups of subjects, different methods (e.g., seed-based FC, ICA and others) and different types of MRI protocols—, showed a large overlap between their results and indicated the robust formation of functionally linked resting state networks in the brain during rest (van den Heuvel and Hulshoff Pol, 2010).

In PD, changes of FC have been reported for different networks. We revise the literature of the most frequent networks: (1) a primary somato-motor network; (2) default mode network (DMN); (3) the left and right parietal-frontal network; (4) the salience network; and (5) a primary visual area and extra-striate visual network.

The Somato-Motor Network

Specific changes in functional neuroimaging for the sensori-motor network of patients with PD have been recently found (Tessitore et al., 2014). Wu et al. (2009) applied graph theory to examine the resting motor network in patients with mild to moderate PD, testing both with and no medication. Patients also performed a finger-tapping task to identify ROIs for the resting state motor network analysis. They found that PD patients after medication withdrawal had significantly decreased FC in supplementary motor area (SMA), left dorsal lateral prefrontal cortex (DLPFC) and left PUT and increased FC in the left cerebellum, left primary motor cortex and left parietal cortex compared to healthy controls. Application of levodopa relatively normalized the pattern of FC in PD patients. This normalization of SMA FC after levodopa administration has also been confirmed by a recent study of Esposito et al. (2013), combining an FC analysis and a spectral frequency analysis. Levodopa stimulated reduced signal fluctuations in the SMA with a selective frequency band of the sensorimotor network. Under dopaminergic therapy, Göttlich et al. (2013) even found increased connectivity within the sensorimotor network and parietal areas besides decreased connectivity in the CD nucleus, orbitofrontal and occipital regions. In another study, Wu et al. (2011) analyzed PD patients after >12 h withdrawal of levodopa compared to healthy controls *via* FC analysis. They investigated the interplay between the rostral SMA (also known as pre-SMA; mainly involved in motor preparation and initiation) and the primary motor cortex (M1; mainly involved in motor execution) by choosing these two regions as seed regions. Without dopaminergic medication, connectivity within the pre-SMA in patients with PD compared to healthy controls was increased to the right M1 and decreased to the left PUT, right insula, right premotor cortex and left inferior parietal lobule. Stronger connectivity was only found in M1 within its own local region in PD patients compared to controls. In contrast to these findings, Yu et al. (2013) found enhanced connectivity between the PUT and the SMA, although patients were also withdrawn >12 h from dopaminergic medication.

But functional changes have been found not only in cortical regions. Helmich et al. (2010) for example compared the FC profile of the posterior PUT, the anterior PUT and the CD nucleus between 41 patients and 36 matched controls and found that the posterior PUT was uniquely coupled to cortical motor areas (like SMA and M1), the anterior PUT to the pre-SMA and anterior cingulate cortex and the CD nucleus to the DLPFC. PD patients had decreased connectivity between the posterior PUT and the cortex (bilateral M1 and secondary somatosensory cortex, intra-parietal cortex, insula and cingulate motor area) after 12 h dopaminergic withdrawal. Differences between PD and healthy controls were, however, specific to the PUT: although PD patients showed decreased coupling between posterior PUT and the inferior parietal cortex, this region showed increased FC with the anterior PUT, suggesting a (maybe compensatory) modulation of existing functional networks.

In light of the study design of Helmich et al. (2010), Manza et al. (2016) also subdivided the striatum in an anterior, posterior PUT and ventral and posterior CD nucleus in early-stage PD. First, they found that higher motor deficit rating was associated with a weaker coupling between the anterior PUT and midbrain including SN; second, a decline in cognitive function, particularly in the memory and visuo-spatial domains, was associated with stronger coupling between dorsal CD nucleus and rostral anterior cingulate cortex. Following Braak's theory (Braak et al., 2004), a recent study by Hacker et al. (2012) focussed on changes in functional network integrity regarding the brainstem. They compared 13 patients with PD and 19 age-matched controls and found that the PD group had markedly lower striatal correlations with the THA, midbrain, pons and cerebellum. Comparing PD to controls, focally altered FC was also observed in sensori-motor and visual areas of the cerebral cortex, as well as in the supramarginal gyrus.

By applying a seed-based approach with four ROI's in each hemisphere (CD, PUT, GP and THA), Agosta et al. (2014) compared cortico-striatal-thalamic network FC in treated and untreated PD patients and controls to study the effect of levodopa on these networks. Patients without dopaminergic stimulation had an increased FC between the left and right basal ganglia and decreased connectivity of the affected CD

nucleus and THA with ipsilateral frontal and insular cortices. Compared with healthy controls and untreated PD patients, PD patients under dopaminergic stimulation showed a decreased FC among the striatal and thalamic regions and increased FC between the striatum and temporal cortex and between the THA and several sensori-motor, parietal and occipital regions. Summing up, levodopa in this study was able to facilitate a compensation of functional abnormalities through an increased FC in the THA. In both groups (untreated/treated), patients with a more severe motor disability had an increased striatal and/or thalamic FC with temporal, parietal, occipital and cerebellar regions.

Sharman et al. (2013) found in general reduced sensori-motor circuit connections within the basal ganglia and between basal ganglia and the THA in PD patients without dopaminergic medication compared to healthy controls. The sensori-motor cortex showed reduced connectivity with the THA. The globus pallidus showed reduced connectivity with both the PUT and the THA in PD patients. Connections of the SN were reduced with the globus pallidus, the PUT and THA in PD patients compared to controls. Increased FC was only observed for non-sensori-motor connections between PUT and associative cortex, THA and limbic cortex as well as between the PUT and THA.

Bell et al. (2015) also found impaired striatal interconnectivity in PD without dopaminergic medication with a pathological decoupling of the striatum from the thalamic and sensori-motor networks. The application of dopaminergic medication significantly improved connectivity across striatal subdivisions.

Kwak et al. (2010) applied FC and frequency content analysis to study the modulation in basal ganglia thalamo-cortical networks in six striatal seed regions [(1) inferior; (2) superior ventral striatum; (3) dorsal CD; (4) dorsal caudal; (5) rostral; and (6) ventral rostral PUT]. In apparent contradiction with the results of Kwak et al. (2010), Esposito et al. (2013) reported that levodopa treatments reduce, rather than increase, the amplitude of low-frequency oscillations, thereby restoring the normal oscillations in an otherwise functionally hyperconnected resting brain. Both studies have, however, remarkable methodological differences (drug-naïve PD vs. levodopa withdrawal in chronically treated PD patients; ICA vs. "full variance" voxel-level time course), so these results should be interpreted carefully.

By studying the sensori-motor system, one important nucleus should not be neglected: the STN. Baudrexel et al. (2011) investigated alterations in the FC profile of the STN in a voxel-by-voxel fMRI study by comparing early-stage PD patients (n = 31) after dopaminergic withdrawal with healthy controls (n = 44). The analysis revealed increased FC between the STN and cortical motor areas [primary motor cortex (M1), premotor cortex and SMA] in line with electrophysiological studies. FC analysis in the M1 hand area elucidated that the FC increase was primarily found in the STN area within the BG, suggesting that increased STN-motor cortex synchronicity mediated *via* the so-called hyperdirect motor cortex-subthalamic pathway might play a crucial role in the pathophysiology of PD. Increased FC between these two areas was also found in early drug-naïve PD patients before application of dopamine (Kurani et al., 2015). Few articles reported FC of STN and motor area in PD patients during the intake of dopaminergic medication. Fernández-Seara et al. (2015) showed an increased FC between the STN and motor cortex just like in PD patients after dopaminergic medication by using arterial spin-labeled perfusion fMRI, whereas Mathys et al. (2016) did not find a change in the FC between the two areas. Shen et al. (2017) compared changes in 31 PD patients under dopaminergic medication with healthy controls and found that, in line with the findings of Braudexel, an increased FC was found between the STN and the sensorimotor cortex, which was related to motor symptom severity in on-medicated patients. All results are summarized in **Supplementary Table S3**.

The Default Mode Network

The DMN consists of the following brain regions: the precuneus, medial frontal, inferior parietal cortical regions and medial temporal lobe. Studies analyzing changes in the DMN in PD have produced diverse results. Applying ICA, Krajcovicova et al. (2012) found no differences in the DMN between patients and controls, comparing cognitively intact patients and controls; patients were however on dopaminergic medication and were not subdivided by the different phenotypes (AR; TD). Comparing PD cognitively unimpaired patients and controls by applying ICA *via* resting state MRI, FC have been found to be decreased in the right medial temporal lobe and bilateral inferior parietal cortex within the DMN (Tessitore et al., 2012b). Karunanayaka et al. (2016) again applied ICA and questioned whether PD_{AR} has different FC patterns in the DMN when compared to PD_{TD} and healthy controls; they found that there was a decreased activity in the left inferior parietal cortex and the left posterior cingulate cortex. PD patients were treated with anti-parkinsonian medication, except for two subjects, who had very mild symptoms and were drug-naïve. Due to the fact that dopamine replacement therapy has an influence on resting state networks (Tahmasian et al., 2015), Hou et al. (2017) included cognitively unimpaired and drug-naïve PD_{AR} patients in his study. Still, they found a decline in FC of the posterior DMN and enhanced compensatory FC of the anterior DMN in early-stage drug-naïve PD_{AR} prior to clinical evidence of cognitive impairment. Non-demented PD patients with and without hallucinations showed reduced connectivity during resting state in the DMN compared to healthy controls. Patients with hallucinations had however significantly greater connectivity in the DMN compared to patients without visual hallucinations. The levodopa dosage was controlled for both groups (Yao et al., 2014).

Disbrow et al. (2014) found a dependency between FC in the DMN and the cognitive dysfunction in non-demented PD patients compared to healthy controls. They found that DMN FC was decreased in the PD group, specifically between posterior cingulate, medial prefrontal and inferior parietal nodes. Greater DMN-FC was related to faster processing speed in the PD group.

Amboni et al. (2014) went one step further and investigated whether patients with mild cognitive impairment (MCI) have differences in FC in the DMN compared to patients without MCI. Both groups were then further compared to healthy controls. Again, both PD groups showed a general decrease

in the DMN connectivity compared with controls. But PD patients with MCI additionally showed a decreased FC of the bilateral prefrontal cortex within the fronto-parietal network. The decreased prefrontal cortex connectivity correlated with cognitive parameters, but not with clinical variables. Hou et al. (2016) compared drug-naïve patients with MCI with patients with unimpaired cognition and healthy controls in a seed-based approach. They also found reduced FC in the DMN in patients with MCI compared to healthy controls, but also in a set of other regions including the precentral gyrus, middle temporal gyrus, insula, anterior inferior parietal lobule and middle frontal gyrus. In the DMN patients with MCI had decreased FC between the hippocampal formation and inferior frontal gyrus, between the posterior cingulate gyrus and posterior inferior parietal lobule and between the anterior temporal lobe and inferior frontal gyrus compared to controls. In another seed-based approach, Gorges et al. (2015) compared the intrinsic FC in cognitively-unimpaired and cognitively-impaired patients. They found that cognitively-impaired patients compared to healthy controls mainly had decreased FC in the DMN. Patients who were cognitively unimpaired had network expansions with significantly increased intrinsic FC in cortical, limbic and basal-ganglia-thalamic areas; as suggested by the authors this might be an adaptive (compensatory mechanism) by recruiting additional resources to maintain normal cognitive performance. Changes in the DMN associated with cognitive impairment have also been confirmed by a recent study of Lucas-Jiménez et al. (2016). Changes of FC in the DMN have also been related to saccadic performance in PD (Gorges et al., 2013); changes in saccadic performance are described to be associated with cognitive changes (Mosimann et al., 2005).

The interaction of the DMN with other structures in the brain also needs to be considered. Hu et al. (2015), for example, compared 20 depressed with 40 non-depressed PD patients and 43 controls. They found stronger connectivity between the left median cingulate cortex and the DMN in depressed PD patients.

The Fronto-Parietal Network

Via functional activation studies it has been shown that the fronto-parietal network, which consists of the DLPFC and the posterior parietal cortex (PPC) is involved in the "top down" control of executive control (Markett et al., 2014; Gratwicke et al., 2015). Tessitore et al. (2012a) reported in a fMRI resting state paradigm that patients with freezing of gait (FOG) had a different pattern of activation in the executive attentional network e.g., the right fronto-parietal network (right middle frontal gyrus) as well as in visual networks (right occipito-temporal gyrus). Their findings suggested that a disruption of "executive-attention" and visual neural networks is associated with the development of FOG. Regarding the amplitude of low-frequency fluctuation (ALFF), Zang et al. (2007) hypothesized that ALFF measures the amplitude of low-frequency (0.01–0.08 Hz) BOLD signal and can be used as an index of local spontaneous neural activity in resting state. Mi et al. (2017) applied this resting state method in PD patients with FOG and compared resulting ALFF measures to patients without FOG and HC. They found that FOG is associated with a dysfunction within fronto-parietal regions, along with increased inhibitory output from the basal ganglia. Additionally, they reported altered activity of cerebellum, implicating its role in the pathophysiology of FOG. Comparing patients with postural instability and gate disorder to TD patients, the latter group had specific hyper-connectivity between motor cortical areas and the inferior parietal lobule. These findings, correlated with a reduced behavioral impairment, suggest compensatory mechanisms in PD patients with tremor (Vervoort et al., 2016). FOG is frequently associated with depression (Giladi and Hausdorff, 2006) and interestingly also depressive PD patients show increased FC in the left fronto-parietal network in addition to increased FC in basal ganglia and decreased FC in salience network and DMN (Wei et al., 2017). The authors also reported hyper-connectivity between the DMN and the left fronto-parietal network in depressed PD. Boord et al. (2017) examined task activated attentional networks and their possible relationship with FC changes in resting state; they found that a weakened interaction between the default mode and task-positive networks might alter the way in which the executive response is processed in PD. Higher activation was found in patients with PD in four regions of the dorsal attention and fronto-parietal networks, namely right frontal eye field, left and right intraparietal sulcus, and precuneus during increased executive challenges. In three regions, they worked out reduced resting state connectivity to the DMN. Further, whereas higher task activation in the right intraparietal sulcus correlated with reduced resting state connectivity between right intraparietal sulcus and the precuneus in healthy controls, this relationship was absent in PD subjects.

The Salience Network

The salience network is an intrinsically connected large-scale network anchored in the anterior insula (AI) and dorsal anterior cingulate cortex (dACC; Menon and Uddin, 2010). Next to the AI and the dACC, it includes three key subcortical structures: the amygdala, the ventral striatum and the SN/ventral tegmental area. In the past, the insula was thought to be primarily a limbic cortical structure. Nowadays, it has become clearer that this part of the brain is highly involved in integrating somatosensory, autonomic and cognitive-affective information to guide behavior. Thus, it acts as a central hub for processing relevant information related to the state of the body as well as cognitive and mood states. According to Braak's staging hypothesis of PD progression, alpha-synuclein is highly deposited in the insula when Braak's stage 5 is reached (Braak et al., 2006). An involvement of the insula in the generation of non-motor symptoms in PD seems likely (Christopher et al., 2014).

Nowadays, apart from pure task-related activations in fMRI, resting state analysis allows the measurement of FC in the salience network at rest. Wu et al. (2011) for example found that the right mid-AI has reduced FC to the pre-SMA in PD compared with healthy controls (Wu et al., 2011). In addition to motor symptoms, non-motor symptoms, as they are frequently present in PD, should also be considered: fatigue might be explained by a dysfunction of the salience network (Li et al., 2017; Zhang et al., 2017). But also a role in the cognitive decline in PD has

been found for the salience network. Especially the coordination of switching between different networks (like DMN, central executive or dorsal attention network) in cognitive tasks seems to be regulated by e.g., the AI and the ACC (Sridharan et al., 2008; Baggio et al., 2015). The central executive network (CEN) is a fronto-parietal network that is crucial to working memory and cognitive control of thought, emotion and behavior (Menon, 2011). Regarding impulsive control behaviors (ICB), the presence of ICB symptoms was associated with increased connectivity in the salience network and the DMN, as well as with decreased connectivity within the CEN (Tessitore et al., 2017b). Drug-naïve PD patients who develop ICB in a 36 months observation time period showed at baseline a decreased connectivity in the DMN and CEN and increased connectivity in the salience network. These results suggest that these cognitive and limbic connectivity changes are predictive for the development of ICB in PD (Tessitore et al., 2017a).

Visual Network

Visual hallucinations are the most common manifestation of psychosis in PD and are predictive of a rapid cognitive decline. Rektorova et al. (2012) compared patients with Parkinson's disease dementia (PDD) with patients without dementia and controls *via* seed-based fMRI. Using the Cd nucleus as a seed for the extra-striatal visual resting state network, they found significant decreases of connectivity in the left and right inferior occipital gyrus in PDD as compared to HC, in addition to connectivity changes within the DMN.

Summing up, in rs-MRI analyses, patients with PD present with multiple network changes like: (1) abnormal signaling in the SMA; (2) decreased functional connectivity between the striatum and cortical regions; (3) abnormal STN-motor-cortex synchronicity resulting in motor impairment, like bradykinesia. Functional connectivity changes in the (4) DMN are frequently found not only in cognitively impaired PD patients, but also in patients with FOG and depression. Fatigue, but also cognitive decline, are caused by impaired functional connectivity of the; (5) salience network. In addition to connectivity changes within the DMN, significant decreases of connectivity; and (6) in the left and right inferior occipital gyrus appear in patients with PDD (Rektorova et al., 2012).

Limitations of Functional rs-fMRI

It is important to note that we only referred to articles about "functional connectivity" (FC) in this review article. FC only refers to the statistical interdependence of the signal from different areas (for an overview see e.g., Friston, 2011). In addition, other possibilities to measure connectivity exist in neuroimaging: (i) structural connectivity or so-called anatomical connectivity, which refers to the existence and structural integrity of tracts connecting different brain areas (Jbabdi et al., 2015); (ii) effective connectivity, which brings the element of causation into the connection analysis, that means that activity in one area causally affects activity in another area (for further details see Friston, 2011).

The rs-fMRI for functional connectome, to which we referred to in this review, has obvious limitations, as it is neither able to give information about the underlying structure nor the direction and how different areas are influenced by each other. Therefore, our proposal of combining different methodological approaches (QSM, rs-fMRI, MEG) should be seen as an idea/starting point but does still not tell the whole truth of the underlying network. The interpretation of combinations between the different connectome analyses are challenging and are part of actual discussions, see e.g., Uddin (2013), Wang and Liu (2015) and Stam et al. (2016). To characterize brain networks properly, structural and effective connectivity analyses should also be part of combination studies in order to adequately elucidate pathological network changes in e.g., neurodegenerative diseases to classify parkinsonian phenotypes.

DISCUSSION

In this review article, we present three different imaging entities, which enable a view into structural and functional abnormalities in PD patients: (1) QSM imaging; (2) MEG; and (3) rs-fMRI. All described methods have a high potential to analyze pathophysiological changes in PD networks with a different accentuation of network changes in both the motor and non-motor domain, as summed up exemplary in **Supplementary Tables S1–S3**.

As can be seen in the different tables, the most challenging factor for the prediction of the parkinsonian phenotype is a proper control of the heterogeneity of parkinsonian symptoms. In all studies we found: (i) PD-independent factors (e.g., age, handedness, gender); (ii) PD-characteristic factors like the existence of (a) non-motor symptoms (cognitive functioning, obstipation, hallucinations e.g. Wu et al., 2017); (b) motor symptoms (tremor, rigor, akinesia, postural instability e.g., Obeso et al., 2017). Additionally, (c) symptom onset; (d) disease duration; and (e) duration of dopaminergic treatment with dopaminergic agonists or levodopa and the (f) treatment response to dopamine were important to characterize the individual PD phenotype. All these symptoms and characteristics can appear simultaneously in one patient; but some patients solely have one single symptom. This heterogeneity makes a prediction of a single course of the disease challenging and methods are needed to better understand the pathophysiological background of differences in the development of the clinical phenotype. This knowledge could help to potentially modulate the disease course of each patient individually.

Despite these challenges, a combination of structural (QSM) and functional data (rs-MRI, MEG) might allow a further classification and a possible prediction of the parkinsonian phenotypes as exemplarily proposed for the impaired motor network in **Figure 1** and cognitively-impaired/demented patients in **Figure 2**: (1) whereas the key knowledge in QSM imaging in PD lies at the actual time point in the ROI-analysis at subcortical level (specifically in the SN) and correlation analyses with disease-specific changes regarding the motor domain; (2) MEG studies predominantly investigate the influence of network changes explaining motor symptoms (e.g., *via* changes

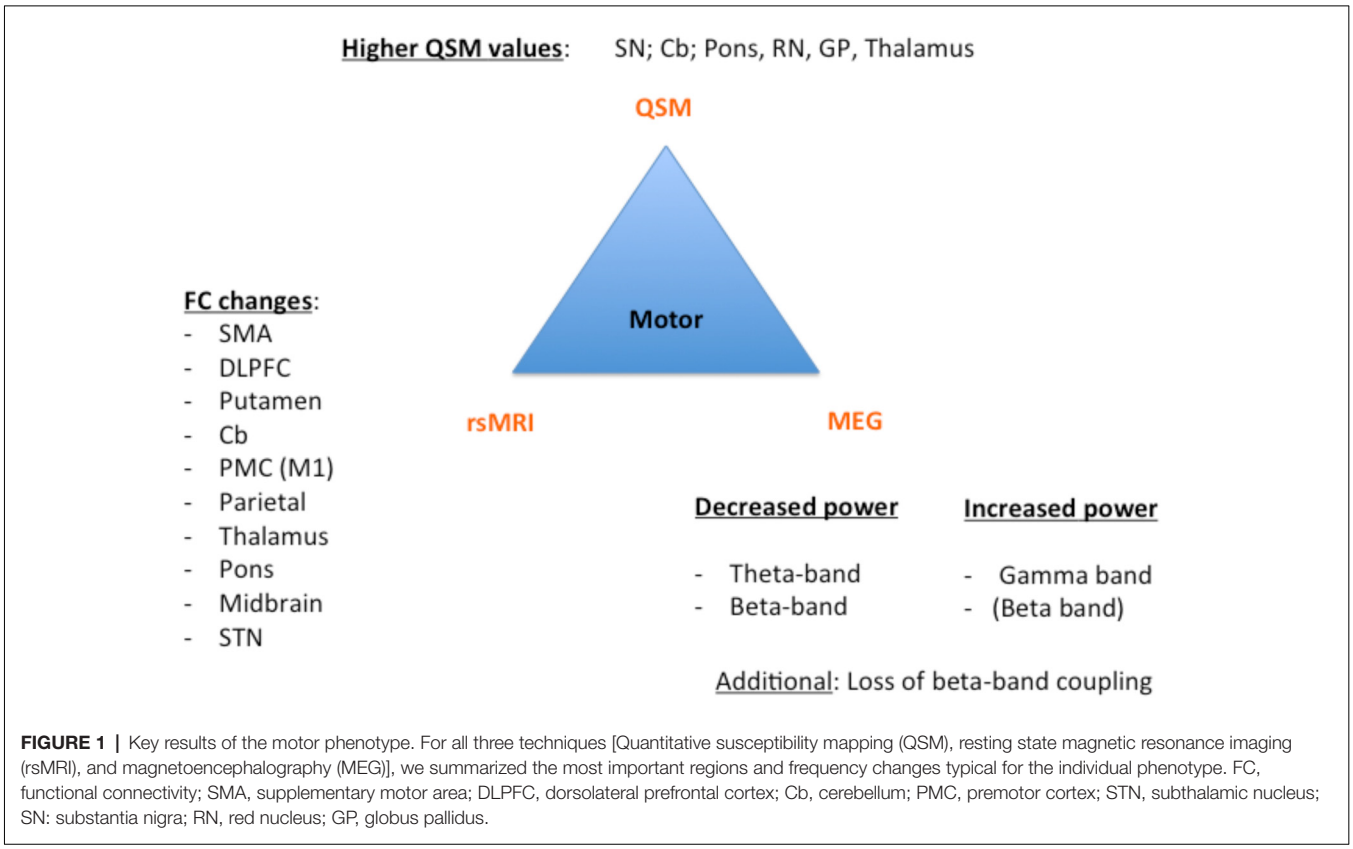

FIGURE 1 | Key results of the motor phenotype. For all three techniques [Quantitative susceptibility mapping (QSM), resting state magnetic resonance imaging (rsMRI), and magnetoencephalography (MEG)], we summarized the most important regions and frequency changes typical for the individual phenotype. FC, functional connectivity; SMA, supplementary motor area; DLPFC, dorsolateral prefrontal cortex; Cb, cerebellum; PMC, premotor cortex; STN, subthalamic nucleus; SN: substantia nigra; RN, red nucleus; GP, globus pallidus.

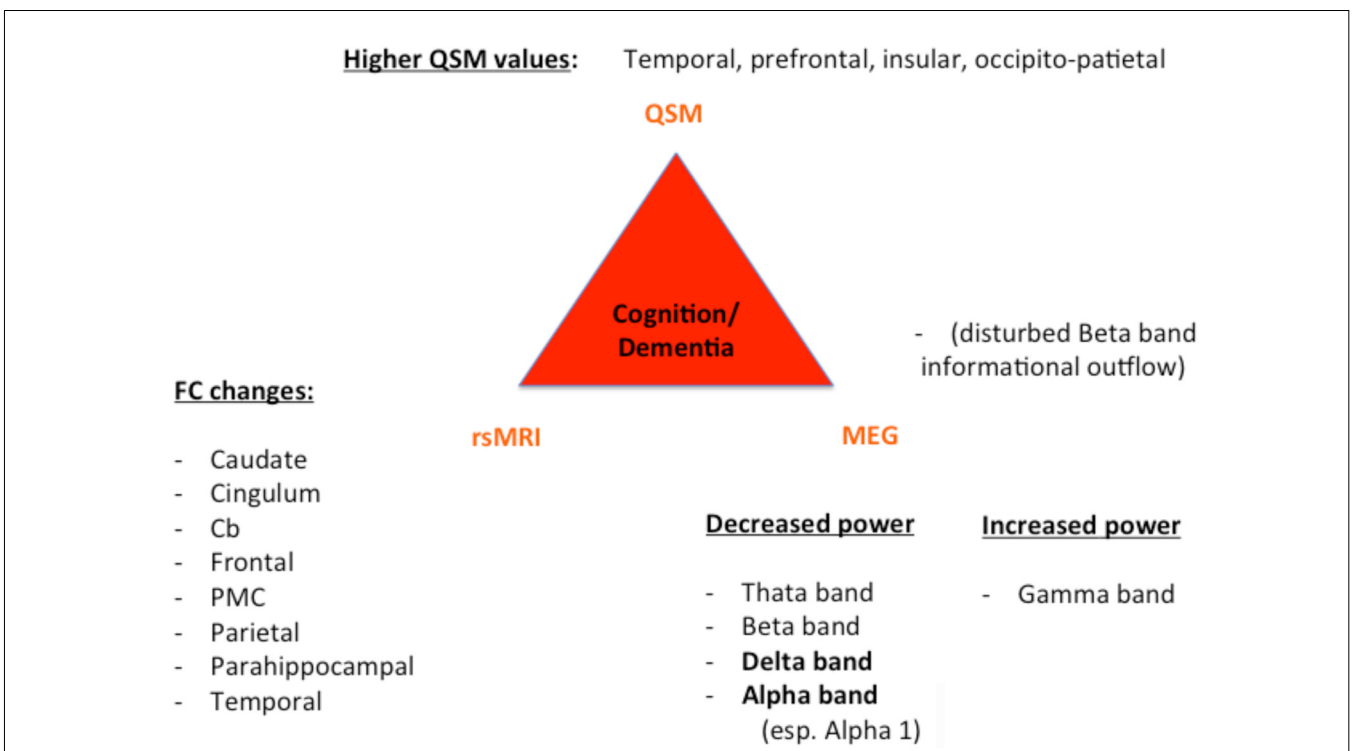

FIGURE 2 | Key results of patients with cognitive decline/dementia. For all three techniques (QSM, rsMRI, and MEG), we summarized the most important regions and frequency changes typical for the individual phenotype. FC, functional connectivity; Cb, cerebellum; PMC, premotor cortex.

in the beta band) and non-motor symptoms (e.g., *via* the increase of slowing of brain activity specifically in demented PD patients) at cortical level. The whole-brain analyses of (3) rs-fMRI build a bridge between QSM imaging and MEG to combine subcortical and cortical network changes. Rs-fMRI, as already mentioned above, has a high impact to improve our understanding of global network changes, especially for the non-motor domain; but, it has also obvious limitations, as it is neither able to give information about the underlying structure nor the direction, how different areas are influenced by each other. Due to its importance, we point to the section "Limitations of Functional rsMRI" (see above), which should not be neglected in the context of rs-fMRI network analyses.

One additional fact has to be mentioned: whereas MEG has the ability to measure activity changes in different networks with a high temporal resolution (but low spatial resolution), rs-fMRI shows changes in different brain networks with a high spatial resolution (as here exemplary described for the somato-motor, DMN, frontal-parietal, salience and visual network). However, despite this very high spatial resolution, it measures BOLD changes, which are the hemodynamic, indirect, answers to brain activity; hence the temporal resolution of rs-fMRI is low. Herewith the combination of rs-fMRI and MEG analyses seems reasonable to close the gap between temporal and spatial resolution in order to capture the full disease pathology. QSM imaging might herewith give an additional answer of the structural disease pathology underlying these functional changes (Wang et al., 2016).

Central to the pathophysiology of PD is the oxidative stress and a pathological protein aggregation, which leads to the degeneration of neurons (Dias et al., 2013; Hwang, 2013); specifically dopaminergic neurons are affected in PD. A number of mechanisms for the generation of reactive oxygen species exist, including the metabolism of dopamine itself, mitochondrial dysfunction, iron, neuro-inflammatory cells, calcium, and aging (Medeiros et al., 2016). QSM imaging enables the analysis of intrinsic tissue property with a mapping of iron (Haacke et al., 2015) and herewith QSM imaging delivers a new method to get basic information about the disease pathology in PD and should be integrated with studies about non-motor symptoms in PD. The accumulation of α-synuclein is a key neuro-pathological finding in parkinsonian brains. It is a small soluble protein and the primary structural component of Lewy bodies (Spillantini et al., 1997). Hence, Rietdijk et al. (2017) postulated a distribution of Lewy bodies throughout the whole brain, although the predictive value for disease stage of PD has been re-evaluated critically (Burke et al., 2008). It has been found that the interactions between α-synuclein and iron are closely related and the appearance of each other yields to a vicious circle, in which higher levels of α-synuclein evoke increased iron accumulation. This iron accumulation hence triggers the aggregation of α-synuclein (Lingor et al., 2017) and increases the oxidative stress with a destruction of neurons (Sian-Hülsmann et al., 2011); therefore QSM imaging, measuring the impaired iron distribution in the parkinsonian brain, might give the neuropathological answer to dysfunctional neuronal networks (measured by MEG and rs-fMRI) in PD.

Although QSM imaging has a strong impact on the imaging of subcortical levels (especially of the SN), the role of QSM at the cortical level for non-motor symptom studies is still questionable. In most of the QSM imaging studies using the regularization method [except for **C**alculation **o**f **s**usceptibility through **m**ultiple **o**rientation **s**ampling, COSMOS (Liu et al., 2015), which is not practical, but can obtain the gold-standard map through QSM imaging in various directions] discussions exists of how to overcome the artificial errors in cortical levels. Problems exist especially in overcoming the inverse problem of QSM imaging due to the missing discrimination of iron at cortical levels, their relations between QSM value and the aggregation of α-synuclein (Wang and Liu, 2015). The complex underlying physics raises the question "of how the signal is influenced in QSM imaging" (Acosta-Cabronero et al., 2016): (i) excessive background susceptibility effects, imperfect QSM inversion, registration errors; (ii) signal changes due to individual parameters (e.g., age, symptom onset); (iii) other paramagnetic metals (e.g., copper, manganese). All these factors require a careful handling and make the interpretation of whole-brain QSM imaging challenging. The new whole-brain approach of Acosta-Cabronero et al. (2017) should, from our point of view, be integrated in future QSM analyses to enable a pathophysiological interpretation of functional changes also in the non-motor domain. In line with this, the feasibility of integration of whole-brain QSM analyses in the non-motor domain has been recently shown for cognitive decline in patients with PD, showing that a higher iron load in the bilateral hippocampus is present in PDD patients (Li et al., 2018). The on-going development of new QSM imaging schemes (Jang et al., 2019) and higher field strengths in QSM imaging (e.g., 7T; Deistung et al., 2013) opens the additional possibility for *in vivo* histology and might herewith yield to a better comprehension of the development of parkinsonian phenotypes and their relationship to the iron metabolism.

CONCLUSION

QSM imaging is a new method that is applicable to detect pathophysiological changes in the parkinsonian brain, which rely on iron accumulation indirectly interfering with the α-synuclein pathology. Together with functional measurements (like rsMRI and MEG) QSM imaging might open the possibility to better classify different parkinsonian phenotypes (including both the motor and non-motor domain) *via* a combination of structure and function. The further classification of parkinsonian phenotypes could provide insights into different disease patterns and courses, which might open the way to new therapeutic strategies to reduce parkinsonian symptoms.

AUTHOR CONTRIBUTIONS

EP: substantial contributions to the conception and design of the work. Additionally, substantial contribution to

the acquisition, analysis and interpretation of data for the work. EF: critically revising the manuscript and providing additional information in the MEG section. AS: drafting the work and revising it critically for important intellectual content.

FUNDING

EF gratefully acknowledges support by the Volkswagen Foundation (Lichtenberg program 89387).

SUPPLEMENTARY MATERIAL

The Supplementary Material for this article can be found online at: https://www.frontiersin.org/articles/10.3389/fncir.2019.00050/full#supplementary-material

TABLE S1 | Overview of key results for QSM imaging studies.

TABLE S2 | Overview of key results for resting state analyses of MEG studies.

TABLE S3 | Overview of key results in resting state analyses for fMRI studies at the example of the somato-motor network.

REFERENCES

Acosta-Cabronero, J., Betts, M. J., Cardenas-Blanco, A., Yang, S., and Nestor, P. J. (2016). *In vivo* MRI mapping of brain iron deposition across the adult lifespan. *J. Neurosci.* 36, 364–374. doi: 10.1523/JNEUROSCI.1907-15.2016

Acosta-Cabronero, J., Cardenas-Blanco, A., Betts, M. J., Butryn, M., Valdes-Herrera, J. P., Galazky, I., et al. (2017). The whole-brain pattern of magnetic susceptibility perturbations in Parkinson's disease. *Brain* 140, 118–131. doi: 10.1093/brain/aww278

Agosta, F., Caso, F., Stankovic, I., Inuggi, A., Petrovic, I., Svetel, M., et al. (2014). Cortico-striatal-thalamic network functional connectivity in hemiparkinsonism. *Neurobiol. Aging* 35, 2592–2602. doi: 10.1016/j.neurobiolaging.2014.05.032

Alexander, G. E., and Crutcher, M. D. (1990). Functional architecture of basal ganglia circuits: neural substrates of parallel processing. *Trends Neurosci.* 13, 266–271. doi: 10.1016/0166-2236(90)90107-l

Alkemade, A., de Hollander, G., Keuken, M. C., Schäfer, A., Ott, D. V. M., Schwarz, J., et al. (2017). Comparison of T2*-weighted and QSM contrasts in Parkinson's disease to visualize the STN with MRI. *PLoS One* 12:e0176130. doi: 10.1371/journal.pone.0176130

Amboni, M., Tessitore, A., Esposito, F., Santangelo, G., Picillo, M., Vitale, C., et al. (2014). Resting-state functional connectivity associated with mild cognitive impairment in Parkinson's disease. *J. Neurol.* 262, 425–434. doi: 10.1007/s00415-014-7591-5

An, H., Zeng, X., Niu, T., Li, G., Yang, J., Zheng, L., et al. (2018). Quantifying iron deposition within the substantia nigra of Parkinson's disease by quantitative susceptibility mapping. *J. Neurol. Sci.* 386, 46–52. doi: 10.1016/j.jns.2018.01.008

Azuma, M., Hirai, T., Yamada, K., Yamashita, S., Ando, Y., Tateishi, M., et al. (2016). Lateral asymmetry and spatial difference of iron deposition in the substantia nigra of patients with Parkinson disease measured with quantitative susceptibility mapping. *Am. J. Neuroradiol.* 37, 782–788. doi: 10.3174/ajnr.a4645

Baggio, H.-C., Segura, B., Sala-Llonch, R., Marti, M.-J., Valldeoriola, F., Compta, Y., et al. (2015). Cognitive impairment and resting-state network connectivity in Parkinson's disease. *Hum. Brain Mapp.* 36, 199–212. doi: 10.1002/hbm.22622

Barbosa, J. H. O., Santos, A. C., Tumas, V., Liu, M., Zheng, W., Haacke, E. M., et al. (2015). Quantifying brain iron deposition in patients with Parkinson's disease using quantitative susceptibility mapping, R2 and R2. *Magn. Reson. Imaging* 33, 559–565. doi: 10.1016/j.mri.2015.02.021

Baudrexel, S., Witte, T., Seifried, C., von Wegner, F., Beissner, F., Klein, J. C., et al. (2011). Resting state fMRI reveals increased subthalamic nucleus-motor cortex connectivity in Parkinson's disease. *Neuroimage* 55, 1728–1738. doi: 10.1016/j.neuroimage.2011.01.017

Bell, P. T., Gilat, M., O'Callaghan, C., Copland, D. A., Frank, M. J., Lewis, S. J. G., et al. (2015). Dopaminergic basis for impairments in functional connectivity across subdivisions of the striatum in Parkinson's disease. *Hum. Brain Mapp.* 36, 1278–1291. doi: 10.1002/hbm.22701

Boon, L. I., Hillebrand, A., Olde Dubbelink, K. T. E., Stam, C. J., and Berendse, H. W. (2017). Changes in resting-state directed connectivity in cortico-subcortical networks correlate with cognitive function in Parkinson's disease. *Clin. Neurophysiol.* 128, 1319–1326. doi: 10.1016/j.clinph.2017.04.024

Boord, P., Madhyastha, T. M., Askren, M. K., and Grabowski, T. J. (2017). Executive attention networks show altered relationship with default mode network in PD. *Neuroimage Clin.* 13, 1–8. doi: 10.1016/j.nicl.2016.11.004

Bosboom, J. L. W., Stoffers, D., Stam, C. J., van Dijk, B. W., Verbunt, J., Berendse, H. W., et al. (2006). Resting state oscillatory brain dynamics in Parkinson's disease: an MEG study. *Clin. Neurophysiol.* 117, 2521–2531. doi: 10.1016/j.clinph.2006.06.720

Bosboom, J. L. W., Stoffers, D., Wolters, E. C., Stam, C. J., and Berendse, H. W. (2008). MEG resting state functional connectivity in Parkinson's disease related dementia. *J. Neural Transm.* 116, 193–202. doi: 10.1007/s00702-008-0132-6

Braak, H., Bohl, J. R., Müller, C. M., Rüb, U., de Vos, R. A. I., and Del Tredici, K. (2006). Stanley Fahn Lecture 2005: the staging procedure for the inclusion body pathology associated with sporadic Parkinson's disease reconsidered. *Mov. Disord.* 21, 2042–2051. doi: 10.1002/mds.21065

Braak, H., Ghebremedhin, E., Rüb, U., Bratzke, H., and Del Tredici, K. (2004). Stages in the development of Parkinson's disease-related pathology. *Cell Tissue Res.* 318, 121–134. doi: 10.1007/s00441-004-0956-9

Brown, P. (2006). "Bad oscillations in Parkinson's disease," in *Parkinson's Disease and Related Disorders*, eds P. Riederer, H. Reichmann, M. B. H. Youdim and M. Gerlach (Vienna: Springer), 27–30. doi: 10.1007/978-3-211-45295-0_6

Burke, R. E., Dauer, W. T., and Vonsattel, J. P. G. (2008). A critical evaluation of the Braak staging scheme for Parkinson's disease. *Ann. Neurol.* 64, 485–491. doi: 10.1002/ana.21541

Cao, C., Li, D., Jiang, T., Ince, N. F., Zhan, S., Zhang, J., et al. (2015). Resting state cortical oscillations of patients with Parkinson disease and with and without subthalamic deep brain stimulation: a magnetoencephalography study. *J. Clin. Neurophysiol.* 32, 109–118. doi: 10.1097/WNP.0000000000000137

Chaudhuri, K. R., Healy, D. G., and Schapira, A. H. (2006). Non-motor symptoms of Parkinson's disease: diagnosis and management. *Lancet Neurol.* 5, 235–245. doi: 10.1016/S1474-4422(06)70373-8

Christopher, L., Koshimori, Y., Lang, A. E., Criaud, M., and Strafella, A. P. (2014). Uncovering the role of the insula in non-motor symptoms of Parkinson's disease. *Brain* 137, 2143–2154. doi: 10.1093/brain/awu084

de Rochefort, L., Liu, T., Kressler, B., Liu, J., Spincemaille, P., Lebon, V., et al. (2010). Quantitative susceptibility map reconstruction from MR phase data using bayesian regularization: validation and application to brain imaging. *Magn. Reson. Med.* 63, 194–206. doi: 10.1002/mrm.22187

Deistung, A., Schäfer, A., Schweser, F., Biedermann, U., Turner, R., and Reichenbach, J. R. (2013). Toward *in vivo* histology: a comparison of quantitative susceptibility mapping (QSM) with magnitude-, phase-, and R2*-imaging at ultra-high magnetic field strength. *Neuroimage* 65, 299–314. doi: 10.1016/j.neuroimage.2012.09.055

Dias, V., Junn, E., and Mouradian, M. M. (2013). The role of oxidative stress in Parkinson's disease. *J. Parkinsons Dis.* 3, 461–491. doi: 10.3233/JPD-130230

Disbrow, E. A., Carmichael, O., He, J., Lanni, K. E., Dressler, E. M., Zhang, L., et al. (2014). Resting state functional connectivity is associated with cognitive dysfunction in non-demented people with Parkinson's disease. *J. Parkinsons Dis.* 4, 453–465. doi: 10.3233/JPD-130341

Du, G., Liu, T., Lewis, M. M., Kong, L., Wang, Y., Connor, J., et al. (2016). Quantitative susceptibility mapping of the midbrain in Parkinson's disease. *Mov. Disord.* 31, 317–324. doi: 10.1002/mds.26417

Esposito, F., Tessitore, A., Giordano, A., De Micco, R., Paccone, A., Conforti, R., et al. (2013). Rhythm-specific modulation of the sensorimotor network in drug-naive patients with Parkinson's disease by levodopa. *Brain* 136, 710–725. doi: 10.1093/brain/awt007

Fernández-Seara, M. A., Mengual, E., Vidorreta, M., Castellanos, G., Irigoyen, J., Erro, E., et al. (2015). Resting state functional connectivity of the subthalamic nucleus in Parkinson's disease assessed using arterial spin-labeled perfusion fMRI. *Hum. Brain Mapp.* 36, 1937–1950. doi: 10.1002/hbm.22747

Fox, M. D., and Raichle, M. E. (2007). Spontaneous fluctuations in brain activity observed with functional magnetic resonance imaging. *Nat. Rev. Neurosci.* 8, 700–711. doi: 10.1038/nrn2201

Friston, K. J. (2011). Functional and effective connectivity: a review. *Brain Connect.* 1, 13–36. doi: 10.1089/brain.2011.0008

Gómez, C., Olde Dubbelink, K. T. E., Stam, C. J., Abásolo, D., Berendse, H. W., and Hornero, R. (2011). Complexity analysis of resting-state MEG activity in early-stage Parkinson's disease patients. *Ann. Biomed. Eng.* 39, 2935–2944. doi: 10.1007/s10439-011-0416-0

Göttlich, M., Münte, T. F., Heldmann, M., Kasten, M., Hagenah, J., and Krämer, U. M. (2013). Altered resting state brain networks in Parkinson's disease. *PLoS One* 8:e77336. doi: 10.1371/journal.pone.0077336

Giladi, N., and Hausdorff, J. M. (2006). The role of mental function in the pathogenesis of freezing of gait in Parkinson's disease. *J. Neurol. Sci.* 248, 173–176. doi: 10.1016/j.jns.2006.05.015

Gorges, M., Müller, H.-P., Lulé, D., LANDSCAPE Consortium, Pinkhardt, E. H., Ludolph, A. C., et al. (2015). To rise and to fall: functional connectivity in cognitively normal and cognitively impaired patients with Parkinson's disease. *Neurobiol. Aging* 36, 1727–1735. doi: 10.1016/j.neurobiolaging.2014.12.026

Gorges, M., Müller, H.-P., Lulé, D., Ludolph, A. C., Pinkhardt, E. H., and Kassubek, J. (2013). Functional connectivity within the default mode network is associated with saccadic accuracy in Parkinson's disease: a resting-state FMRI and videooculographic study. *Brain Connect.* 3, 265–272. doi: 10.1089/brain.2013.0146

Gratwicke, J., Jahanshahi, M., and Foltynie, T. (2015). Parkinson's disease dementia: a neural networks perspective. *Brain* 138, 1454–1476. doi: 10.1093/brain/awv104

Griffiths, P. D., Dobson, B. R., Jones, G. R., and Clarke, D. T. (1999). Iron in the basal ganglia in Parkinson's disease. An *in vitro* study using extended X-ray absorption fine structure and cryo-electron microscopy. *Brain* 122, 667–673. doi: 10.1093/brain/122.4.667

Guan, X., Xuan, M., Gu, Q., Huang, P., Liu, C., Wang, N., et al. (2017). Regionally progressive accumulation of iron in Parkinson's disease as measured by quantitative susceptibility mapping. *NMR Biomed.* 30:e3489. doi: 10.1002/nbm.3489

Hämäläinen, M., Hari, R., Ilmoniemi, R. J., Knuutila, J., and Lounasmaa, O. V. (1993). Magnetoencephalography—theory, instrumentation, and applications to noninvasive studies of the working human brain. *Rev. Mod. Phys.* 65, 413–497. doi: 10.1103/revmodphys.65.413

Haacke, E. M., Cheng, N. Y. C., House, M. J., Liu, Q., Neelavalli, J., Ogg, R. J., et al. (2005). Imaging iron stores in the brain using magnetic resonance imaging. *Magn. Reson. Imaging* 23, 1–25. doi: 10.1016/j.mri.2004.10.001

Haacke, E. M., Liu, S., Buch, S., Zheng, W., Wu, D., and Ye, Y. (2015). Quantitative susceptibility mapping: current status and future directions. *Magn. Reson. Imaging* 33, 1–25. doi: 10.1016/j.mri.2014.09.004

Hacker, C. D., Perlmutter, J. S., Criswell, S. R., Ances, B. M., and Snyder, A. Z. (2012). Resting state functional connectivity of the striatum in Parkinson's disease. *Brain* 135, 3699–3711. doi: 10.1093/brain/aws281

Hammond, C., Bergman, H., and Brown, P. (2007). Pathological synchronization in Parkinson's disease: networks, models and treatments. *Trends Neurosci.* 30, 357–364. doi: 10.1016/j.tins.2007.05.004

He, N., Ling, H., Ding, B., Huang, J., Zhang, Y., Zhang, Z., et al. (2015). Region-specific disturbed iron distribution in early idiopathic Parkinson's disease measured by quantitative susceptibility mapping. *Hum. Brain Mapp.* 36, 4407–4420. doi: 10.1002/hbm.22928

Heinrichs-Graham, E., Kurz, M. J., Becker, K. M., Santamaria, P. M., Gendelman, H. E., and Wilson, T. W. (2014). Hypersynchrony despite pathologically reduced β oscillations in patients with Parkinson's disease: a pharmaco-magnetoencephalography study. *J. Neurophysiol.* 112, 1739–1747. doi: 10.1152/jn.00383.2014

Helmich, R. C., Derikx, L. C., Bakker, M., Scheeringa, R., Bloem, B. R., and Toni, I. (2010). Spatial remapping of cortico-striatal connectivity in Parkinson's disease. *Cereb. Cortex* 20, 1175–1186. doi: 10.1093/cercor/bhp178

Hillebrand, A., Barnes, G. R., Bosboom, J. L., Berendse, H. W., and Stam, C. J. (2012). Frequency-dependent functional connectivity within resting-state networks: an atlas-based MEG beamformer solution. *Neuroimage* 59, 3909–3921. doi: 10.1016/j.neuroimage.2011.11.005

Hou, Y., Luo, C., Yang, J., Ou, R., Liu, W., Song, W., et al. (2017). Default-mode network connectivity in cognitively unimpaired drug-naïve patients with rigidity-dominant Parkinson's disease. *J. Neurol.* 264, 152–1560. doi: 10.1007/s00415-016-8331-9

Hou, Y., Yang, J., Luo, C., Song, W., Ou, R., Liu, W., et al. (2016). Dysfunction of the default mode network in drug-naïve Parkinson's disease with mild cognitive impairments: a resting-state fMRI study. *Front. Aging Neurosci.* 8:247. doi: 10.3389/fnagi.2016.00247

Hu, X., Song, X., Li, E., Liu, J., Yuan, Y., Liu, W., et al. (2015). Altered resting-state brain activity and connectivity in depressed Parkinson's disease. *PLoS One* 10:e0131133. doi: 10.1371/journal.pone.0131133

Hwang, O. (2013). Role of oxidative stress in Parkinson's disease. *Exp. Neurobiol.* 22, 11–17. doi: 10.5607/en.2013.22.1.11

Ide, S., Kakeda, S., Ueda, I., Watanabe, K., Murakami, Y., Moriya, J., et al. (2015). Internal structures of the globus pallidus in patients with Parkinson's disease: evaluation with quantitative susceptibility mapping (QSM). *Eur. Radiol.* 25, 710–718. doi: 10.1007/s00330-014-3472-7

Jang, H., Lu, X., Carl, M., Searleman, A. C., Jerban, S., Ma, Y., et al. (2019). True phase quantitative susceptibility mapping using continuous single-point imaging: a feasibility study. *Magn. Reson. Med.* 81, 1907–1914. doi: 10.1002/mrm.27515

Jbabdi, S., Sotiropoulos, S. N., Haber, S. N., Van Essen, D. C., and Behrens, T. E. (2015). Measuring macroscopic brain connections *in vivo*. *Nat. Neurosci.* 18, 1546–1555. doi: 10.1038/nn.4134

Karunanayaka, P. R., Lee, E.-Y., Lewis, M. M., Sen, S., Eslinger, P. J., Yang, Q. X., et al. (2016). Default mode network differences between rigidity- and tremor-predominant Parkinson's disease. *Cortex* 81, 239–250. doi: 10.1016/j.cortex.2016.04.021

Kim, E. Y., Sung, Y. H., Shin, H.-G., Noh, Y., Nam, Y., and Lee, J. (2018). Diagnosis of early-stage idiopathic Parkinson's disease using high-resolution quantitative susceptibility mapping combined with histogram analysis in the substantia nigra at 3 T. *J. Clin. Neurol.* 14, 90–97. doi: 10.3988/jcn.2018.14.1.90

Krajcovicova, L., Mikl, M., Marecek, R., and Rektorova, I. (2012). The default mode network integrity in patients with Parkinson's disease is levodopa equivalent dose-dependen. *J. Neural Transm.* 119, 443–454. doi: 10.1007/s00702-011-0723-5

Kurani, A. S., Seidler, R. D., Burciu, R. G., Comella, C. L., Corcos, D. M., Okun, M. S., et al. (2015). Subthalamic nucleus--sensorimotor cortex functional connectivity in *de novo* and moderate Parkinson's disease. *Neurobiol. Aging* 36, 462–469. doi: 10.1016/j.neurobiolaging.2014.07.004

Kwak, Y., Peltier, S., Bohnen, N. I., Müller, M. L. T. M., Dayalu, P., and Seidler, R. D. (2010). Altered resting state cortico-striatal connectivity in mild to moderate stage Parkinson's disease. *Front. Syst. Neurosci.* 4:143. doi: 10.3389/fnsys.2010.00143

Langkammer, C., Krebs, N., Goessler, W., Scheurer, E., Ebner, F., Yen, K., et al. (2010). Quantitative MR imaging of brain iron: a postmortem validation study. *Radiology* 257, 455–462. doi: 10.1148/radiol.10100495

Langkammer, C., Pirpamer, L., Seiler, S., Deistung, A., Schweser, F., Franthal, S., et al. (2016). Quantitative susceptibility mapping in Parkinson's disease. *PLoS One* 11:e0162460. doi: 10.1371/journal.pone.0162460

Lempel, A., and Ziv, J. (1976). On the complexity of finite sequences. *IEEE Trans. Inform. Theor.* 22, 75–81. doi: 10.1109/TIT.1976.1055501

Li, D. T. H., Hui, E. S., Chan, Q., Yao, N., Chua, S. E., McAlonan, G. M., et al. (2018). Quantitative susceptibility mapping as an indicator of subcortical and limbic iron abnormality in Parkinson's disease with dementia. *Neuroimage Clin.* 20, 365–373. doi: 10.1016/j.nicl.2018.07.028

Li, J., Yuan, Y., Wang, M., Zhang, J., Zhang, L., Jiang, S., et al. (2017). Alterations in regional homogeneity of resting-state brain activity in fatigue of Parkinson's diseas. *J. Neural Transm.* 124, 1187–1195. doi: 10.1007/s00702-017-1748-1

Lingor, P., Carboni, E., and Koch, J. C. (2017). α-synuclein and iron: two keys unlocking Parkinson's diseas. *J. Neural Transm.* 124, 973–981. doi: 10.1007/s00702-017-1695-x

Liu, T., Eskreis-Winkler, S., Schweitzer, A. D., Chen, W., Kaplitt, M. G., Tsiouris, A. J., et al. (2013). Improved subthalamic nucleus depiction with quantitative susceptibility mapping. *Radiology* 269, 216–223. doi: 10.1148/radiol.13121991

Liu, C., Li, W., Tong, K. A., Yeom, K. W., and Kuzminski, S. (2015). Susceptibility-weighted imaging and quantitative susceptibility mapping in the brain. *J. Magn. Reson. Imaging* 42, 23–41. doi: 10.1002/jmri.24768

Lucas-Jiménez, O., Ojeda, N., Peña, J., Díez-Cirarda, M., Cabrera-Zubizarreta, A., Gómez-Esteban, J. C., et al. (2016). Altered functional connectivity in the default mode network is associated with cognitive impairment and brain anatomical changes in Parkinson's disease. *Parkinsonism Relat. Disord.* 33, 58–64. doi: 10.1016/j.parkreldis.2016.09.012

Manza, P., Zhang, S., Li, C.-S. R., and Leung, H.-C. (2016). Resting-state functional connectivity of the striatum in early-stage Parkinson's disease: cognitive decline and motor symptomatology. *Hum. Brain Mapp.* 37, 648–662. doi: 10.1002/hbm.23056

Markett, S., Reuter, M., Montag, C., Voigt, G., Lachmann, B., Rudorf, S., et al. (2014). Assessing the function of the fronto-parietal attention network: insights from resting-state fMRI and the attentional network test. *Hum. Brain Mapp.* 35, 1700–1709. doi: 10.1002/hbm.22285

Mathys, C., Caspers, J., Langner, R., Südmeyer, M., Grefkes, C., Reetz, K., et al. (2016). Functional connectivity differences of the subthalamic nucleus related to Parkinson's disease. *Hum. Brain Mapp.* 37, 1235–1253. doi: 10.1002/hbm.23099

Medeiros, M. S., Schumacher-Schuh, A., Cardoso, A. M., Bochi, G. V., Baldissarelli, J., Kegler, A., et al. (2016). Iron and oxidative stress in Parkinson's disease: an observational study of injury biomarkers. *PLoS One* 11:e0146129. doi: 10.1371/journal.pone.0146129

Menon, V. (2011). Large-scale brain networks and psychopathology: a unifying triple network model. *Trends Cogn. Sci.* 15, 483–506. doi: 10.1016/j.tics.2011.08.003

Menon, V., and Uddin, L. Q. (2010). Saliency, switching, attention and control: a network model of insula function. *Brain Struct. Funct.* 214, 655–667. doi: 10.1007/s00429-010-0262-0

Mi, T.-M., Mei, S.-S., Liang, P.-P., Gao, L.-L., Li, K.-C., Wu, T., et al. (2017). Altered resting-state brain activity in Parkinson's disease patients with freezing of gait. *Sci. Rep.* 7:16711. doi: 10.1038/s41598-017-16922-0

Montez, T., Linkenkaer-Hansen, K., van Dijk, B. W., and Stam, C. J. (2006). Synchronization likelihood with explicit time-frequency priors. *Neuroimage* 33, 1117–1125. doi: 10.1016/j.neuroimage.2006.06.066

Mosimann, U. P., Müri, R. M., Burn, D. J., Felblinger, J., Oandapos;Brien, J. T., and McKeith, I. G. (2005). Saccadic eye movement changes in Parkinson's disease dementia and dementia with Lewy bodies. *Brain* 128, 1267–1276. doi: 10.1093/brain/awh484

Moustafa, A. A., Chakravarthy, S., Phillips, J. R., Gupta, A., Keri, S., Polner, B., et al. (2016). Motor symptoms in Parkinson's disease: a unified framework. *Neurosci. Biobehav. Rev.* 68, 727–740. doi: 10.1016/j.neubiorev.2016.07.010

Murakami, Y., Kakeda, S., Watanabe, K., Ueda, I., Ogasawara, A., Moriya, J., et al. (2015). Usefulness of quantitative susceptibility mapping for the diagnosis of Parkinson disease. *Am. J. Neuroradiol.* 36, 1102–1108. doi: 10.3174/ajnr.A4260

Nambu, A., Tokuno, H., and Takada, M. (2002). Functional significance of the cortico-subthalamo-pallidal 'hyperdirect' pathway. *Neurosci. Res.* 43, 111–117. doi: 10.1016/s0168-0102(02)00027-5

Obeso, J. A., Stamelou, M., Goetz, C. G., Poewe, W., Lang, A. E., Weintraub, D., et al. (2017). Past, present and future of Parkinson's disease: a special essay on the 200th Anniversary of the Shaking Palsy. *Mov. Disord.* 32, 1264–1310. doi: 10.1002/mds.27115

Olde Dubbelink, K. T. E., Hillebrand, A., Twisk, J. W. R., Deijen, J. B., Stoffers, D., Schmand, B. A., et al. (2014). Disrupted brain network topology in Parkinson's disease: a longitudinal magnetoencephalography study. *Brain* 137, 197–207. doi: 10.1093/brain/awt316

Olde Dubbelink, K. T. E., Stoffers, D., Deijen, J. B., Twisk, J. W. R., Stam, C. J., and Berendse, H. W. (2013a). Cognitive decline in Parkinson's disease is associated with slowing of resting-state brain activity: a longitudinal study. *Neurobiol. Aging* 34, 408–418. doi: 10.1016/j.neurobiolaging.2012.02.029

Olde Dubbelink, K. T. E., Stoffers, D., Deijen, J. B., Twisk, J. W. R., Stam, C. J., Hillebrand, A., et al. (2013b). Resting-state functional connectivity as a marker of disease progression in Parkinson's disease: a longitudinal MEG study. *Neuroimage Clin.* 2, 612–619. doi: 10.1016/j.nicl.2013.04.003

Oswal, A., Beudel, M., Zrinzo, L., Limousin, P., Hariz, M., Foltynie, T., et al. (2016). Deep brain stimulation modulates synchrony within spatially and spectrally distinct resting state networks in Parkinson's disease. *Brain* 139, 1482–1496. doi: 10.1093/brain/aww048

Pollok, B., Krause, V., Martsch, W., Wach, C., Schnitzler, A., and Südmeyer, M. (2012). Motor-cortical oscillations in early stages of Parkinson's disease. *J. Physiol.* 590, 3203–3212. doi: 10.1113/jphysiol.2012.231316

Ponsen, M. M., Stam, C. J., Bosboom, J. L. W., Berendse, H. W., and Hillebrand, A. (2013). A three dimensional anatomical view of oscillatory resting-state activity and functional connectivity in Parkinson's disease related dementia: an MEG study using atlas-based beamforming. *Neuroimage Clin.* 2, 95–102. doi: 10.1016/j.nicl.2012.11.007

Prodoehl, J., Burciu, R. G., and Vaillancourt, D. E. (2014). Resting state functional magnetic resonance imaging in Parkinson's disease. *Curr. Neurol. Neurosci. Rep.* 14:448. doi: 10.1007/s11910-014-0448-6

Rektorova, I., Krajcovicova, L., Marecek, R., and Mikl, M. (2012). Default mode network and extrastriate visual resting state network in patients with Parkinson's disease dementia. *Neurodegener. Dis.* 10, 232–237. doi: 10.1159/000334765

Rietdijk, C. D., Perez-Pardo, P., Garssen, J., van Wezel, R. J. A., and Kraneveld, A. D. (2017). Exploring Braak's hypothesis of Parkinson's disease. *Front. Neurol.* 8:37. doi: 10.3389/fneur.2017.00037

Schnitzler, A., and Gross, J. (2005). Normal and pathological oscillatory communication in the brain. *Nat. Rev. Neurosci.* 6, 285–296. doi: 10.1038/nrn1650

Schoffelen, J.-M., and Gross, J. (2009). Source connectivity analysis with MEG and EEG. *Hum. Brain Mapp.* 30, 1857–1865. doi: 10.1002/hbm.20745

Sharman, M., Valabregue, R., Perlbarg, V., Marrakchi-Kacem, L., Vidailhet, M., Benali, H., et al. (2013). Parkinson's disease patients show reduced cortical-subcortical sensorimotor connectivity. *Mov. Disord.* 28, 447–454. doi: 10.1002/mds.25255

Shen, B., Gao, Y., Zhang, W., Lu, L., Zhu, J., Pan, Y., et al. (2017). Resting state fMRI reveals increased subthalamic nucleus and sensorimotor cortex connectivity in patients with Parkinson's disease under medication. *Front. Aging Neurosci.* 9:74. doi: 10.3389/fnagi.2017.00074

Sian-Hülsmann, J., Mandel, S., Youdim, M. B. H., and Riederer, P. (2011). The relevance of iron in the pathogenesis of Parkinson's disease. *J. Neurochem.* 118, 939–957. doi: 10.1111/j.1471-4159.2010.07132.x

Silberstein, P., Pogosyan, A., Kühn, A. A., Hotton, G., Tisch, S., Kupsch, A., et al. (2005). Cortico-cortical coupling in Parkinson's disease and its modulation by therapy. *Brain* 128, 1277–1291. doi: 10.1093/brain/awh480

Sjöström, H., Granberg, T., Westman, E., and Svenningsson, P. (2017). Quantitative susceptibility mapping differentiates between parkinsonian disorders. *Parkinsonism Relat. Disord.* 44, 51–57. doi: 10.1016/j.parkreldis.2017.08.029

Spillantini, M. G., Schmidt, M. L., Lee, V. M., Trojanowski, J. Q., Jakes, R., and Goedert, M. (1997). α-synuclein in Lewy bodies. *Nature* 388, 839–840. doi: 10.1038/42166

Sridharan, D., Levitin, D. J., and Menon, V. (2008). A critical role for the right fronto-insular cortex in switching between central-executive and default-mode networks. *Proc. Natl. Acad. Sci. U S A* 105, 12569–12574. doi: 10.1073/pnas.0800005105

Stam, C. J., Nolte, G., and Daffertshofer, A. (2007). Phase lag index: assessment of functional connectivity from multi channel EEG and MEG with diminished bias from common sources. *Hum. Brain Mapp.* 28, 1178–1193. doi: 10.1002/hbm.20346

Stam, C. J., van Straaten, E. C. W., Van Dellen, E., Tewarie, P., Gong, G., Hillebrand, A., et al. (2016). The relation between structural and functional connectivity patterns in complex brain networks. *Int. J. Psychophysiol.* 103, 149–160. doi: 10.1016/j.ijpsycho.2015.02.011

Stoffers, D., Bosboom, J. L. W., Deijen, J. B., Wolters, E. C., Berendse, H. W., and Stam, C. J. (2007). Slowing of oscillatory brain activity is a stable

characteristic of Parkinson's disease without dementia. *Brain* 130, 1847–1860. doi: 10.1093/brain/awm034

Stoffers, D., Bosboom, J. L. W., Deijen, J. B., Wolters, E. C., Stam, C. J., and Berendse, H. W. (2008a). Increased cortico-cortical functional connectivity in early-stage Parkinson's disease: an MEG study. *Neuroimage* 41, 212–222. doi: 10.1016/j.neuroimage.2008.02.027

Stoffers, D., Bosboom, J. L. W., Wolters, E. C., Stam, C. J., and Berendse, H. W. (2008b). Dopaminergic modulation of cortico-cortical functional connectivity in Parkinson's disease: an MEG study. *Exp. Neurol.* 213, 191–195. doi: 10.1016/j.expneurol.2008.05.021

Tahmasian, M., Bettray, L. M., van Eimeren, T., Drzezga, A., Timmermann, L., Eickhoff, C. R., et al. (2015). A systematic review on the applications of resting-state fMRI in Parkinson's disease: does dopamine replacement therapy play a role? *Cortex* 73, 80–105. doi: 10.1016/j.cortex.2015.08.005

Tessitore, A., Amboni, M., Esposito, F., Russo, A., Picillo, M., Marcuccio, L., et al. (2012a). Resting-state brain connectivity in patients with Parkinson's disease and freezing of gait. *Parkinsonism Relat. Disord.* 18, 781–787. doi: 10.1016/j.parkreldis.2012.03.018

Tessitore, A., Esposito, F., Vitale, C., Santangelo, G., Amboni, M., Russo, A., et al. (2012b). Default-mode network connectivity in cognitively unimpaired patients with Parkinson disease. *Neurology* 79, 2226–2232. doi: 10.1212/WNL.0b013e31827689d6

Tessitore, A., de Micco, R., Giordano, A., di Nardo, F., Caiazzo, G., Siciliano, M., et al. (2017a). Intrinsic brain connectivity predicts impulse control disorders in patients with Parkinson's disease movement disorders. *Mov. Disord.* 32, 1710–1719. doi: 10.1002/mds.27139

Tessitore, A., Santangelo, G., de Micco, R., Giordano, A., Raimo, S., Amboni, M., et al. (2017b). Resting-state brain networks in patients with Parkinson's disease and impulse control disorders. *Cortex* 94, 63–72. doi: 10.1016/j.cortex.2017.06.008

Tessitore, A., Giordano, A., de Micco, R., Russo, A., and Tedeschi, G. (2014). Sensorimotor connectivity in Parkinson's disease: the role of functional neuroimaging. *Front. Neurol.* 5:180. doi: 10.3389/fneur.2014.00180

Timmermann, L., Gross, J., Dirks, M., Volkmann, J., Freund, H.-J., and Schnitzler, A. (2003). The cerebral oscillatory network of parkinsonian resting tremor. *Brain* 126, 199–212. doi: 10.1093/brain/awg022

Uddin, L. Q. (2013). Complex relationships between structural and functional brain connectivity. *Trends Cogn. Sci.* 17, 600–602. doi: 10.1016/j.tics.2013.09.011

van den Heuvel, M. P., and Hulshoff Pol, H. E. (2010). Exploring the brain network: a review on resting-state fMRI functional connectivity. *Eur. Neuropsychopharmacol.* 20, 519–534. doi: 10.1016/j.euroneuro.2010.03.008

Vervoort, G., Alaerts, K., Bengevoord, A., Nackaerts, E., Heremans, E., Vandenberghe, W., et al. (2016). Functional connectivity alterations in the motor and fronto-parietal network relate to behavioral heterogeneity in Parkinson's disease. *Parkinsonism Relat. Disord.* 24, 48–55. doi: 10.1016/j.parkreldis.2016.01.016

Wang, Y., and Liu, T. (2015). Quantitative susceptibility mapping (QSM): decoding MRI data for a tissue magnetic biomarker. *Magn. Reson. Med.* 73, 82–101. doi: 10.1002/mrm.25358

Wang, S., Lou, M., Liu, T., Cui, D., Chen, X., and Wang, Y. (2013). Hematoma volume measurement in gradient echo MRI using quantitative susceptibility mapping. *Stroke* 44, 2315–2317. doi: 10.1161/STROKEAHA.113.001638

Wang, Y., Spincemaille, P., Liu, Z., Dimov, A., Deh, K., Li, J., et al. (2017). Clinical quantitative susceptibility mapping (QSM): biometal imaging and its emerging roles in patient care. *J. Magn. Reson. Imaging* 46, 951–971. doi: 10.1002/jmri.25693

Wang, J.-Y., Zhuang, Q.-Q., Zhu, L.-B., Zhu, H., Li, T., Li, R., et al. (2016). Meta-analysis of brain iron levels of Parkinson's disease patients determined by postmortem and MRI measurements. *Sci. Rep.* 6:36669. doi: 10.1038/srep36669

Wei, L., Hu, X., Zhu, Y., Yuan, Y., Liu, W., and Chen, H. (2017). Aberrant intra- and internetwork functional connectivity in depressed Parkinson's disease. *Sci. Rep.* 7:2568. doi: 10.1038/s41598-017-02127-y

Wu, S.-L., Liscic, R. M., Kim, S., Sorbi, S., and Yang, Y.-H. (2017). Nonmotor symptoms of Parkinson's disease. *Parkinsons Dis.* 2017, 1–2. doi: 10.1155/2017/4382518

Wu, T., Long, X., Wang, L., Hallett, M., Zang, Y., Li, K., et al. (2011). Functional connectivity of cortical motor areas in the resting state in Parkinson's disease. *Hum. Brain Mapp.* 32, 1443–1457. doi: 10.1002/hbm.21118

Wu, T., Wang, L., Chen, Y., Zhao, C., Li, K., and Chan, P. (2009). Changes of functional connectivity of the motor network in the resting state in Parkinson's disease. *Neurosci. Lett.* 460, 6–10. doi: 10.1016/j.neulet.2009.05.046

Yao, B., Li, T.-Q., Gelderen, P. V., Shmueli, K., de Zwart, J. A., and Duyn, J. H. (2009). Susceptibility contrast in high field MRI of human brain as a function of tissue iron content. *Neuroimage* 44, 1259–1266. doi: 10.1016/j.neuroimage.2008.10.029

Yao, N., Shek-Kwan Chang, R., Cheung, C., Pang, S., Lau, K. K., Suckling, J., et al. (2014). The default mode network is disrupted in Parkinson's disease with visual hallucinations. *Hum. Brain Mapp.* 35, 5658–5666. doi: 10.1002/hbm.22577

Yu, R., Liu, B., Wang, L., Chen, J., and Liu, X. (2013). Enhanced functional connectivity between putamen and supplementary motor area in Parkinson's disease patients. *PLoS One* 8:e59717. doi: 10.1371/journal.pone.0059717

Zhang, J.-J., Ding, J., Li, J.-Y., Wang, M., Yuan, Y.-S., Zhang, L., et al. (2017). Abnormal resting-state neural activity and connectivity of fatigue in Parkinson's disease. *CNS Neurosci. Ther.* 23, 241–247. doi: 10.1111/cns.12666

Zang, Y.-F., He, Y., Zhu, C.-Z., Cao, Q.-J., Sui, M.-Q., Liang, M., et al. (2007). Altered baseline brain activity in children with ADHD revealed by resting-state functional MRI. *Brain Dev.* 29, 83–91. doi: 10.1016/j.braindev.2006.07.002

Zhao, X., An, H., Liu, T., Shen, N., Bo, B., Zhang, Z., et al. (2017). Quantitative susceptibility mapping of the substantia nigra in Parkinson's disease. *Appl. Magn. Reson.* 48, 533–544. doi: 10.1007/s00723-017-0877-x

Conflict of Interest Statement: The authors declare that the research was conducted in the absence of any commercial or financial relationships that could be construed as a potential conflict of interest.

frontiers in Neural Circuits

ORIGINAL RESEARCH
published: 26 September 2019
doi: 10.3389/fncir.2019.00062

Projections of Brodmann Area 6 to the Pyramidal Tract in Humans: Quantifications Using High Angular Resolution Data

Zhen-Ming Wang[1,2], *Yi Shan*[1,2], *Miao Zhang*[1,2], *Peng-Hu Wei*[3], *Qiong-Ge Li*[1,2], *Ya-Yan Yin*[1,2] *and Jie Lu*[1,2,4]*

[1]Department of Radiology, Xuanwu Hospital, Capital Medical University, Beijing, China, [2]Beijing Key Laboratory of Magnetic Resonance Imaging and Brain Informatics, Beijing, China, [3]Department of Neurosurgery, Xuanwu Hospital, Capital Medical University, Beijing, China, [4]Department of Nuclear Medicine, Xuanwu Hospital, Capital Medical University, Beijing, China

Primate studies indicate that the pyramidal tract (PyT) could originate from Brodmann area (BA) 6. However, in humans, the accurate origin of PyT from BA 6 is still uncertain owing to difficulties in visualizing anatomical features such as the fanning shape at the corona radiata and multiple crossings at the semioval centrum. High angular-resolution diffusion imaging (HARDI) could reliably replicate these anatomical features. We explored the origin of the human PyT from BA 6 using HARDI. With HARDI data of 30 adults from the Massachusetts General Hospital-Human Connectome Project (MGH-HCP) database and the HCP 1021 template (average of 1021 HCP diffusion data), we visualized the PyT at the 30-averaged group level and the 1021 large-sample level and validated the observations in each of the individuals. Endpoints of the fibers within each subregion were quantified. PyT fibers originating from the BA 6 were consistently visualized in all images. Specifically, the bilateral supplementary motor area (SMA) and dorsal premotor area (dPMA) were consistently found to contribute to the PyT. PyT fibers from BA 6 and those from BA 4 exhibited a twisting topology. The PyT contains fibers originating from the SMA and dPMA in BA 6. Infarction of these regions or aging would result in incomplete provision of information to the PyT and concomitant decreases in motor planning and coordination abilities.

Keywords: supplementary motor area, dorsal premotor area, high angular resolution diffusion imaging, pyramidal tract, human connectome project

OPEN ACCESS

Edited by:
Lijun Bai,
Xi'an Jiaotong University, China

Reviewed by:
Hesheng Liu,
Harvard Medical School, United States
Baoci Shan,
Chinese Academy of Sciences, China
J.H. Gao,
Peking University, China

***Correspondence:**
Jie Lu
imaginglu@hotmail.com

Received: *30 April 2019*
Accepted: *12 September 2019*
Published: *26 September 2019*

Citation:
Wang Z-M, Shan Y, Zhang M, Wei P-H, Li Q-G, Yin Y-Y and Lu J (2019) Projections of Brodmann Area 6 to the Pyramidal Tract in Humans: Quantifications Using High Angular Resolution Data. Front. Neural Circuits 13:62. doi: 10.3389/fncir.2019.00062

INTRODUCTION

The pyramidal tract (PyT) is a longitudinal pathway that delivers information regarding voluntary motor behavior. It is constituted of the corticospinal tract and the corticobulbar tract (Rea, 2015). According to experiments using non-human primates, beside the primary motor area, the PyT could still originate from Brodmann area (BA) 6. Specifically, in the BA 6, the PyT predominately derives from the supplementary motor area (SMA), dorsal premotor area (dPMA), and cingulate cortex (Dum and Strick, 1991; Galea and Darian-Smith, 1994). In humans, diffusion tensor imaging (DTI) has been introduced to visualize the PyT (Kumar et al., 2009; Zolal et al., 2012; George et al., 2014). As the DTI technique cannot discriminate fanning or crossing fibers, or flipped angles

(Fernandez-Miranda et al., 2012), it cannot decode either the fanning shape of the corona radiate (Rea, 2015) or the multiple crossing fibers at the semioval centrum (Fernandez-Miranda et al., 2012). A failure to visualize these anatomical features means that the origin of the PyT from regions other than BA 4 (e.g., fibers from BA 6) remains unknown in humans (Archer et al., 2018; Chenot et al., 2019).

With the introduction of multi-band techniques (Moeller et al., 2010), many diffusion directions and multiple *b*-values became available. Consequently, high angular resolution acquisition techniques, such as diffusion spectrum imaging (DSI) and high angular-resolution diffusion imaging (HARDI) have been developed to solve the aforementioned shortcomings of DTI. Besides, high angular resolution acquisition approaches could determine both the origin and termination with accuracy compared with traditional DTI, specifically, the accurate termination could even outline the shape of cortical gyrus (Fernandez-Miranda et al., 2012). In addition to the scanning technique, quantitative anisotropy (QA)-based deterministic tracking methods (Yeh et al., 2013) were also developed with specific focus on high angular-resolution data. This algorithm can interpolate multiple orientations directly to a single voxel by considering the anisotropy of different b-vectors and the trajectory, and can reliably present anatomical features such as fanning, crossing, and angular-flipping fibers, and fiber terminations (Fernandez-Miranda et al., 2012; Yoshino et al., 2016; Wei et al., 2017). In addition to the high angular resolution techniques, high magnetic gradient strength could shorten the diffusion encoding time enormously and decrease the signal loss owing to T2 decay (Fan Q. et al., 2016). The advantages of the high magnetic gradient have been validated by the comparison of tractographies under different gradients of 300 mT/m, 80 mT/m and 40 mT/m (Chamberland et al., 2018). Thus, constraints that previously hindered explorations of the termination of the PyT have largely been eliminated. Accordingly, in the present study, we explored projections from BA 6 to the PyT using these high angular-resolution diffusion techniques and high magnetic gradient data.

MATERIALS AND METHODS

In the present study, 30 groups of the Massachusetts General Hospital-Human Connectome Project (MGH-HCP) individual diffusion data from the HCP were used[1]. This dataset was acquired at the MGH, using the Siemens 3T connectome scanner, which has 300 mT/m maximum gradient strength (McNab et al., 2013; Setsompop et al., 2013). High gradient strength can improve the angular resolution of the diffusion image (Fan Q. et al., 2016). First, the 30 individual datasets were averaged to the same Montreal Neurological Institute (MNI) space to create a 30-subjects-averaged template which was created by ourselves. Fiber tracking was performed for this template. Then, we performed the fiber tracking using another open source template[2], which consisted of 1,021 healthy young adults from the HCP (Q1-Q4, 2017) and did not need data preprocessing. Finally, fiber tracking was performed for the 30 participants at the individual level in individual space to validate the findings from the two templates. For each type of data or template, the fiber tracking process was divided into two stages. In the first stage, we performed fiber tracking to test whether the fanning shape of the corona radiata and multiple crossings could be reliably presented, as this constituted the basis of exploring the origin of the PyT. In the second stage, we quantified the effective connectivity of the projections from BA6 and its relationship with BA4. Thus, these two stages were performed at the individual level, group level (30-subjects-averaged template), and the large population level (HCP 1021 template). Parameters of the scanning protocol are available at: http://protocols.humanconnectome.org/HCP/3T/imaging-protocols.html and http://protocols.humanconnectome.org/HCP/MGH/. The study was reviewed and approved by Xuanwu Ethical Committee.

Data Preprocessing

We used the open access software DSI-studio[3] to analyze the data. First, we reconstructed the spin distribution function (SDF) of each participant and simultaneously warped the SDF to the MNI space, using the q-space diffeomorphic reconstruction method (Yeh and Tseng, 2011). A value of 1.1 was used as the diffusion sampling length ratio. All these 30 groups of SDFs were averaged to the same MNI space to create the 30-subjects-averaged template. Then fiber tracking was performed with this template.

For the preprocessing in the individual space, the SDF was reconstructed using the generalized q-sampling imaging method. The following parameters were used: diffusion sampling length ratio 1:1, 20-fold SDF tessellation, 10 resolved fibers. The SDF was used to conduct further fiber tracking in the individual space to validate the findings.

Fiber Tracking

Fiber tracking was performed for the 30 individuals, the 30-subjects-averaged template, and the HCP 1021 template. To track the multiple crossing fibers, we first visualized the left-right oriented fibers that extended from the corpus callosum by drawing a region of interest (ROI) at the corpus callosum and lateral side of the semioval centrum in sagittal slices. The frontal-posterior oriented fibers of the arcuate fasciculus were visualized by setting the superior temporal gyrus and premotor cortex as ROIs. The superior temporal gyrus and the premotor cortex were defined by the non-liner registration of the automatic anatomical labeling (AAL) atlas and Brodmann atlas, respectively, to the individual space within the DSI-studio software. The superior-inferior oriented fibers of the pyramidal tract were visualized as follows: to track the potential PyT fibers issuing from BA 4 (PyT4) and 6 (PyT6), we introduced the Brainnetome Atlas[4], which is a structural connectome based template (Fan L. et al., 2016) in which BA 6 was parceled into the caudal dorsolateral region (A6cdl), caudal ventrolateral region

[1]https://db.humanconnectome.org
[2]https://pitt.box.com/v/HCP1021-1mm
[3]http://dsi-studio.labsolver.org/dsi-studio-download
[4]http://atlas.brainnetome.org/download.html

(A6cvl), dorsolateral region (A6dl, or dPMA), ventrolateral region (A6vl), and medial region (A6m, or SMA), while BA 4 was parceled into the head and face region (A4hf), upper-limb region (A4ul), trunk region (A4t), tongue and larynx region (A4tl), and lower limb region (A4ll). During fiber tracking, these cortical regions were used as seed regions. Additionally, ROIs in the white matter included the cerebral peduncle (imported from the JHU white-matter tractography atlas, which is embedded in the DSI-studio software) and the pyramid (drawn by a neurologist with 10 years of experience). In each round of fiber tracking, one cortical seed region was paired simultaneously with the cerebral peduncle and pyramid to visualize the PyT.

Most of the ROIs within the present study were imported to the native space by non-linear registration using open access atlas, the whole processes were performed without subjective manipulations. For the pyramid, it is an obvious anatomical structure which was bordered medially by the anterior median fissure and laterally by the anterolateral sulcus. Therefore, the repeatability of defining the regions was also guaranteed.

The QA threshold was set at the optimal threshold such that the orientation distribution signal best fit the brain tissue in the SDF map, with the least amount of the orientation signal falling outside the pial boundary or into the ventricle. Here, values of the QA thresholds ranged from 0.05 to 0.1 for the individual data, while the value was 0.15 for the 30-subjects-averaged template and 0.1 for the HCP 1021 template. Other tracking parameters were as follows: angular threshold = 90, step size = 0.5, smoothing = 0.8, min length = 5.0 mm, max length = 300.0 mm, trilinear algorithm, and streamlined. The tracking process was set to terminate if the seed number reached 50,000.

Connectome Evaluation

To evaluate whether a given region within BA 6 is an effective region that constituted the PyT, we defined the effective index (EI) as the number of endpoints that fell within the region divided by the number of voxels in the region; this reflects the average fiber distribution within the region. Calculation of the EI was performed for the 30-subjects-averaged template and HCP 1021 template, to estimate the composition of the PyT at the group or population level. Here, 0.5 was chosen as the EI threshold; that is, if more than half of the total voxels within a certain region had at least one endpoint, we considered this region to reliably contribute fibers to the PyT. Origin analysis (EI), shape, and course of the fiber tracts were observed for the 30-subjects-averaged template and HCP 1021 template, and verified in 30 of the MGH-HCP individuals.

RESULTS

In the 30-subjects-averaged template, HCP 1021 template, and all 30 individuals, fibers of BA 6 were consistently observed to contribute to the PyT. Additionally, the trajectory and shape of the PyT were also visualized at individual, group, and population levels.

Fanning Shape and Triple Cross of the PyT

We first checked whether an inability to reconstruct the fanning shape and triple cross, which would prevent visualization of the endpoints of the PyT, were present for the templates and individual-level data. Fanning shapes were present in most of the data (**Figures 1**, **2**). Additionally, triple crossings were visualized at the semioval centrum, which consisted of fibers of the corpus callosum in a left-right direction; arcuate fasciculus in the anterior-posterior direction; and PyT in the superior-inferior direction (**Figure 2**).

Quantitative Evaluation of PyT Distribution in BA 6

For the 30-subjects-averaged template and HCP 1021 template, we calculated the EI according to subregions of BA 6 (**Figure 3**). For the former template, subregions where EI was larger than 0.5 were bilateral A6dl and A6m, as well as the right A6cvl. On the latter template, these areas were bilateral A6dl and A6m. Notably, subregions with consistent effective distributions between templates were bilateral A6dl and A6m. These findings were further verified in the individuals; we observed that the subregions of bilateral A6dl, A6m, and right A6cvl, had relatively high frequencies of being areas with effective distribution to the PyT (**Figure 3**). Details of the fiber tractography that originated from A6dl and A6m is shown in **Figure 4**.

Twisting Relationship Between PyT6 and PyT4

In both the 30-subjects-averaged template and HCP 1021 template (**Figure 5**), PyT6 was typically located anterior and medial to PyT4. Specifically, from the level of the cortex to the semioval centrum, PyT6 predominately coursed in front of PyT4. When descending into the internal capsule and the cerebral peduncle, PyT6 was located at the anteromedial side of PyT4. After further descending into the pons, PyT6 was located at the medial side of PyT4. At the level of the foramen magnum, PyT6 rotated to the medial posterior side of PyT4. These observations also applied to individual participants.

DISCUSSION

Using the large population data of the HCP and high magnet gradient HARDI data, we found the existence of PyT6 in humans. Specifically, A6dl, or the dPMA, and A6m, or the SMA, have consistently contributed to the PyT. To the best of our knowledge, there is a lack of extant literature that explores the distribution of fibers from BA 6 to the PyT in human beings.

Currently, most knowledge regarding the origin of the PyT was obtained from axonal tracing studies of non-human primates. These animal studies revealed that besides the primary motor cortex, the remaining projections originated from the SMA, arcuate premotor area, and caudal cingulate motor areas (Dum and Strick, 1991; Galea and Darian-Smith, 1994). Concerning the PyT in humans, although five decades ago postmortem observation of the human brain observed the PyT had origins other than the precentral gyrus (Jane et al., 1967), the definite origin of the PyT in humans remains to be defined

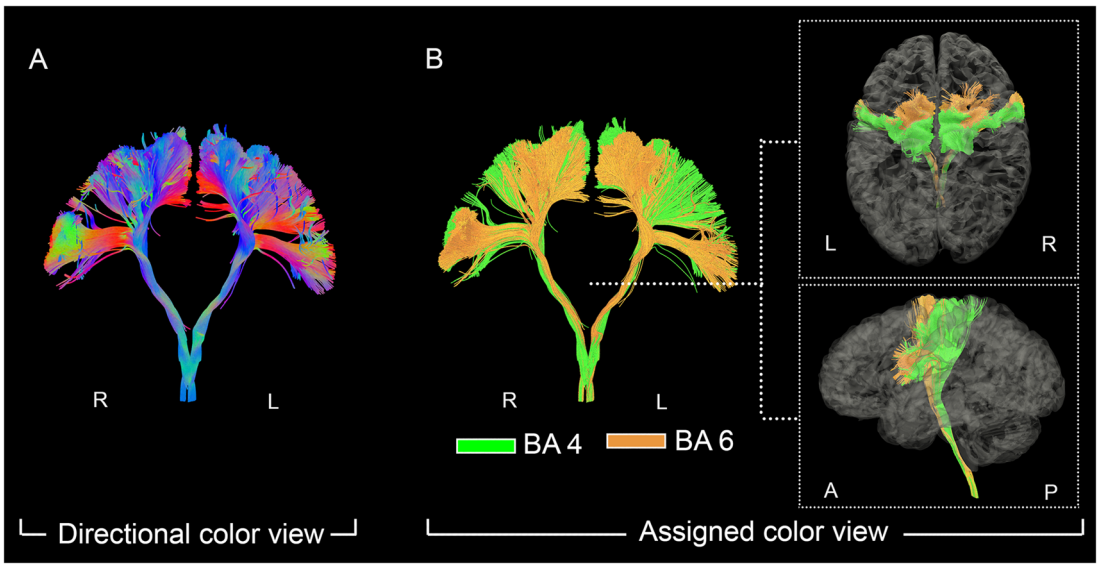

FIGURE 1 | The fanning shape of pyramidal tract (PyT) visualized in individual level. On the left panel **(A)**, the fanning shape of PyT was visualized in the directional view. On the right panel **(B)**, PyT4 and PyT6 are shown in green and orange, respectively, together with top and lateral views.

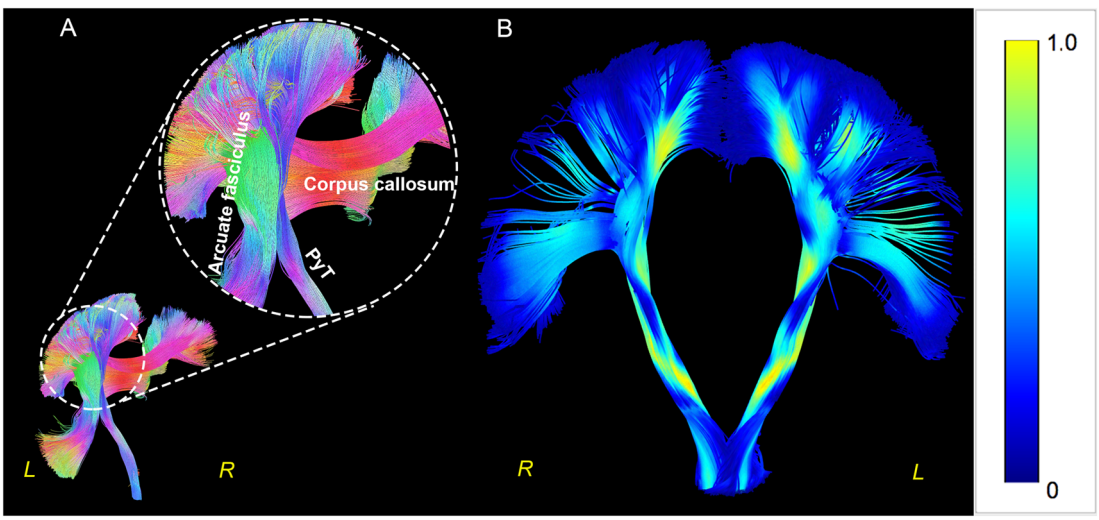

FIGURE 2 | Triple crossings and fanning shape in Human Connectome Project (HCP) 1021. Triple crossings at the semioval centrum, PyT, corpus callosum, and arcuate fasciculus are shown in the left panel **(A)**. The fanning shape is shown in the right panel **(B)**, with color-code indicating the quantitative anisotropy (QA) value. The QA values were observed to be higher in white matters and lower within the gray matters.

(Archer et al., 2018; Chenot et al., 2019). Several DTI studies have explored the PyT (Kumar et al., 2009; Zolal et al., 2012; George et al., 2014); however, due to angular resolution limits, the fanning shape of the PyT and multiple crossings of the semioval centrum have been barriers to reliably evaluating the origin and course of the PyT. Additionally, most of these previous studies primarily focused on the precentral area. With respect to BA 6 projections to the PyT in humans, Seo and Jang (2013) investigated different diffusion indices of the SMA and dPMA, recognizing that the origin of the PyT at the SMA and dPMA was chosen by default in animal studies, rather than by defining explicitly which subregions project to the PyT (Seo and Jang, 2013). In a more recent study, Chenot et al. (2019) used DTI to create a PyT template. They observed the origin of the PyT as the premotor area; nevertheless, they also mentioned that the distribution to the PyT from the premotor area in humans remains to be defined (Chenot et al., 2019).

In the present study, the triple crossing fibers at the semioval centrum and the fanning shape of the PyT were visualized successfully, indicating that prior barriers that

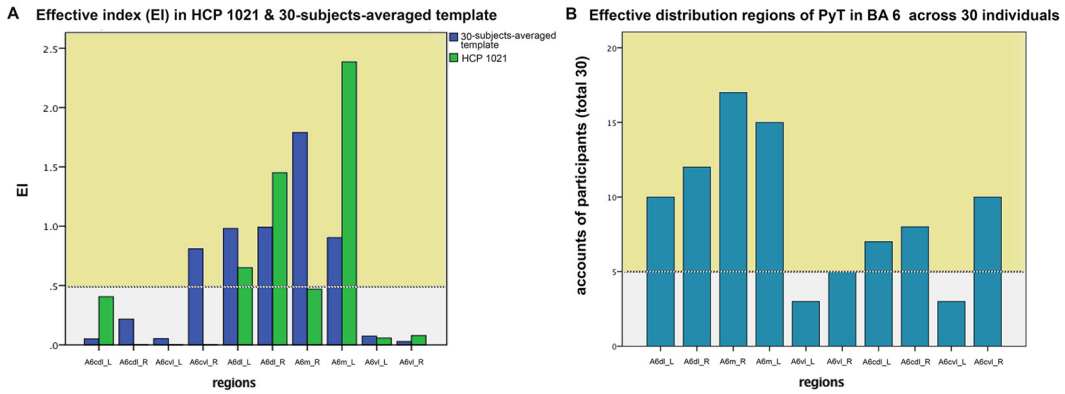

FIGURE 3 | Effective index (EI) in HCP 1021, 30-subjects-averaged template and across 30 individuals. On the left panel **(A)**, subregions where EI was larger than 0.5 were bilateral A6dl and A6m, as well as the right A6cvl for the 30-subjects-averaged template. For the HCP template, these areas were bilateral A6dl and A6m. On the right panel **(B)**, bilateral A6dl and A6m, as well as the right A6cvl were the most frequently observed to be effectively contributed to the PyT across 30 individuals. Effective distributions are shown in yellow background.

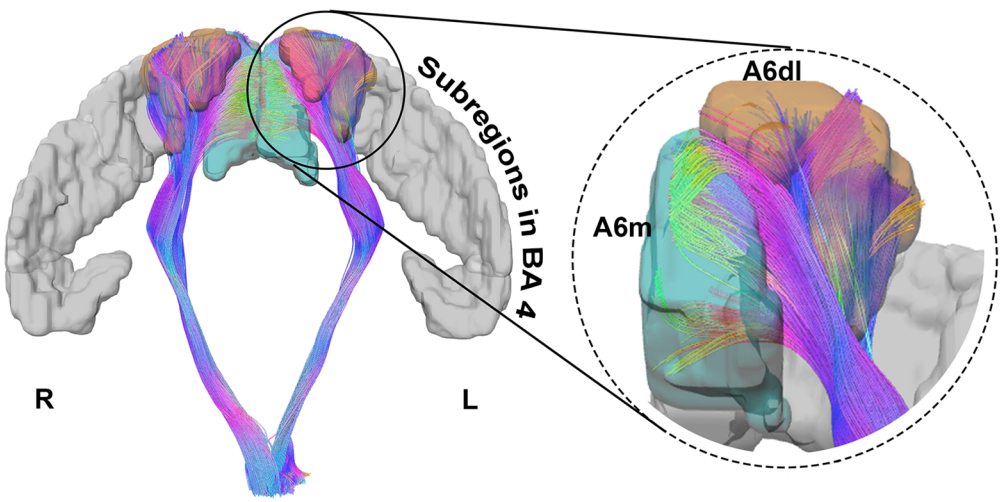

FIGURE 4 | Details of the fiber tractography originating from A6dl and A6m in HCP 1021 template. The left side shows bilateral fibers that originated from A6dl and A6m, together with all subregions in Brodmann area (BA) 4 in gray. The right side shows details of fiber tractography origins from left A6dl and A6m. Left A6dl is shown in orange and left A6m in green.

prevented visualization of the terminations had been removed. The QA values were observed to be slightly lower in the gray matter than in the white matter (**Figure 2**). This was due to white matter typically consists of axons in a certain direction, therefore, the diffusional movement of the water molecules are directive within the membrane (Alexander et al., 2007), and this resulted in a higher QA value. However, when approaching the gray matter, different layers of cytoarchitecture (Fatterpekar et al., 2002) typically decreased the water diffusion, thus, the QA value exhibited a reduction at regions of gray matter.

By using different subregions from the BN atlas that fully covered the entire BA 6, and by introducing EI as a quantitative evaluation of the effective distribution, we observed that the dPMA and SMA consistently contributed to the PyT; these observations are consistent with previous studies of non-human primates. According to the literature, the dPMA is primarily concerned with addressing external cues and adjusting movement plans (Paus, 2001; Hartwigsen et al., 2012). Additionally, the dPMA plays a role in the recovery of motor paresis after stroke (Watson et al., 1986; Seitz et al., 1998; Di Pino et al., 2014); injury to the dPMA can be accompanied by limb-kinetic apraxia (Freund and Hummelsheim, 1985; Jang and Seo, 2016). In contrast, the SMA is involved in self-initiated movements (Passingham et al., 2010), action monitoring (Bonini et al., 2014), and sequencing (Tanji, 2001). Infarction of the SMA can result in apraxia of the extremities (Marchetti and Della Sala,

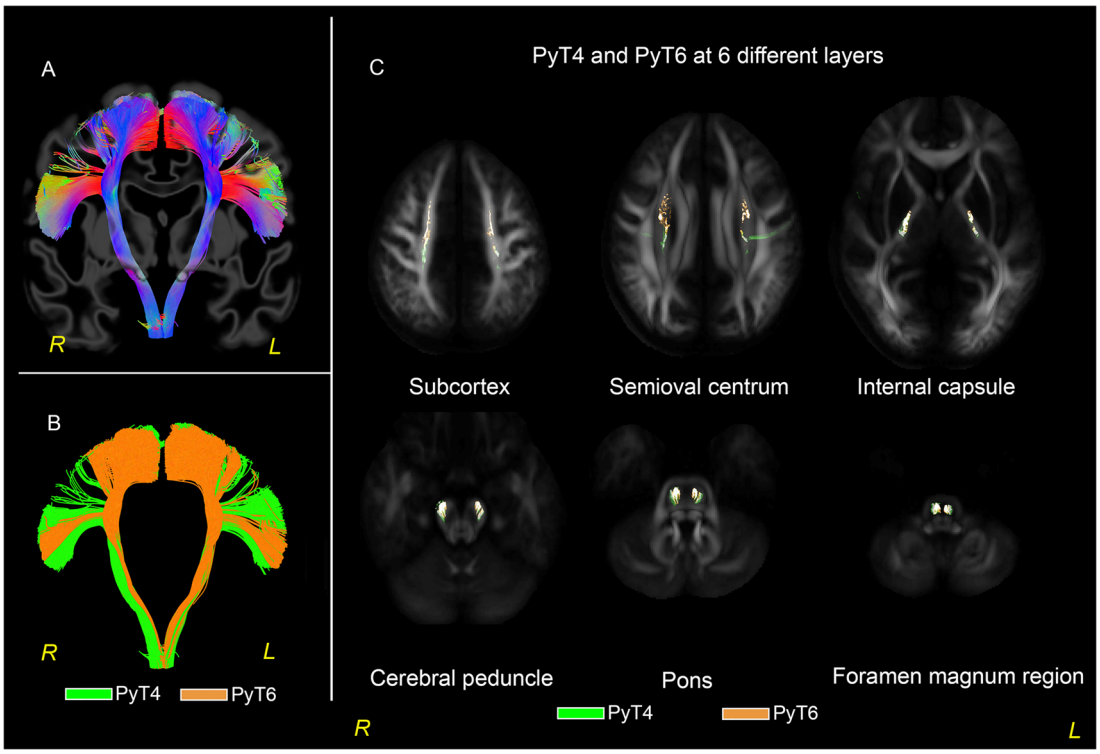

FIGURE 5 | PyT6 and PyT4 in 30-subjects-averaged template. **(A)** Fibers distributed in a fanning shape ranged from the medial wall of the frontal lobe to the opercula region. **(B)** PyT4 and PyT6 are shown in green and orange, respectively. **(C)** PyT4 and PyT6 at layers of subcortex, semioval centrum, internal capsule, cerebral peduncle, pons, and foramen magnum region.

1997; Chang and Chun, 2015). Watson et al. (1986) reported two patients with left mesial hemisphere infarctions that included the SMA who had bilateral apraxia for lower limb movements. Ito et al. (2013) reported a patient who was unable to move his left leg intentionally either by verbal command or by imitation after the SMA injury. Chang and Chun (2015) reported a patient with SMA infarction who presented lower limb apraxia and even noted that this apraxia might accompany disruption of the PyT. Therefore, this study might still have important clinical meanings.

Regarding organization of the PyT at different descending levels, we found that the PyT4 and PyT6 exhibited a twisting relationship from the level of cortex to the level of the medulla oblongata. The twisting organization of the PyT from the cortex to the internal capsule has been observed in previous studies (Park et al., 2008; Pan et al., 2012; Chenot et al., 2019), most of which focused on discussing the somatopology of the primary motor area in the internal capsule. Studies that explicitly assess the relationship between PyT6 and PyT4 are lacking.

There are limitations to the present study. First, it was previously reported that the PyT contains fibers from the cingulate cortex in non-human primates. However, in the present study, we did not find these projections after tracking all data carefully, even though the diffusion data we used in the present study is of high angular resolution. Thus, it remains to be elucidated whether the cingulate cortex is an origin of the PyT in humans. Next, in addition to the consistent regions of A6m and A6dl, other regions were variable and could not be defined meaningfully in the current study. Furthermore, there is only one modality and a lack of functional experiments exists in this study. Thus, the present study focused on discussing the structural basis of the PyT6. Future studies are also needed to explore the functional aspects of the fibers.

CONCLUSION

Using HARDI images, our findings indicated that the PyT contains fibers originating from BA 6, most probably from the SMA and dPMA. Injury to the SMA and dPMA (e.g., infarction, aging) would result in incomplete receipt of information by the PyT, and further decrease motor planning and coordination abilities.

DATA AVAILABILITY STATEMENT

Publicly available datasets were analyzed in this study. The datasets analyzed for this study can be found at https://db.humanconnectome.org.

ETHICS STATEMENT

This study was carried out with written informed consent from all subjects. All subjects gave written informed consent in accordance with the Declaration of Helsinki. The protocol was approved by the "Ethical committee of Xuanwu Hospital."

AUTHOR CONTRIBUTIONS

Z-MW, P-HW and JL: conception and design. Z-MW, YS, MZ, Q-GL and Y-YY: development of methodology and data management. Z-MW: analysis and interpretation of data. Z-MW and JL: writing and/or revision of the manuscript. JL: study supervision.

FUNDING

This study was supported by the National Natural Science Foundation of China (Grant numbers 81671662, 81522021), Beijing Municipal Administration of Hospitals' Ascent Plan (Grant number DFL20180802) and the National Natural Science Foundation of China (Grant numbers 81871009, 81801288). Data were provided by the Human Connectome Project, MGH-USC Consortium (Principal Investigators: Bruce R. Rosen, Arthur W. Toga, and Van Wedeen; U01MH093765) funded by the NIH Blueprint Initiative for Neuroscience Research grant; the National Institutes of Health grant P41EB015896; and the Instrumentation Grants S10RR023043, 1S10RR023401, 1S10RR019307.

REFERENCES

Alexander, A. L., Lee, J. E., Lazar, M., and Field, A. S. (2007). Diffusion tensor imaging of the brain. *Neurotherapeutics* 4, 316–329. doi: 10.1016/j.nurt.2007.05.011

Archer, D. B., Vaillancourt, D. E., and Coombes, S. A. (2018). A template and probabilistic atlas of the human sensorimotor tracts using diffusion MRI. *Cereb. Cortex* 28, 1685–1699. doi: 10.1093/cercor/bhx066

Bonini, F., Burle, B., Liégeois-Chauvel, C., Régis, J., Chauvel, P., and Vidal, F. (2014). Action monitoring and medial frontal cortex: leading role of supplementary motor area. *Science* 343, 888–891. doi: 10.1126/science.1247412

Chamberland, M., Tax, C. M. W., and Jones, D. K. (2018). Meyer's loop tractography for image-guided surgery depends on imaging protocol and hardware. *Neuroimage Clin* 20, 458–465. doi: 10.1016/j.nicl.2018.08.021

Chang, M. C., and Chun, M. H. (2015). Right lower limb apraxia in a patient with left supplementary motor area infarction: intactness of the corticospinal tract confirmed by transcranial magnetic stimulation. *Neural Regen. Res.* 10, 325–327. doi: 10.4103/1673-5374.152389

Chenot, Q., Tzourio-Mazoyer, N., Rheault, F., Descoteaux, M., Crivello, F., Zago, L., et al. (2019). A population-based atlas of the human pyramidal tract in 410 healthy participants. *Brain Struct. Funct.* 224, 599–612. doi: 10.1007/s00429-018-1798-7

Di Pino, G., Pellegrino, G., Assenza, G., Capone, F., Ferreri, F., Formica, D., et al. (2014). Modulation of brain plasticity in stroke: a novel model for neurorehabilitation. *Nat. Rev. Neurol.* 10, 597–608. doi: 10.1038/nrneurol.2014.162

Dum, R. P., and Strick, P. L. (1991). The origin of corticospinal projections from the premotor areas in the frontal lobe. *J. Neurosci.* 11, 667–689. doi: 10.1523/JNEUROSCI.11-03-00667.1991

Fan, L., Li, H., Zhuo, J., Zhang, Y., Wang, J., Chen, L., et al. (2016). The human brainnetome atlas: a new brain atlas based on connectional architecture. *Cereb. Cortex* 26, 3508–3526. doi: 10.1093/cercor/bhw157

Fan, Q., Witzel, T., Nummenmaa, A., Van Dijk, K. R., Van Horn, J. D., Drews, M. K., et al. (2016). MGH-USC Human Connectome Project datasets with ultra-high b-value diffusion MRI. *Neuroimage* 124, 1108–1114. doi: 10.1016/j.neuroimage.2015.08.075

Fatterpekar, G. M., Naidich, T. P., Delman, B. N., Aguinaldo, J. G., Gultekin, S. H., Sherwood, C. C., et al. (2002). Cytoarchitecture of the human cerebral cortex: MR microscopy of excised specimens at 9.4 Tesla. *Am. J. Neuroradiol.* 23, 1313–1321.

Fernandez-Miranda, J. C., Pathak, S., Engh, J., Jarbo, K., Verstynen, T., Yeh, F. C., et al. (2012). High-definition fiber tractography of the human brain: neuroanatomical validation and neurosurgical applications. *Neurosurgery* 71, 430–453. doi: 10.1227/neu.0b013e3182592faa

Freund, H. J., and Hummelsheim, H. (1985). Lesions of premotor cortex in man. *Brain* 108, 697–733. doi: 10.1093/brain/108.3.697

Galea, M. P., and Darian-Smith, I. (1994). Multiple corticospinal neuron populations in the macaque monkey are specified by their unique cortical origins, spinal terminations, and connections. *Cereb. Cortex* 4, 166–194. doi: 10.1093/cercor/4.2.166

George, E., Heier, L., Kovanlikaya, I., and Greenfield, J. (2014). Diffusion tensor imaging of pyramidal tract reorganization after pediatric stroke. *Childs Nerv. Syst.* 30, 1135–1139. doi: 10.1007/s00381-013-2351-x

Hartwigsen, G., Bestmann, S., Ward, N. S., Woerbel, S., Mastroeni, C., Granert, O., et al. (2012). Left dorsal premotor cortex and supramarginal gyrus complement each other during rapid action reprogramming. *J. Neurosci.* 32, 16162–16171a. doi: 10.1523/JNEUROSCI.1010-12.2012

Ito, I., Ito, K., and Shindo, N. (2013). Left leg apraxia after anterior cerebral artery territory infarction: functional analysis using single-photon emission computed tomography. *Eur. Neurol.* 69, 252–256. doi: 10.1159/000342222

Jane, J. A., Yashon, D., Demyer, W., and Bucy, P. C. (1967). The contribution of the precentral gyrus to the pyramidal tract of man. *J. Neurosurg.* 26, 244–248. doi: 10.3171/jns.1967.26.2.0244

Jang, S. H., and Seo, J. P. (2016). Limb-kinetic apraxia due to injury of corticofugal tracts from secondary motor area in patients with corona radiata infarct. *Acta Neurol. Belg.* 116, 467–472. doi: 10.1007/s13760-016-0600-y

Kumar, A., Juhasz, C., Asano, E., Sundaram, S. K., Makki, M. I., Chugani, D. C., et al. (2009). Diffusion tensor imaging study of the cortical origin and course of the corticospinal tract in healthy children. *Am. J. Neuroradiol.* 30, 1963–1970. doi: 10.3174/ajnr.a1742

Marchetti, C., and Della Sala, S. (1997). On crossed apraxia. Description of a right-handed apraxic patient with right supplementary motor area damage. *Cortex* 33, 341–354. doi: 10.1016/s0010-9452(08)70010-8

McNab, J. A., Edlow, B. L., Witzel, T., Huang, S. Y., Bhat, H., Heberlein, K., et al. (2013). The human connectome project and beyond: initial applications of 300 mT/m gradients. *Neuroimage* 80, 234–245. doi: 10.1016/j.neuroimage.2013.05.074

Moeller, S., Yacoub, E., Olman, C. A., Auerbach, E., Strupp, J., Harel, N., et al. (2010). Multiband multislice GE-EPI at 7 tesla, with 16-fold acceleration using partial parallel imaging with application to high spatial and temporal whole-brain fMRI. *Magn. Reson. Med.* 63, 1144–1153. doi: 10.1002/mrm.22361

Pan, C., Peck, K. K., Young, R. J., and Holodny, A. I. (2012). Somatotopic organization of motor pathways in the internal capsule: a probabilistic diffusion tractography study. *Am. J. Neuroradiol.* 33, 1274–1280. doi: 10.3174/ajnr.a2952

Park, J. K., Kim, B. S., Choi, G., Kim, S. H., Choi, J. C., and Khang, H. (2008). Evaluation of the somatotopic organization of corticospinal tracts in the internal capsule and cerebral peduncle: results of diffusion-tensor MR tractography. *Korean J. Radiol.* 9, 191–195. doi: 10.3348/kjr.2008.9.3.191

Passingham, R. E., Bengtsson, S. L., and Lau, H. C. (2010). Medial frontal cortex: from self-generated action to reflection on one's own performance. *Trends Cogn. Sci.* 14, 16–21. doi: 10.1016/j.tics.2009.11.001

Paus, T. (2001). Primate anterior cingulate cortex: where motor control, drive and cognition interface. *Nat. Rev. Neurosci.* 2, 417–424. doi: 10.1038/35077500

Rea, P. (2015). *Essential Clinical Anatomy of the Nervous System.* Cambridge, MA: Academic Press.

Seitz, R. J., Höflich, P., Binkofski, F., Tellmann, L., Herzog, H., and Freund, H. J. (1998). Role of the premotor cortex in recovery from middle cerebral artery infarction. *Arch. Neurol.* 55, 1081–1088. doi: 10.1001/archneur.55.8.1081

Seo, J. P., and Jang, S. H. (2013). Different characteristics of the corticospinal tract according to the cerebral origin: DTI study. *Am. J. Neuroradiol.* 34, 1359–1363. doi: 10.3174/ajnr.a3389

Setsompop, K., Kimmlingen, R., Eberlein, E., Witzel, T., Cohen-Adad, J., McNab, J. A., et al. (2013). Pushing the limits of *in vivo* diffusion MRI for the Human Connectome Project. *Neuroimage* 80, 220–233. doi: 10.1016/j.neuroimage.2013.05.078

Tanji, J. (2001). Sequential organization of multiple movements: involvement of cortical motor areas. *Annu. Rev. Neurosci.* 24, 631–651. doi: 10.1146/annurev.neuro.24.1.631

Watson, R. T., Fleet, W. S., Gonzalez-Rothi, L., and Heilman, K. M. (1986). Apraxia and the supplementary motor area. *Arch. Neurol.* 43, 787–792. doi: 10.1001/archneur.1986.00520080035016

Wei, P. H., Mao, Z. Q., Cong, F., Yeh, F. C., Wang, B., Ling, Z. P., et al. (2017). *In vivo* visualization of connections among revised Papez circuit hubs using full q-space diffusion spectrum imaging tractography. *Neuroscience* 357, 400–410. doi: 10.1016/j.neuroscience.2017.04.003

Yeh, F. C., and Tseng, W. Y. (2011). NTU-90: a high angular resolution brain atlas constructed by q-space diffeomorphic reconstruction. *Neuroimage* 58, 91–99. doi: 10.1016/j.neuroimage.2011.06.021

Yeh, F. C., Verstynen, T. D., Wang, Y., Fernández-Miranda, J. C., and Tseng, W. Y. (2013). Deterministic diffusion fiber tracking improved by quantitative anisotropy. *PLoS One* 8:e80713. doi: 10.1371/journal.pone.0080713

Yoshino, M., Abhinav, K., Yeh, F. C., Panesar, S., Fernandes, D., Pathak, S., et al. (2016). Visualization of cranial nerves using high-definition fiber tractography. *Neurosurgery* 79, 146–165. doi: 10.1227/NEU.0000000000001241

Zolal, A., Hejčl, A., Vachata, P., Bartoš, R., Humhej, I., Malucelli, A., et al. (2012). The use of diffusion tensor images of the corticospinal tract in intrinsic brain tumor surgery: a comparison with direct subcortical stimulation. *Neurosurgery* 71, 331–340; discussion 340. doi: 10.1227/neu.0b013e31825b1c18

Conflict of Interest: The authors declare that the research was conducted in the absence of any commercial or financial relationships that could be construed as a potential conflict of interest.

frontiers in Neural Circuits

ORIGINAL RESEARCH
published: 06 November 2019
doi: 10.3389/fncir.2019.00072

Altered Cerebro-Cerebellar Limbic Network in AD Spectrum: A Resting-State fMRI Study

Zhigang Qi[1,2], *Yanhong An*[1,2], *Mo Zhang*[1,2], *Hui-Jie Li*[3]* and *Jie Lu*[1,2]*

[1]Department of Radiology, Xuanwu Hospital, Capital Medical University, Beijing, China, [2]Beijing Key Laboratory of Magnetic Resonance Imaging and Brain Informatics, Beijing, China, [3]Key Laboratory of Behavioral Science, Institute of Psychology, Chinese Academy of Sciences, Beijing, China

Recent evidence suggests that the cerebellum is related to motor and non-motor cognitive functions, and that several coupled cerebro-cerebellar networks exist, including links with the limbic network. Since several limbic structures are affected by Alzheimer pathology, even in the preclinical stages of Alzheimer's disease (AD), we aimed to investigate the cerebral limbic network activity from the perspective of the cerebellum. Twenty patients with mild cognitive impairment (MCI), 18 patients with AD, and 26 healthy controls (HC) were recruited to acquire Resting-state functional MRI (rs-fMRI). We used seed-based approach to construct the cerebro-cerebellar limbic network. Two-sample *t*-tests were carried out to explore the differences of the cerebellar limbic network connectivity. The first result, a sub-scale network including the bilateral posterior part of the orbitofrontal cortex (POFC) extending to the anterior insular cortex (AIC) and left inferior parietal lobule (L-IPL), showed greater functional connectivity in MCI than in HC and less functional connectivity in AD than in MCI. The location of this sub-scale network was in accordance with components of the ventral attention network. Second, there was decreased functional connectivity to the right mid-cingulate cortex (MCC) in the AD and MCI patient groups relative to the HC group. As the cerebellum is not compromised by Alzheimer pathology in the prodromal stage of AD, this pattern indicates that the sub-scale ventral attention network may play a pivotal role in functional compensation through the coupled cerebro-cerebellar limbic network in MCI, and the cerebellum may be a key node in the modulation of social cognition.

Keywords: mild cognitive impairment, Alzheimer's disease, cerebro-cerebellar connectivity, limbic network, resting-state functional MRI, compensation

OPEN ACCESS

Edited by:
Lijun Bai,
Xi'an Jiaotong University, China

Reviewed by:
J. H. Gao,
Peking University, China
Stefano Delli Pizzi,
Università degli Studi G. d'Annunzio Chieti e Pescara, Italy

***Correspondence:**
Hui-Jie Li
lihj@psych.ac.cn
Jie Lu
imaginglu@hotmail.com

Received: *29 April 2019*
Accepted: *17 October 2019*
Published: *06 November 2019*

Citation:
Qi Z, An Y, Zhang M, Li H-J and Lu J (2019) Altered Cerebro-Cerebellar Limbic Network in AD Spectrum: A Resting-State fMRI Study. Front. Neural Circuits 13:72. doi: 10.3389/fncir.2019.00072

INTRODUCTION

The most prominent feature of Alzheimer's disease (AD) is the compromise of episodic memory, even in its prodromal stage that is referred to as mild cognitive impairment (MCI). It is natural that the pathogenesis of the impairment of memory became a focus on the research of AD. Although it is also involved in memory function, the limbic system has attracted little attention in AD-related research (Rolls, 2015). However, the common neuropsychiatric symptoms (NPS) of AD, including agitation and aggression, can result in potential harm that affects the patients and their caregivers and may become a much more serious burden on the family than the amnesia (Craig et al., 2005). For most psychiatric conditions, dysfunction of the limbic structures affects emotion regulation,

social interaction, and other behaviors. Understanding the limbic network would be meaningful for deeply probing brain functions, such as memory, and for clarifying the pathogenesis of psychiatric disorders, such as depression (Bennett, 2011), bipolar disorder (Leow et al., 2013), and psychosocial stress (Pruessner et al., 2008). To date, very few reports have focused on the significance of the limbic network in the evaluation of the biological underpinnings of AD (Trzepacz et al., 2013).

A series of clinical studies exploring NPS in patients with MCI and AD indicated that greater agitation was correlated with decreased gray matter (GM) density in the left insula and bilateral anterior cingulate (Bruen et al., 2008) and the left inferior frontal, insular, and bilateral retrosplenial cortices (Hu et al., 2015). Similarly, Trzepacz et al. (2013) reported that agitation and aggression severity was positively correlated to frontolimbic atrophy. Limbic dysfunction mainly includes the entorhinal cortex extending to the parietal cortex (Khan et al., 2014) and inferior frontal areas. Several limbic structures are involved by tau pathology even in AD patients (Spires-Jones and Hyman, 2014). With combined positron emission tomography (PET) and magnetic resonance imaging (MRI), severe reductions of metabolism were observed throughout a network of limbic structures, including the hippocampus, medial thalamus, and posterior cingulate cortex (PCC) in mild AD patients; the same pattern was seen in amnestic MCI to a lesser degree (Nestor et al., 2003).

Resting-state functional MRI (rs-fMRI) can be used to evaluate the functional connectivity and large-scale functional network such as the default mode network (DMN) and limbic network. A typical finding is impairment of DMN activity, which is considered to be the origin of episodic memory damage in MCI and AD (Greicius et al., 2004; Li et al., 2015). Rs-fMRI may be particularly useful in the early detection of pathological change, due to neural function alterations may precede neuronal atrophy. Since the structure of the limbic system is compromised in MCI and AD, it is reasonable to hypothesize that functional changes of the limbic system occur in AD, even in the prodromal stages. A resting-state magnetoencephalography study on patients with MCI due to AD showed that patients with phosphorylated tau pathology had decreased functional connectivity such as the PCC, orbitofrontal cortex (OFC), and paracentral lobule, which could affect the limbic structures (Canuet et al., 2015).

The cerebellum has long been considered as mainly being involved in motor function; recently, it was also found to contribute to some non-motor cognitive functions. In other words, in addition to sensorimotor function, cognition, emotion, and autonomic functions can also be localized to the cerebellum, just like with the cerebrum. The cognitive/limbic cerebellum is found to be located in the cerebellar posterior lobe, which has been connected to cerebral cortex association areas. Moreover, lesions in the cerebellar posterior lobe lead to the cerebellar cognitive affective syndrome (CCAS). New evidence regarding cerebellar organization and functional connections have been provided by rs-fMRI studies in humans that have found distributed cerebral networks that underlie movement, attention, and limbic valence, as well as frontoparietal and default systems concerned with multiple different functions map onto the cerebellum with topographic specificity (Habas et al., 2009; O'Reilly et al., 2010). Patients with focal infarcts to the hemipons, present disrupted functional coupling between the cerebrum and contralateral cerebellum (Lu et al., 2011). Buckner et al. (2011) proposed an rs-fMRI-based approach to comprehensively explore the organization of cerebro-cerebellar circuits in the human brain. Seven networks, including the limbic network, within the cerebellum were observed to connect to the associated cerebral networks.

Because cerebellum plays crucial roles in higher cortical functions through a cerebro-cerebellar circuit, and it is not compromised by AD-related pathology in the early stages (Braak and Braak, 1991), here, we wanted to evaluate the pattern of cerebral limbic network activity of the AD spectrum through the coupled cerebro-cerebellar network.

MATERIALS AND METHODS

Participants Recruitment

Twenty patients with MCI, 18 patients with AD, and 26 healthy controls (HC) were recruited in the study. The MCI and AD participants were recruited from the memory clinic of the Department of Neurology in hospital. HC were enrolled through volunteer posters from a community-based epidemiological study. Participants all provided written informed consent in accordance with the guidelines set by the Medical Research Ethics Committee of Beijing Xuanwu Hospital.

Clinical Examination

For each subject, clinical examination was composed of medical history, neurological examination, informant interview, and neuropsychological assessment including the Mini-Mental State Examination (MMSE) and Clinical Dementia Rating (CDR). Potential participants with a history of stroke, drug abuse, moderate to serious hypertension, psychiatric diseases, or other systemic diseases were excluded from the study.

HC did not have any subjective or reported cognitive impairments, and a CDR score of 0 and MMSE score $\geq$28. The inclusion criteria for MCI patients were based on previous studies (Winblad et al., 2004; Zhang et al., 2017) and were as follows: had a subjective cognitive complaint (corroborated by an informant), episodic memory deficit on neuropsychological testing (CDR score = 0.5 and MMSE score >24), and could complete daily living independently. AD patients met both the DSM-IV criteria for dementia and the National Institute of Neurological and Communicative Diseases and Stroke/AD and Related Disorders Association criteria for probable AD dementia.

The demographic and neuropsychological findings of the AD, MCI, and HC groups are summarized in **Table 1**. Age, gender ratio, and years of education were matched across the three groups. The age of participants was similar between the three diagnostic groups (one-way ANOVA, $F = 0.590$, $p = 0.559$) with similar medians and ranges, whereas the MMSE scores were significantly different between the three groups (one-way ANOVA, $F = 78.552$, $p < 0.0001$).

TABLE 1 | Demographics of Alzheimer's disease (AD) and mild cognitive impairment (MCI) patients, and healthy controls (HC).

	Age	Female/Male	Education (year)	MMSE	CDR
AD patients (n = 20)	73.1 ± 6.7	11/9	10.5 ± 0.6	17.5 ± 0.1	1
MCI patients (n = 18)	70.5 ± 6.3	10/8	12.3 ± 1	26.1 ± 0.6	0.5
Healthy controls (n = 26)	71.3 ± 6.8	12/14	11 ± 0.9	28.3 ± 0.5	0

No significant difference ($p > 0.05$) was observed in age, sex, or years of education between the three groups. Significant differences in Mini-Mental State Examination (MMSE) scores were seen between the three groups ($p < 0.0001$).

MRI Data Acquisition

All MRI data were acquired using a 3-T Siemens Trio system. Participants' heads were positioned within a 12-channel head coil. Foam padding was provided for comfort and to minimize head movement. During the rs-fMRI scanning, all participants were informed to close their eyes and to restrain from initiating attention-demanding activity. Functional images were collected using a gradient echo sequence [echo time (TE) = 40 ms, repetition time (TR) = 2,000 ms, flip angle = 90°, field of view (FoV) = 256 mm^2, matrix = 64 × 64, 28 slices, slice thickness = 4 mm, and 0 mm inter-slice gap] for a period of 8 min and 4 s, resulting in a total of 239 imaging volumes. A T1-weighted anatomical image was also obtained using a magnetization-prepared rapid acquisition gradient echo sequence [TE = 2.2 ms, TR = 1,900 ms, inversion time (TI) = 900 ms, flip angle = 9°, FoV = 256 mm^2, matrix = 224 × 256, 176 slices, and 1 mm^3 voxel]. 3D T1 structural images were collected for anatomical co-registration.

MR Image Preprocessing and Individual Limbic Network Mapping

We preprocessed all MRI data using the Connectome Computation System pipeline consisting of anatomical and functional image processing steps (Xu et al., 2015). The anatomical preprocessing firstly denoised individual MRI structural images with a spatially adaptive non-local means filter (Xing et al., 2011). It stripped the skull of the denoised image and integrated manual edits to achieve a better brain extraction and segmented the brain volume into cerebrospinal fluid (CSF), white matter (WM), and GM tissues across both cerebral cortex and cerebellum. Individual pial (GM/CSF boundary) and white (GM/WM boundary) surfaces were subsequently generated and spatially normalized to match a group-level template surface in Montreal Neurological Institute (MNI) space. The subsequent functional preprocessing removed the first five volumes (10 s), detected and fixed temporal spikes by interpolation, corrected temporal acquisition difference in slice order and spatial head motion across volumes and performed intensity normalization on the 4D global mean intensity of 10,000. This pipeline uses individual white surfaces to complete a boundary-based registration (BBR) for building spatial matching between multimodal (functional vs. anatomical) images in a single individual. Friston's 24-parameter motion curves, WM and CSF mean time series, as well as linear and quadratic trends were regressed out from the individual rs-fMRI time series using multiple linear regressions. As the final step in the CCS, the rs-fMRI time series were transferred into a 1-mm MNI surface grid and down-sampled to the 4-mm MNI surface grid (fsaverage5).

Seed-based method was employed to construct a cerebro-cerebellar limbic network. In this study, seed was chosen following these steps: first, cerebellar limbic network template was chosen from the 7-network parcellation of the cerebellum using 1,500 subjects (Buckner et al., 2011); second, the average time sequence of all the vertex in the template was extracted. Pearson's correlation coefficient between the individual mean time series of the cerebellar limbic network and preprocessed rs-fMRI time series of each vertex on the fsaverage5 was calculated and further converted into Fisher-z value to quantify the limbic functional connectivity. This resulted in individual surface mapping of the limbic network connectivity for subsequent statistical tests across the three groups.

Correlational Analysis

Two-sample t-tests were applied to explore cerebellar limbic network connectivity differences between each pair of the three groups. Vertex-wise statistical cortical surface maps were corrected for multiple comparisons with cluster-level random field theory of family-wise errors (corrected $p < 0.05$). Correlations between MMSE score and mean cerebellar limbic network connectivity across all vertices within each cluster exhibiting significant differences in functional connectivity were performed.

RESULTS

Cerebral Areas Showing Significant Functional Connectivity to Cerebellar Limbic Network

In HC, a set of distributed areas showed positive functional connectivity to the cerebellar limbic network, including the frontal lobe, parietal lobe, and temporal lobe, mainly in the medial part of the hemispheres. Some areas also showed negative functional connectivity to the cerebellar limbic network, distributing in the convexity of the hemispheres (see **Figure 1A**). In the MCI group, fewer cerebral areas showed positive functional connectivity to the cerebellar limbic network than in HC; however, the t-values were higher in some areas on visual inspection, mainly in the frontoparietal lobes (see **Figure 1B**). Many fewer areas exhibited positive functional connectivity to the cerebellar limbic network in AD than in MCI and HC; these areas were mostly distributed in the frontal and temporal pole (see **Figure 1C**). At the same time, the number of areas showing negative functional connectivity to the cerebellar limbic network was higher in MCI and AD groups than in the HC. These areas

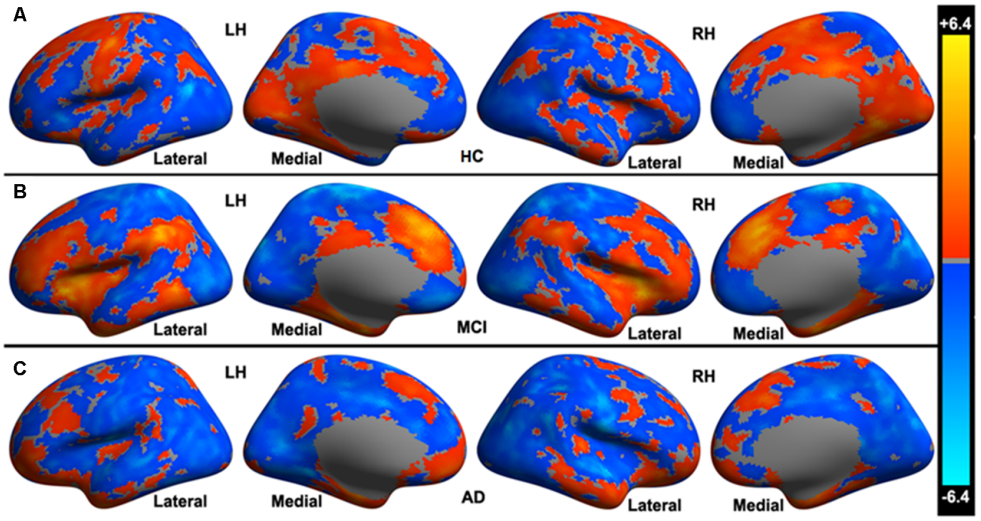

FIGURE 1 | Cerebral areas showing significant functional connectivity to the cerebellar limbic network in **(A)** healthy controls (HC), **(B)** mild cognitive impairment (MCI), and **(C)** Alzheimer's disease (AD) groups.

showing functional connectivity to the cerebellar limbic network were nearly symmetrically distributed in bilateral hemispheres.

Significant Differences of the Functional Connectivity Between Cerebellar Limbic Network and Cerebral Cortex Between HC, MCI, and AD Groups

HC vs. AD: HC present increased functional connectivity in the right mid-cingulate cortex (MCC), right lingual gyrus to the cerebellar limbic network and decreased functional connectivity in the left temporal pole to cerebellar limbic network in comparison with AD (see **Figure 2A**).

HC vs. MCI: compared with MCI, HC show increased functional connectivity in the left paracentral lobule, right paracentral lobule extending to the right MCC to the cerebellar limbic network and decreased functional connectivity in the bilateral posterior part of the orbitofrontal cortex (POFC) extending to the anterior insular cortex (AIC), left inferior parietal lobule (L-IPL), and right fusiform gyrus to the cerebellar limbic network (see **Figure 2B**).

MCI vs. AD: increased functional connectivity between the bilateral POFC extending to the AIC (POFC-AIC), L-IPL and the cerebellar limbic network were found in MCI patients. No decreased functional connectivity was observed in MCI relative to AD (see **Figure 2C**).

Table 2 illustrated Talairach coordinates of clusters showing significant differences in functional connectivity with the cerebellar limbic network between HC, MCI, and AD groups.

Relationships Between Functional Connectivity and MMSE Score

A Pearson correlation was calculated between MMSE score and significant clusters. Among these clusters, the right MCC (HC vs. AD), right lingual gyrus (HC vs. AD), bilateral posterior part of orbital-frontal cortex extending to the AIC (MCI vs. AD), and left inferior parietal lobule (MCI vs. AD) showed positive correlations with the MMSE score ($p < 0.05$). Negative correlation was observed between the left temporal pole (HC vs. AD) and MMSE score ($p < 0.01$; see **Table 3**). Clusters showing positive or negative correlation with the MMSE score are those with a significant difference in HC vs. AD, and MCI vs. AD. No significant correlations were observed between MMSE score and clusters showing significant differences between HC and MCI patients.

DISCUSSION

The current study evaluated changes in the cerebral limbic network in MCI and AD from the perspective of cerebro-cerebellar functional connectivity because regions of the cerebellum are functionally coupled to specific cerebral networks (Buckner et al., 2011). In other words, we aimed to study the cerebral areas showing significant functional connectivity to the cerebellar limbic network and discriminate differences between HC, MCI, and AD groups. The pattern of the cerebral areas showing functional connectivity to the cerebellar limbic network, which was nearly symmetrically distributed in bilateral hemispheres, was similar in the three groups. The significant differences between the three group indicated that: (1) a sub-scale network, including the bilateral POFC-AIC and left IPL, showed greater functional connectivity in MCI relative to HC and lower connectivity in AD relative to MCI; (2) decreased functional connectivity in the left paracentral lobule and right paracentral lobule extending to right MCC in MCI relative to HC and decreased functional connectivity in the right MCC in AD relative to HC and

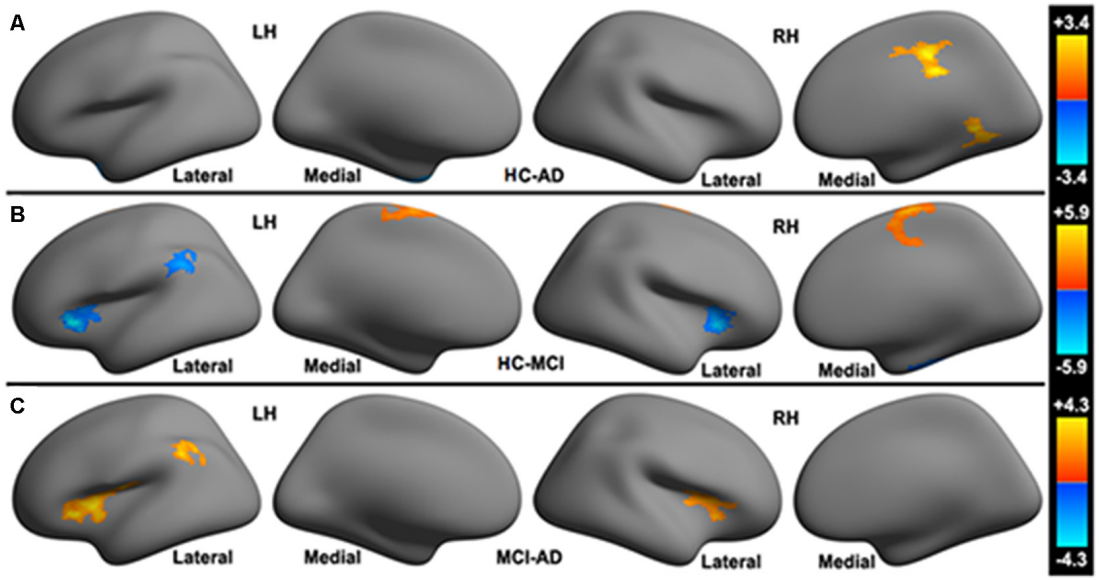

FIGURE 2 | Significant differences in the functional connectivity to the cerebellar limbic network between **(A)** HC, **(B)** MCI and **(C)** AD groups.

TABLE 2 | Talairach coordinates of clusters showing significant differences in functional connectivity with the cerebellar limbic network between HC, MCI, and AD groups.

	Size (mm^2)	X	Y	Z	BA	Area	T
HC-MCI							
	511	−11	−7	63	6	Left paracentral lobule	1.929
	1,021	13	−16	36	24	Right mid-cingulate cortex/paracentral lobule	3.376
	639	−55	−47	30	40	Left inferior parietal lobule	−1.915
	559	39	22	8		Right posterior part of orbital-fronto cortex and anterior part of insular cortex	−2.554
	499	39	−11	−23	20	Right fusiform gyrus	−2.038
	679	−28	25	5		Left posterior part of orbital-fronto cortex and anterior part of insular cortex	−2.988
HC-AD							
	624	13	−16	36	24	Right mid-cingulate cortex	2.171
	845	13	−64	1		Right lingual gyrus	1.851
	539	−31	−6	−28	20	Left temporal pole	−2.022
MCI-AD							
	1,314	−47	−12	17		Left posterior part of orbital-fronto cortex and anterior part of insular cortex	5.043
	703	−49	−45	43	40	Left inferior parietal lobule	2.192
	734	32	14	10		Right posterior part of orbital-fronto cortex and anterior part of insular cortex	2.865

TABLE 3 | Significant correlations between the MMSE score and functional connectivity of brain regions.

	R-MCC	R-LG	L-POFC-AIC	L-IPL	R-POFC-AIC	L-TP
Correlation coefficient	0.366	0.366	0.341	0.325	0.313	−0.439
P-value	0.017	0.017	0.027	0.036	0.043	0.004

Note: R-MCC, right mid-cingulate cortex; R-LG, right lingual gyrus; L-POFC-AIC, left posterior part of orbital-fronto cortex and anterior part of insular cortex; L-IPL, left inferior parietal lobule; R-POFC-AIC, right posterior part of orbital-fronto cortex and anterior part of insular cortex; L-TP, left temporal pole.

(3) decreased functional connectivity in the left temporal pole in HC relative to AD and in the right fusiform gyrus in HC relative to MCI, increased functional connectivity in the right lingual gyrus in HC relative to AD. The dual change of the cerebral limbic network in the current study is consistent with a previous study on MCI due to AD patients (Canuet et al., 2015). They found patients with abnormal CSF p-tau and Aβ42 levels showed both decreased and increased functional connectivity affecting limbic structures, with resting-state magnetoencephalography.

The limbic network was proposed by Papez (1995) to be a system involved in emotion and memory. It is well known that AD is characterized by impairment of episodic memory. However, since NPS was verified to occur in

AD and MCI (Bruen et al., 2008; Trzepacz et al., 2013), and several previous studies have reported GM atrophy in the limbic network in AD and MCI (Bruen et al., 2008; Trzepacz et al., 2013; Hu et al., 2015), it is reasonable to consider that the limbic network is compromised in AD spectrum disorders.

Although the cerebellum has long been considered to be mainly involved in motor control, evidence has been accumulating that the cerebellum also contributes to higher cognitive function (Buckner, 2013; Bernard and Seidler, 2014; Sokolov et al., 2017; Schmahmann, 2019). Patients with left-sided lesions showed deficits in visuo-spatial processing while patients with right-sided lesions had verbal memory defects, indicating dysfunction of the contralateral cerebral hemispheres (Hokkanen et al., 2006). Other studies related to ADHD (Tomasi and Volkow, 2012), depression (Alalade et al., 2011), and aging (Bernard et al., 2013) without visible parenchymal lesions also revealed that cerebellar function might change accordingly. Moreover, a recent multi-study analysis showed that cerebellar activity during domain-specific mentalizing functionality is strongly connected with a corresponding mentalizing network in the cerebrum (Van Overwalle and Mariën, 2016). However, in the AD spectrum, the cerebellum was considered to be free from Alzheimer pathology until the severe phase of the disease, and always a normal reference in the evaluation of cerebral metabolism (Ni et al., 2013). Bai et al. (2011) reported that longitudinal functional connectivity between the hippocampus subregion and cerebellum may be a valuable biomarker to classify aMCI converters from aMCI non-converters. Similarly, in a recent report (Delli Pizzi et al., 2019), hippocampal/entorhinal functional connectivity were evaluated in individuals with MCI those who did not convert to AD or show the presence of AD pathological load compared to those who converted to AD or showed presence of AD pathological load, increased functional connectivity to the selected regions, especially the cerebellum, were considered to be the strategy in maintaining the cognitive reserve. According to the MMSE and CDR score, AD patients in our study were classified as mild to moderate. It is feasible to illuminate the role of the cerebellum in the evaluation of the limbic network in the AD spectrum by examining coupled cerebro-cerebellar functional connectivity.

POFC-AIC and IPL

In the current study, the bilateral POFC-AIC, together with the left IPL, formed a sub-scale network that showed a dual pattern in MCI and AD patients. Increased functional connectivity between the sub-scale network and cerebellar limbic network was observed in MCI relative to HC and decreased functional connectivity was observed in AD relative to MCI. The result provided support for a nonlinear trajectory of this sub-scale network activity in the evolution from MCI to AD, similar to the pattern of memory-related neural activity reported by Celone et al. (2006). The OFC and other regions of the prefrontal cortex have been considered important in personality and social behavior. The lateral part of the OFC, which is also a component of limbic cortices, is mainly involved in behavioral inhibition, response inhibition, selective responses, and emotional cognitive adjustment. The OFC is not an area of onset for AD pathology in the brain; however, a large number of neurofibrillary tangles (NFTs) can be observed in the OFC in AD. The density of NFTs in the OFC was only secondary to that of the medial temporal lobe (MTL) even in healthy elderly with normal aging and MCI (Guillozet et al., 2003). These tangles may lead to the changes in OFC activity seen in AD. The anterior insula is an important hub in the emotional limbic system, with the ventral part of anterior insula, just ventral to the primary taste cortex, a part of the limbic system. The ventral anterior insula, together with the anterior cingulate cortex (ACC) and MCC, form the visceromotor limbic cortices. Most researches on the insula have concentrated on its influence on affective disorders. In individuals with depression, task-induced fMRI study showed hypoactivation of the right insula in response to negative affective pictures (Lee et al., 2007), and resting-state fMRI showed decreased Regional Homogeneity (ReHo) in the right insula, which was positively correlated with anxiety severity (Yao et al., 2009). The ventral anterior insular region has strong projections to the OFC and receives inputs from the OFC and ACC (Price, 2007), involving in decoding and representing reward and punishment signals that produce autonomic/visceral responses.

The IPL is not a component of the limbic system and was considered to exhibit strong evidence of a direct role in episodic memory retrieval. Vilberg and Rugg (2008) speculated that the IPL is involved in the maintenance or representation of retrieved information in something like the episodic buffer. In a study of focal lateral parietal damage, Davidson et al. (2008) showed evidence of disrupted recollection in an anterograde memory task. Since some links from the emotional system to the memory system are present, we would like to speculate that the IPL might play a role in limbic activity from the connected network.

The bilateral POFC-AIC and left IPL showed a more positive correlation with the MMSE score in MCI than in AD ($p < 0.05$), whereas no significant difference in correlation was observed between HC and MCI. This indicates that this sub-scale network activity was correlated with Alzheimer pathology, and may be a key biomarker in limbic activity. Moreover, the difference between HC and MCI was much less than that between MCI and AD. Compensatory activity is thought to occur during the progression of AD, especially in individuals at risk of AD (Bookheimer et al., 2000). That is to say, normal-appearing brain areas may be recruited for cognitive activity compensation in the progression of AD (Celone et al., 2006). In Yeo's Atlas (Yeo et al., 2011), the locations of bilateral POFC-AIC and left IPL are consistent with components of the ventral attention network, so we may speculate that limbic network activity compensation can be verified in MCI through a sub-scale ventral attention network, in addition to decompensation in AD. This coincides with the progress of Alzheimer pathology.

Paracentral Lobule and MCC

The paracentral lobule and MCC showed a consistent change in MCI and AD relative to HC. The left paracentral lobule

and right paracentral lobule extending to right MCC showed compromised functional connectivity to the cerebellar limbic network in MCI, and right MCC in AD. Structural connectivity also showed shorter fibers in the cingulum connecting the MCC with adjacent areas, such as the paracentral lobule, and lingual and fusiform gyri. Generally, the sensorimotor function is spared until severe disease; therefore, the paracentral lobule was not considered to be involved in AD patients in the current study. However, recent reports showed some functional changes in this area, such as increased ReHo index in MCI (Wang et al., 2015), and a significant increase in the nodal centrality in APOE $\varepsilon 4$ carriers relative to APOE $\varepsilon 4$ non-carriers based on a graph theory brain network analysis (Yao et al., 2015). Unlike the results of previous reports, the paracentral lobule showed decreased functional connectivity in MCI in this study. The MCC is one part of the limbic cortex, belonging to the hippocampal-centric division, and is also part of the posterior part of the medial DMN. The Pearson correlation indicated that the right MCC showed a more positive correlation with the MMSE score in HC than in AD ($p < 0.05$). No difference in correlation was observed between the right MCC and MMSE scores between HC and MCI, which is analogous to the pattern observed in the POFC-AIC and IPL.

Fusiform and Lingual Gyri, and Temporal Lobe

The fusiform gyrus is not a component of the cerebral limbic cortices, unlike the lingual gyrus. However, they both participate in mediating the perception of face identity (Hoffman and Haxby, 2000). The fusiform gyrus was also activated in a memory task. With associative encoding of novel picture-word pairs task, MCI subjects showed greater fMRI responses in the fusiform regions, which was believed to be a compensatory change due to the incipient atrophy in the anterior MTL (Hämäläinen et al., 2007). In the present study, the right fusiform showed increased functional connectivity in MCI relative to HC, which was consistent with previous reports. Both the lingual gyrus and temporal pole are parts of the olfactocentric division of the limbic network (Catani et al., 2013). In the comparison between AD and HC, the right lingual gyrus showed decreased while the temporal pole showed increased functional connectivity in AD. However, the correlation analysis showed that a positive correlation with MMSE score was observed in the right lingual gyrus and a negative correlation observed in the right temporal pole. To some degree, the negative correlation between the left temporal pole and MMSE score may indicate that the lower MMSE score in AD patients corresponds to stronger functional activity in this area. Mesulam (1998) has theorized that the temporal poles act as "transmodal epicenters" where information from the multiple sensory modalities is combined to form complex, symbolic, personalized representations. This area was always focused in the study of frontotemporal dementia, especially in the behavioral variant frontotemporal dementia (Hornberger et al., 2011). Zahn et al. (2009) showed that OFC and temporal pole atrophy was associated with disinhibited social behavior. The interaction of the OFC with temporal regions *via* the uncinate fasciculus might be crucial in maintaining normal behavior (Green et al., 2010). A large-scale functional connectivity study showed that the medial part of the left temporal pole is connected to paralimbic structures (Pascual et al., 2015). We should consider that the temporal pole is also a pivotal area in the evaluation of AD and deserves to be studied further.

CONCLUSION

The current study investigated the pattern of limbic network activity in the AD spectrum by examining the cerebro-cerebellar functional connectivity as the cerebellum is involved in the modulation of cognitive function. Functional connectivity to the cerebellar limbic network was significantly more compromised in AD than in MCI patients. This coincides with the progress of Alzheimer pathology. However, the dual pattern of the sub-scale ventral attention network, increased in MCI vs. HC and decreased in AD vs. MCI, indicating a compensatory mechanism in the MCI period, may be significant in the illumination of the limbic network in the AD spectrum. And this is consistent with Delli's report (Delli Pizzi et al., 2019) that increased functional connectivity between the hippocampus and the cerebellar functional associated regions, including the limbic system, was observed in individuals with MCI those who did not convert to AD compared to those who converted to AD. In Skouras' report (Skouras et al., 2019), cerebellum showed increased functional connectivity to PCC in asymptomatic preclinical AD and to MCC in MCI, these were also considered as functional compensation. Considering that the cerebellum was spared in the early stages of the AD, it is reasonable to believe that the cerebellum is crucial in this process. In addition, the change in left temporal pole activity supports the notion that more attention should be paid to this area in the limbic network in AD.

LIMITATION

Although this is a pilot study, we think it was meaningful to investigate the cerebral limbic network activity from the perspective of coupled cerebro-cerebellar functional connectivity. Nonetheless, there were some limitations in this study. The first was the small sample in each group. The second item may be the incomplete neuropsychological study without the use of the Neuropsychiatric Inventory (NPI). Third, we believe it would be more helpful to take the DMN into consideration and analyze the interrelationship between them.

DATA AVAILABILITY STATEMENT

The raw data supporting the conclusions of this manuscript will be made available by the authors, without undue reservation, to any qualified researcher.

ETHICS STATEMENT

The study was approved by the local ethics committee of Xuanwu Hospital. Written informed consent was obtained from

all participants in accordance with the Declaration of Helsinki prior to the study.

AUTHOR CONTRIBUTIONS

ZQ, H-JL and JL contributed to the conception and design of the study. ZQ organized the database. H-JL performed the statistical analysis. ZQ, YA and MZ wrote the first draft of the manuscript. All authors contributed to manuscript revision, read and approved the submitted version.

FUNDING

This work was supported by Beijing Municipal Geriatric Medical Research Center Project (PXM2019_026283_000003), Beijing Municipal Commission of Science and Technology (Z171100000117001), Beijing Municipal Administration of Hospitals' Ascent Plan (DFL20180802), Natural Science Foundation of China (81141018, 31871143), and National Key Research and Development Program of China (2016YFC0107100).

REFERENCES

Alalade, E., Denny, K., Potter, G., Steffens, D., and Wang, L. (2011). Altered cerebellar-cerebral functional connectivity in geriatric depression. *PLoS One* 6:e20035. doi: 10.1371/journal.pone.0020035

Bai, F., Xie, C., Watson, D. R., Shi, Y., Yuan, Y., Wang, Y., et al. (2011). Aberrant hippocampal subregion networks associated with the classifications of aMCI subjects: a longitudinal resting-state study. *PLoS One* 6:e29288. doi: 10.1371/journal.pone.0029288

Bennett, M. R. (2011). The prefrontal-limbic network in depression: Modulation by hypothalamus, basal ganglia and midbrain. *Prog. Neurobiol.* 93, 468–487. doi: 10.1016/j.pneurobio.2011.01.006

Bernard, J. A., Peltier, S. J., Wiggins, J. L., Jaeggi, S. M., Buschkuehl, M., Fling, B. W., et al. (2013). Disrupted cortico-cerebellar connectivity in older adults. *Neuroimage* 83, 103–119. doi: 10.1016/j.neuroimage.2013.06.042

Bernard, J. A., and Seidler, R. D. (2014). Moving forward: age effects on the cerebellum underlie cognitive and motor declines. *Neurosci. Biobehav. Rev.* 42, 193–207. doi: 10.1016/j.neubiorev.2014.02.011

Bookheimer, S. Y., Strojwas, M. H., Cohen, M. S., Saunders, A. M., Pericak-Vance, M. A., Mazziotta, J. C., et al. (2000). Patterns of brain activation in people at risk for Alzheimer's disease. *N. Engl. J. Med.* 343, 450–456. doi: 10.1056/NEJM200008173430701

Braak, H., and Braak, E. (1991). Neuropathological stageing of Alzheimer-related changes. *Acta Neuropathol.* 82, 239–259. doi: 10.1007/bf00308809

Bruen, P. D., McGeown, W. J., Shanks, M. F., and Venneria, A. (2008). Neuroanatomical correlates of neuropsychiatric symptoms in Alzheimer's disease. *Brain* 131, 2455–2463. doi: 10.1093/brain/awn151

Buckner, R. L. (2013). The cerebellum and cognitive function: 25 years of insight from anatomy and neuroimaging. *Neuron* 80, 807–815. doi: 10.1016/j.neuron.2013.10.044

Buckner, R. L., Krienen, F. M., Castellanos, A., Diaz, J. C., and Yeo, B. T. (2011). The organization of the human cerebellum estimated by intrinsic functional connectivity. *J. Neurophysiol.* 106, 2322–2345. doi: 10.1152/jn.00339.2011

Canuet, L., Pusil, S., López, M. E., Bajo, R., Pineda-Pardo, J. Á., Cuesta, P., et al. (2015). Network disruption and cerebrospinal fluid amyloid-beta and phospho-tau levels in mild cognitive impairment. *J. Neurosci.* 35, 10325–10330. doi: 10.1523/jneurosci.0704-15.2015

Catani, M., Dell'acqua, F., and Thiebaut de Schotten, M. (2013). A revised limbic system model for memory, emotion and behaviour. *Neurosci. Biobehav. Rev.* 37, 1724–1737. doi: 10.1016/j.neubiorev.2013.07.001

Celone, K. A., Calhoun, V. D., Dickerson, B. C., Atri, A., Chua, E. F., Miller, S. L., et al. (2006). Alterations in memory networks in mild cognitive impairment and Alzheimer's disease: an independent component analysis. *J. Neurosci.* 26, 10222–10231. doi: 10.1523/JNEUROSCI.2250-06.2006

Craig, D., Mirakhur, A., Hart, D. J., McIlroy, S. P., and Passmore, A. P. (2005). A cross-sectional study of neuropsychiatric symptoms in 435 patients with Alzheimer's disease. *Am. J. Geriatr. Psychiatry* 13, 460–468. doi: 10.1176/appi.ajgp.13.6.460

Davidson, P. S., Anaki, D., Ciaramelli, E., Cohn, M., Kim, A. S., Murphy, K. J., et al. (2008). Does lateral parietal cortex support episodic memory? Evidence from focal lesion patients. *Neuropsychologia* 46, 1743–1755. doi: 10.1016/j.neuropsychologia.2008.01.011

Delli Pizzi, S., Punzi, M., Sensi, S. L., and Alzheimer's Disease Neuroimaging Initiative. (2019). Functional signature of conversion of patients with mild cognitive impairment. *Neurobiol. Aging* 74, 21–37. doi: 10.1016/j.neurobiolaging.2018.10.004

Green, S., Ralph, M. A., Moll, J., Stamatakis, E. A., Grafman, J., and Zahn, R. (2010). Selective functional integration between anterior temporal and distinct fronto-meso limbic regions during guilt and indignation. *Neuroimage* 52, 1720–1726. doi: 10.1016/j.neuroimage.2010.05.038

Greicius, M. D., Srivastava, G., Reiss, A. L., and Menon, V. (2004). Default-mode network activity distinguishes Alzheimer's disease from healthy aging: evidence from functional MRI. *Proc. Natl. Acad. Sci. U S A* 101, 4637–4642. doi: 10.1073/pnas.0308627101

Guillozet, A. L., Weintraub, S., Mash, D. C., and Mesulam, M. M. (2003). Neurofibrillary tangles, amyloid, and memory in aging and mild cognitive impairment. *Arch. Neurol.* 60, 729–736. doi: 10.1001/archneur.60.5.729

Habas, C., Kamdar, N., Nguyen, D., Prater, K., Beckmann, C. F., Menon, V., et al. (2009). Distinct cerebellar contributions to intrinsic connectivity networks. *J. Neurosci.* 29, 8586–8594. doi: 10.1523/JNEUROSCI.1868-09.2009

Hämäläinen, A., Pihlajamäki, M., Tanila, H., Hänninen, T., Niskanen, E., Tervo, S., et al. (2007). Increased fMRI responses during encoding in mild cognitive impairment. *Neurobiol. Aging* 28, 1889–1903. doi: 10.1016/j.neurobiolaging.2006.08.008

Hoffman, E. A., and Haxby, J. V. (2000). Distinct representations of eye gaze and identity in the distributed human neural system for face perception. *Nat. Neurosci.* 3, 80–84. doi: 10.1038/71152

Hokkanen, L. S. K., Kauranen, V., Roine, R. O., Salonen, O., and Kotila, M. (2006). Subtle cognitive deficits after cerebellar infarcts. *Eur. J. Neurol.* 13, 161–170. doi: 10.1111/j.1468-1331.2006.01157.x

Hornberger, M., Geng, J., and Hodges, J. R. (2011). Convergent grey and white matter evidence of orbitofrontal cortex changes related to disinhibition in behavioural variant frontotemporal dementia. *Brain* 134, 2502–2512. doi: 10.1093/brain/awr173

Hu, X., Meiberth, D., Newport, B., and Jessen, F. (2015). Anatomical correlates of the neuropsychiatric symptoms in Alzheimer's disease. *Curr. Alzheimer Res.* 12, 266–277. doi: 10.2174/1567205012666150302154914

Khan, U. A., Liu, L., Provenzano, F. A., Berman, D. E., Profaci, C. P., Sloan, R., et al. (2014). Molecular drivers and cortical spread of lateral entorhinal cortex dysfunction in preclinical Alzheimer's disease. *Nat. Neurosci.* 17, 304–311. doi: 10.1038/nn.3606

Lee, B. T., Cho, S. W., Khang, H. S., Lee, B. C., Choi, I. G., Lyoo, I. K., et al. (2007). The neural substrates of affective processing toward positive and negative affective pictures in patients with major depressive disorder. *Prog. Neuropsychopharmacol. Biol. Psychiatry* 31, 1487–1492. doi: 10.1016/j.pnpbp.2007.06.030

Leow, A., Ajilore, O., Zhan, L., Arienzo, D., GadElkarim, J., Zhang, A., et al. (2013). Impaired inter-hemispheric integration in bipolar disorder revealed with brain network analyses. *Biol. Psychiatry* 73, 183–193. doi: 10.1016/j.biopsych.2012.09.014

Li, H. J., Hou, X. H., Liu, H. H., Yue, C. L., He, Y., and Zuo, X. N. (2015). Toward systems neuroscience in mild cognitive impairment and Alzheimer's disease: a meta-analysis of 75 fMRI studies. *Hum. Brain Mapp.* 36, 1217–1232. doi: 10.1002/hbm.22689

Lu, J., Liu, H., Zhang, M., Wang, D., Cao, Y., Ma, Q., et al. (2011). Focal pontine lesions provide evidence that intrinsic functional connectivity reflects polysynaptic anatomical pathways. *J. Neurosci.* 31, 15065–15071. doi: 10.1523/jneurosci.2364-11.2011

Mesulam, M. M. (1998). From sensation to cognition. *Brain* 121, 1013–1052. doi: 10.1093/brain/121.6.1013

Nestor, P. J., Fryer, T. D., Smielewski, P., and Hodges, J. R. (2003). Limbic hypometabolism in Alzheimer's disease and mild cognitive impairment. *Ann. Neurol.* 54, 343–351. doi: 10.1002/ana.10669

Ni, R., Gillberg, P. G., Bergfors, A., Marutle, A., and Nordberg, A. (2013). Amyloid tracers detect multiple binding sites in Alzheimer's disease brain tissue. *Brain* 136, 2217–2227. doi: 10.1093/brain/awt142

O'Reilly, J. X., Beckmann, C. F., Tomassini, V., Ramnani, N., and Johansen-Berg, H. (2010). Distinct and overlapping functional zones in the cerebellum defined by resting state functional connectivity. *Cereb. Cortex* 20, 953–965. doi: 10.1093/cercor/bhp157

Papez, J. W. (1995). A proposed mechanism of emotion. *J. Neuropsychiatry Clin. Neurosci.* 7, 103–112. doi: 10.1176/jnp.7.1.103

Pascual, B., Masdeu, J. C., Hollenbeck, M., Makris, N., Insausti, R., Ding, S. L., et al. (2015). Large-scale brain networks of the human left temporal pole: a functional connectivity MRI study. *Cereb. Cortex* 25, 680–702. doi: 10.1093/cercor/bht260

Price, J. L. (2007). Definition of the orbital cortex in relation to specific connections with limbic and visceral structures and other cortical regions. *Ann. N Y Acad. Sci.* 1121, 54–71. doi: 10.1196/annals.1401.008

Pruessner, J. C., Dedovic, K., Khalili-Mahani, N., Engert, V., Pruessner, M., Buss, C., et al. (2008). Deactivation of the limbic system during acute psychosocial stress: evidence from positron emission tomography and functional magnetic resonance imaging studies. *Biol. Psychiatry* 63, 234–240. doi: 10.1016/j.biopsych.2007.04.041

Rolls, E. T. (2015). Limbic systems for emotion and for memory, but no single limbic system. *Cortex* 62, 119–157. doi: 10.1016/j.cortex.2013.12.005

Schmahmann, J. D. (2019). The cerebellum and cognition. *Neurosci. Lett.* 688, 62–75. doi: 10.1016/j.neulet.2018.07.005

Skouras, S., Falcon, C., Tucholka, A., Rami, L., Sanchez-Valle, R., Lladó, A., et al. (2019). Mechanisms of functional compensation, delineated by eigenvector centrality mapping, across the pathophysiological continuum of Alzheimer's disease. *Neuroimage Clin.* 22:101777. doi: 10.1016/j.nicl.2019.101777

Sokolov, A. A., Miall, R. C., and Ivry, R. B. (2017). The cerebellum: adaptive prediction for movement and cognition. *Trends Cogn. Sci.* 21, 313–332. doi: 10.1016/j.tics.2017.02.005

Spires-Jones, T. L., and Hyman, B. T. (2014). The intersection of amyloid beta and tau at synapses in Alzheimer's disease. *Neuron* 82, 756–771. doi: 10.1016/j.neuron.2014.05.004

Tomasi, D., and Volkow, N. D. (2012). Abnormal functional connectivity in children with attention-deficit/hyperactivity disorder. *Biol. Psychiatry* 71, 443–450. doi: 10.1016/j.biopsych.2011.11.003

Trzepacz, P. T., Yu, P., Bhamidipati, P. K., Willis, B., Forrester, T., Tabas, L., et al. (2013). Frontolimbic atrophy is associated with agitation and aggression in mild cognitive impairment and Alzheimer's disease. *Alzheimers Dement.* 9, S95.e1–S104.e1. doi: 10.1016/j.jalz.2012.10.005

Van Overwalle, F., and Mariën, P. (2016). Functional connectivity between the cerebrum and cerebellum in social cognition: a multi-study analysis. *Neuroimage* 124, 248–255. doi: 10.1016/j.neuroimage.2015.09.001

Vilberg, K. L., and Rugg, M. D. (2008). Memory retrieval and the parietal cortex: review of evidence from a dual-process perspective. *Neuropsychologia* 46, 1787–1799. doi: 10.1016/j.neuropsychologia.2008.01.004

Wang, Y., Zhao, X., Xu, S., Yu, L., Wang, L., Song, M., et al. (2015). Using regional homogeneity to reveal altered spontaneous activity in patients with mild cognitive impairment. *Biomed Res. Int.* 2015:807093. doi: 10.1155/2015/807093

Winblad, B., Palmer, K., Kivipelto, M., Jelic, V., Fratiglioni, L., Wahlund, L. O., et al. (2004). Mild cognitive impairment-beyond controversies, towards a consensus: report of the international working group on mild cognitive impairment. *J. Intern. Med.* 256, 240–246. doi: 10.1111/j.1365-2796.2004.01380.x

Xing, X. X., Zhou, Y. L., Adelstein, J. S., and Zuo, X. N. (2011). PDE-based spatial smoothing: a practical demonstration of impacts on MRI brain extraction, tissue segmentation and registration. *Magn. Reson. Imaging* 29, 731–738. doi: 10.1016/j.mri.2011.02.007

Xu, T., Yang, Z., Jiang, L., Xing, X.-X., and Zuo, X.-N. (2015). A Connectome Computation System for discovery science of brain. *Sci. Bull.* 60, 86–95. doi: 10.1007/s11434-014-0698-3

Yao, Z., Hu, B., Zheng, J., Zheng, W., Chen, X., Gao, X., et al. (2015). A FDG-PET study of metabolic networks in Apolipoprotein E ϵ4 allele carriers. *PLoS One* 10:e0132300. doi: 10.1371/journal.pone.0132300

Yao, Z., Wang, L., Lu, Q., Liu, H., and Teng, G. (2009). Regional homogeneity in depression and its relationship with separate depressive symptom clusters: a resting-state fMRI study. *J. Affect. Disord.* 115, 430–438. doi: 10.1016/j.jad.2008.10.013

Yeo, B. T., Krienen, F. M., Sepulcre, J., Sabuncu, M. R., Lashkari, D., Hollinshead, M., et al. (2011). The organization of the human cerebral cortex estimated by intrinsic functional connectivity. *J. Neurophysiol.* 106, 1125–1165. doi: 10.1152/jn.00338.2011

Zahn, R., Moll, J., Iyengar, V., Huey, E. D., Tierney, M., Krueger, F., et al. (2009). Social conceptual impairments in frontotemporal lobar degeneration with right anterior temporal hypometabolism. *Brain* 132, 604–616. doi: 10.1093/brain/awn343

Zhang, Y. W., Zhao, Z. L., Qi, Z., Hu, Y., Wang, Y. S., Sheng, C., et al. (2017). Local-to-remote cortical connectivity in amnestic mild cognitive impairment. *Neurobiol. Aging* 56, 138–149. doi: 10.1016/j.neurobiolaging.2017.04.016

Conflict of Interest: The authors declare that the research was conducted in the absence of any commercial or financial relationships that could be construed as a potential conflict of interest.

Advantages of publishing in Frontiers

OPEN ACCESS
Articles are free to read for greatest visibility and readership

FAST PUBLICATION
Around 90 days from submission to decision

HIGH QUALITY PEER-REVIEW
Rigorous, collaborative, and constructive peer-review

TRANSPARENT PEER-REVIEW
Editors and reviewers acknowledged by name on published articles

Frontiers
Avenue du Tribunal-Fédéral 34
1005 Lausanne | Switzerland

Visit us: www.frontiersin.org
Contact us: info@frontiersin.org | +41 21 510 17 00

REPRODUCIBILITY OF RESEARCH
Support open data and methods to enhance research reproducibility

DIGITAL PUBLISHING
Articles designed for optimal readership across devices

FOLLOW US
@frontiersin

IMPACT METRICS
Advanced article metrics track visibility across digital media

EXTENSIVE PROMOTION
Marketing and promotion of impactful research

LOOP RESEARCH NETWORK
Our network increases your article's readership